7 December 2012 | $10

Science

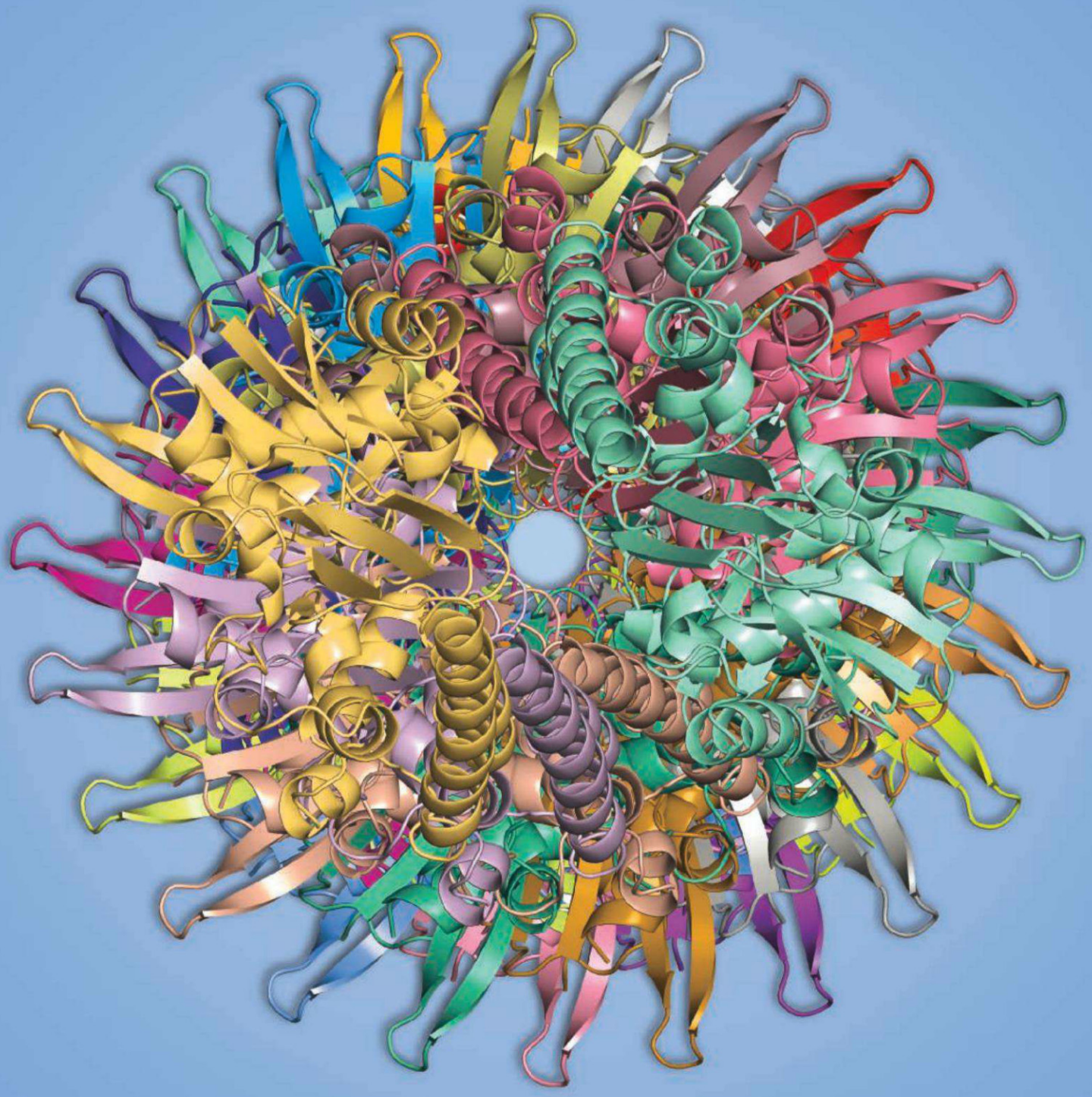

AAAS

One source for all your immunoassay needs

abcam®
discover more

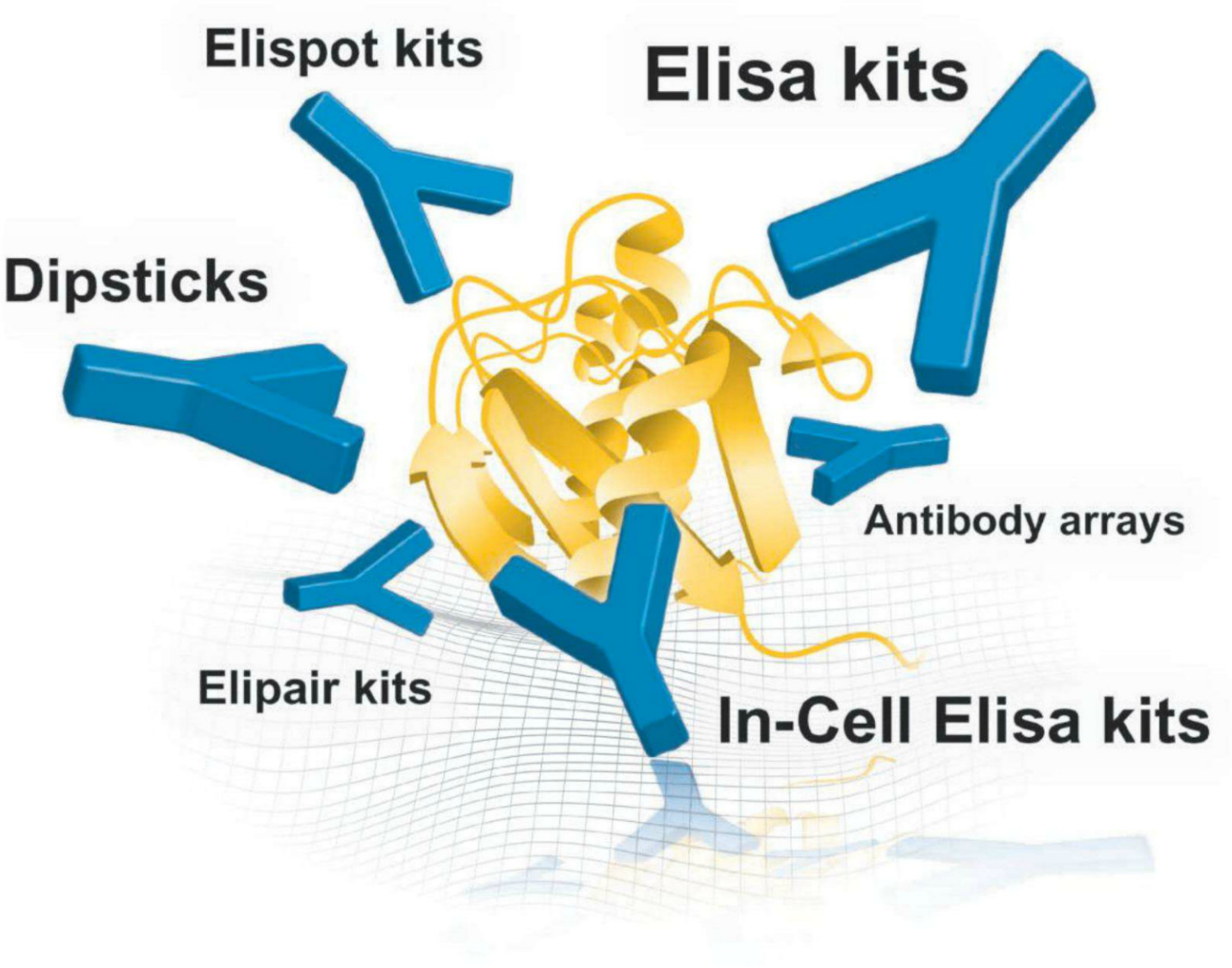

Choose from a range of easy-to-use kits for over **600 targets**. Get coverage of an extremely wide range of analysis including both extracellular and intracellular pathway targets such as cytokines, angiogenesis, adipokines, cell differentiation, growth factors, oncoproteins, signal transduction and many more.

Discover more at abcam.com/science

EPITOMICS®
an abcam® company

SPECIAL OFFER
$99 ANTIBODY SPECIAL
Find out more @
www.epitomics.com/promo

THE RABBIT MONOCLONAL ADVANTAGE

- More diverse epitope recognition
- High specificity and affinity
- Improved response to mouse antigens
- Highly validated - every antibody tested in WB, IHC, ICC, Flow Cytometry, and IP

Rabbit Monoclonal Antibodies (RabMAbs®) provide the combined benefits of superior antigen recognition of the rabbit immune system with the specificity and consistency of a monoclonal antibody, bringing you the highest quality antibody possible.

Over ***4000 RabMAbs®*** online, visit www.epitomics.com

CDX2 RabMAb | CDX2 Mouse MAb

Paraffin-embedded human colon tissue stained with Epitomics' CDX2 RabMAb (Cat.# 2475-1) and Vendor A's CDX2 Mouse Monoclonal under optimal conditions

Find out more @ www.epitomics.com/advantage

100% SATISFACTION GUARANTEE *Antibody Satisfaction Guarantee*

www.epitomics.com

US & Canada | 1-877-772-2622
Outside NA | 650-583-6688

NEW ENGLAND BioLabs® Inc.
enabling technologies in the life sciences

Stick together.

New DNA Ligases and Ligase Master Mixes

New England Biolabs offers the most extensive selection of high-quality and performance-optimized DNA ligases and ligase master mixes to streamline your cloning experiments.

Our expanded portfolio now includes:

- Blunt/TA Ligase Master Mix, optimized for blunt-end and single-base overhang substrates
- Instant Sticky-end Ligase Master Mix, uniquely formulated for the rapid ligation of sticky-end substrates
- T7 DNA Ligase, specific for sticky ends
- ElectroLigase,™ directly compatible with electroporation

Stick together with DNA Ligases and Ligase Master Mixes from NEB.

To request a FREE SAMPLE of our new DNA Ligase Master Mixes, visit **NEBStickTogether.com**

Blunt/TA Ligase Master Mix outperforms the competition

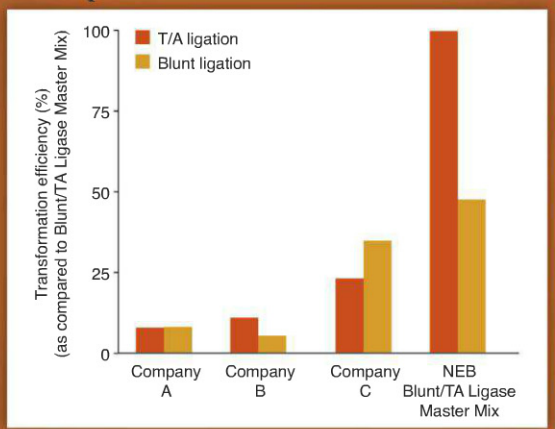

Duplicate ligation reactions of blunt or T/A vector/insert pairs were set up according to the master mix vendors' suggestions. Equal amounts of ligated DNA were used to transform NEB 10-beta Competent E. coli (NEB #C3019) and triplicate plating was performed. Transformation results were averaged and graphed as a percentage of the highest performing reaction, T/A ligation using the Blunt/TA Ligase Master Mix.

ELECTROLIGASE™ is a trademark of New England Biolabs.

EDITORIAL

1263 Failure of Skin-Deep Learning
Bruce Alberts

NEWS OF THE WEEK

1268 A roundup of the week's top stories

NEWS & ANALYSIS

1270 Final Report on Stapel Also Blames Field As a Whole

1271 Proposed H5N1 Research Reviews Raise Concerns

1272 Peering Inside the Moon to Read Its Earliest History
>> Science *Express Reports by M. T. Zuber* et al., *M. A. Wieczorek* et al., *and J. C. Andrews-Hanna* et al.; Science *Podcast*

1273 River Basin Management Plan Secures Water for the Environment

1274 White House Panel Urges Agencies to Take More Risks

1275 India Barred Entry to U.S. Author of Seismic Review

NEWS FOCUS

1276 Growing Pains in the Desert

1282 All Eyes on RNA

LETTERS

1285 Voles, Vasopressin, and the Ethics of Framing
D. J. McKaughan and K. C. Elliott

Disease Prevention: Data Integration
V. J. H. Powell and A. Acharya

Risk Communication on Shaky Ground
M. Sirota and M. Juanchich

1287 CORRECTIONS AND CLARIFICATIONS

BOOKS *ET AL.*

1289 Some Suggestions from 2012—The SB&F Prizes Finalists
>> Science *Podcast*

1293 Finalists for the Royal Society's Young People's Book Prize

POLICY FORUM

1296 U.S. Regulation of Stem Cells as Medical Products
D. Sipp and L. Turner

PERSPECTIVES

1298 Putting a Greenhouse Gas to Work
G. Haufe
>> *Report p. 1324*

1299 Redder Than Red
T. P. Sakmar
>> *Report p. 1340*

1300 Atomic Layer Electrodeposition
J. A. Switzer
>> *Report p. 1327*

1301 The Utility of Mouse Models in Post-GWAS Research
A. Lewis and I. Tomlinson
>> *Report p. 1360*

1303 Inflammation to Rebuild a Brain
N. Stella
>> *Report p. 1353*

1304 Platelets Kill the Parasite Within
C. R. Engwerda and M. F. Good
>> *Report p. 1348*

1305 Global Decline in Large Old Trees
D. B. Lindenmayer et al.

CONTENTS continued >>

page 1276

page 1289

COVER

End-on view of the atomic model of the bacterial actinlike ParM protein double-helical filament, generated from an electron microscopic reconstruction. A bipolar spindle of antiparallel ParM filaments pushes plasmids to the cell poles, constituting the simplest known apparatus for the segregation of genetic information. The loops on the outside of the 8- to 9-nanometer-thick filaments are involved in spindle formation. See page 1334.

Image: Jan Löwe

DEPARTMENTS

1259 This Week in *Science*
1264 Editors' Choice
1266 *Science* Staff
1369 New Products
1370 *Science* Careers

The Highest Quality
Cytokines & Growth Factors
...from Cell Signaling Technology

The world's highest quality antibody provider has now extended its expertise to cytokine production.

- Produced and bioassayed in house with the highest purity and bioactivity.
- Comparison of multiple lots, stringent product specifications, and rigorous quality control ensures maximum lot-to-lot consistency.
- Endotoxin levels are routinely tested and are less than 0.01 ng/µg cytokine.
- Many products are produced in mammalian cells to maximize natural conformation and glycosylation.
- Multi-milligram quantities available.

Human Interleukin-17A (hIL-17A) #8928

Purity

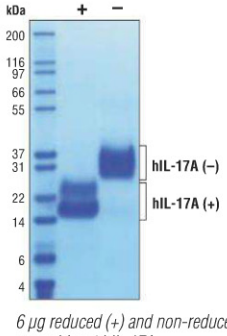

6 µg reduced (+) and non-reduced (-) recombinant hIL-17A.

Bioactivity

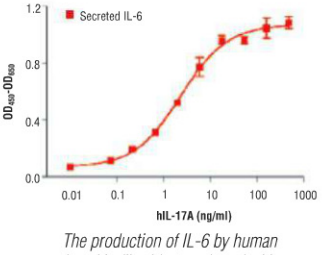

The production of IL-6 by human foreskin fibroblasts cultured with increasing concentrations of hIL-17A for 48 hours was assessed.

Downstream Signaling

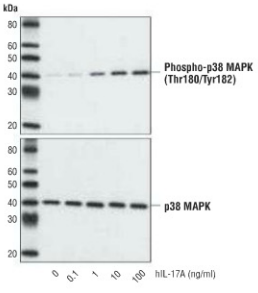

Human foreskin fibroblasts treated with hIL-17A for 15 minutes were examined using phospho- and total p38 MAPK antibodies.

for quality products you can trust...

www.cellsignal.com

Cell Signaling TECHNOLOGY®

For Research Use Only. Not For Use In Diagnostic Procedures.

Orders (toll-free) 1-877-616-2355 | **Inquiries** info@cellsignal.com | **Environmental Commitment** eco.cellsignal.com

© 2012 Cell Signaling Technology, Inc. Cell Signaling Technology® is a trademark of Cell Signaling Technology, Inc.

BREVIA

1307 Drought in Africa Caused Delayed Arrival of European Songbirds
A. P. Tøttrup et al.
A severe drought in the Horn of Africa delayed the spring arrival in Europe of two migratory species.

RESEARCH ARTICLE

1308 Crystal Structure of the Calcium Release–Activated Calcium Channel Orai
X. Hou et al.
The unusual architecture of this ion-channel pore regulates the flow of calcium into cells.

REPORTS

1314 Binary Millisecond Pulsar Discovery via Gamma-Ray Pulsations
H. J. Pletsch et al.
A computer-intensive search revealed gamma-ray pulsations from an exotic binary star system in data from the Fermi Telescope.

1317 Mapping Local Charge Recombination Heterogeneity by Multidimensional Nanospectroscopic Imaging
W. Bao et al.
A near-field optical probe designed to maximize its own signal enhancement can be used to image nonmetallic samples.

1321 Robust Photogeneration of H_2 in Water Using Semiconductor Nanocrystals and a Nickel Catalyst
Z. Han et al.
A photoreduction system combining nanoparticulate light absorbers with a soluble molecular catalyst proves stable for weeks.

1324 Taming of Fluoroform: Direct Nucleophilic Trifluoromethylation of Si, B, S, and C Centers
G. K. S. Prakash et al.
Proper choice of base and solvent renders fluoroform a useful reagent to introduce trifluoromethyl groups into a range of compounds.
>> *Perspective p. 1298*

1327 Self-Terminating Growth of Platinum Films by Electrochemical Deposition
Y. Liu et al.
Control over the presence of adsorbed hydrogen enables rapid sequential deposition of metal monolayers from aqueous solution.
>> *Perspective p. 1300*

1330 Phase Transformations and Metallization of Magnesium Oxide at High Pressure and Temperature
R. S. McWilliams et al.
Mantle minerals conductive at the high pressures and temperatures of planetary interiors could induce a magnetic field.

1334 A Bipolar Spindle of Antiparallel ParM Filaments Drives Bacterial Plasmid Segregation
P. Gayathri et al.
A bipolar spindle, formed by antiparallel actinlike filaments, pushes sister plasmids apart.

1337 Kinetic Responses of β-Catenin Specify the Sites of Wnt Control
A. R. Hernández et al.
Reducing the rate of phosphorylation of β-catenin leads to an increase in the steady-state level of the unmodified form.

1340 Tuning the Electronic Absorption of Protein-Embedded All-*trans*-Retinal
W. Wang et al.
Opsin-based light absorption was tuned over a 200-nanometer range by rationally engineering retinol-binding protein.
>> *Perspective p. 1299*

1344 Identity and Function of a Large Gene Network Underlying Mutagenic Repair of DNA Breaks
A. A. M. Al Mamun et al.
The complete set of proteins required for a mutagenic DNA-repair pathway is defined in *Escherichia coli*.

1348 Platelet Factor 4 and Duffy Antigen Required for Platelet Killing of *Plasmodium falciparum*
B. J. McMorran et al.
Interaction of a platelet protein and a red cell protein enables platelets to attack malarial parasites inside red cells.
>> *Perspective p. 1304*

1352 Developmental Progression to Infectivity in *Trypanosoma brucei* Triggered by an RNA-Binding Protein
N. G. Kolev et al.
The developmental stages of the sleeping sickness parasite can now be observed without the tsetse fly.
>> Science *Podcast*

1353 Acute Inflammation Initiates the Regenerative Response in the Adult Zebrafish Brain
N. Kyritsis et al.
An inflammatory response to traumatic injury promotes neurogenesis and repair in the zebrafish brain.
>> *Perspective p. 1303*

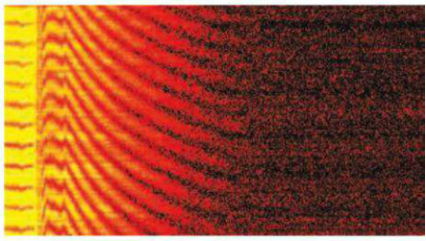

page 1330

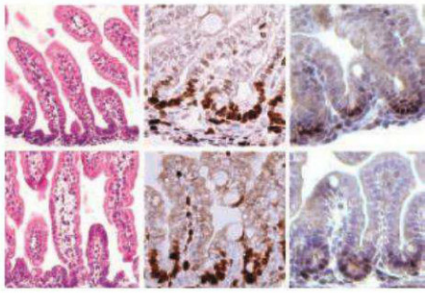

pages 1301 & 1360

1357 Sexually Dimorphic BDNF Signaling Directs Sensory Innervation of the Mammary Gland
Y. Liu et al.
Androgen-driven changes in receptor expression disrupt a neuronal signaling pathway and de-innervation.

1360 Mice Lacking a *Myc* Enhancer That Includes Human SNP rs6983267 Are Resistant to Intestinal Tumors
I. K. Sur et al.
A human genetic variant, identified in genome-wide association studies as increasing cancer risk, alters tumorigenesis in mice.
>> *Perspective p. 1301*

1363 Evolution of an MCM Complex in Flies That Promotes Meiotic Crossovers by Blocking BLM Helicase
K. P. Kohl et al.
Minichromosome maintenance proteins have been co-opted to make meiotic recombination safe in flies.

CONTENTS continued >>

BE INSPIRED WHEN YOU PCR WITH BIO-RAD.

(FEEL FREE TO RETHINK WHAT'S POSSIBLE.)

INTEGRATED PCR SOLUTIONS

It's time to rethink what you know about PCR. From digital PCR to real-time PCR, from thermal cyclers to reagents to our new wet-lab validated gene expression assays, Bio-Rad has been improving PCR for close to 25 years. Our philosophy is simple: give researchers an easier path to the best results. That way you can spend your time and focus on driving your research to new discoveries.

Find out more at bio-rad.com/ad/pcr2

BIO-RAD

ONLINE**HIGHLIGHTS**

*SCIENCE*XPRESS

www.sciencexpress.org

Publication Ahead of Print

Gravity Field of the Moon from the Gravity Recovery and Interior Laboratory (GRAIL) Mission
M. T. Zuber et al.
10.1126/science.1231507

The Crust of the Moon as Seen by GRAIL
M. A. Wieczorek et al.
10.1126/science.1231530

Ancient Igneous Intrusions and Early Expansion of the Moon Revealed by GRAIL Gravity Gradiometry
J. C. Andrews-Hanna et al.
10.1126/science.1231753
>> News story p. 1272

Neural Basis of a Pollinator's Buffet: Olfactory Specialization and Learning in *Manduca sexta*
J. A. Riffell et al.
10.1126/science.1225483

Suppression of Oxidative Stress by β-Hydroxybutyrate, an Endogenous Histone Deacetylase Inhibitor
T. Shimazu et al.
10.1126/science.1227166

JNK Expression by Macrophages Promotes Obesity-Induced Insulin Resistance and Inflammation
M. S. Han et al.
10.1126/science.1227568

Germline DNA Demethylation Dynamics and Imprint Erasure Through 5-Hydroxymethylcytosine
J. A. Hackett et al.
10.1126/science.1229277

*SCIENCE*NOW

www.sciencenow.org

Highlights From Our Daily News Coverage

The First Signs of Ancient Life on Mars?
The Curiosity rover has detected organic matter, but it may never have been alive.
http://scim.ag/Life-Mars

Why Old People Get Scammed
The anterior insula may make us less suspicious as we age.
http://scim.ag/Brain_Region

Read My Hips
Intense emotions are easier to read in the body than in the face.
http://scim.ag/Intense_Emotions

*SCIENCE*SIGNALING

www.sciencesignaling.org

The Signal Transduction Knowledge Environment

4 December issue: http://scim.ag/ss120412

RESEARCH ARTICLE: RNF4-Dependent Hybrid SUMO-Ubiquitin Chains Are Signals for RAP80 and Thereby Mediate the Recruitment of BRCA1 to Sites of DNA Damage
C. M. Guzzo et al.
DNA repair proteins find sites of damage marked by hybrid SUMO-ubiquitin chains.

RESEARCH ARTICLE: G Protein–Coupled Receptor–Mediated Activation of p110β by Gβγ Is Required for Cellular Transformation and Invasiveness
H. A. Dbouk et al.
Loss of the phosphatase PTPN22 enhances the functions of both effector and regulatory T cells.

PERSPECTIVE: Cdc42 Oscillations in Yeasts
F. O. Bendezú and S. G. Martin
Oscillations in the localization of active Cdc42 govern polarized cell growth in yeasts.

PRESENTATION: SCF-Mediated Degradation of p100 (NF-κB2): Mechanisms and Relevance in Multiple Myeloma
L. Busino et al.
Degradation of an inhibitor of noncanonical NF-κB signaling promotes cell survival.

*SCIENCE*TRANSLATIONAL MEDICINE

www.sciencetranslationalmedicine.org

Integrating Medicine and Science

5 December issue: http://scim.ag/stm120512

FOCUS: The Goldilocks Effect
M. Boothby and C. L. Williams

RESEARCH ARTICLE: Overexpression of Methyl-CpG Binding Protein 2 Impairs T_H1 Responses
T. Yang et al.
MECP2 gene duplication causes immune dysregulation by suppressing IFN-γ production from T helper cells.

FOCUS: Creating a Space for Innovative Device Development
M. McMurry-Heath and M. A. Hamburg
The FDA announces a nonprofit partnership to advance regulatory science for medical technology development.

RESEARCH ARTICLE: α-Synuclein–Induced Down-Regulation of Nurr1 Disrupts GDNF Signaling in Nigral Dopamine Neurons
M. Decressac et al.
Nurr1 mediates protection of dopamine neurons by GDNF in response to α-synuclein–mediated toxicity.

RESEARCH ARTICLE: Decreased Tonic Inhibition in Cerebellar Granule Cells Causes Motor Dysfunction in a Mouse Model of Angelman Syndrome
K. Egawa et al.
Ube3a deficiency causes decreased cerebellar tonic inhibition by preventing degradation of GAT1 in Angelman syndrome.

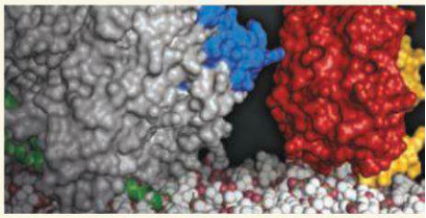

SCIENCE**SIGNALING**
Targeting the interaction site.

*SCIENCE*CAREERS

www.sciencecareers.org/career_magazine

Free Career Resources for Scientists

http://scim.ag/SciCareers7December2012

Getting Back Your Mojo
M. Price
Psychologists share tips for figuring out what is sapping your enthusiasm—and how to get it back.

Taken for Granted: How Not to Attract Minorities to STEM
B. L. Benderly
Research shows that large admissions preferences stymie studies in science and technical subjects.

myIDP: What Do You Care About?
B. Lindstaedt et al.
Analyzing and prioritizing your deeply held values are crucial steps in choosing a scientific career.

*SCIENCE*PODCAST

www.sciencemag.org/multimedia/podcast

Free Weekly Show for 7 December 2012

Listen to stories on sleeping sickness, prize-winning children's books, the GRAIL project, and more.

SCIENCE (ISSN 0036-8075) is published weekly on Friday, except the last week in December, by the American Association for the Advancement of Science, 1200 New York Avenue, NW, Washington, DC 20005. Periodicals Mail postage (publication No. 484460) paid at Washington, DC, and additional mailing offices. Copyright © 2012 by the American Association for the Advancement of Science. The title SCIENCE is a registered trademark of the AAAS. Domestic individual membership and subscription (51 issues): $149 ($74 allocated to subscription). Domestic institutional subscription (51 issues): $990; Foreign postage extra: Mexico, Caribbean (surface mail) $55; other countries (air assist delivery) $85. First class, airmail, student, and emeritus rates on request. Canadian rates with GST available upon request, GST #1254 88122. Publications Mail Agreement Number 1069624. **Printed in the U.S.A.**

Change of address: Allow 4 weeks, giving old and new addresses and 8-digit account number. **Postmaster:** Send change of address to AAAS, P.O. Box 96178, Washington, DC 20090–6178. **Single-copy sales:** $10.00 current issue, $15.00 back issue prepaid includes surface postage; bulk rates on request. **Authorization to photocopy** material for internal or personal use under circumstances not falling within the fair use provisions of the Copyright Act is granted by AAAS to libraries and other users registered with the Copyright Clearance Center (CCC) Transactional Reporting Service, provided that $30.00 per article is paid directly to CCC, 222 Rosewood Drive, Danvers, MA 01923. The identification code for *Science* is 0036-8075. *Science* is indexed in the *Reader's Guide to Periodical Literature* and in several specialized indexes.

AAAS
ADVANCING SCIENCE, SERVING SOCIETY

CREDIT: OSCAR VADAS/MRC LABORATORY OF MOLECULAR BIOLOGY, CAMBRIDGE

MILLIONS OF STUDENTS AND RESEARCHERS USE ENDNOTE TO MANAGE THEIR REFERENCES AND CREATE BIBLIOGRAPHIES. WHY NOT YOU?

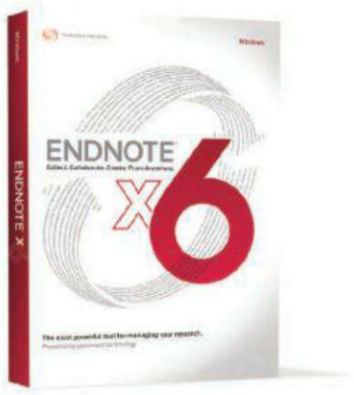

INTRODUCING

ENDNOTE® X6

Collect. Collaborate. Create. From Anywhere.

With *EndNote*, you can:

- Access your references from anywhere and manage your *EndNote* library from multiple computers with *EndNoteSync*.
- Search hundreds of online resources to collect references and PDFs
- Format references for any project with patented *Cite While You Write*® technology
- Use the new PubMed direct export format to import records in fewer steps
- Create and share custom groups, smart groups, or combined groups
- Enjoy a FREE 2-year subscription to *EndNote Web* with advanced features
- And so much more!

1-800-722-1227 • rs.sales@thomson.com

endnote.com

© Copyright 2012 Thomson Reuters. EndNote is a registered trademark of Thomson Reuters. All trademarks are the property of their respective companies.

THOMSON REUTERS™

EDITED BY STELLA HURTLEY

Platelets Poison Parasites

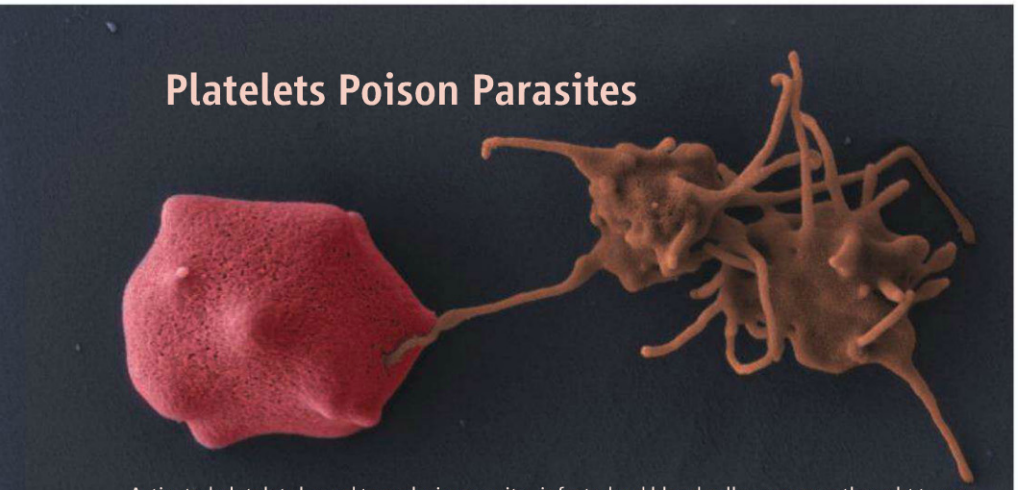

Activated platelets bound to malaria parasite–infected red blood cells were once thought to contribute to pathogenesis, but recently the platelets have been found to have a protective effect. **McMorran *et al.*** (p. 1348; see the Perspective by **Engwerda and Good**) extended this discovery to show that platelet activation releases intracellular granules containing a chemokine, PF4, which is internalized by *Plasmodium falciparum*–infected red cells. Subsequently, mature parasites within the cells die. The Duffy blood-group factor on red blood cells is known to act as a nonspecific receptor for chemokines, such as PF4, as well as a receptor for cell invasion by other species of malaria parasite. When the Duffy antigen was blocked by antibody treatment, platelets and PF4 were less able to kill the *P. falciparum* parasites within.

CREDITS (TOP TO BOTTOM): ANDREAS GRETH/AUSTRALIAN SCHOOL OF ADVANCED MEDICINE, MACQUARIE UNIVERSITY; STEPHEN B. LONG/MEMORIAL SLOAN-KETTERING CANCER CENTER

Exotic Pulsations

The launch of the Fermi Gamma-ray Space Telescope in 2008 enabled the detection of large numbers of pulsars. Millisecond pulsars, neutron stars with millisecond periods, are much more difficult to find in gamma-ray data. In a computational tour de force, **Pletsch *et al.*** (p. 1314, published online 25 October) detected gamma-ray pulsations from a formerly unidentified gamma-ray source in the Fermi Large Area Telescope Second Source Catalog. The pulsating neutron star orbits a companion star more rapidly than any other such neutron star known, and the system may belong to an exotic class of binary systems where the neutron star is systematically destroying its companion.

Atomic Layers from Solution

Growth of flat thin films is often plagued by the formation of mounds and pyramids. To avoid this problem, atomic-layer deposition (ALD) can be used whereby alternating self-termination reactions stop the layer growth. Electrochemical approaches to ALD use surface alloys to slow film growth, but often lead to film contamination. **Yihua Liu *et al.*** (p. 1327; see the Perspective by **Switzer**) show that for platinum films, controlling surface potential can lead to adsorbed hydrogen on the surface, which can terminate film growth at one layer, leaving platinum species in solution available for further reduction. Rapid changes in applied potential can oxidize the hydrogen, which allows efficient contamination-free growth of an additional atomic layer.

Robust Reduction

A major challenge in the design of artificial photosynthesis catalysts has been their instability under the reaction conditions—a problem that plants and other autotrophs address by perpetually reproducing their biochemical machinery. **Han *et al.*** (p. 1321, published online 8 November) now demonstrate a system for photoreductive hydrogen generation in water that manifests undiminished activity for weeks at a time. Semiconductor nanoparticles for light absorption were combined with a soluble nickel complex for the catalytic chemistry. The system currently requires a sacrificial electron donor, but its robustness shows promise for future pairing with an integrated oxidation catalyst.

CF_3 from Fluoroform

Fluoroform (CF_3H) is a by-product from the manufacture of fluorocarbon-based materials used, for example, in nonstick coatings and refrigerants. Fluoroform's potency as a greenhouse gas is a growing concern as supplies continue to accumulate. In this context, **Prakash *et al.*** (p. 1324; see the Perspective by **Haufe**) show that fluoroform can be used to transfer CF_3 to silicon, sulfur, and carbon centers in the development of CF_3-bearing pharmaceutical and agrochemical structures.

Planetary Interiors Under Pressure

The interiors of Earth and other rocky planets generally consist of a few common minerals. Depending largely on the size of the planet, the distribution and relative abundance of these minerals varies; for example, MgO is abundant in the mantles of Earth and large Earth-like planets, but is present in Jupiter's core. The properties of MgO also vary with planetary size as a function of temperature and pressure. **McWilliams *et al.*** (p. 1330, published online 22 November) performed laser-shock experiments at pressures over three times higher than Earth's inner core. MgO underwent two phase transformations, first to a solid with a modified crystal structure, and then to a conductive liquid. In terrestrial planets greater than eight Earth masses, MgO in the mantle could generate a magnetic field–generating dynamo such as those that typically found in planetary cores.

Architecture of a CRAC

The calcium release–activated calcium (CRAC) channel generates intracellular calcium signals in response to depletion of calcium from the endoplasmic reticulum. **Hou *et al.*** (p. 1308, published online 22 November) report a high-resolution crystal structure of Orai, the CRAC channel pore from *Drosophila melanogaster*. Six Orai subunits surround a central pore that extends into the cytosol. The pore is in a closed conformation that is stabilized by anions binding to a basic region near the intracellular side. A ring of glutamates on the extracellular side form a selectivity filter. The channel architecture allows calcium permeation while regulating the flow to prevent overloading the cell with calcium.

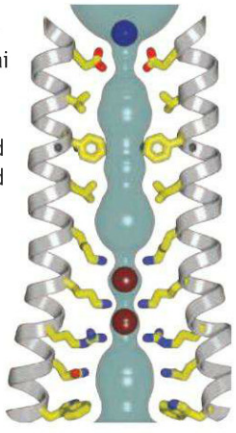

Plasmid Partitioning

Bacterial plasmids need to be able to partition faithfully into daughter cells. Combining structural data and advanced microscopy, **Gayathri**

Continued on page 1261

LightCycler®

Reveal Your qPCR Super Powers!

Introducing the LightCycler® 96 Real-Time PCR System

- **Innovative optics for accurate results**
  Simultaneously capture 96 wells of data for maximum well-to-well consistency.
- **Intuitive touchscreen interface and powerful data analysis software**
  Speed time to results with an advanced yet easy-to-use system designed for both novices and experienced users.
- **Built on 14 years of real-time PCR excellence**
  Rely on Roche's expertise in providing fast, flexible, and accurate real-time PCR systems that enable research breakthroughs.

Become a qPCR Superhero with the NEW LightCycler® 96 Real-Time PCR System from Roche! See the video at *www.lightcycler96.com*

Contact your Roche representative or call **800 262 1640** for more information.

For life science research only.
Not for use in diagnostic procedures.

LIGHTCYCLER is a trademark of Roche.

Roche Diagnostics Corporation
Roche Applied Science
Indianapolis, Indiana

Roche

© 2012 Roche Diagnostics.
All rights reserved.

Continued from page 1259

et al. (p. 1334, published online 25 October; see the cover) describe how actin-like ParM filaments form a bipolar spindle for the faithful segregation of low-copy-number plasmids to the two cell poles of *Escherichia coli*, despite being polar, with two distinct ends. ParM filaments are elongated by a small adaptor protein ParR that physically links the filament end(s) to a centromere-like region on the plasmid. Antiparallel filament bundling and sliding appear to produce a bipolar spindle made of filaments that elongate unidirectionally so that all the plasmids are segregated together in one large bundle.

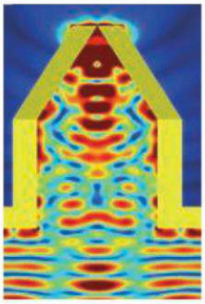

Mind the Gap

Near-field microscopy has benefited from subwavelength near-field plasmonic probes that make use of the field-concentrating properties of gaps. These probes achieve maximum enhancement only in the tip-substrate gap mode, which can yield large near-field signals, but only for a metallic substrate and for very small tip-substrate gap distances. **Bao *et al.*** (p. 1317) designed a probe that unites broadband field enhancement and confinement with bidirectional coupling between far-field and near-field electromagnetic energy. Their tips primarily rely on the internal gap modes of the tip itself, thereby enabling it to image nonmetallic samples.

Dissecting Wnt Signaling

The Wnt signaling pathway plays a key role in regulating a broad range of functions from development to cancer. But a precise understanding of how Wnt proteins act through their receptors (Frizzled proteins) has been elusive. By paring the system down to its core reactions and performing kinetic analysis in cultured cells, **Hernández *et al.*** (p. 1337, published online 8 November) were able to deduce the mechanism of Wnt action without invoking any previous assumptions. Such quantitative analysis of mass balance may offer a way to identify essential control points in other complicated signaling systems, and thus help define targets for therapeutic intervention.

The Good Side of Inflammation

The zebrafish brain is much more adept than the human brain at recovering after traumatic injury. **Kyritsis *et al.*** (p. 1353, published online 8 November; see the Perspective by **Stella**) investigated the cellular events that support regeneration in the zebrafish brain. Although inflammation is part of the response in both settings, the zebrafish brain goes on to initiate proliferation of replacement neurons. By inciting inflammation without neuronal damage, radial glial cells could be pushed into neurogenesis.

Androgen-Driven Sequestration

Male and female mice differ in the neuronal patterns that serve the mammary glands. **Yin Liu *et al.*** (p. 1357) now describe how gonadal hormones drive development of distinct male and female sensory innervations. Although both male and female mammary glands develop their sensory innervation similarly in early embryogenesis, once the androgens take effect, the developmental trajectories diverge. By birth, the rich network of sensory neurons present in the female is absent in the male. Androgens cause a switch from expression of the full-length neurotrophin receptor TrkB to its truncated form, TrkB.T1, both of which are expressed on the neurons. In males, truncated TrkB.T1 sequesters brain-derived neurotrophic factor (BDNF) from further activity, whereas in females, full-length TrkB binds BDNF and supports neuronal development.

From Man to Mouse

Genome-wide association studies of humans have identified single-nucleotide polymorphisms (SNPs) that increase an individual's risk of developing common diseases like cancer. Most of these SNPs have only a modest effect on risk, and many map to noncoding regions of the genome. **Sur *et al.*** (p. 1360, published online 1 November; see the Perspective by **Lewis and Tomlinson**) used a mouse model to study the functional impact of a particular SNP that resides 300 kilobases upstream of the *MYC* oncogene on human chromosome 8q24 and has been linked to cancer risk in humans. When a sequence encompassing this SNP was deleted in mice that were predisposed to develop intestinal tumors, the mice displayed fewer tumors than control mice. This SNP may thus play a causal role in human cancer, presumably through altered regulation of *MYC*.

CREDIT: BAO *ET AL.*

NEVER!
Phase Separate Again
RNA *directly* from TRIzol®, TRI Reagent® & more with the Direct-zol™ RNA Kits

RNA Shield™
One Reagent for
30-day RNA sample storage at ambient temperature

RNA from a single cell

Selective Purification of large micro small RNAs

High-Throughput & Automated purification of high-quality total RNA

THE NEW RNA WORLD

Get more info & sign up to receive The New RNA World Newsletter at
www.zymoresearch.com
TRI-Reagent® and TRIzol® are registered trademarks of Molecular Research Center, Inc.

ZYMO RESEARCH
The Beauty of Science is to Make Things Simple

Call for 2012 Cozzarelli Prize Nominations

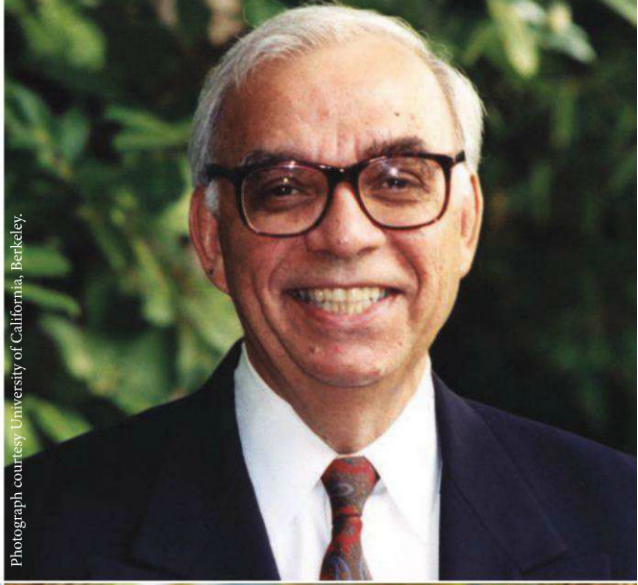

Photograph courtesy University of California, Berkeley.

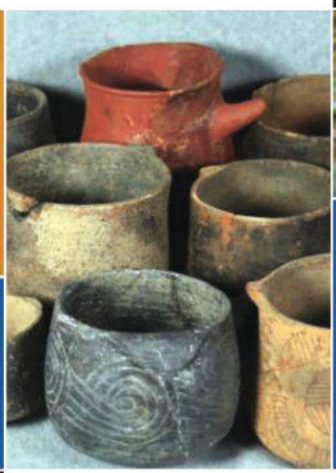

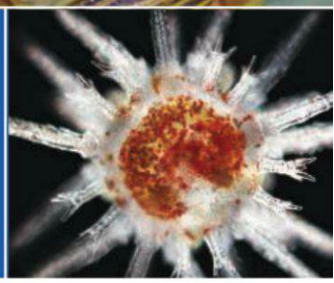

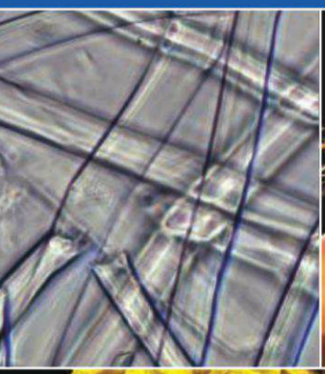

The PNAS Editorial Board is now accepting nominations through January 11, 2013, for the 2012 Cozzarelli Prize. This award recognizes scientific excellence and is given to six papers published in PNAS during the past year.

Nominations should include a citation and brief explanation of the merits of the work. The award recipients will be recognized during the PNAS Editorial Board Meeting and the NAS Annual Meeting Awards Ceremony on April 28, 2013, in Washington, DC.

PNAS

www.pnas.org

For more information and a list of previous winners visit www.pnas.org/cozzarelliprize.

Bruce Alberts is Editor-in-Chief of *Science*.

Failure of Skin-Deep Learning

THERE IS A DISCONNECT AT THE HEART OF THE U.S. EDUCATION SYSTEM THAT IS HAVING A DEVASTATING effect on how and what children learn. Research shows that the most meaningful learning takes place when students are challenged to address an issue in depth, which can only be done for a relatively small number of topics in any school year.* But the traditional process of setting standards tends to promote a superficial "comprehensive coverage" of a field, whether it be biology or history, leaving little room for in-depth learning. The curricula and textbooks that result are skin-deep and severely flawed.

The factoid-filled textbooks that most young U.S. students are assigned for biology class make science seem like gibberish—an unending list of dry, meaningless names and relationships to be memorized. Take, for example, my 12-year-old grandson's life science textbook. Approved by the State of California, it is filled with elaborate drawings and covers an astonishingly broad range of biology. But the text is largely incomprehensible for its student audience, reminding me of a commercial exam-cramming guide that proudly states: "We'll show you that you don't really have to understand anything. You just have to make a couple of simple *associations*, like these. Aerobic respiration with: presence of oxygen, more ATP produced . . . Anaerobic respiration with: absence of oxygen, less ATP produced." When my grandson and his classmates successfully complete that book and the class based on it, it is clear that they will know nothing of the kind of biology that inspires passion in the souls of the scientists working in the labs around me at the University of California, San Francisco. How might we instead give schoolchildren the gift of experiencing the profound joys of science, or history, or literature?

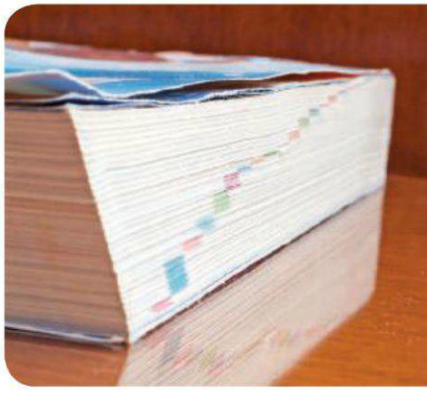

My answer is based on a remarkable year-long history course I took as an undergraduate at Harvard—Social Sciences 2, Western Thought and Institutions—that demonstrated the critical importance of in-depth learning for students. The course, taught for three decades by the legendary Professor Samuel Beer, focused intensively on six brief periods of time from the Magna Carta to the rise of Communism. In attempting to analyze each period of 50 or so years in depth, we read original documents as well as essays by famous historians, and through term papers and exams we explored the forces that have shaped human history. Although I had taken history courses in high school, memorizing enough facts and dates to be awarded an A grade, I had learned nothing essential about history. It was only in Professor Beer's class that history came alive for me as a critical tool for understanding human societies.

I believe that the above course has important lessons for all educators. At all levels of schooling, we need to replace the current "comprehensive" overviews of subjects with a series of in-depth explorations. To do so, we will need to abandon the one-size-fits-all textbooks used in schools in favor of a large set of much shorter curriculum units, each designed to facilitate the active exploration of one important topic in depth for a month or so. Importantly, the teachers in each school district should be empowered to cover only a fraction of the topics available for their grade level. Rather than attempt to cover an entire subject such as biology, an impossible task, the goal of each unit should be to challenge students to explore one narrow topic deeply. To this end, it will be important to avoid the fatally flawed, state-based textbook-adoption process.† For science education, could a national process of curriculum unit validation be parceled out to a set of major scientific societies? More about this in my next Editorial, focused on the biology of cells and organisms. **– Bruce Alberts**

10.1126/science.1233422

*M. S. Schwartz, P. M. Sadler, G. Sonnert, R. H. Tai, *Sci. Educ.* **93**, 798 (2009); W. B. Wood, *Science* **325**, 1627 (2009).
†H. Tyson-Bernstein, *A Conspiracy of Good Intentions: America's Textbook Fiasco* (Council for Basic Education, Washington, DC, 1988).

CREDITS: (TOP LEFT) TOM KOCHEL; (RIGHT) ISTOCKPHOTO.COM

EDITED BY STELLA HURTLEY AND JAKE YESTON

ECOLOGY

Desert Invaders

The popular conception of an invasive plant species is of one that rapidly achieves abundance or even dominance after its introduction into a new region. However, in natural communities, many native species can persist at low population densities, reaching greater abundance only when changes occur in ecological factors such as resource abundance, competitors, or herbivores. This could be a feature of some invasive species too. A decade ago, Shea and Chesson advanced the notion of "niche opportunities" for invasive species, whereby such a species might be able to occupy a new habitat at low density, biding its time until conditions become right for more rapid expansion and spread. Observation of such behavior requires long-term monitoring. Allington *et al*. have now documented a case of niche opportunity in an invasive herbaceous annual, *Erodium cicutarium*, in the Chihuahuan desert. For the first two of three decades of monitoring, *E. cicutarium* remained at low densities. After 20 years, however, a coincidental decrease in the abundance of rodents and a shift in the precipitation regime combined to create an opportunity for populations of *E. cicutarium* to increase rapidly, outcompeting native species and becoming the dominant plant in the community. — AMS

Ecol. Lett. 10.1111/ele.12023 (2012).

PHYSICS

A Topo-Superconducting Hybrid

Soon after the discovery of topological insulators (TIs)—exotic materials that have a surface state similar to graphene's—physicists conjectured that "mating" a TI with a superconductor would give rise to an even more exotic state dubbed the topological superconductor (TSC); such a material might support Majorana states, thought to be a promising platform for quantum computing. A bulk TI can be doped until it becomes superconducting, while preserving its signature surface states. This approach led to the discovery of $Cu_xBi_2Se_3$, a possible TSC, but intrinsic inhomogeneities in that material made progress difficult. Now, Sasaki *et al.* observe a possible TSC state in $Sn_{1-x}In_xTe$ by point-contact spectroscopy, which shows a signature peak in the density of states at the Fermi energy instead of the gap expected in an ordinary superconductor. Coupled with theoretical considerations, this result indicates that the material is an unconventional superconductor. The similarity in the band structure and the spin-orbit coupling strength in the two materials ($Cu_xBi_2Se_3$ and $Sn_{1-x}In_xTe$) suggests a more general approach in the search for topological superconductivity. — JS

Phys. Rev. Lett. **109**, 217004 (2012).

DEVELOPMENTAL BIOLOGY

Chick Limb Regeneration

Classic regeneration experiments with planaria and newts have demonstrated the amazing abilities of some animals to regrow amputated parts. Unfortunately, such phenomena are generally not possible in birds and mammals. The chicken limb does not normally regenerate; however, regeneration can occur after fibroblast growth factor is added or a limited part of the mesenchyme is removed. With this limited regenerative potential in mind, Oezpolat *et al.* examined the elbow joint. The joint was identified by histological and cell-fate mapping, and a section of tissue containing the joint was excised. When the two ends were placed together, the bones fused without generation of a joint. However, if a "window" of space was maintained after excision, the elbow joint regenerated. Regeneration followed the same molecular program as that taken during normal embryonic development. Furthermore, cell labeling experiments revealed that posterior cells migrated to the site of injury. Chick limb regeneration thus resembles that of amphibian limbs, where cells migrate to a wounded area and reinitiate the normal developmental program. — BAP

Dev. Biol. **372**, 229 (2012).

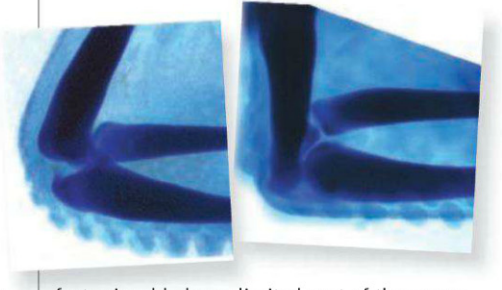

CREDITS (TOP TO BOTTOM): MORGAN ERNEST/UTAH STATE UNIVERSITY; B. DUYGUET *ET AL., DEV. BIOL.*, **372**, 229 (2012)

CHEMISTRY

A Bit of Charge Is Plenty

For nanoparticles to find use in an array of applications, new techniques are needed to deposit and order the individual particles into large structures. Electrophoretic deposition, in which charged particles in a solution are exposed to a uniform electric field, has been used to close-pack spherical particles or deposit them into trenches or order a layer of nanocrystal rods. Singh *et al.* show that control over net particle charge and

dipole can lead to the formation of well-ordered, tightly packed multilayers of vertically aligned rods. The best ordering was obtained for CdS rods, where a low net charge (or zeta potential) on the as-synthesized rods facilitated the slow deposition necessary for good ordering. Increasing the zeta potential by ligand exchange led to much poorer ordering. In contrast to CdS, CdSe rods showed a tapered rice shape less amenable to close-packing. However, it was still possible to pack the rods in a vertical orientation at high density, an arrangement needed for application of this material as a solar cell photoabsorber. — MSL

J. Phys. Chem. B 10.1021/jp305184n (2012).

ENVIRONMENTAL MICROBIOLOGY

Programmed Death Machines All at Sea

The interaction between viruses and phytoplankton blooms can influence marine carbon export. In culture, it has been established that giant double-stranded DNA coccolithoviruses invoke glycosphingolipid synthesis to trigger programmed cell death in neighboring uninfected cells, thus amplifying lysis. Using mesocosm enclosures in a Norwegian fjord, Vardi *et al.* probed the dynamics of *Emiliania huxleyi* and its associated virus at sea. They discovered several conserved molecular correlates for concurrent ecological observations, including release of the same viral death-inducing lipids that had been observed in culture. The viral glycosphingolipids induce intracellular reactive oxygen species, which prompt the programmed cell death machinery in algal cells to assemble, providing an environment that includes everything the virus needs for successful replication. Furthermore, the stressed algal cells produce expolymer particles that form aggregates called marine snow, and it is this that accelerates carbon export to deep water. Finally, virus infection induces a subset of the algal cells to form haploid sexual stages that can evade infection and live to die another year. — CA

Proc. Natl. Acad. Sci. U.S.A. 10.1073/pnas.1208895109 (2012).

CELL BIOLOGY

Smell of Genes Packed Away

To allow responses to specific odorants, mammalian olfactory sensory neurons form clusters that express just 1 of almost 3000 olfactory receptor alleles. Clowney *et al.* explored the mechanism by which the promoters of all the rest of these genes are maintained in an inactive state. In mouse olfactory sensory neurons, the unused promoters were spatially organized in about five large foci from which the active gene was excluded. Unlike most cells, where inactive heterochromatin is localized to the periphery of the nucleus, the olfactory receptor genes were located near the center of the nuclei. This "inside-out" morphology is similar to that observed in mice lacking functional lamin b receptor, a protein of the nuclear envelope that interacts with lamins and heterochromatin. Indeed, lamin b receptor was down-regulated during sensory neuron differentiation. Forced expression of the lamin b receptor reversed the morphological sequestration of the olfactory receptor genes and also decreased the expression of the chosen active allele, probably because the thousands of transcription factor binding sites of the normally sequestered olfactory receptor genes were now competing for binding of activating factors. Thus, spatial organization in the nucleus appears to have an essential role in control of this extreme example of monoallelic gene expression. — LBR

Cell **151**, 724 (2012).

CREDIT CREATAS/THINKSTOCK

CLIMATE SCIENCE

Feeling Is Believing

Weather is generally much more variable than climate, and a single person's experience of either is restricted in both space and time. Still, at some point, or even right now, it is expected that climate change will become more apparent even to an average person, at least in some regions. Mahlstein *et al.* point out that the locations that will provide the earliest individually apparent evidence are those where the magnitude of some manifestation of climate change is greater than local weather variability: presently, that means lower latitudes, where the annual range of seasonal temperatures is the smallest. They therefore use observational temperature data from every longitude to investigate if and where emergent local warming signals are apparent and when those warming trends became clear. They find that some locations, mainly at low latitudes, began to reveal rising temperatures as early as during the 1960s, but that far more areas still do not show a clear local signal. However, the frequency of emerging signals is increasing with time, and it is clear that the pattern of emergence reflects a steadily warming climate. — HJS

Geophys. Res. Lett. **39**, L21711 (2012).

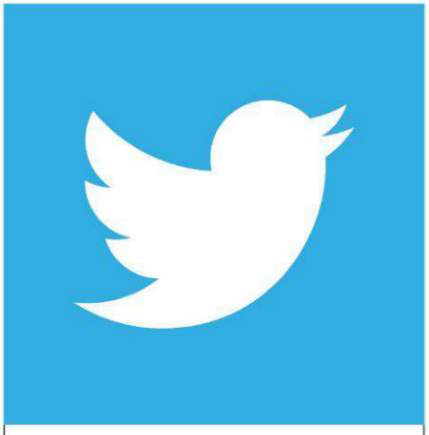

Join the Conversation!

Twitter is a great way to connect with AAAS members and staff about the issues that matter to you most. Be a part of the discussion while staying up-to-date on the latest news and information about your personal member benefits.

Follow us @AAASmember and join the conversation with #AAAS

AAAS MEMBERCENTRAL

MemberCentral.aaas.org

www.sciencemag.org

Science

1200 New York Avenue, NW
Washington, DC 20005
Editorial: 202-326-6550, FAX 202-289-7562
News: 202-326-6581, FAX 202-371-9227
Bateman House, 82-88 Hills Road
Cambridge, UK CB2 1LQ
+44 (0) 1223 326500, FAX +44 (0) 1223 326501

Subscription Services For change of address, missing issues, new orders and renewals, and payment questions: 866-434-AAAS (2227) or 202-326-6417, FAX 202-842-1065. Mailing addresses: AAAS, P.O. Box 96178, Washington, DC 20090-6178 or AAAS Member Services, 1200 New York Avenue, NW, Washington, DC 20005

Institutional Site Licenses please call 202-326-6755 for any questions or information

Reprints: Author Inquiries 800-635-7181
Commercial Inquiries 803-359-4578

Permissions 202-326-7074, FAX 202-682-0816

Member Benefits AAAS Travels: Betchart Expeditions 800-252-4910; Apple Store www.store.apple.com/us/go/eppstore/aaas; NASA Federal, 1-888-NASA-FCU (1-888-627-2328) or www.nasafcu.com; Cold Spring Harbor Laboratory Press Publications www.cshlpress.com/affiliates/aaas.htm; GEICO Auto Insurance www.geico.com/landingpage/go51.htm?logo=17624; Hertz 800-654-2200 CDP#343457; Office Depot https://bsd.officedepot.com/portalLogin.do; Seabury & Smith Life Insurance 800-424-9883; Subaru VIP Program 202-326-6417; VIP Moving Services www.vipmayflower.com/domestic/index.html; Other Benefits: AAAS Member Services 202-326-6417 or www.aaasmember.org.

science_editors@aaas.org (for general editorial queries)
science_letters@aaas.org (for queries about letters)
science_reviews@aaas.org (for returning manuscript reviews)
science_bookrevs@aaas.org (for book review queries)

Published by the American Association for the Advancement of Science (AAAS), *Science* serves its readers as a forum for the presentation and discussion of important issues related to the advancement of science, including the presentation of minority or conflicting points of view, rather than by publishing only material on which a consensus has been reached. Accordingly, all articles published in *Science*—including editorials, news and comment, and book reviews—are signed and reflect the individual views of the authors and not official points of view adopted by AAAS or the institutions with which the authors are affiliated.

AAAS was founded in 1848 and incorporated in 1874. Its mission is to advance science, engineering, and innovation throughout the world for the benefit of all people. The goals of the association are to: enhance communication among scientists, engineers, and the public; promote and defend the integrity of science and its use; strengthen support for the science and technology enterprise; provide a voice for science on societal issues; promote the responsible use of science in public policy; strengthen and diversify the science and technology workforce; foster education in science and technology for everyone; increase public engagement with science and technology; and advance international cooperation in science.

Information for Authors
See pages 752 and 753 of the 10 February 2012 issue or access www.sciencemag.org/about/authors

EDITOR-IN-CHIEF **Bruce Alberts**
EXECUTIVE EDITOR **Monica M. Bradford** NEWS EDITOR **Colin Norman**
MANAGING EDITOR, RESEARCH JOURNALS **Katrina L. Kelner**
DEPUTY EDITORS **R. Brooks Hanson, Barbara R. Jasny, Andrew M. Sugden, Valda J. Vinson**

Editorial senior editors/commentary Lisa D. Chong, Brad Wible; **senior editors** Gilbert J. Chin, Pamela J. Hines, Paula A. Kiberstis (Boston), Marc S. Lavine (Toronto), Beverly A. Purnell, L. Bryan Ray, Guy Riddihough, H. Jesse Smith, Phillip D. Szuromi (Tennessee), Jake S. Yeston, Laura M. Zahn (San Diego); **associate editors** Melissa R. McCartney (Education Projects), Kristen L. Mueller, Jelena Stajic, Sacha Vignieri (Oregon), Nicholas S. Wigginton; **book review editor** Sherman J. Suter; **associate letters editor** Jennifer Sills; **editorial manager** Cara Tate; **senior copy editors** Jeffrey E. Cook, Cynthia Howe, Harry Jach, Lauren Kmec, Barbara P. Ordway, Trista Wagoner; **copy editor** Chris Filiatreau; **senior editorial coordinators** Carolyn Kyle, Beverly Shields; **editorial coordinators** Joi S. Granger, Anita Wynn; **publications assistants** Ramatoulaye Diop, Aneera Dobbins, Jeffrey Hearn, Lisa Johnson, Dona Mathieu, Le-Toya Mayne Flood, Shannon McMahon, Scott Miller, Jerry Richardson, Teresa R. Sakon, Brian White; **editorial assistant** Patricia M. Moore; **executive editorial assistant** Yolanda O'Bannon (San Francisco); **executive assistant** Alison Crawford; **administrative support** Maryrose Madrid

Editorial director, web and new media Stewart Wills; **senior web editor** Sarah Crespi; **web editor** Kerry Klein; **web development manager** Martyn Green; **web developers** Corinna Cohn, Andrew Whitesell; **intern** Edward Hurme

News deputy news editors Robert Coontz, David Grimm (Online), Eliot Marshall, Jeffrey Mervis, Leslie Roberts, John Travis; **contributing editors** Elizabeth Culotta, Polly Shulman; **news writers** Yudhijit Bhattacharjee, Adrian Cho, Jennifer Couzin-Frankel, Carolyn Gramling, Jocelyn Kaiser, Richard A. Kerr, David Malakoff, Greg Miller, Elizabeth Pennisi, Robert F. Service (Pacific NW), Erik Stokstad; **web developer** Daniel Berger; **social media strategist** Meghna Sachdev; **intern** Emily Underwood; **contributing correspondents** John Bohannon, Jon Cohen (San Diego, CA), Ann Gibbons, Sam Kean, Eli Kintisch, Andrew Lawler, Mitch Leslie, Charles C. Mann, Virginia Morell, Gary Taubes; **copy editors** Melissa Raimondi, Kara Estelle, Linda B. Felaco; **administrative support** Scherraine Mack; **bureaus** San Diego, CA: 760-942-3252, FAX 760-942-4979; Pacific Northwest: 503-963-1940

Production director Wendy K. Shank; **assistant managers** Rebecca Doshi, Lori Murphy; **senior specialists** Steve Forrester, Christopher Redwood, Anthony Rosen; **Preflight director** David M. Tompkins; **manager** Marcus Spiegler; **specialists** Jason Hillman, Tara Kelly

Art director Yael Fitzpatrick; **associate art director** Laura Creveling; **senior illustrators** Chris Bickel, Katharine Sutliff; **illustrator** Yana Hammond; **senior art associates** Holly Bishop, Preston Huey; **art associates** Kay Engman, Garvin Grullón, Chrystal Smith; **photo editor** Leslie Blizard

***Science* International**

Europe (science@science-int.co.uk) **editorial: international managing editor** Andrew M. Sugden; **senior editor/commentary** Julia Fahrenkamp-Uppenbrink; **senior editors** Caroline Ash, Stella M. Hurtley, Ian S. Osborne, Peter Stern; **associate editor** Maria Cruz; **contributing editor** Helen Pickersgill; **editorial support** Rachel Roberts, Alice Whaley; **administrative support** Janet Clements, John Wood; **news: deputy news editor, u.k.** Daniel Clery; **contributing editor, europe** Martin Enserink; **contributing correspondents** Michael Balter (Paris), Kai Kupferschmidt (Berlin), Gretchen Vogel (Berlin)

Asia Japan Office: Asca Corporation, Tomoko Furusawa, Rustic Bldg. 7F, 77 Tenjin-cho, Shinjuku-ku, Tokyo 162-0808, Japan; +81 3 6802 4616, FAX +81 3 6802 4615, inquiry@sciencemag.jp; **asia news editor** Richard Stone (Beijing: rstone@aaas.org); **contributing correspondents** Dennis Normile [Japan: +81 (0) 3 3391 0630, FAX +81 (0) 3 5936 3531; dnormile@gol.com]; Hao Xin [China: cindyhao@gmail.com]; Mara Hvistendahl [China: mhvisten@aaas.org]; Pallava Bagla [South Asia: +91 (0) 11 2271 2896; pbagla@vsnl.com]

EXECUTIVE PUBLISHER **Alan I. Leshner**
PUBLISHER **Beth Rosner**

Fulfillment Systems and Operations (membership@aaas.org); **customer service supervisor** Pat Butler; **specialists** LaToya Casteel, Michelle Ofordire, April Marshall; **manager, data entry** Mickie Napoleoni; **data entry specialists** Tarrika Hill, JJ Regan, Eva Mae Campbell

Business Operations and Administration director Deborah Rivera-Wienhold; **business systems and financial analysis director** Randy Yi; **manager, fulfillment systems** Frits Buningh; **systems analyst** Nicole Mehmedovich; **manager, business analysis** Eric Knott; **manager, business operations** Jessica Tierney; **business analysts** Cory Lipman, Celeste Troxler; Christine Wehrli; **financial analyst** Julia Nguyen; **rights and permissions: administrator** Emilie David; **associate** Elizabeth Sandler; **marketing director** Ian King; **marketing managers** Allison Pritchard, Alison Chandler, Julianne Wielga, Samantha Smith; **marketing associates** Aimee Aponte, Mary Ellen Crowley, Elizabeth Sattler, Rebecca Riffkin; **senior marketing executive** Jennifer Reeves; **director, site licensing** Tom Ryan; **director, corporate relations** Eileen Bernadette Moran; **senior publisher relations specialist** Kiki Forsythe; **publisher relations manager** Catherine Holland; **publisher relations, eastern region** Keith Layson; **publisher relations, western region** Ryan Rexroth; **customer relations manager** Iquo Edim; **marketing manager** Christina Schlecht; **marketing associates** Paulina Curto, Mitchell Edmund; **customer relations associate:** Joe Horn; **electronic media: director** Lizabeth Harman; **assistant manager** Lisa Stanford; **production specialists** Antoinette Hodal, Nichele Johnston, Kimberly Oster; **web and new media: senior project manager** Trista Smith, **project leader** Luke Johnson **computer specialists** Walter Jones, Kai Zhang, **web developer** Jeremy Bates; **program director, aaas member central** Peggy Mihelich

director, global collaboration, custom publications, advertising Bill Moran
editor, custom publishing Sean Sanders: 202-326-6430
assistant editor, custom publishing Tianna Hicklin 202-326-6463
associate director, collaboration, custom publications/china/taiwan/korea/singapore Ruolei Wu +86-1367-101-5294

Product (science_advertising@aaas.org); **midwest** Rick Bongiovanni: 330-405-7080, FAX 330-405-7081; **east coast/e. canada** Laurie Faraday: 508-747-9395, FAX 617-507-8189; **west coast/w. canada** Lynne Stickrod: 415-931-9782, FAX 415-520-6940; **uk europe/asia** Roger Goncalves: TEL/FAX +41 43 243 1358; **japan,** Makiko Hara: +81 (0) 3 6802 4616, FAX +81 (0) 3 6802 4615; ads@sciencemag.jp; **china/taiwan** Ruolei Wu: +86 1367 1015 294 rwu@aaas.org

worldwide associate director of *Science* Careers Tracy Holmes: +44 (0) 1223 326525, FAX +44 (0) 1223 326532

Classified (advertise@sciencecareers.org); **u.s.: east coast/west coast/south central/south america** Tina Burks: 202-326-6577; **midwest/canada/industry** Allyson Rosen: 202-326-6578; **sales administrator** Marci Gallun; **europe/row sales** Benjamin Asfaha, Lucy Nelson; **sales assistant** Kelly Grace; **japan** Yuri Kobayashi +81 (6) 6627-9250; careerads@sciencemag.jp; **china/taiwan** Ruolei Wu: +86 1367 1015 294 rwu@aaas.org; **advertising support manager** Karen Foote: 202-326-6740; **advertising production operations manager** Deborah Tompkins; **senior production specialist/graphic designer** Amy Hardcastle; **production specialist** Yuse Lajiminmuhip; **senior traffic associate** Christine Hall; **sales coordinator** Shirley Young

AAAS Board of Directors retiring president, chair Nina V. Fedoroff; **president** William H. Press; **president-elect** Phillip A. Sharp; **treasurer** David E. Shaw; **chief executive officer** Alan I. Leshner; **board** May R. Berenbaum, Bonnie L. Bassler, Stephen L. Mayo, Raymond Orbach, Julia M. Phillips, Sue V. Rosser, David D. Sabatini, Inder M. Verma

AAAS
ADVANCING SCIENCE, SERVING SOCIETY

SENIOR EDITORIAL BOARD

A. Paul Alivisatos, *Lawrence Berkeley Nat'l. Laboratory*
Cori Bargmann, *The Rockefeller Univ.*
Ernst Fehr, *Univ. of Zurich*
Erin O'Shea, *Harvard Univ.*
Michael S. Turner, *University of Chicago*

BOARD OF REVIEWING EDITORS

Adriano Aguzzi, *Univ. Hospital Zürich*
Takuzo Aida, *Univ. of Tokyo*
Sonia Altizer, *Univ. of Georgia*
Sebastian Amigorena, *Institut Curie*
Angelika Amon, *MIT*
Kathryn Anderson, *Memorial Sloan-Kettering Cancer Center*
Siv G. E. Andersson, *Uppsala Univ.*
Peter Andolfatto, *Princeton Univ.*
Meinrat O. Andreae, *Max Planck Inst., Mainz*
Johan Auwerx, *EPFL*
David Awschalom, *Univ. of California Santa Barbara*
Ben Barres, *Stanford Medical School*
Jordi Bascompte, *Estación Biológica de Doñana, CSIC*
Facundo Batista, *London Research Inst.*
Ray H. Baughman, *Univ. of Texas, Dallas*
David Baum, *Univ. of Wisconsin*
Mark Bear, *Massachusetts Inst. of Technology*
Yasmine Belkaid, *NIAID, NIH*
Philip Benfey, *Duke Univ.*
Stephen J. Benkovic, *Penn State Univ.*
Christophe Bernard, *Aix-Marseille Univ.*
Gregory C. Beroza, *Stanford Univ.*
Gabriele Bergers, *Univ. of California, San Francisco*
Peer Bork, *EMBL*
Bernard Bourdon, *Ecole Normale Superieure de Lyon*
Ian Boyd, *Univ. of St. Andrews*
Christian Büchel, *Universitätsklinikum Hamburg-Eppendorf*
Joseph A. Burns, *Cornell Univ.*
William P. Butz, *Population Reference Bureau*
Gyorgy Buzsaki, *New York Univ., School of Medicine*
Mats Carlsson, *Univ. of Oslo*
Mildred Cho, *Stanford Univ.*
David Clapham, *Children's Hospital, Boston*
David Clary, *Univ. of Oxford*
Jonathan D. Cohen, *Princeton Univ.*
Robert Cook-Deegan, *Duke Univ.*
James Collins, *Boston Univ.*
Alan Cowman, *Walter & Eliza Hall Inst.*
Robert H. Crabtree, *Yale Univ.*
Wolfgang Cramer, *Mediterranean Inst. of Biodiversity and Ecology*
F. Fleming Crim, *Univ. of Wisconsin*
Jeff L. Dangl, *Univ. of North Carolina*
Tom Daniel, *Univ. of Washington*
Frans de Waal, *Emory Univ.*
Stanislas Dehaene, *Collège de France*
Robert Desimone, *MIT*
Claude Desplan, *New York Univ.*
Ap Dijksterhuis, *Radboud Univ. of Nijmegen*
Dennis Discher, *Univ. of Pennsylvania*
Gerald W. Dorn II, *Washington Univ. School of Medicine*
Jennifer A. Doudna, *Univ. of California, Berkeley*
Julian Downward, *Cancer Research UK*
Bruce Dunn, *Univ. of California, Los Angeles*
Christopher Dye, *WHO*
David Ehrhardt, *Carnegie Inst. of Washington*
Tim Elston, *Univ. of North Carolina at Chapel Hill*
Gerhard Ertl, *Fritz-Haber-Institut, Berlin*
Barry Everitt, *Univ. of Cambridge*
Paul G. Falkowski, *Rutgers Univ.*
Ernst Fehr, *Univ. of Zurich*
Tom Fenchel, *Univ. of Copenhagen*
Michael Feuer, *The George Washington Univ.*
Alain Fischer, *INSERM*
Susan Fiske, *Princeton Univ.*
Anne C. Ferguson-Smith, *Univ. of Cambridge*
Wulfram Gerstner, *EPFL Lausanne*
Karl-Heinz Glassmeier, *TU Braunschweig*
Elizabeth Grove, *Univ. of Chicago*
Kip Guy, *St. Jude's Children's Research Hospital*
Taekjip Ha, *Univ. of Illinois at Urbana-Champaign*
Christian Haass, *Ludwig Maximilians Univ.*
Steven Hahn, *Fred Hutchinson Cancer Research Center*
Gregory J. Hannon, *Cold Spring Harbor Lab.*
Martin Heimann, *Max Planck Inst., Jena*
Isaac Held, *NOAA*
James A. Hendler, *Rensselaer Polytechnic Inst.*
Janet G. Hering, *Swiss Fed. Inst. of Aquatic Science & Technology*
Ray Hilborn, *Univ. of Washington*
Michael E. Himmel, *National Renewable Energy Lab.*
Kai-Uwe Hinrichs, *Univ. of Bremen*
Kei Hirose, *Tokyo Inst. of Technology*
David Hodell, *Univ. of Cambridge*
David Holden, *Imperial College*
Lora Hooper, *UT Southwestern Medical Ctr at Dallas*
Jeffrey A. Hubbell, *EPFL Lausanne*
Thomas Hudson, *Ontario Inst. for Cancer Research*
Steven Jacobsen, *Univ. of California, Los Angeles*
Kai Johnsson, *EPFL Lausanne*
Peter Jonas, *Universität Freiburg*
William Kaelin Jr., *Dana-Farber Cancer Inst.*
Daniel Kahne, *Harvard Univ.*
Daniel Kammen, *Univ. of California, Berkeley*
Joel Kingsolver, *Univ. of North Carolina at Chapel Hill*
Robert Kingston, *Harvard Medical School*
Roberto Kolter, *Harvard Medical School*
Alberto R. Kornblihtt, *Univ. of Buenos Aires*
Leonid Kruglyak, *Princeton Univ.*
Thomas Langer, *Univ. of Cologne*
Mitchell A. Lazar, *Univ. of Pennsylvania*
David Lazer, *Harvard Univ.*
Virginia Lee, *Univ. of Pennsylvania*
Ottoline Leyser, *Cambridge Univ.*
Olle Lindvall, *Univ. Hospital, Lund*
Marcia C. Linn, *Univ. of California, Berkeley*
John Lis, *Cornell Univ.*
Jianguo Liu, *Michigan State Univ.*
Jonathan Losos, *Harvard Univ.*
Ke Lu, *Chinese Acad. of Sciences*
Christian Lüscher, *Univ. of Geneva*
Laura Machesky, *CRUK Beatson Inst. for Cancer Research*
Anne Magurran, *Univ. of St Andrews*
Oscar Marin, *CSIC & Univ. Miguel Hernández*
Charles Marshall, *Univ. of California, Berkeley*
Martin M. Matzuk, *Baylor College of Medicine*
Graham Medley, *Univ. of Warwick*
Yasushi Miyashita, *Univ. of Tokyo*
Richard Morris, *Univ. of Edinburgh*
Edvard Moser, *Norwegian Univ. of Science and Technology*
Sean Munro, *MRC Lab. of Molecular Biology*
Thomas Murray, *The Hastings Center*
Naoto Nagaosa, *Univ. of Tokyo*
James Nelson, *Stanford Univ. School of Med.*
Timothy W. Nilsen, *Case Western Reserve Univ.*
Pär Nordlund, *Karolinska Inst.*
Helga Nowotny, *European Research Advisory Board*
Luke O'Neill, *Trinity College, Dublin*
Stuart Newman, *New York Medical College*
N. Phuan Ong, *Princeton Univ.*
Joe Orenstein, *Univ. of California, Berkeley & Lawrence Berkeley National Lab*
Stuart H. Orkin, *Dana-Farber Cancer Inst.*
Harry Orr, *Univ. of Minnesota*
Christine Ortiz, *MIT*
Andrew Oswald, *Univ. of Warwick*
Steve Palumbi, *Stanford Univ.*
Jane Parker, *Max-Planck Inst. of Plant Breeding Research*
Donald R. Paul, *Univ. of Texas at Austin*
P. David Pearson, *Univ. of California, Berkeley*
Reginald M. Penner, *Univ. of California, Irvine*
John H. J. Petrini, *Memorial Sloan-Kettering Cancer Center*
Simon Phillpot, *Univ. of Florida*
Joshua Plotkin, *Univ. of Pennsylvania*
Philippe Poulin, *CNRS*
Colin Renfrew, *Univ. of Cambridge*
Trevor Robbins, *Univ. of Cambridge*
Barbara A. Romanowicz, *Univ. of California, Berkeley*
Jens Rostrup-Nielsen, *Haldor Topsoe*
Mike Ryan, *Univ. of Texas, Austin*
Shimon Sakaguchi, *Kyoto Univ.*
Miquel Salmeron, *Lawrence Berkeley National Lab*
Jürgen Sandkühler, *Medical Univ. of Vienna*
Randy Seeley, *Univ. of Cincinnati*
Vladimir Shalaev, *Purdue Univ.*
Joseph Silk, *Institut d'Astrophysique de Paris*
Denis Simon, *Arizona State Univ.*
Alison Smith, *John Innes Centre*
Davor Solter, *Inst. of Medical Biology, Singapore*
Peter Sorger, *Harvard Medical School*
John Speakman, *Univ. of Aberdeen*
Allan C. Spradling, *Carnegie Institution of Washington*
Jonathan Sprent, *Garvan Inst. of Medical Research*
Paula Stephan, *Georgia State Univ. and National Bureau of Economic Research*
Elsbeth Stern, *ETH Zürich*
Ira Tabas, *Columbia Univ.*
Yoshiko Takahashi, *Kyoto University*
Sarah Teichmann, *Cambridge Univ.*
John Thomas, *Duke Univ.*
Herbert Virgin, *Washington Univ.*
Bert Vogelstein, *Johns Hopkins Univ.*
Cynthia Volkert, *Univ. of Göttingen*
Bruce D. Walker, *Harvard Medical School*
Douglas Wallace, *Dalhousie Univ.*
Ian Walmsley, *Univ. of Oxford*
David A. Wardle, *Swedish Univ. of Agric Sciences*
David Waxman, *Fudan Univ.*
Jonathan Weissman, *Univ. of California, San Francisco*
Sue Wessler, *Univ. of California, Riverside*
Kathy Willis, *Oxford Univ.*
Ian A. Wilson, *The Scripps Res. Inst.*
Timothy D. Wilson, *Univ. of Virginia*
Rosemary Wyse, *Johns Hopkins Univ.*
Jan Zaanen, *Leiden Univ.*
Kenneth Zaret, *Univ. of Penn. School of Medicine*
Mayana Zatz, *University of Sao Paolo*
Jonathan Zehr, *Univ. of California, Santa Cruz*
Maria Zuber, *MIT*

BOOK REVIEW BOARD

John Aldrich, *Duke Univ.*
David Bloom, *Harvard Univ.*
Angela Creager, *Princeton Univ.*
Richard Shweder, *Univ. of Chicago*
Ed Wasserman, *DuPont*
Lewis Wolpert, *Univ. College London*

THE SECOND MOST NECESSARY EQUIPMENT IN THE LAB?

You never go into the lab without your goggles, so why would you start your project without SciFinder®? Used by top researchers, SciFinder is the only tool that provides access to the most comprehensive and trustworthy chemistry-related content. And that's why SciFinder is the choice for chemistry research.™

Find out more at www.cas.org.

SciFinder®

The choice for chemistry research.™

AROUND THE WORLD

Washington, D.C. **1**

U.S. Supreme Court Reconsiders Gene Patents

The US Supreme Court intends to address a far-reaching question in biology and law: Are human genes patentable? The biotech world thought that the answer was clear already: Many companies have been built on the assumption that DNA sequences can be patented exclusively. But on 30 November, the court indicated that may not be so. It granted certiorari to a case known as *Association for Molecular Pathology v. Myriad Genetics*, agreeing to hear a challenge against Myriad, a diagnostics firm

in Salt Lake City, which owns patents on the human breast and ovarian cancer genes *BRCA1* and *BRCA2*. Myriad has created a database of DNA variants and uses a patented test to check individuals for cancer risk. The group challenging Myriad argues that the key genes are a product of nature and, therefore, not patentable—a position backed by many researchers—including Nobel winner James Watson—and a number of medical groups, including the American Medical Association. The court will hear the case this term, which ends in June.

Rome **2**

Italy Cancels €1 Billion Accelerator Project

The Italian government has scrapped plans to build a particle accelerator known as SuperB in the outskirts of Rome after a new study calculated its total cost to be about €1 billion—some €350 million more than previously estimated. SuperB was to have been built on the campus of the University of Rome Tor Vergata by an international collaboration of scientists. It would have collided beams of electrons and positrons to produce B mesons and other exotic particles.

The Italian government had promised €250 million; other countries, including France and Russia, said they might pay a share of the costs; and the United States had agreed to donate parts from a decommissioned accelerator at the SLAC laboratory in California. But the growing price tag and an unbridgeable funding gap sank the project. The Italian government has invited Italy's National Institute of Nuclear Physics to pitch proposals for new projects that could be funded with the €250 million it had originally promised. **http://scim.ag/NoSuperB**

Argonne, Illinois **3**

Science 'Hub' to Focus On Batteries

Argonne National Laboratory will receive $120 million over 5 years to create a scientific "hub" that focuses on batteries and energy storage research, the U.S. Department of Energy (DOE) announced. DOE already has three hubs in other places working on generating fuels from sunlight, modeling of nuclear reactors, and increasing the energy efficiency of buildings. A fifth hub on relatively scarce "critical materials" has

Proposed electrochemical design lab, JCESR

yet to be sited. The brainchild of Secretary of Energy Steven Chu, the hubs are supposed to recreate the more focused, yet free-wheeling culture with which Bells Labs and the Manhattan Project addressed specific scientific challenges. These five could be the only ones DOE builds, as observers do not expect Chu, a Bell Labs alum and a Nobel Prize–winning physicist, to stay on for President Barack Obama's second term.

Washington, D.C. **4**

Lamar Smith to Head House Science Panel

Republicans in the House of Representatives have chosen Lamar Smith (R–TX) to be the next chair of the House Committee on Science, Space, and Technology. He was

nominated by the Republication leadership over two other contenders: F. James Sensenbrenner Jr. (R–WI) and Dana Rohrabacher (R–CA).

Smith, who last month was elected to his 14th term in Congress, has served on the science panel for 26 years. A former chair of the House Judiciary Committee, he's known for his conservative views on immigration and criminal justice issues, but also as a skilled legislator who is able to work with Democrats. He's a skeptic when it comes to government action on climate change. Still, many Washington-based lobbyists for uni-

NOTED

>*eLife*, the much anticipated open access journal bankrolled by three heavyweight research funders—the Howard Hughes Medical Institute, the Wellcome Trust, and the Max Planck Society—is scheduled to make its official debut next week.

CREDITS (TOP TO BOTTOM): ARGONNE NATIONAL LABORATORY; DREW ANGERER/FILE/AP PHOTO; ISTOCKPHOTO

versities and science organizations privately said that they hoped Smith would win the job. They see him as a pragmatic lawmaker who is the most likely to revive the science committee, which has been perceived as relatively quiet under current chair, Ralph Hall (R–TX). Smith will formally take his new post in the Congress that begins in January.

NEWSMAKERS

Harvard Biologist Chosen As HHMI Vice President

O'Shea

The Howard Hughes Medical Institute has named biochemist **Erin O'Shea** as its next vice president and chief scientific officer. O'Shea, an HHMI investigator at Harvard University, will join the giant biomedical research charity in January.

O'Shea will oversee an $800 million research budget that includes HHMI's flagship Investigator Program as well as education programs and support for early career scientists in the United States and abroad. A former postdoc in the lab of HHMI President Robert Tjian, O'Shea studies gene regulation and signal transduction. For the past 7 years, she has also directed Harvard's Center for Systems Biology. She says the HHMI position will be "an opportunity to influence research and science education at a much broader level."

O'Shea replaces Jack Dixon, who after 6 years at HHMI will return to his lab at the University of California, San Diego. With an endowment of $16.1 billion in 2011, HHMI is the largest private funder of academic biomedical research in the United States.

BY THE NUMBERS

$65.1 billion Amount spent on research at U.S. universities in 2011 from all funding sources, up 6.3% from 2010 and the highest ever, according to the National Science Foundation.

$1.08 million Value of the Klaus J. Jacobs Research Prize 2012, awarded by the Jacobs Foundation to Dante Cicchetti of the University of Minnesota, Twin Cities, for "groundbreaking achievements in child and youth development."

Country	2011 New HIV Infections	2011 Increase in New Patients on Treatment	Ratio of New HIV Infections to Increase in New Patients on Treatment
Botswana	8,500	17,811	0.5
Cote d'Ivoire	13,000	6,844	1.9
DRC	46,000*	9,375	4.9
Ethiopia	11,000	40,507	0.3
Kenya	91,000	93,912	1.0
Lesotho	22,000	5,845	3.8
Mozambique	100,000	48,912	2.0
Namibia	80,000	14,539	0.6
Nigeria	270,000	56,789	4.8
Rwanda	8,400	4,083	2.1
South Africa	350,000	276,017	1.3
Swaziland	12,000	11,751	1.0
Tanzania	120,000	31,700**	3.8
Uganda	120,000	60,014	2.0
Zambia	42,000	66,479	0.6
Zimbabwe	60,000	142,155	0.4

* Official data not available for new HIV infections; data generated through internal PEPFAR modeling.
** Due to concerns about data validity, the ratio shown for Tanzania was calculated using the increase in new patients on ART directly supported by PEPFAR in 2011.
Source: UNAIDS 2012 World AIDS Day Report.

The Tipping Point For AIDS-Free Generations

The President's Emergency Plan for AIDS Relief (PEPFAR) has suggested a novel metric to gauge whether countries are moving toward the goal of an "AIDS-Free Generation": the ratio of new infections to the increase in patients started on antiretroviral treatment. PEPFAR suggests that a ratio of 1 represents a "programmatic 'tipping point.' " As the table on the left shows, Ethiopia has made great progress, with a ratio of 0.3. At the other end of the spectrum, the war-torn Democratic Republic of the Congo had a ratio of 4.9 last year.

Random Sample

Are You Listening to Me?

Eurasian jays, a bird found from Western Europe to Southeast Asia, are known for remembering the thousands of locations where they've stashed nuts and seeds for the winter—and not just their own, but those of other jays, which they pilfer. Jays don't like being watched while hiding their nuts; if they've been observed, they'll re-cache their treasure. But what's their response when another bird can only hear—but not see—them in the act of stashing? To find out, researchers at the University of Cambridge tested eight captive jays, providing them with 30 peanuts and two trays for caching. One tray contained sand, the other gravel, a noisier substrate. The researchers report in the *Proceedings of the Royal Society B* that jays generally avoided hiding the nuts in the noisy gravel if their competitors could hear them, but not see them. But they hid in both the noisy and quiet trays when their rivals could both hear and see them. The spying jays were also less vocal when watching another jay hiding food compared with other situations. The experiments suggest that the jays understand that others can hear what they are doing, and that they must behave stealthily to protect their caches, and to successfully spy on others. **http://scim.ag/Jayscache**

Science LIVE

Join us on Thursday, 13 December, at 3 p.m. EST for a live chat on **the prospects for new male contraceptives. http://scim.ag/science-live**

CREDITS (TOP TO BOTTOM): KYLIE MILLAR; KATHLEEN DOOHER; PEPFAR BLUEPRINT

SCIENTIFIC ETHICS

Final Report on Stapel Also Blames Field As a Whole

AMSTERDAM—Just when it seemed time to close the book on Diederik Stapel, a new one was opened, quite literally, by Stapel himself. On 28 November, the day on which three investigative panels presented their exhaustive final report on the disgraced social psychologist, Stapel made his first media appearance in more than a year. In a video statement taped at his home by Dutch public television, he said he was deeply sorry and announced he had written an autobiography to explain how it all happened.

The 2:20-minute clip and the appearance of the book the next day caused a new media storm in a country already obsessed with the "Lying Dutchman," as a blogger with *The Washington Post* called him. Many felt that Stapel, fired from Tilburg University in September 2011, was hogging the limelight once again. "Making the announcement on the same day … he's still an ego-tripper," says psychologist Pieter Drenth of the Free University Amsterdam, who chaired one of the committees. Others dispute Stapel's right to earn money off his tale.

But the key message in the joint report—there was one committee for each of the universities where Stapel worked—was a different one: It's not just about Stapel. Colleagues, co-authors, reviewers, and editors at even the most prestigious journals deserve some degree of blame for letting Stapel get away with "blatant" fraud, says the report, which concludes that "the critical function of science has failed on all levels."

The final tally concludes that Stapel made up data in 55 of his 137 papers and in the Ph.D. theses of 10 students he supervised. In another 10 papers, scientific misconduct could not be established beyond a reasonable doubt, either because the original data were missing or Stapel did not confess to fraud, but statistical analyses on the published papers showed "evidence of fraud," says Drenth, who chaired the Amsterdam committee.

These analyses were based partly on the work of psychologist and fraud detective Uri Simonsohn of the Wharton School at the University of Pennsylvania, who sent shockwaves through the field earlier this year with a new method to find suspicious statistical patterns in published papers (*Science*, 6 July, p. 21). Simonsohn has raised questions about the work of several social psychologists, including Dirk Smeesters of Erasmus University Rotterdam and Lawrence Sanna of the University of Michigan, Ann Arbor. Amsterdam panel member and statistician Chris Klaassen adapted the method to further reduce chances of a false alarm, Drenth says, adding that the technique "could be used far more broadly when there are suspicions."

Off the tracks. A pirated copy of Stapel's autobiography appeared on the Internet 2 days after it was published.

In what the report describes as "bycatch," it says that Stapel and his co-authors committed a whole range of smaller sins in papers that weren't outright fraudulent. (It even coins a new Dutch word for sloppy science, "slodderwetenschap," to describe them.) For example, research subjects were struck from the data on dubious grounds, certain parts of experiments weren't reported, or data from experiments were merged, all to reach statistical significance. There were numerous statistical errors in the studies as well as discrepancies between the actual experiments and published papers.

> ***"I had become addicted to the rhythm of digging, discovering, testing, publishing, scoring, and applause."***
>
> **—DIEDERIK STAPEL**

The implications go beyond Stapel, says psycholinguist Willem Levelt, who chaired the Tilburg committee and coordinated the entire investigation. "We're not saying all of social psychology is sloppy science," he says. "But the fact that this could happen shows that the review process has failed from the bottom to the top." Levelt believes the field is taking the message to heart, however. The report praises the "reproducibility project," a large collaborative effort to replicate psychology studies set up by Brian Nosek of the University of Virginia in Charlottesville (*Science*, 30 March, p. 1558), as well as the November issue of *Perspectives on Psychological Science*, which is devoted to analyses of what ails the field and proposals to cure it. "I was impressed by many of the papers," Levelt says. "I have faith that they're cleaning up their shop."

Nosek says the Stapel inquiry is highly unusual in its transparency, the fact that it looked at Stapel's entire corpus of work, and dug deep into the surrounding circumstances. In the case of Harvard University evolutionary biologist Marc Hauser, for instance, a federal investigation found misconduct in six studies, but the university has not released its own report, which reportedly described eight instances of misconduct (*Science*, 14 September, p. 1283). Sanna resigned in May and several of his papers have been retracted, but neither the University of Michigan nor his previous employer, the University of North Carolina, have revealed further information about the case. "We have no idea which of his papers we can trust," Nosek says. "I see the Stapel investigation as a paradigmatic example of how to do it right."

In the wake of the Stapel report, Erasmus University announced that it will take an in-depth look at all of Smeesters's papers, instead of the three that a previous committee studied. Erasmus MC, the university's hospital, will investigate whether the same is possible for Don Poldermans, a cardiologist who was fired in November 2011 after an investigation found "violations of scientific integrity," including fictitious data, in five studies. The job would be huge, because Poldermans has authored about 600 papers.

Stapel's book, meanwhile, poses a problem for curious fellow psychologists and the pubic at large: Buy it or not? "I probably will, but I have very mixed feelings about it," Drenth says. "It would be less of a problem if he shared the proceeds with the Ph.D. stu-

PHOTO CREDIT: TILBURG UNIVERSITY

dents he deceived." Yet there may be an alternative. A 324-page PDF of the book showed up on a file sharing Web site 2 days after publication; the URL was tweeted and retweeted extensively, often with undisguised schadenfreude. The file was removed 2 days later, only to pop up on a new site.

In the book, entitled *Ontsporing* (*Derailment*), Stapel does not deny his fraud, but says that once he started, he did not know how to stop. "I had become addicted to the rhythm of digging, discovering, testing, publishing, scoring, and applause," he writes. The book includes details on how he designed studies with Ph.D. students and colleagues, and then insisted on doing the actual data collection himself, usually at a high school or university where he said he had good contacts. The carefully prepared questionnaires weren't used and ended up in a dumpster; Stapel grew fat, he writes, from eating small bags of M&M's that supposedly were the rewards for his research subjects.

The collapse of his house of cards devastated his family and led him to consider suicide. "I was too weak even for that," he writes. "I hated myself." **–MARTIN ENSERINK**

AVIAN INFLUENZA

Proposed H5N1 Research Reviews Raise Concerns

Researchers are giving a mixed reception to a draft U.S. government plan to do more stringent funding reviews of certain kinds H5N1 avian influenza research—and perhaps even require some studies to be kept secret.

The proposal, presented last week at a meeting of the government's National Science Advisory Board for Biosecurity (NSABB) in Bethesda, Maryland, is the latest fallout from the controversy surrounding two studies in which scientists engineered the H5N1 virus, which normally causes deadly infections in birds, to move between mammals, potentially opening the door to a human pandemic (*Science*, 22 June, p. 1494). The controversy prompted H5N1 influenza researchers to impose a voluntary moratorium on such potentially risky "gain-of-function" studies, and it renewed calls from biosecurity experts for funding agencies to do more to identify problematic experiments before they begin.

No gain? The U.S. government wants tighter review of experiments that enable the H5N1 virus (purple) to gain new capabilities.

The new proposal is designed to do just that, Amy Patterson, associate director for science policy at the National Institutes of Health (NIH), told NSABB on 27 November. At its heart is a list of seven criteria that a study would have to meet to be eligible for NIH funding. A researcher would have to show that a gain-of-function experiment has "high significance to public health," for instance, and that there were "no feasible alternative methods" for doing it. A study that fails to meet any one of the criteria would get a more intensive review by NIH's parent, the Department of Health and Human Services (HHS), and other agencies—and possibly a recommendation that it be transferred to an agency that does classified research, such as the defense or homeland security departments.

Patterson emphasized that the new reviews would not apply to routine studies that characterize naturally occurring H5N1 viruses. NIH officials are currently aware of just "four or five" proposed H5N1 experiments that might trigger the special reviews.

The criterion sparking the most debate would require researchers to provide "evidence" that the H5N1 virus they want to create "could be produced through a natural evolutionary process in the foreseeable future." The idea is to focus studies on viral variants that public health experts might actually encounter in the wild—and to avoid the risks associated with exotic and dangerous synthetic strains. Still, that wording has been "very controversial" among scientists and biosecurity experts, Patterson said. "I've heard questions like: 'What constitutes evidence? What's the foreseeable future?' "

Several NSABB members echoed those concerns, including panel chair Samuel Stanley, a physician and president of Stony Brook University in New York. "My read of this is that it really would put a stop … to most of this research," he said at the meeting. "I think it sets a bar that may be too high."

The leader of one of the controversial H5N1 studies that prompted the creation of the criteria also has doubts. "In my opinion our research meets all of these criteria," virologist Ron Fouchier of Erasmus MC in Rotterdam, the Netherlands, wrote in an e-mail. But the evolutionary criterion "is a tough one, as I fail to see how one would get such evidence." Virologist Peter Palese of Mount Sinai Hospital in New York City believes the government "is misguided in making gain-of-function experiments … such an issue." One problem is that the policy looks "only at one side of the coin," he wrote in an e-mail; genetic changes that enable a virus to gain transmissibility, for instance, can also make it lose lethality.

The plan gets a better review from biologist Richard Ebright of Rutgers University, Busch Campus, who has long pushed for tighter biosecurity reviews. It is "a step forward," he wrote in an e-mail, but has "crucial flaws," including the lack of "a bona fide risk-benefit assessment."

The debate will get a full airing over the next few months. NIH says it will soon release for public comment a white paper that details the plan, and officials will present it at an international workshop on H5N1 research that HHS is hosting in Bethesda on 17 and 18 December. "We definitely want to hear what other countries are thinking about this," Patterson said.

–DAVID MALAKOFF

CREDIT: © 3D4MEDICAL.COM/CORBIS

PLANETARY SCIENCE

Peering Inside the Moon to Read Its Earliest History

A few billion years ago, huge impacts and massive volcanic eruptions created the Man (or Woman) in the Moon for all to see, but that pummeling and unnumbered smaller impacts seem to have erased any traces of the moon's earliest history. Planetary scientists have struggled to peer inside the moon to glimpse some vestige of its formative years, but the view has been fuzzy.

GRAIL has changed all that. The two spacecraft of NASA's Gravity Recovery and Interior Laboratory mission have been orbiting the moon since the beginning of the year measuring the subtlest of variations in the moon's gravitational pull. Those variations have now painted a picture of a moon even more badly battered than had been thought. Still, GRAIL is seeing past the pummeling to the formation of the lunar crust and the moon's early expansion. Eventually, GRAIL will explore the moon from crust to core. "My first reaction on seeing GRAIL's results up close was simple astonishment," says planetary physicist William McKinnon of Washington University in St. Louis. "It's a tour de force, totally amazing." And the amazement is likely not over.

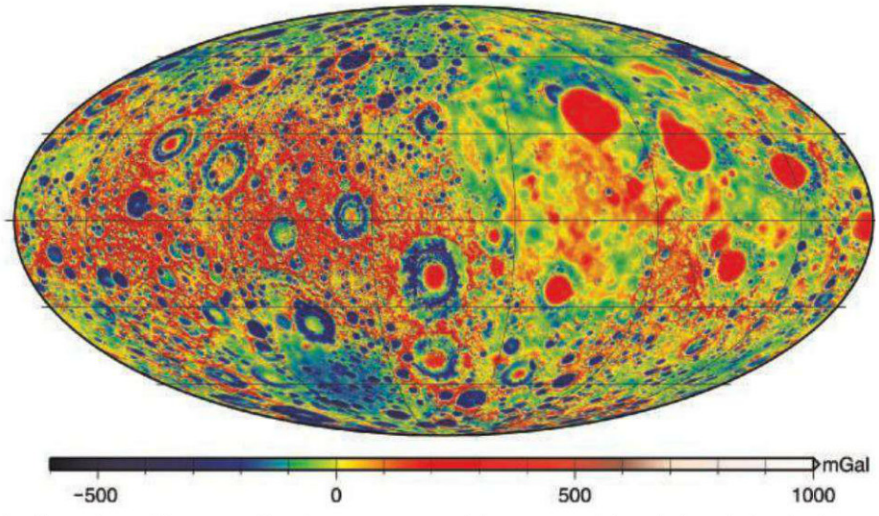

The fine points of lunar gravity. The GRAIL spacecraft have mapped the subtle variations in the moon's gravitational pull (reds higher, blues lower) in unprecedented detail, including the farside (*left side*).

GRAIL's secret to success is using a gravity mapping technique that had never been attempted with the moon but has been working beautifully on Earth for years. The GRAIL mission team, led by planetary geophysicist Maria Zuber of the Massachusetts Institute of Technology in Cambridge, borrowed the concept as well as the instrument hardware used in the Gravity Recovery and Climate Experiment (GRACE) mission still orbiting Earth.

In the GRACE approach, two satellites orbit a body, one leading and the other following by as much as a couple of hundred kilometers, while they precisely measure the distance between them. When the leading spacecraft passes over a spot with extra mass beneath it—say, a crater rim or a buried clump of extra-dense rock—the slightly higher gravity there will pull the leading spacecraft (named Flow in GRAIL) ahead, opening its lead over the trailing spacecraft (Ebb). The opening and closing of the gap can be converted into a map of varying gravitational pull and then into a three-dimensional map of internal density.

The GRAIL approach to lunar gravity proved to be near perfect, as Zuber and her teammates report online in *Science* (http://scim.ag/MZuber). The onboard microwave-based hardware measured the Ebb-to-Flow change of distance to a precision of 20 to 50 nanometers per second, five times better than the conservative design goal. And with no atmosphere to worry about, GRAIL could fly at an average altitude of only 55 kilometers, far closer than GRACE could fly to Earth. The resulting gravity map reveals features as small as 13 kilometers, a resolution about five times as good as previous lunar missions achieved. "Sometimes science advances in little steps," McKinnon says, but "this is a giant leap for planetary science."

GRAIL's "leitmotif is the role of impacts on the lunar crust," Zuber says. "The crust of the moon has absolutely been battered." As planetary geophysicist Mark Wieczorek of the Institute of Physics of the Globe of Paris and his GRAIL teammates report online in *Science* (http//scim.ag/MWieczorek), impacts left the crust with fractures ranging from hairline cracks to through-going faults that reach down at least a few kilometers in places and perhaps tens of kilometers in others. Because GRAIL data have reduced the best estimate of lunar crustal thickness from 50 or 60 kilometers to between 34 and 43 kilometers, this newly recognized fracturing could span the lunar crust and even penetrate the underlying mantle.

Deep fracturing could have broad implications. All the rocky planets of the inner solar system would have suffered similar batterings. Mercury's pulverized crust would have acted like an insulating blanket holding in the planet's inner fires and encouraging volcanic activity. On Mars, where there was plenty of water early on, deep fracturing would have provided lots of wet, hot rock, just the place for early life.

The moon may be beat up, but GRAIL can still see through the fog of fractures. Also online in *Science*, planetary geophysicist Jeffrey Andrews-Hanna of the Colorado School of Mines in Golden and GRAIL teammates report the discovery of 20 or more great sheets of denser rock that formed early in lunar history (http://scim.ag/JA-Hanna). They rose up as magma through vertical crustal fractures typically a few hundred kilometers long. These fractures weren't impact damage. Rather, they must have opened after the nascent moon's ocean of magma warmed a cooler interior, driving an early expansion of the moon. That conclusion confirms a sometimes scoffed-at 1977 hypothesis of how the moon came together.

The end is nigh for GRAIL. Its operators brought the spacecraft down from their 55-kilometer orbits to 22 kilometers in late summer for even more detailed mapping. At press time, the two were scheduled to soon drop to a hair-raising 11 kilometers average altitude. And then in the coming weeks, as they run low on thruster fuel to control their altitude, Ebb and Flow will crash into the moon. "I'll probably cry," Zuber says, "but it should be a celebration." **–RICHARD A. KERR**

Online
sciencemag.org
Podcast interview with author Richard A. Kerr (http://scim.ag/pod_6112).

CREDIT: ZUBER ET AL., *SCIENCE*

AUSTRALIA

River Basin Management Plan Secures Water for the Environment

MELBOURNE, AUSTRALIA—In the scramble to secure water for drinking and agriculture, the environment often gets overlooked. Australia is aiming to set an example of how to balance all three needs in its agricultural heartland. The Murray-Darling basin plan, adopted by the government on 22 November, "is historic," says Richard Kingsford, a conservation biologist at the University of New South Wales in Sydney. South Australian River Murray Minister Paul Caica praised the expected environmental gains: "It will help floodplains support healthy red gum forests, waterbird and fish breeding habitats. … It will keep water levels high enough to prevent acidification in the lower lakes … and reduce the risk of the Murray [m]outh needing to be dredged."

Water managers worldwide "see it as a model" for the use of technical advice and involvement of government at all levels, says water policy expert Sharon Megdal of the University of Arizona in Tucson. The plan's deft balancing of societal and ecological needs, adds Clifford Dahm, an aquatic ecologist at the University of New Mexico, Albuquerque, "gives us some useful ideas for science, planning, and the political tightrope that such decisionmaking requires."

The 1-million-square-kilometer Murray-Darling basin stretches across four states that have been brawling over water for more than a century. Rising from tributaries in Queensland and New South Wales, the Darling River flows southwest, joining the Murray River at the Victorian border, and finally enters the sea near Adelaide. Although the two rivers and their tributaries account for less than 7% of the nation's stream flow, the basin, which draws most of its water from the Murray, produces about 40% of the food grown in Australia. Its ecological treasures include Chowilla wetlands, Macquarie marshes, and, near the mouth of the Murray, the iconic Coorong with its 140-kilometer-long lagoon that provides sanctuary for a cornucopia of waterbirds.

Beginning in the 1950s, dams and irrigation channels transformed the free-flowing waterways into a highly managed system. Prior to the arrival of Europeans in the 1800s, more than 40% of rainwater entering the system annually, or 12,200 billion liters, made it to the sea, according to a 2008 study by the Commonwealth Scientific and Industrial Research Organisation. By 2008, even with normal rainfall, flow in the rivers' lower reaches had dwindled to nearly one-third of historical levels, about 4700 billion liters. The decadelong Millennium Drought starting in the late 1990s exacerbated the water shortage. Along the lower Murray, three-quarters of once-extensive red gum forests withered and died. The Goolwa wetlands dried up, oxidizing sulfates in the soil to sulfuric acid, which acidified the wetlands and adjacent farms once the waters returned and spread it. The Coorong was cut off from the Murray for 3 years. Its salinity jumped to five to seven times that of seawater, turning half of the estuary into a dead sea. "Paleoecological evidence indicates it was unusual even for the last 7000 years," Rebecca Lester, an environmental scientist at Deakin University in Melbourne, penned on *The Conversation*, a research news Web site.

Upstream, nutrients accumulating in the Murray and Darling rivers fueled toxic algal blooms, setting a world record in 1991 for a bloom that extended 1000 kilometers along the Darling River. Residents of Adelaide, the city last in line to draw water from the river system, had to contend with some of the world's saltiest drinking water. In 2009, experts raised the alarm with some predicting that within the year, the city would have to turn to bottled water.

The Millennium Drought led to a number of measures, including the establishment in 2008 of the Murray-Darling Basin Authority (MDBA), which is an independent federal agency charged with finding the right balance between agricultural, social, and environmental values. Restoring river and wetlands health meant primarily removing less water for irrigation. "How much to take back is open for lots of debate," says Tony Minns, director of the Goyder Institute for Water Research in Adelaide. MDBA planners also called for fixing leaky irrigation systems to retain more water in rivers and proposed that flows could be bolstered by pumping in groundwater.

In June 2010, the Wentworth Group of Concerned Scientists, an independent conservation organization, called for water flows to be returned to two-thirds of historical levels, a target that won broad though not universal support among environmentalists. MDBA issued a preliminary plan in November 2010 that

Free-flowing. Balancing competing demands will keep water flowing through the Murray-Darling river system.

CREDITS (TOP TO BOTTOM): RICHARD KINGSFORD; DISCOVER MURRAY RIVER, WWW.MURRAYRIVER.COM.AU

looked at three water recovery scenarios—none of which pleased farmers, who tossed it into bonfires. A final plan issued a year later improved modeling to assess how different scenarios would affect 18 key indicators of environmental health. One indicator is to keep salinity in the Coorong below 60 grams per liter—a safe level for seagrasses that fish and birds depend on. (Pre-European salinity was 24 grams per liter; by 2009 it had risen to 62 grams per liter.) Returning 3200 billion liters to the Murray-Darling system would satisfy 17 of 18 indicators and come close to the Wentworth target of two-thirds of historical flows. But it poses another problem: Infrastructure along the rivers' lower reaches built to suit reduced flows would be swamped. To accommodate more flow, the government earmarked $1.85 billion in October to raise bridges, build levees, and compensate landowners. Much of that water will come from buying water rights from farmers; better irrigation infrastructure will spread it further. The basin plan is expected to be fully implemented by 2024.

The plan still faces hurdles. "There are many ways the states could frustrate the deal," says Rhondda Dickson, MDBA chief executive. For instance, states still own the water and could cap the amount of irrigation rights MDBA can purchase, as New South Wales has threatened to do. "To make it work," Dickson says, "the government needs the states' support, however grudging." The environment ministry is working on an implementation agreement with the states.

Ecological recovery could take decades. MDBA's water purchases and infrastructure upgrades so far have returned 1327 billion liters to the rivers, rejuvenating parched wetland systems, Kingsford says. The numbers of nesting waterfowl species have bounced back, but *Ruppia tuberosa*, a key seagrass species that fish and waterfowl feed on, has disappeared. Soil acidification still affects wetlands and farm fields. "It's not clear whether these changes are permanent," Minns says, referring to both biodiversity loss and acidification.

The basin's future will depend not just on the volume of water flowing through the system, but how it's added. "We have to develop ecological watering plans [to decide] how much, how often and when [to release water] to achieve the environmental outcomes," Minns says. One goal is to restore natural flow variability. "Ecologically, occasional flooding is important for these river systems," Kingsford says. Now that MDBA is getting the water it needs, it will have to learn how to best manage it. As Minns says, "The real work starts now."

–ELIZABETH FINKEL AND DENNIS NORMILE

U.S. SCIENCE POLICY

White House Panel Urges Agencies to Take More Risks

Be bolder.

A new report by a presidential advisory panel urges U.S. research agencies to make a bigger commitment to supporting high-risk, interdisciplinary research by investigators with a strong track record. Current efforts by the National Institutes of Health (NIH) and the National Science Foundation (NSF) to do so are "a drop in the bucket of total agency funding," says a report released last week by the President's Council of Advisors on Science and Technology (PCAST).

The new PCAST report, entitled *Transformation and Opportunity: The Future of the U.S. Research Enterprise*, offers 17 recommendations to shore up the $450-billion-a-year U.S. research enterprise, both public and private, and increase its eventual economic payoff. Most of the ideas—including the need to ease the regulatory burden on universities, strengthen ties with industry, improve science and math education, and ensure a steady, predictable rate of growth for federal spending on science—will sound familiar to readers of other recent reports by equally prestigious panels. "The majority of these recommendations have been made by other groups," admits University of Texas, Austin, computer scientist William Press, who co-chaired the working group that produced the report. (Press is also president of AAAS, which publishes *Science*.) In fact, PCAST's suggestions to boost overall research spending to 3% of the nation's gross domestic product, make permanent a research tax credit for industry, and help foreign scientists remain in the United States after graduation have already been embraced by its intended audience: President Barack Obama. But advocates for the research community say that it never hurts to remind the administration that such proposed policy changes are important—especially when the White House and Congress are engaged in tense negotiations to avoid heading over the so-called fiscal cliff next month.

Presidential prodding. William Press led the PCAST panel that wants changes in U.S. research practices.

CREDIT: SARA PRESS

One area where the PCAST report breaks from the pack is its call for research agencies to adopt "revolutionary … interdisciplinary ... and people-based awards." Too much of federal spending—which amounts to about one-third of the nation's total investment in research—backs incremental advances, according to the report. And one of the culprits is a conservative merit review process that rewards safe bets.

NIH is taking small steps away from that approach with its Pioneer, New Innovator, and Early Independence awards from the director's office, the report notes. Likewise, the report praises NSF's Rapid Response Research grants and its planned expansion of programs to reward "creative … transformative interdisciplinary ventures." But Press says "the funding agencies have been slower than we would like to see in moving in these directions." And the report documents those baby steps: This year, it notes, NIH will make 50 awards in the three director's categories out of a total of 35,944 research grants. "While this plethora of initiatives, each worthy in its own way, gives an illusion of significant progress," the report notes, "in truth the sum of all these programs is tiny, almost invisible, in comparison to each agency's dominant" form of research support.

The report also urges Congress and the executive branch to find a way to provide research agencies with multiyear budgets, or at least funding guarantees for individual projects. Other countries operate on 5-year budgets, notes NSF Director Subra Suresh. But Suresh says "it's very difficult to carry out long-term planning with our sister agencies" under the current U.S. system of annual appropriations.

–JEFFREY MERVIS

GEOPHYSICS

India Barred Entry to U.S. Author Of Seismic Review

Seismologists have been buzzing in recent meetings about the harsh treatment of peers who give public advice—the L'Aquila effect, some call it. It's a reference to the jail sentences given to experts who gave overly reassuring advice that a major earthquake was unlikely to strike L'Aquila, Italy, just days before a quake devastated the town and killed 308 people. Some scientists say they have seen a flipside effect as well: sanctions for public warnings that seem too dire.

This happened in India recently, according to seismologist Max Wyss, director of the World Agency of Planetary Monitoring and Earthquake Risk Reduction in Geneva, Switzerland, who's scheduled to discuss the topic on 6 December at the American Geophysical Union meeting in San Francisco, California. He says that Roger Bilham, a geophysicist at the University of Colorado, Boulder, was detained at the New Delhi airport in May and sent home like a "criminal." Bilham's misdeed, Wyss believes, was to go public with his view that seismic hazards in India are underestimated, and that a nuclear project needs more review.

Bilham, who has a Ph.D. in geophysics from the University of Cambridge in the United Kingdom, described what happened: "I was on my way to Bhutan," stopping over in New Delhi to change planes on 18 May, he says, when "I was forcibly escorted back to the U.S. flight I had just arrived on." At customs, he says, "I was told I was on 'a list.' I was given no reason what the list was, or why I was on it." His round trip took 29 hours and halted field work on the seismicity of Bhutan.

When *Science* asked why Bilham was denied entry, the Indian Ministry of Home Affairs (MHA) indicated that Bilham, traveling on a tourist visa, was not in compliance with regulations. The official response: "Activity of visitor not commensurate with the type of visa granted, hence entry denied." Bilham says he has been to India more than 10 times since 1967—always traveling on a tourist visa—and has written 81 articles on Indian tectonics. He hasn't tried to return since.

A top MHA official, speaking on condition of anonymity, dismissed Bilham's seismic warnings as "scare-mongering" and claimed that Bilham and a co-author were unfair to target "only India." Bilham's assessment that a magnitude-8.7 earthquake could strike in the Kashmir Himalayas—more than 10 times stronger than the widely accepted upper bound of magnitude 8—has irked some in the Indian disaster management community.

Bilham also co-authored a review in the 25 November 2011 issue of *Current Science*, an Indian journal, with Vinod K. Gaur titled, "Historical and Future Seismicity Near Jaitapur, India." Jaitapur is the proposed home of a 9900 megawatt nuclear plant in western India, potentially the world's largest single nuclear electricity producer. Gaur, a leading seismologist at the CSIR Centre for Mathematical Modelling and Computer Simulation in Bangalore, and Bilham wrote that the seismic record near Jaitapur is too scant to support a long-term hazard assessment, which would require data reaching back 1000 years. They concluded that the present "seismic quietness of Jaitapur does not mean that a severe earthquake cannot occur there." To highlight the issue of seismic risk, Bilham spoke at a press conference organized by Greenpeace in Mumbai on 12 January, explaining how a magnitude-6 quake might lead to intensity VII shaking at the plant.

AREVA, the French company that's supplying six EPR reactors for Jaitapur, sees nothing new in this analysis. In an e-mail, the company wrote: "The EPR can definitely resist intensity VII shaking and is designed to withstand a peak ground acceleration of 0.25g, which would correspond to a 6.5 magnitude earthquake occurring 15 kilometers away from the plant site." The Nuclear Power Corporation of India Limited, the responsible utility, also dismissed concerns early this year, saying that "seismic aspects have been addressed" at Jaitapur. In July, B.K. Rastogi at the Institute of Seismological Research in Gandhinagar rebutted Bilham and Gaur in *Current Science*, pointing to "many errors" and concluding that the paper's concerns had all been previously considered.

Bilham concedes there were "factual errors" in the paper but emphasizes that the seismic risks at Jaitapur are not well understood and may be larger than people assume. "Scientists have a duty to inform the public of their findings," Bilham says. Silencing the "discussion of large future earthquakes will not prevent their occurrence." "The site at Jaitapur is safe for a nuclear park," says Ratan K. Sinha, chair of the Atomic Energy Commission in Mumbai, adding that the nuclear establishment had nothing to do with Bilham's expulsion.

PHOTO CREDIT: PHOTO BY UNIVERSITY OF COLORADO

Blacklisted? Roger Bilham was marched onto a return flight to the United States after landing in New Delhi in May.

India's decision to hustle Bilham out of the country was "a travesty—but of a different kind [from L'Aquila]," Wyss says. Bilham was denied entry for "speaking out about seismic hazard not for hiding it." Gaur agrees, saying the deportation was a "draconian step to silence science." But "nobody has asked for my head," Gaur says.

Bilham and Gaur seem to be right on one point—the seismic risk map of India is based on meager data, says Khadg Singh Valdiya, a specialist on neotectonics at the Jawaharlal Nehru Centre for Advanced Scientific Research in Bangalore. "The country has thousands of hidden and locked faults, all waiting to break free, but we have not cataloged them." There is an "urgent need to map the geodynamic hot spots," before building on them he says. As for Bilham's deportation, Valdiya thinks it was an error: "We should have the courage to stand up to open criticism." He thinks that India may have seismic studies held in secret that would answer some of the many questions about earthquake risk at Jaitapur. If so, Valdiya says, they should be declassified.

–PALLAVA BAGLA

Growing Pains in the Desert

A 3-year-old graduate research university in Saudi Arabia is finding that it will take more than money to create a global research powerhouse

TONY EASTHAM WASN'T PLANNING TO FINISH HIS ACADEMIC career in Saudi Arabia. And David Ketcheson didn't think his first faculty job would be at a new, graduate-only research university in the Middle East. But in 2009, both Eastham, a British physicist with an international CV, and Ketcheson, a U.S.-born-and-bred applied mathematician, wound up working at King Abdullah University of Science and Technology (KAUST).

The country's octogenarian monarch gave his name—and an estimated $20 billion—to what he hoped would be a *Bayt al-Hikma*, a house of wisdom, in the grand tradition of Islamic scholarship (*Science*, 16 October 2009, p. 354). The money, in addition to providing KAUST with a huge endowment to be tapped for operating expenses, has bought what Eastham describes as "resources not available to any other university in the world."

For many faculty members, the job has exceeded their expectations. "The funding opportunities are astounding, and I've had the chance to do things that wouldn't normally be possible for someone at my level," says Ketcheson, born and educated in the United States, who was hired at age 29 right out of graduate school as an assistant professor. "Coming here also appealed to my sense of adventure," he adds, noting that his wife and three small children also enjoy living within the gated community that surrounds the campus.

The British-born Eastham, now 67, has had a different, and ultimately much less satisfying, experience. "There was a tremendous sense of camaraderie the first year," recalls Eastham, who agreed to run KAUST's core labs after having spent the previous 13 years managing research and technology development at Hong Kong University of Science and Technology, an institution whose rapid rise KAUST hopes to emulate (*Science*, 7 September, p. 1162). "We were all part of this pioneering experiment."

But for Eastham, the initial excitement gave way to frustration, disappointment, and, finally, disillusionment. In December 2011, Eastham left what he had begun to call the King Abdullah University of Stress and Tension and retired to his beloved Vancouver. (He had spent more than 2 decades as a Canadian academic before going to Hong Kong.) "The atmosphere had become poisoned, and KAUST was no longer a comfortable place to work. After 3 years, I decided I had had enough."

Eastham is one of several senior administrators who have left KAUST in the past year. All still embrace the king's vision but believe that it is being undermined by management decisions that have trampled upon the openness, collegiality, and transparency common at Western institutions. Those decisions include sudden changes in admissions standards to increase the share of Saudi students, revisions in the rules governing internal funding, and a failure to uphold agreements with international collaborators. Compounding the problem, current and former staff members say, is a work environment that discourages any airing of these concerns.

Without a change in leadership, they worry, KAUST will fall short of its quest to become a global research university.

GLOBAL RESEARCH UNIVERSITIES

www.sciencemag.org/extra/global

This is the fourth in a series of articles on global research universities. Previous stories have examined the role of student and faculty mobility (7 September, p. 1162), the phenomenon of satellite laboratories (28 September, p. 1600), and efforts by France and Germany to strengthen research at a handful of elite universities (2 November, p. 597).

More than a vision

KAUST owes its existence to King Abdullah's belief that the country needed a top-rated research university. In 2007, he assigned the task of building one to his oil minister—an ironic choice given that one of KAUST's goals is to wean the kingdom from its dependence on oil—and the minister chose Saudi Aramco to make it happen.

Deploying a round-the-clock crew of 30,000 and up to 50 cranes poking skyward, the state-owned giant oil company completed the 36-million-square-meter campus in only 2 years. And in September 2009, the king himself pre-

CREDITS (TOP TO BOTTOM): COURTESY OF KAUST; ISTOCKPHOTO

Looking ahead. Provost Stefan Catsicas (*standing, right*) meets with KAUST's senior academic management team.

sided over a gala opening celebration for foreign dignitaries and scientific luminaries.

In retrospect, however, building the institution was the easy part. Making it work like a research university is proving to be much harder.

In addition to Eastham, the list of senior academics who have left KAUST in the past year includes the director of admissions, the heads of two of the university's nine initial research centers, the founding provost, the first dean of life sciences and engineering, and the head of university communications. Without exception, these former employees are still rooting for KAUST to succeed. They believe that a world-class university in Saudi Arabia would strengthen global science, provide technology-based solutions to pressing problems in the region, and perhaps even ease political tensions in this volatile part of the world. And they agree that the unprecedented investment in equipment and facilities has attracted talented scientists from around the world.

KAUST's tight control over information makes it hard to generalize about how most faculty members and administrators feel about their employer. Even so, *Science* has learned that some have tried to express their concerns through private channels, with uncertain results.

Happier times. King Abdullah greets James Luyten, a founding research center director who last year resigned in frustration.

In one notable case, several senior KAUST officials and scientists responded to a request last fall from the king's inner circle for information on KAUST management practices. Their statements, which *Science* obtained after agreeing not to identify the authors, provide a frank assessment of what they regard as pressing problems. And the same themes recur. "The current atmosphere in the administration and finance of the university is one of brutality," notes one writer, adding that "dedicated talents who believed in the dream of the university from the start are leaving because they can no longer tolerate this hostile climate." The author ends with a plea: "The management of a university must be in the hands of academic professionals."

Eastham was at first reluctant to speak out and says he decided to do so only because he believes KAUST's fate is important to the scientific community. (Several persons requested anonymity as a condition of talking to *Science*, saying that they feared reprisals.) Another former senior administrator who has come forward publicly is James Luyten, who resigned last December as founding director of KAUST's Red Sea Research Center.

Luyten is a former head of the Woods Hole Oceanographic Institution (WHOI) in Massachusetts, which in 2007 became KAUST's first international research partner. Saudi officials made a splash when they inked a 3-year, $25 million agreement with WHOI to carry out a range of marine activities that included five 16-day cruises on the Red Sea. But even with a 2-year extension, fewer than half the cruises were conducted, and on 31 October the partnership ended with a whimper.

Luyten believes that KAUST hasn't provided the mutual respect and transparency needed to carry out world-class, collaborative research. His repeated efforts to address those problems while he directed the Red Sea center were thwarted by his superiors, he adds.

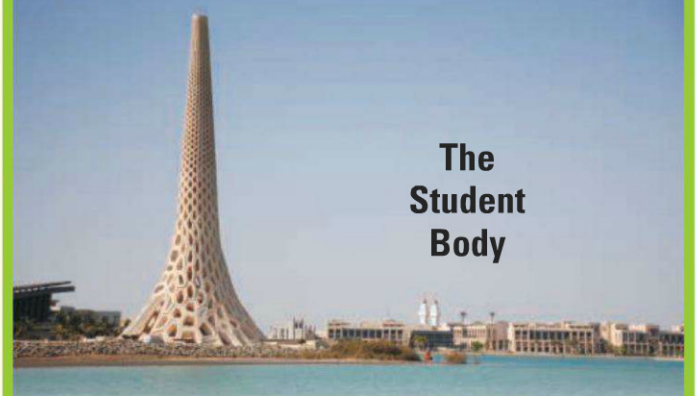

The Student Body

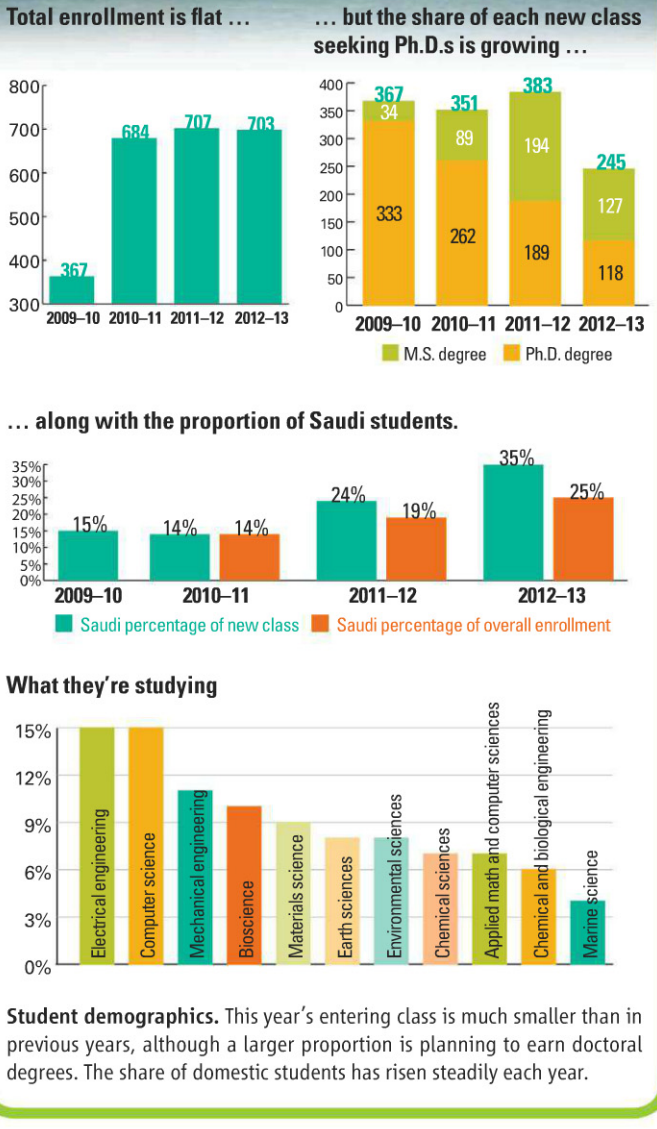

Student demographics. This year's entering class is much smaller than in previous years, although a larger proportion is planning to earn doctoral degrees. The share of domestic students has risen steadily each year.

CREDITS: (PHOTOS) COURTESY OF KAUST (2); (DATA SOURCE) KAUST

"I have to say that every promise that has been made to us has been broken, except for the payment of our actual salaries," he says.

Calling the shots

One fundamental problem, Luyten, Eastham, and others say, is that Aramco has retained a prominent role in running the institution it built. Its top-down management style may be fine for operating an oil-production facility, they say, but that style is ill-suited to a graduate research university. "There's a lack of trust at the top. They just don't trust anybody," says Alyn Rockwood, a professor of applied mathematics and associate director of the Geometric Modeling and Scientific Visualization Center, who this fall announced that he would be leaving KAUST in January.

Critics are particularly unhappy with the management style of one senior KAUST administrator, Nadhmi Al-Nasr. He's a former Aramco vice president for engineering services whose title at KAUST is executive vice president for administration and finance. Although he reports to KAUST's president, Choon Fong Shih, Al-Nasr is widely viewed as the de facto head of the university. (Al-Nasr was interim president before Shih arrived in 2008 as the much-admired president of the National University of Singapore, and Shih's pending retirement, announced in May, appears to have further strengthened Al-Nasr's hand.)

"Personally, I like Nadhmi. But he does some strange things," says Rockwood, who notes that his pending departure gives him greater freedom than other faculty members to express his opinions. "And he's from a culture where fear and intimidation are part of the way you do business. He's not an academic. He's an oil manager, and I guess that you have to be pretty hard-nosed to be successful in that field."

"Learning how to work in an academic culture was a totally new game for me."

—NADHMI AL NASR, KAUST EXECUTIVE VICE PRESIDENT FOR ADMINISTRATION AND FINANCE

Al-Nasr, who has never before been a university administrator and who holds a bachelor's degree in chemical engineering, acknowledges that he was jumping into the deep end when he joined KAUST. "Learning how to work in an academic culture was a totally new game for me," he explained during an interview in which he was by turns combative, cagey, and cajoling. "In industry, business decisions are all top-down. The corporation decides, and the staff executes the plan. Academia is different. The ideas of people at all levels count, and you need to learn how to listen."

A successful academic administrator needs to be patient, Al-Nasr adds. "Faculty debate things for a long time," he notes. "In industry, time is money, so you don't have that luxury."

There was no template for Aramco to follow for building such a well-endowed graduate research university from scratch. And even if there had been one, it probably wouldn't have applied to a country without such institutions.

Although the administrative and classroom buildings opened on time, equipping the labs to do science took much, much longer. The delays were especially hard on researchers with wet labs. "It was horrible for those people," says David Keyes, an applied mathematician who left a tenured professorship at Columbia University to join KAUST in 2009 as a founding dean. "They were very much impacted by the unexpected difficulties in starting supply chains and getting clearances."

Keyes has spent the past 3 years dealing with those problems as head of two of KAUST's three academic divisions—one spanning the physical sciences and engineering and the second encompassing applied mathematics and computer science and engineering. But he doesn't fault the university or Aramco. "Any start-up has challenges. I'd like to see General Electric run a university," he says. "Maybe Google could do it and get it right the first time. But for a company that is used to ordering valves to suddenly be asked to order spectrometers and textbooks, everything is likely to go wrong."

Al-Nasr acknowledges the slow start but doesn't think there was much that KAUST could have done differently. "It was a big shock to the system," he admits. "Our demands were way more than the kingdom has ever seen before, in terms of both our focus on research and the absolute amount of research that faculty wanted to do. People had come from all over the world, and we wanted to meet their expectations. It was pretty frustrating for faculty. But I think most of those problems have been worked out."

Keyes certainly hopes so. Once his successors are in place—in August, Yves Gnanou of the École Polytechnique in Paris became dean of physical sciences, and the appointment of a dean for math and computer sciences is imminent—Keyes can return to his first love: research. He's currently working on algorithms for extreme computing applications.

Arguably the university's most prominent active scientist, Keyes believes that KAUST has survived the worst and is starting to make real progress. "People here still have faith in the unique opportunity represented by an interdisciplinary, graduate science and engineering institution with 5-year funding for research," he says. "So the things that made it distinctive in the first place are still there."

One area where KAUST has been able to hit the ground running is in the mathematical and computer sciences and engineering, which are less dependent on good supply chains. Keyes says that the division "has carved out a niche of developing enabling technologies while continuing to do good research." In turn, Ketcheson says that Keyes is the reason he decided to start his academic career in the Arabian desert after earning a Ph.D. in applied mathematics from the University of Washington.

"David's famous in the field," Ketcheson says. "He mentioned KAUST when I called him about possible positions at Columbia while I was still in graduate school. At first I shrugged it off. You don't go to the Middle East if you want a tenure-track position at a top university, because that caliber of institution doesn't generally exist there. But once I looked into it, I was really impressed."

Admissions reversal

Academics like to say that a university is only as good as the graduate students it attracts. That truism also explains why the researchers who spoke with *Science* are so troubled by how the 2011 entering class was chosen.

CREDIT: NICK CRETTIER/KAUST

"I've had the chance to do things that wouldn't normally be possible for someone at my level."

—DAVID KETCHESON, ASSISTANT PROFESSOR, KAUST

KAUST has no shortage of applicants thanks to its full scholarships, generous stipends, subsidized housing, and outstanding facilities. And while one of KAUST's missions is to train the next generation of Saudi scientists, KAUST hasn't been able to find enough high-quality candidates from the kingdom to fill all the available slots. "I realize that this is a sensitive topic," says the provost, Stefan Catsicas, a neurobiologist who came to KAUST in January 2011 from the Swiss Federal Institute of Technology in Lausanne. "But we are a university in Saudi Arabia."

At the same time, Catsicas says, KAUST does not want an entirely domestic class and believes that a good mix of international students is essential. So the university has tried to strike a balance without imposing a quota.

The 15% share of Saudi students in each of the first two classes, out of a total of roughly 360, was lower than desired, however, Catsicas says. Even more troubling for a university hoping to become a predominantly doctoral-granting institution was the fact that only 10% of the arriving students seeking doctoral degrees were from the kingdom. (A majority of the students in the first two classes were aiming for master's degrees.)

So in late winter of 2011, KAUST decided to boost the Saudi representation in the next class to 30%. That decision was made so late in the admissions cycle, however, that it forced officials to take the unusual step of sending an update to 125 foreign students who had already received acceptance letters. The students were told that they faced one more hurdle—an interview—before they could enroll.

"The questions were very casual, about my family and my future plans. They could have gotten most of the information from my CV," says one African student who requested anonymity. Two months later, most of the students were told that the offer had been withdrawn. Others discovered that they could not obtain a visa to study at KAUST.

Although faculty members had recruited some of these students, they were shut out of the final selection process. When they learned what had happened, many pleaded with Catsicas to reverse the decisions, and KAUST agreed to welcome back some 30 "high-value" students.

The reshuffling created more slots for Saudi students. In the end, 24% of the entering class of 2011 was from Saudi Arabia, including one-third of those seeking master's degrees.

This year, KAUST upped the percentage of Saudi students to 35% of the whole, including 51% of those seeking master's degrees. But officials did it by reducing the overall size of the entering class. The number of new students plummeted from 383 to 245, and the size of the Asian contingent dropped by more than half, from roughly 120 in each of the first three classes to only 54 in the newest class.

Asked if he thought last year's admissions process had damaged KAUST's reputation among future applicant pools, Catsicas says that quality is more important than quantity. And he doesn't think that KAUST had been hurt: "This is a young institution, and I'm sure we will make mistakes. But it is not an arbitrary process, and the objective is quality."

Building global ties

When it comes to luring prized senior faculty members like Rockwood, KAUST is willing to pull out all the stops. At least, that's how it looked at first to Rockwood, whose career in computer graphics and geometric modeling has straddled industry and academia. Full professors were promised an annual research budget "equivalent to a NSF [National Science Foundation] center," he says—in his case, $1 million—"and we were told that, if we needed more, we could write a two-page grant to the provost and it would be approved."

Rockwood says he wasn't surprised when the second promise never materialized: "It just seemed too easy." But he was disappointed when his package was suddenly trimmed back to $800,000. And he was annoyed to discover the hidden costs within his budget, such as being charged up to $70,000 a year to support a doctoral student. "And then there were just silly things, like having to pay our own phone bills."

Al-Nasr declined to discuss KAUST's operating budget (it's believed to be roughly $750 million a year), explaining that KAUST "doesn't share its financial information with anyone except our board of trustees." But he says that "there haven't been any budget cuts affecting research that I'm aware of." He says the endowment provides "the biggest portion" of the funds needed to operate the university, although officials are hoping a growing share will come from industry, philanthropic organizations, and private donors. At the same time, he says, KAUST has reduced its "nonacademic expenditures" by 20%.

Core labs. KAUST's facilities include nanofabrication and nanobiology labs, NMR machines, and a supercomputer.

Those cost-saving measures may annoy faculty members, Keyes says, but they are hardly unique to KAUST. "Now that the global economy is much less secure, we are striving to live within a budget that will not require breaking promises," he says. "That means every new faculty member's requests for start-up funds and equipment is getting more scrutiny." In addition to growing its own talent, KAUST decided early on that institutional collaborations with global heavyweights would be a good way to jump-start its research activities. So KAUST inked dozens of deals using an array of mechanisms.

The first one, with WHOI, covered research in three areas: coral

CREDITS: DATA AND PHOTOS COURTESY OF KAUST

eppendorf

Spectracular!

Eppendorf BioSpectrometer® and Eppendorf µCuvette™ G1.0

Combining accuracy, sensitivity and guided operation, the Eppendorf BioSpectrometer offers outstanding flexibility in a small and robust instrument.

The µCuvette G1.0 expands the measuring range of the Eppendorf BioSpectrometer and complements Eppendorf's range of products for photometry.

> UV/Vis spectral range from 200 nm to 830 nm
> μCuvette G1.0 for measuring sample volumes ≥ 1.5 μL
> Attractive bundles on offer

www.eppendorf.com

Eppendorf®, the Eppendorf Logo® and Eppendorf BioSpectrometer® are registered trademarks of Eppendorf AG, Hamburg, Germany.
Eppendorf µCuvette™ is a trademark of Eppendorf AG, Hamburg, Germany. All rights reserved, including graphics and images.
Copyright © 2012 by Eppendorf AG.

reef ecology, marine resources and fisheries management, and physical oceanography. Each was designed to take advantage of KAUST's location along the Red Sea, a body of water with special characteristics. It promised to be a boon to scientists around the world who had been prohibited from working there because of its strategic and military importance to the countries—Egypt, Sudan, Somalia, and Ethiopia, as well as Saudi Arabia—along its shores.

The cruises, across all seasons, were designed to generate the first large-scale, top-to-bottom hydrographic survey of this poorly explored sea. But only one came off as originally planned, says Amy Bower, a senior scientist at WHOI and project leader. (Fortunately, it yielded what Bower calls "an unprecedented data set" on nutrient flows into the sea from the Gulf of Aden.)

The first cruise was "pretty much a debacle," Bower says, after WHOI's ship was blocked from working in Saudi coastal waters and rerouted to study brine pools in the middle of the sea, fed by an unknown hydrothermal vent. A second cruise was moved to the Caribbean. WHOI scientists also complain about being left in the dark as to why certain decisions were made. "The one thing I've learned is that there are always 10 more reasons than you've been told," Bower says.

Rough seas. WHOI's Amy Bower and her co-chief scientist, Yasser Abualnaja of KAUST, had hoped to do more cruises aboard the *Aegaeo*.

Summing up her experience, Bower says "I wouldn't say it was a failure. But it was a big disappointment. KAUST was poised to become a major player in oceanography; they had water access and lots of money. They could have done a lot for Red Sea science and for research throughout the region. Instead, this [shift in priorities] makes them a limited, parochial coastal lab, of which there are many around the world."

Xabier Irigoien, who a year ago succeeded Luyten as director of the Red Sea center, sees things quite differently. He says the collaboration was flawed from the beginning because it was not a good match with the research interests of KAUST faculty members. "We do not consider physical oceanography to be a priority," Irigoien says. "We are moving toward a focus on marine biology and the unique systems on hand, here in the Red Sea. Pure basic mapping is less of a priority."

Looking for answers

Such shifts in research focus are easier to make at a small university—KAUST now has about 120 faculty members and 700 students—that is still wet behind the ears. And the more collaborative the research, the better: Instead of departments, faculty members are clustered in three large divisions and carry out most of their research at centers that cover broad interdisciplinary topics such as desalination, catalysis, clean combustion, and solar engineering. KAUST also has no tenure system, instead offering faculty members 5-year contracts that can be extended indefinitely after annual reviews.

Those features appealed to plant geneticist Nina Fedoroff, a renowned academic scientist. After completing a 3-year stint as science adviser to the U.S. Secretary of State, Fedoroff postponed retirement and accepted an invitation last year to create a desert agriculture research center.

"I realized from my experiences at State that, despite all the verbiage about the need to adapt to climate change, there wasn't much going on substantively with respect to food and water needs," she explains. "There are many inefficiencies in how we do agriculture in terms of water, nutrients, and land use. And the reason I came here, in a nutshell, was to see if we could make progress in those areas."

"This is exactly the kind of thing they should be doing," says biochemist Barry Halliwell, deputy president for research and technology at the National University of Singapore and a member of a blue-ribbon International Advisory Council that advises KAUST's president. "It's highly relevant to the kingdom, and it's quite an exciting area. People have messed around with it for awhile. And the place that could really tackle it, and one with unlimited solar energy, is Saudi Arabia."

Another type of collaboration at KAUST begins with competitive research grants of up to $10 million to scientists from around the world (*Science*, 28 March 2008, p. 1748). The hope is that these scientists would find a way to involve KAUST faculty members and students in their work. Ted Sargent, a professor of nanotechnology at the University of Toronto in Canada, says he has been "blown away" by what he has seen at KAUST since receiving one of these global research awards in 2008.

"It's been an incredible partnership because KAUST has hired faculty at the top of their game," Sargent says. "People have chosen KAUST over MIT [the Massachusetts Institute of Technology] or Cornell, and I think it's fast becoming one of the world's top universities." KAUST's microscopy facilities, which he calls "outstanding," have been essential for his work on quantum dots, and Sargent shares students and postdocs with Ghassan Jabbour, who directs the Solar & Photovoltaics Engineering Research Center at KAUST.

Another grant recipient, computational biologist Anna Tramontano of the Sapienza University of Rome, says her 5-year, $5 million award has ushered in "the most productive period of her career" because it has allowed her to pursue a broad, long-range research program. "The scientific atmosphere is very good there, and I think it's going well," says Tramontano, who has also helped KAUST evaluate faculty members and programs in her field.

Energy saver. KAUST has earned a green building designation for its sustainable architecture.

At age 88, King Abdullah probably won't be around to see whether his vision is realized. But senior KAUST administrators believe KAUST can become an example of how to create a global research university attuned to, and serving the needs of, the Middle East.

"Am I worried what will happen after the king dies? A big 'no' to that," Al-Nasr says. "Why should we worry? Things are going well, and KAUST is moving ahead as planned." **–JEFFREY MERVIS**

CREDITS (TOP TO BOTTOM): LEAH TRAFFORD/WOODS HOLE OCEANOGRAPHIC INSTITUTION; COURTESY OF KAUST

NEUROSCIENCE

All Eyes on RNA

The list of RNA-binding proteins linked to amyotrophic lateral sclerosis is growing; RNA may also explain why a common mutation causes this fatal motor neuron disease—and a dementia

In the summer of 2011, a 3-year investigation into the genetics of amyotrophic lateral sclerosis (ALS) by research teams on two continents was coming to a head. This international consortium had narrowed the search for a mutation they knew caused ALS in families to just three genes on chromosome 9. Yet detailed and thorough gene analysis, using a variety of new sequencing technologies and massive computational power, failed to turn up any mutations that could be responsible.

Knowing that something unusual must lurk in this segment of DNA, Bryan Traynor, a geneticist at the U.S. National Institute on Aging in Bethesda, Maryland, took a closer look at one particularly suspicious stretch repeating itself over and over, far more than in unaffected family members. Because this type of mutation has been implicated in some other neurodegenerative diseases—repeated DNA sequences cause Huntington's disease and fragile X syndrome, for example—Traynor was confident that the consortium's long quest was over.

Indeed, a team led by Rosa Rademakers of the Mayo Clinic in Jacksonville, Florida, independently discovered the same repeat in the gene, provisionally dubbed *C9ORF72*, and the two groups published simultaneously in *Neuron* in September 2011. It quickly became apparent this was the most important ALS gene discovered to date, by far. The *C9ORF72*

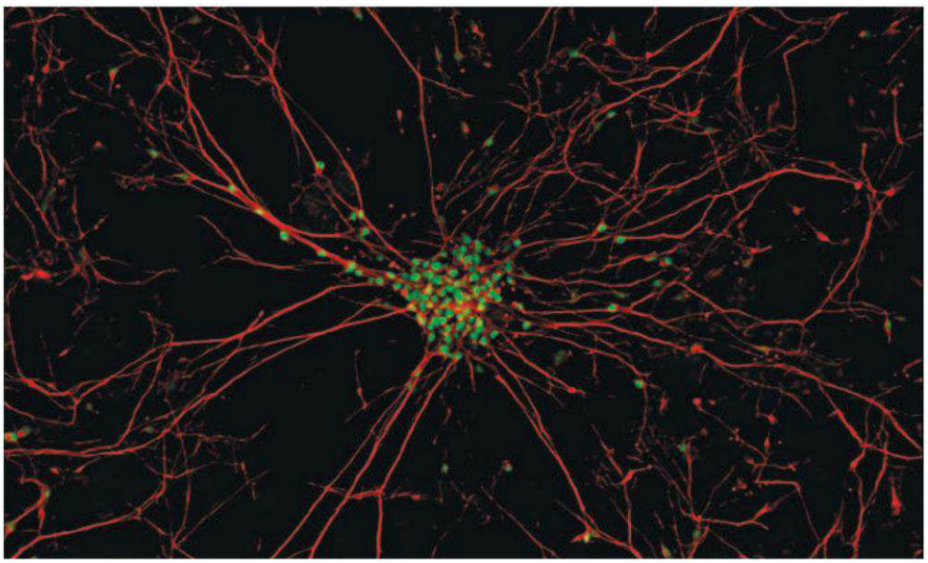

So long. The lengthy axons (red) of these motor neurons, derived from the cells of a person with ALS, may be vulnerable to defects in RNA processing.

patients show symptoms of both diseases to varying degrees.)

The leading hypothesis is that the long DNA repeat spawns a bloated gob of RNA that creates a trap inside cells for one or more RNA-binding proteins necessary for a neuron's function or survival. RNA-binding proteins have been under scrutiny in ALS since 2006, when one of them, TDP-43, was reported to make up the abnormal protein deposits, known as inclusions, found in motor neurons in almost all ALS cases (*Science*, 6 October 2006, p. 42). Mutations in the genes for TDP-43 and in FUS, a related RNA-binding protein, can cause ALS, and mutations in a third RNA-binding protein, ataxin-2, are a powerful risk factor for the disease.

Although ALS neurons suffer many types of dysfunction, the multiple recent discoveries have led to "a convergence of ideas" that errors in RNA processing are central to ALS and they could be linked to all the cellular problems, says biochemist Don Cleveland of the University of California (UC), San Diego. Others in the field caution that ALS might actually be several distinct diseases with different causes, RNA misprocessing being only one. Nevertheless, Cleveland says, "since last September, it's been the most exciting time of discovery in ALS in the history of the planet."

Inward bound

What RNA-binding proteins are doing—or not doing as the case may be—in ALS and FTD remains largely a mystery. That's partly because each protein may bind so many RNAs, thousands in some cases, that it is hard to know which RNAs are important in disease. Among other duties, RNA-binding proteins trim, cap, escort, degrade, and otherwise process messenger RNA, which carries the transcribed DNA sequence from the cell nucleus to the cytoplasm for translation into protein. "There isn't a step in the process [without] a halo of RNA-binding proteins surrounding the RNA," says Robert

NIVERSITY AND PROJECT A.L.S., NEW YORK, NEW YORK

AAAS 2013 ANNUAL MEETING

14-18 FEBRUARY • BOSTON

THE BEAUTY AND BENEFITS OF SCIENCE

HYNES CONVENTION CENTER

The Beauty and Benefits of Science theme highlights the "unreasonable effectiveness" of the scientific enterprise in creating economic growth, solving societal problems, and satisfying the essential human drive to understand the world in which we live.

- Over 150 sessions on a range of scientific topics
- Learn about recent developments in science, engineering, education, and policy
- Network and connect with professionals from around the world
- Deep discounts on hotel and travel

Featured Plenary Speakers

Sherry Turkle
Massachusetts Institute of Technology
The Robotic Moment: What Do We Forget When We Talk to Machines?

Cynthia Kenyon
University of California, San Francisco
Mechanisms for Life Extension in C. elegans

Nathan Myhrvold
Intellectual Ventures
Modernist Cuisine: The Art and Science of Cooking

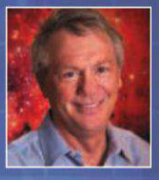

Robert Kirshner
Harvard University
The Beauty of the Accelerating Universe

Register Today at www.aaas.org/meetings

AAAS, publisher of *Science*, thanks the sponsors and supporters of the 2013 Annual Meeting

SUBARU

NSF

European Commission

ACS Chemistry for Life®
American Chemical Society

HELMHOLTZ ASSOCIATION

Canada

AAAS thanks

THE KAVLI FOUNDATION

for its generous support of the Science Journalism Awards

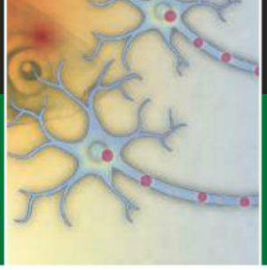

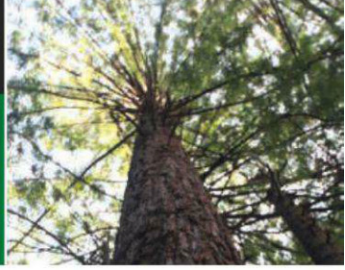

LETTERS

edited by Jennifer Sills

Voles, Vasopressin, and the Ethics of Framing

THE SCIENTIFIC COMMUNITY INCREASINGLY RECOGNIZES THE IMPORTANCE OF COMMUNICATING effectively and responsibly with the public (*1*), but questions remain about whether and how to "frame" scientific information about controversial issues such as climate change, evolution, and embryonic stem cell research (*2*, *3*). Recent discussions about the biological determinants of behavior in voles provide an opportunity to reflect on how scientists can frame information in ways that are both illuminating and responsible.

By modulating the density and distribution of vasopressin receptors in specific regions of the brain, scientists can get ordinarily "promiscuous" montane voles to behave more like "monogamous" prairie voles (*4*). By the time this research was reported in the popular media, it had become a story about the discovery of a "gene for" "monogamy," "fidelity," "promiscuity," or "divorce" in humans (*5*).

Montane vole.

Consider the major frames we identified in the media coverage of this research: (i) "genetic determinism," the idea that a single gene controls even complex social behaviors such as sexual monogamy (*6*); (ii) "triumph for reductionism," the suggestion that soon we will understand love in terms that refer exclusively to physics and chemistry (*7*); (iii) "humans are like voles," a parallel allowing wide-ranging extrapolation (*8*); (iv) "happiness drug," the idea that applying lessons learned from this research to biotechnology efforts could save a relationship or marriage (*9*); and (v) "dangers of social manipulation," which has led to stories about trust sprays of potential use to the military, department stores, politicians, and stalkers (*10*).

These frames, albeit crude and oversimplified, can help members of the public understand how research relates to broader social trends, issues, and debates. By paying close attention to the dominant frames used in highly publicized cases like this one, scientists can take advantage of these strengths while preemptively highlighting their potential weaknesses. For example, to correct a common source of misunderstanding in the "humans are like voles" frame, experts could emphasize that ordinary usage of terms such as "monogamy" can differ substantially from their technical applications in biology. (Spending 56% of the time with one's spouse, 19% of the time alone, and 25% of the time copulating with strangers would not qualify as monogamous by ordinary human standards.) They could also suggest alternative frames that counteract weaknesses in existing ones. Instead of focusing on "happiness drugs," for example, scientists could contextualize this research as a potential treatment for autism, thereby focusing attention on the more realistic relevance of this work.

By recognizing the benefits of particular frames while preempting and mitigating common misperceptions, scientists can work with the media to develop frames that promote public interest in scientific advances without contributing to sensationalism and diminished scientific credibility.

DANIEL J. MCKAUGHAN[1]* AND KEVIN C. ELLIOTT[2]

[1]Department of Philosophy, Boston College, Chestnut Hill, MA 02467, USA. [2]Department of Philosophy, University of South Carolina, Columbia, SC 29208, USA.

*To whom correspondence should be addressed. E-mail: daniel.mckaughan@bc.edu

CREDIT: RICK & NORA BOWERS/ALAMY

References

1. A. I. Leshner, *Science* **315**, 161 (2007).
2. M. C. Nisbet, C. Mooney, *Science* **316**, 56 (2007).
3. E. M. Holland *et al.*, *Science* **317**, 1168 (2007).
4. M. M. Lim *et al.*, *Nature* **429**, 754 (2004).
5. D. McKaughan, *Biol. Philos.* **27**, 521 (2012).
6. C. Holden, "Why men cheat: Study chalks up promiscuous behavior to a single genetic change," *ScienceNOW*, 2 September 2008 (http://news.sciencemag.org/sciencenow/2008/09/02-01.html).
7. L. Young, *Nature* **457**, 148 (2009).
8. J. Silver, "Men are like voles: Vasopressin and bonding—marital fidelity may be affected by a vasopressin polymorphism," *Journal Watch Psychiatry*, 29 September 2008.
9. J. Tierney, "Anti-love drug may be ticket to bliss," *New York Times*, 13 January 2009 (www.nytimes.com/2009/01/13/science/13tier.html).
10. J. Koebler, "Oxytocin, the 'trust hormone,' could become new interrogation tool," *U.S. News and World Report*, 15 May 2012 (www.usnews.com/news/articles/2012/05/15/oxytocin-the-trust-hormone-could-become-new-interrogation-tool).

Disease Prevention: Data Integration

IN HIS PERSPECTIVE "WHY A MACROECONOMIC perspective is critical to the prevention of noncommunicable disease" (special section on Disease Prevention, 21 September, p. 1501), R. Smith fails to acknowledge a fundamental flaw in the design of the delivery of health care: the lack of data integration among each patient's disparate health records. This structural issue in the healthcare system must be addressed in order to optimize preventive care.

For example, research shows a relationship between diabetes and periodontal disease (*1*, *2*). However, the National Committee for Quality Assurance (NCQA) was established by medical health plans that do not typically serve as payers for dental care. It is therefore difficult for the NCQA to require a periodontal screening of diabetes patients as part of a Health Effectiveness Data and Information Set measure, despite the importance of this measure according to the Wisconsin Diabetes Prevention and Control Program Guidelines (*3*).

Furthermore, most private-sector electronic health records technologies fail to integrate medical and dental records. The lack of integrated data hinders the efforts of researchers trying to address the relationships between periodontal disease and diabetes. It also places a technical barrier in the path of disease registries set up to monitor the quality of preventive care delivered by medical home provider teams. The data about a given patient's medical and dental care are only available in separate claim streams and usually cannot be successfully integrated, given disparate and unarticulated patient identification schemes (*4*).

Revising the model of care delivery would affect provider education, the structure and function of healthcare organizations, the design of electronic records systems and health information exchanges, models for quality assurance and meaningful use, and models and operations for payer organizations. True preventive care must be adequately integrated, and provider utilization must be optimized. Before undertaking macroeconomic remedies, let us first address the models of care delivery and patient records.

VALERIE J. H. POWELL[1]* AND AMIT ACHARYA[2]

[1]Computer and Information Systems Department, Clinical Data Integration Project, Robert Morris University, Moon Township, PA 15108, USA. [2]Dental Informatics Postdoctoral Fellowship Program, Dental Informatics Research and Training Program, Biomedical Informatics Research Center, and Marshfield Clinic Research Foundation, Marshfield, WI 54449, USA.

*To whom correspondence should be addressed. E-mail: powell@rmu.edu

References

1. B. L. Mealey, L. F. Rose, *Curr. Opin. Endocrinol., Diabetes Obesity* **15**, 135 (2008).
2. G. W. Taylor, W. S. Borgnakke, *Oral Dis.* **14**, 191 (2008).
3. Wisconsin Diabetes Advisory Group, "Wisconsin essential diabetes mellitus care guidelines" (Wisconsin Diabetes Prevention and Control Program, Madison, WI, 2008), chap. 9; http://dhs.wisconsin.gov/health/diabetes/PDFs/GL09.pdf.
4. S. Foreman, in *Integration of Medical and Dental Care and Patient Data*, V. Powell *et al.*, Eds., (Springer-Verlag, London, 2012), chap. 4.1.

Risk Communication on Shaky Ground

THE VERDICT OF MANSLAUGHTER FOR THE experts who assessed earthquake risk in L'Aquila ("Aftershocks in the courtroom," E. Cartlidge, News & Analysis, 12 October, p. 184 and "Prison terms for L'Aquila experts shock scientists," E. Cartlidge, News Focus, 26 October, p. 451) highlights the need for evidence-based risk communication guidelines. These guidelines should specify which expressions are appropriate to communicate risk, in order to protect both the risk information recipient and the risk information provider. Presumably, if evidence-based risk communication guidelines had been established and followed, experts would have communicated the earthquake risk more appropriately to the citizens of L'Aquila and later would have benefited from legal protection.

Research on risk communication and its sociocognitive and behavioral consequences indicates that the negative verbal proba-

Letters to the Editor

Letters (~300 words) discuss material published in *Science* in the past 3 months or matters of general interest. Letters are not acknowledged upon receipt. Whether published in full or in part, Letters are subject to editing for clarity and space. Letters submitted, published, or posted elsewhere, in print or online, will be disqualified. To submit a Letter, go to www.submit2science.org.

AAAS Travels

Wild & Prehistoric FRANCE

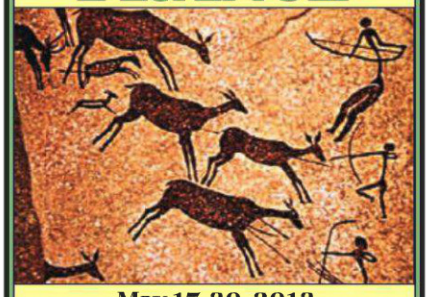

May 17-30, 2013

including Lascaux II & Rouffignac

Discover wild areas and prehistoric sites in Haute Provence, the Massif Central, and the Dordogne. See spectacular gorge country and images of the great cave paintings at Lascaux II and Rouffignac of mammoths. Visit the Vezere Valley, Font de Gaume, Arles, and Les Baux. $3,695 + air

For a detailed brochure, please call (800) 252-4910

All prices are per person twin share + air

BETCHART EXPEDITIONS Inc.

17050 Montebello Rd, Cupertino, CA 95014

Email: AAASInfo@betchartexpeditions.com

www.betchartexpeditions.com

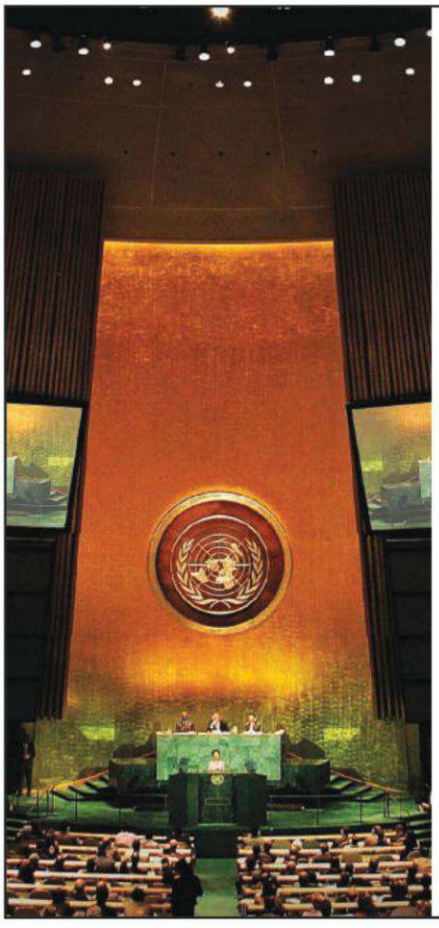

AAAS is here –

Science Funding,
Climate Regulation,
Human Rights.

Around the world, governments turn to AAAS as an objective, multidisciplinary scientific authority to educate public officials and judicial figures on today's most pressing issues. And this is just one of the ways that AAAS is committed to advancing science to support a healthy and prosperous world. Join us. Together we can make a difference.

To learn more, visit
aaas.org/plusyou/policy

AAAS + U = Δ

bilities that were frequently used to quantify the earthquake risk in L'Aquila, such as "unlikely" and "very improbable," express a decreasing trend of risk (*1*). Findings suggest that these terms draw attention toward the nonoccurrence of the outcome and discourage preventive measures (*2*). Negative verbal probabilities also denote a more vague degree of risk than positive expressions (e.g., "there is a small probability") (*3*). Therefore, negative expressions of probabilities should be avoided in risk communications requiring preventive measures.

Recently, a systematic effort was made by the Intergovernmental Panel on Climate Change to provide risk communication guidelines (*4*). The panel generated a set of quantitative scales of likelihood that are associated with different verbal probabilities. However, these recommendations may have overlooked previous research showing that using negative expressions would discourage preventive measures. For example, the panel suggests the use of "unlikely" for probabilities between 10 and 33%, therefore deterring preventive actions, which is not the intention of the IPCC.

Consequently, we call for a more systematic consideration of scientific empirical findings when establishing risk communication guidelines to protect both the recipient and provider of the risk information.

MIROSLAV SIROTA[1]* AND MARIE JUANCHICH[2]

[1]King's College London, SE1 3QD, London, UK. [2]Kingston University London, KT2 7LB, Kingston Upon Thames, UK.

*To whom correspondence should be addressed. E-mail: miroslav.sirota@kcl.ac.uk

References

1. M. Juanchich, K. H. Teigen, G. Villejoubert, *Acta Psychologica* **135**, 267 (2010).
2. K. H. Teigen, W. Brun, *Org. Behav. Hum. Decision Processes* **80**, 155 (1999).
3. M. Smithson, D. V. Budescu, S. B. Broomell, H.-H. Por, *Int. J. Approximate Reasoning* **53**, 1262 (2012).
4. Intergovernmental Panel on Climate Change, "Guidance notes for lead authors of the IPCC fourth assessment report on addressing uncertainties" (2005); www.ipcc.ch/pdf/assessment-report/ar4/wg1/ar4-uncertaintyguidancenote.pdf.

CORRECTIONS AND CLARIFICATIONS

News & Analysis: "Change versus experience?" by D. Malakoff (16 November, p. 875). Representative Dana Rohrabacher is a Republican, not a Democrat. His party affiliation (R–CA) has been corrected in the HTML and PDF versions online.

Letters: "Disease prevention: Experiments in nature" by L. A. Cohen (16 November, p. 883). A reference was missing: C. P. Howson, T. Hiyama, E. L. Wynder, *Epid. Rev.* **8**, 1 (1986). The reference should have been cited at the end of the fourth sentence. The HTML version online has been corrected.

Perspectives: "Cooperative transcription factor complexes in control" by G. J. Martinez and A. Rao (16 November, p. 891). The first line of the figure caption should have cited Ref. 1, the Glasmacher *et al*. Report, not Ref. 2. The citation has been corrected in the HTML and PDF versions online.

Reports: "*Salmonella* inhibits retrograde trafficking of mannose-6-phosphate receptors and lysosome function" by K. McGourty *et al*. (16 November, p. 963). In the acknowledgments note, "*SkipPlekhm2*$^{-/-}$" should have been "*Skip/Plekhm2*$^{-/-}$." The HTML version online has been corrected.

Perspectives: "Driving the formation of molecular knots" by J. S. Siegel (9 November, p. 752). Reference 12 was incorrect. It should be: C. Z. Liang, K. Mislow, *J. Am. Chem. Soc*. **116**, 11189 (1994). The reference has been corrected in the HTML and PDF versions online.

Imagine what you can accomplish by **quantifying** previously **undetectable biomarkers**.

Uncover clinically relevant biomarkers faster and with more confidence. Powered by Singulex digital technology, you can measure low-abundance biomarkers accurately and reliably, even in healthy individuals.

Want to see the data? It's waiting for you at www.singulex.com/imagine

Singulex®

Request for Information: LTAR Network

The Agricultural Research Service (ARS) requests information from long-term research groups (e.g. experimental watersheds or ranges) that are interested in becoming formally affiliated with the USDA Long Term Agro-ecosystem Research (LTAR) Network.

The LTAR will sustain infrastructure for research and education that enables forecasting of the nation's capacity to provide agricultural goods and ecosystem services under changing conditions.

Information should be provided for each of the following criteria to evaluate a site's potential for inclusion into LTAR. 1) Productivity; 2) Infrastructure Capacity; 3) Data Richness; 4) Data Accessibility; 5) Geographic Coverage; 6) Partnerships; 7) Institutional Commitment

Details concerning the RFI and prior successful applications can be found at:

www.ars.usda.gov/ltar

Responses are due on April 1st, 2013.

Contact Mark Walbridge at (301) 504-4731 or at:

mark.walbridge@ars.usda.gov

for more information.

LOCATION: Jackson Park Health Club
ARTICLE: *An Electronic Second Skin*
DATE: Sep 21, 7:43am

LOCATION: University Faculty Lounge
ARTICLE: *The Visual Impact of Gossip*
DATE: Sep 21, 4:22pm

LOCATION: Gyro King
ARTICLE: *Cavemen Craved Carbs, Too*
DATE: Sep 21, 1:13pm

LOCATION: Hemlock Bar
ARTICLE: *Quantum Simulation of Frustrated Classical Magnetism in Triangular Optical Lattices*
DATE: Sep 21, 9:21pm

LOCATION: Bed
ARTICLE: *Consciousness: What, How and Why*
DATE: Sep 21, 10:56pm

A new way to look at science

The new *Science* Reader app for iPad® from AAAS puts *Science* in your hands, wherever you go. Read abstracts, career advice, and highlights from our newest journals, *Science Signaling* and *Science Translational Medicine*. Plus, AAAS members can access full text articles from *Science*. Visit iTunes App Store℠ or content.aaas.org/ipad for details.

Available on the App Store

Science
AAAS

FOR YOUNGER READERS

Some Suggestions from 2012—The SB&F Prizes Finalists

If you are seeking to kindle an interest in science among a younger reader, the finalists for the 2013 Science Books and Films Prizes for Excellence in Science Books may provide some sparks. The prizes, sponsored by AAAS and Subaru, honor books that promote an understanding and appreciation of science in children and young adults. The nearly 170 books considered for the 2013 prizes were published between September 2011 and August 2012. The prize for a hands-on science book returns this year, rejoining three age-based categories: for readers in grades K–4, for those in grades 5–8, and for high school students. The four finalists for the young adult award were written for the general public.

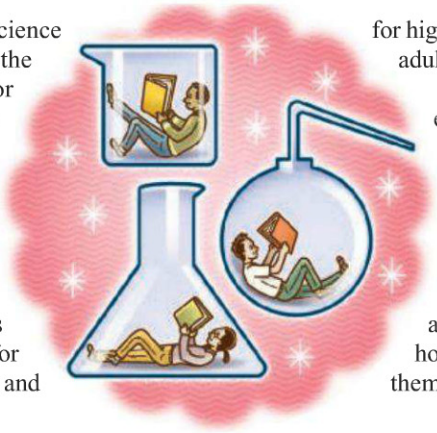

The panel of librarians, scientists, and science literacy experts had a hard time narrowing the fields this year. Short descriptions of the 19 finalists follow. Longer reviews have appeared or been scheduled in Science Books and Films. The winners will be announced in February at the AAAS Annual Meeting in Boston.

The honored books are expected to clearly and accurately present scientific concepts. We hope that children and young adults will also find them enticing.

Children's Science Picture Book

The Beetle Book. Steve Jenkins. Houghton Mifflin Harcourt, Boston, 2012. 36 pp. $16.99, £11.99. ISBN 9780547680842.

Even if one doesn't accept Jenkins's claim that one out of every four kinds of plant or animal on Earth is a beetle, there is no doubt that this order of insects has been extraordinarily successful since its origins about 230 million years ago. Over 350,000 species have been named, and thousands more are discovered each year. Jenkins's striking illustrations (torn- and cut-paper collage) and concise text provide an enticing introduction to the group's "amazing range of shapes, sizes, and colors" and its biology. The author begins his survey with a description of beetles' basic blueprint, including their diagnostic hard or leathery "outer wings" (wing covers). He then introduces their senses, four life stages, and the types of foods that their wide variety of jaw forms allows them to tap. Subsequent spreads highlight their use of sounds (and in some cases, light) for communication and of chemical defenses. Jenkins shows beetles that mimic ants, wasps, or spiders (to discourage other species from eating them or encourage other species to aid them) and beetles that disguise themselves as bird droppings or camouflage themselves to resemble leaves, bark, or lichen. He also provides examples of species that run, crawl, jump, dig, swim, or fly to get around. Silhouettes indicate the actual sizes of the various beetles, and the book ends with a list of scientific names and geographic areas for each of the featured 77 species. **– Sherman J. Suter**

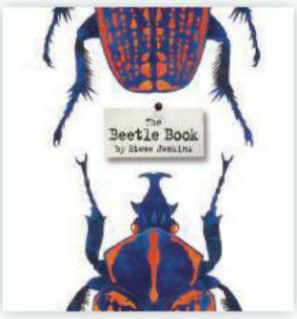

Rachel Carson and Her Book That Changed the World. Laurie Lawlor, illustrated by Laura Beingessner. Holiday House, New York, 2012. 32 pp. $16.99, £10.59. ISBN 9780823423705.

Most people know that Carson wrote *Silent Spring*, the book that rang the alarm bells over our release of damaging chemicals into our environment. Very few may know of the woman biology teacher who inspired her; the battles she fought to become a biologist when women were not welcome; her exciting adventures as an undersea diver or alligator chaser; or that, despite never marrying, throughout her adult life she was the sole breadwinner for a large extended family. Lawlor's accessible text and Beingessner's warm and comfortable images reveal the triumphs and trials of Carson's life, including her death from breast cancer before she was able to witness the impact of her work. As in many biographies written for children, we find the inspirational messages that hard work and following one's dreams pay off and can make the world a better place. Unlike many others, however, the book ends on a melancholy note due to her early death. For all the positive changes that Carson's work inspired, 50 years on fierce resistance to protecting the environment continues. On those grounds, the mix between hope and sadness one feels on closing the cover seems entirely appropriate. **– Sacha Vignieri**

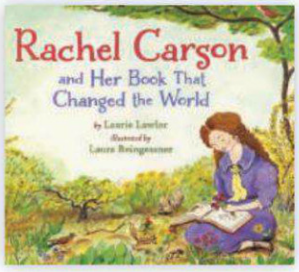

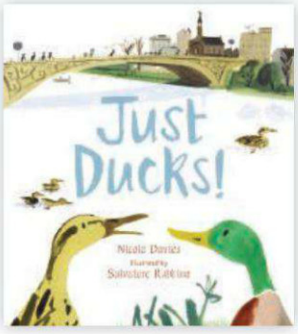

Just Ducks! Nicola Davies, illustrated by Salvatore Rubbino. Candlewick, Somerville, MA, 2012. 32 pp. $15.99, C$18. ISBN 9780763659363. Walker, London. £12. ISBN 9781406327397.

Every morning, the young narrator wakes up to the "quack-quuuack, quack-quaack-quack" of the mallards that live on the river that flows through her town. She recounts the preening, splashing, swimming, and dabbling that she has noticed on her way to and from school; tells how she sometimes stops to feed them when the weather is cold; and reveals that she even heard them one evening eating worms on the lawn outside her choir practice. Davies supplements her narrator's charming and informative story with additional facts about the urban ducks and their lives. Suggestive of quick yet comprehensive field sketches, Rubbino's watercolor illustrations effectively convey the birds' appearances and behaviors. **– Sherman J. Suter**

A Place for Bats. Melissa Stewart, illustrated by Higgins Bond. Peachtree, Atlanta, GA, 2012. 44 pp. $18.99, £10.60. ISBN 9781561456246.

Through her "A Place for …" series, Stewart aims to inform young readers of how people's activities affect animals with which we share our world. In the latest addition to the series, she discusses an often misunderstood

CREDIT: PETER AND MARIA HOEY/WWW.PETERHOEY.COM

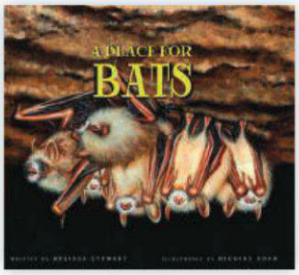

and maltreated group, bats. Presenting 13 of North America's 45 species, she describes aspects of bat behavior, feeding, habitats, and ecological roles. (The endpapers provide range maps for all but the lesser long-nosed bat, and perhaps the depiction of it lapping nectar from a cactus blossom suffices to indicate where it lives.) Her examples include 4 of the 7 bats on the U.S. endangered species list, and Stewart highlights the threats bat populations face—such as disturbance at roosting sites, insecticide use, wind turbines, habitat loss, and white nose syndrome. She also suggests steps that people can take to help ensure that "bats can live and grow," including putting up bat boxes in backyards, keeping cats indoors, gating caves and abandoned mines, and protecting natural areas. Bond's color illustrations place each species in its surroundings (for example, she shows people watching a cloud of Mexican free-tailed bats emerging from their roost beneath a highway bridge). The text concludes with a few "fascinating facts" about bats in general.

– Sherman J. Suter

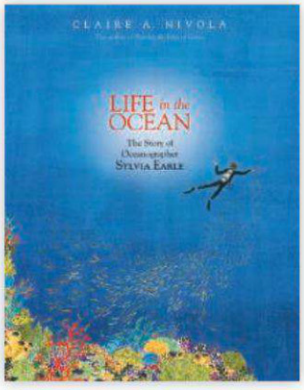

Life in the Ocean: The Story of Oceanographer Sylvia Earle. Claire A. Nivola. Farrar Straus Giroux, New York, 2012. 32 pp. $17.99, £11.25. ISBN 9780374380687.

"We know more about the planets in outer space than we know about the sea," Nivola declares toward the end of this beautifully illustrated biography of oceanographer Sylvia Earle. This book should inspire its young audience to help change that. The artwork conveys Earle's adventurous life beneath the waves learning about the ocean and its diverse inhabitants. After briefly recounting how the young Earle's curiosity led her toward science, Nivola takes readers underwater to show the researcher's work at different depths. I particularly liked the author's note with its labeled portraits of ocean denizens that will be unfamiliar to most children. Collectively, the varied images, atypical seascapes, and account of how one individual was able to realize her goal to see these wonders should spark the imaginations of countless budding scientists.

– Laura M. Zahn

Ocean Sunlight: How Tiny Plants Feed the Seas. Molly Bang and Penny Chisholm. Scholastic, New York, 2012. 44 pp. $18.99, £11.85. ISBN 9780545273220.

This charming book explains how the Sun feeds the dark depths of the ocean.

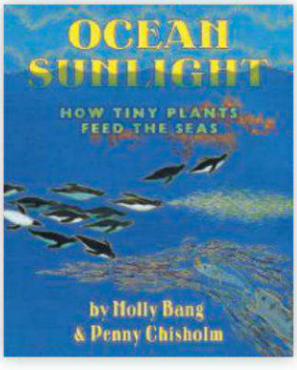

Bang and Chisholm begin with the more familiar case of sunlight falling onto land plants. They then show that the same principles help us understand how detritus from ocean phytoplankton supports denizens of the deep. They boil the chemistry of photosynthesis down to its simplest components: water, carbon dioxide, and sunlight produce sugar and oxygen. Several food chains woven into the illustrations reveal how plant productivity supports animal and human life. Visually striking images present microscopic views of macroscopic events and inform the theme of food webs with a sense of quantity, size, and habitat. The depictions of molecular structures are graphically appealing without sacrificing accuracy. Particularly eye-catching drawings of phytoplankton convey all their morphological glory. The text will challenge early readers, but the book will work well when read to a child, as the illustrations provide plenty for parent and child to exclaim over. Details supplied in the final pages will help adult readers fill out the story.

– Pamela J. Hines

Middle Grades Science Book

The Book of Blood: From Legends and Leeches to Vampires and Veins. H. P. Newquist. Houghton Mifflin Harcourt, Boston, 2012. 160 pp. $17.99, £11.25. ISBN 9780547315843.

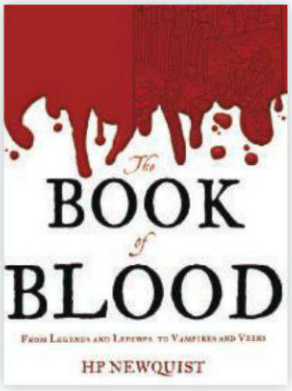

Given the title, it's not surprising that faux blood spots decorate the book's pages. Covering a sizeable range of topics, Newquist mixes science, history, and some fiction. (Yes, he includes descriptions and depictions of famous vampires.) His account's strongest points include the historical sections on how blood has been studied. The effort to bring sophisticated topics such as blood chemistry and immunology to younger readers suffers from some oversimplifications. However, those readers will likely come away knowing more about the components of blood and their functions, the circulatory system in cold- and warm-blooded animals, blood transfusion, and diseases associated with blood or blood flow.

– Barbara R. Jasny

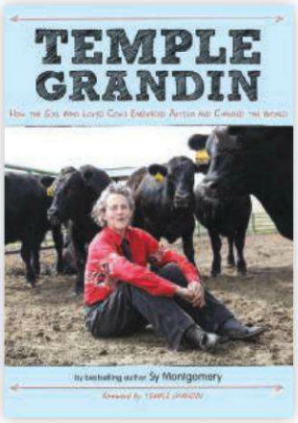

Temple Grandin: How the Girl Who Loved Cows Embraced Autism and Changed the World. Sy Montgomery. Houghton Mifflin Harcourt, Boston, 2012. 160 pp. $17.99, £11.25. ISBN 9780547443157.

Humans equate language with intelligence and tend to regard species, or individuals, lacking language skills as cognitively inferior. This perspective presumes intelligence operates on a single scale. Montgomery's biography of animal-welfare advocate Grandin demonstrates the flaw in such thinking. Autistic and nonverbal as a child, Grandin came to understand that her thought process was much like that of animals—largely visual and without verbal language, but also powerful and insightful. The author describes clearly how Grandin harnessed her insight to improve the welfare of animals, another group that often suffers greatly for its lack of language and inability to be measured by our regular cognitive rules. As we follow Grandin's growing understanding of her own mind, how it works, and what it can do, we can see the world in an alternative way. Montgomery's compelling presentation will encourage young readers to develop their own understanding of and appreciation for different minds, be they human or animal.

– Sacha Vignieri

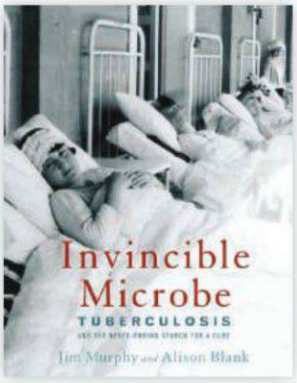

Invincible Microbe: Tuberculosis and the Never-Ending Search for a Cure. Jim Murphy and Alison Blank. Clarion, New York, 2012. 160 pp. $18.99, £11.86. ISBN 9780618535743.

Tuberculosis (TB, once known as consumption), the disease caused by the *Mycobacterium tuberculosis* bacteria, has afflicted the human race since our origins. Murphy and Blank provides an exceptionally thorough up-to-date scientific history of this scourge and its impacts on humanity (and especially on European and U.S. cultures). Their biography of the pathogen also illuminates aspects of the history of medicine and medical sociology. The informative text and many interesting historical images chart how we have benefited from improved understanding of the transmission, treatment, and cures of one of the most prevalent infectious diseases. **– Laura M. Zahn**

Moonbird: A Year on the Wind with the Great Survivor B95. Phillip Hoose. Farrar Straus Giroux, New York, 2012. 148 pp. $21.99, £13.75. ISBN 9780374304683.

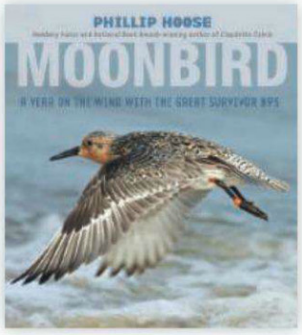

Each year, red knots (*Calidris canutus*) of the *rufa* population travel some 144,000 km from Tierra del Fuego to their breeding grounds in the Canadian Arctic and later return south. One bird, first banded in 1995 as an adult, has made the trip at least 18 times. Hoose uses its story to present the knots' biology and migration. In between their multiday flights, the birds rest and refuel at a few stopover sites (such as Delaware Bay, where they feast on the eggs of horseshoe crabs in late May). Changes, many caused by human activities, at some of these crucial locations have reduced the available food, and over the past two decades the population has dropped by nearly 80%. In addition to describing the challenges that B95 has repeatedly surmounted, Hoose introduces readers to biologists and conservationists whose work underlies his narrative and who are collaborating to save these shorebirds. (An appendix suggests ways to help.) He accompanies his engaging prose with informative and evocative photographs, several of which show the remarkable survivor whose endurance he celebrates. **– Sherman J. Suter**

Hands-On Science Book

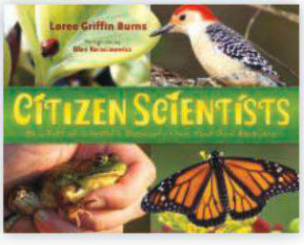

Citizen Scientists: Be a Part of Scientific Discovery from Your Own Backyard. Loree Griffin Burns, photographs by Ellen Harasimowicz. Holt, New York, 2012. 80 pp. $19.99, £12.49. ISBN 9780805090628. Paper, $12.99, £8.11. ISBN 9780805095173.

Whether they live in a city, in the suburbs, or on a farm, children can feel the excitement of being involved in real science. Burns descibes four activities (one per season, from fall through summer) that can contribute to research projects that can only be carried out by armies of volunteers: tagging butterflies to monitor migration pathways, counting winter birds, listening for mating calls to survey frog populations, and identifying ladybugs to help find species thought to be extinct. (What a great class trip—taking kids with nets on long poles out to a field to gather and photograph ladybugs.) Harasimowicz's many photos portray young investigators in action as well as the objects of their studies. The text includes lists of items the citizen scientist will need, discussions of precautions to take, and "quizzes" to help with identifications. Toward the back of the book, Burns points out other resources for these and other projects (from counting stars to tracking the movements of money around the globe) that welcome observations from children studying the world they live in. **– Barbara R. Jasny**

Crazy Concoctions: A Mad Scientist's Guide to Messy Mixtures. Jordan D. Brown, illustrated by Anthony Owsley. Charlesbridge, Watertown, MA, 2012. 80 pp. $14.95, £9.99. ISBN 9781936140510.

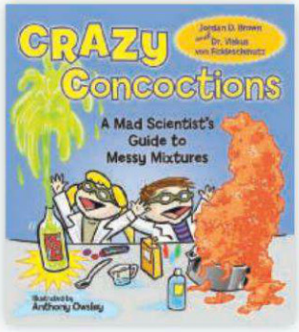

Exclamations such as "Cool!" "Gross!" and "Wow!" are sure to be heard coming from young experimenters exploring this book of kitchen chemistry. Brown provides six chapters of recipes to make things such as slime and fake blood, tells how to generate gas explosions, and encourages readers to try some of their own concoctions. Science lessons abound among the recipes. Educational snippets follow each experiment, sometimes building on unlikely hooks such as the explanation of polymers (relevant to gelatin) after the recipe to make "pretend puke." On occasion, the author tosses in history lessons, explaining contributions from well-known scientists (e.g., Dmitri Mendeleev and Robert Boyle) as well as less-familiar ones (e.g., James Wright and William A. Mitchell, respectively the inventors of silly putty and pop rocks). The science fun comes sprinkled with intriguing facts and trivia as well as nonsensical handwritten annotation by a reportedly fired coauthor. While getting the nod from parents for its educational content along with the attention to safety and cleanup, the book will certainly appeal to kids. **– Beverly Purnell**

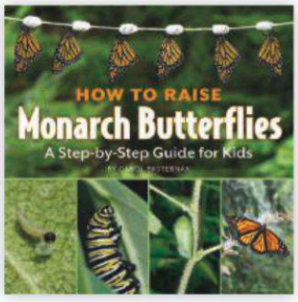

How to Raise Monarch Butterflies: A Step-by-Step Guide for Kids. Carol Pasternak. Firefly, Richmond Hill, ON, 2012. 160 pp. $19.95, C$19.95, £13.46. ISBN 9781770850019. Paper, $8.95, C$8.95, £5.59. ISBN 9781770850026.

Kids who love insects often want to bring them inside, put them in jars, and watch them grow. Unfortunately, jars aren't the ideal habitat, and these efforts usually don't turn out well for the insects. Pasternak's book may help tip them toward more positive outcomes. It describes how to find, raise, and release monarchs—from the eggs to the beautiful adults heading out for their long migration. The clear, though not simplistic, instructions could easily be followed by upper-elementary-school children. The author provides valuable information on butterfly morphology and ecology as well as bright photographs that highlight her directions and the butterflies themselves. Given the widespread sale of butterfly-growing kits with little apparent concern for potential introduction of nonnative species, it is refreshing that she focuses on finding butterfly eggs locally and releasing the adults where the eggs were found. A monarch enthusiast, Pasternak clearly wants to encourage readers to develop their own fascination through experience and further education. **– Sacha Vignieri**

Potatoes on Rooftops: Farming in the City. Hadley Dyer. Annick, Toronto, 2012. 148 pp. $24.95, C$24.95. ISBN 9781554514250. Paper, $14.95, C$14.95, £9.34. ISBN 9781554514243.

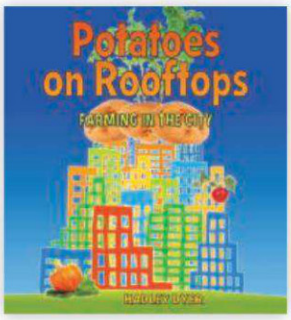

While showing how easy it is to grow potatoes on rooftops, Dyer encourages children to reflect on the food they eat, the environment they live in, and how the two are related. She starts by describing urban challenges, such as increasing populations and decreasing green space, that place the importance of urban farming into context. She then reveals simple steps for introducing green patches, however small, into concrete landscapes. Accompanying photos—portraying vertical, rooftop, raised, community, and even underground gardens—highlight the importance of creativity in urban farming. Text boxes present additional fascinating facts and ideas. For example, one describes how an old kiddie pool can be transformed into a lettuce garden. Dryer challenges her readers to take the environmental concepts they learn through gardening and apply them to similar conservation efforts, such as harvesting water and composting. She also offers a multitude of ways (including a list of organizations and websites) to help children become involved in ongoing urban gardening projects. **– Melissa McCartney**

The World in Your Lunch Box: The Wacky History and Weird Science of Everyday Foods. Claire Eamer, illustrated by Sa Boothroyd. Annick, Toronto, 2012. 148 pp. $22.95, C$22.95. ISBN 9781554513932. Paper, $14.95, C$14.95, £9.34. ISBN 9781554513925.

Before reading this book, I thought my packed-from-home lunch would bore the spots off a frog. I see now that my lunch includes Egyptian history, microbiology (of good bugs and bad), and the consequences of world exploration. Go a little crazy, and you might have a water source from the Kalahari Desert as well as crunchy fiber from Kazakhstan (those would be watermelon and apples). This colorful and entertaining book tells the story behind some of our common foods. Eamer and Booth weave together science and history, with a sprinkling of kid-friendly jokes, to explain how today's foods have long antecedents. Particularly fascinating snippets describe how food shaped world history, as in the trading routes and wars founded on the searches for pepper, salt, and spices. The book addresses a range of science topics such as risks of monoculture, health impacts of excessive salt, improvements in food safety, plant hormones that promote fruit ripening, and one plant's solution to locust attack. School kids may never look at their lunches the same again. Neither will you—just close your eyes when you snack on the bee vomit. **– Pamela J. Hines**

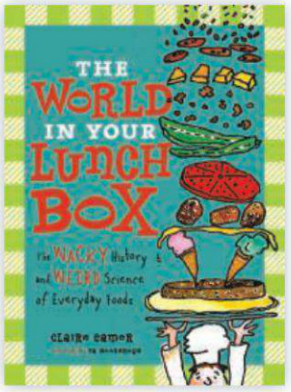

Young Adult Science Book

Death at SeaWorld: Shamu and the Dark Side of Killer Whales in Captivity. David Kirby. St. Martin's, New York, 2012. 479 pp. $26.99, C$31, £18.99. ISBN 9781250002020.

Probably few of the awed spectators at SeaWorld's Shamu show consider what it must be like for the majestic star to live in captivity. Wild orcas swim 160 km a day, live for 50 years or more in complex matriarchal societies, and show intense intelligence. Kirby details the true story of Tilikum, a 6-ton bull orca and 20-year Shamu star, who became sadly infamous for the tragic deaths of three devoted trainers. Unresolved lawsuits over the most recent death dispute whether it was an unfortunate accident or a deliberate act of aggression induced by the stress of decades of captivity. Kirby's narrative unfolds through the eyes of two protagonists who take the latter position: Naomi Rose, a Ph.D. orca expert at the U.S. Humane Society, and Jeffrey Ventre, a disillusioned ex-SeaWorld trainer. Overly long, the book is at its best when focused on orcas not humans. The fascinating lives of wild orcas contrast poignantly with the extreme limitations of their mundane captive existence. Like the 1993 film *Free Willy*, the book sharpens the rhetoric on both sides of debates over whether animals, particularly large mammals, should be kept in captivity. Zoo and aquarium supporters emphasize benefits such as saving endangered species and educating the public. Although noble, these pursuits are unlikely to sway readers of this tragic story, who may join the author in concluding that orcas should never be kept in captivity. **– Orla Smith**

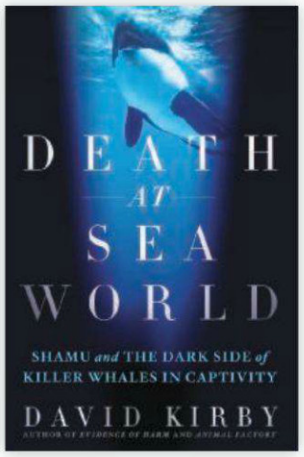

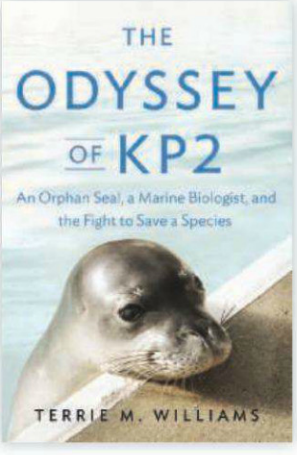

The Odyssey of KP2: An Orphan Seal, a Marine Biologist, and the Fight to Save a Species. Terrie M. Williams. Penguin, New York, 2012. 301 pp. $27.95, £17.46. ISBN 9781594203398.

Organismal biologists have long been taught that when it comes to research, it is populations that matter. Recently we have become more aware of the importance of individuals; some species are now so threatened that a single member can contribute substantially to their persistence. In her story of an orphaned, endangered Hawaiian monk seal, KP2, physiologist Williams takes readers on a moving exploration of these considerations. In her research, she has largely toed the "individuals don't matter" line. However, her account reveals an appreciation for individual animals as unique beings, even as her focus remains on their potential contribution to species conservation. Her inspiring tale of this seal, and the people he ensnares with his charisma, provides insights into the history, biology, and predicament of monk seals. While KP2's saga is captivating, perhaps more compelling is the author's own story, especially the emotional strands evident between the lines. The scientific life generally comes with a price. But, Williams argues, saving species, and sometimes even individuals, is worth the cost. **– Sacha Vignieri**

Zoobiquity: What Animals Can Teach Us About Health and the Science of Healing/What Animals Can Teach Us About Being Human. Barbara Natterson-Horowitz and Kathryn Bowers. Knopf, New York, 2012. 320 pp. $26.95. ISBN 9780307593481. Virgin, London. Paper, £12. ISBN 9780753539835.

As a pet owner, I can attest to the recent explosion of veterinary care for domestic animals. This has expanded both diagnostic and treatment options

available for a slew of animal diseases, many of which have names the same as or very similar to those of human aliments. Yet few pet owners or zoo visitors likely reflect on how the knowledge of animal illnesses help inform human medicine. Cardiologist Natterson-Horowitz and writer Bowers take us through the doctor's perspective of the veterinary world for domestic, zoo, and wild animals. Through discussions with many expert specialists, they link human and zoonotic behaviors (such as nonprocreative sex) as well as pathological states that any one of us might someday experience (including heart ailments, drug addiction, infectious diseases, and compulsive behavior). Telling the story from Natterson-Horowitz's perspective, they paint vivid, easily accessible scenarios that illuminate how the study of animals helps improve human health.

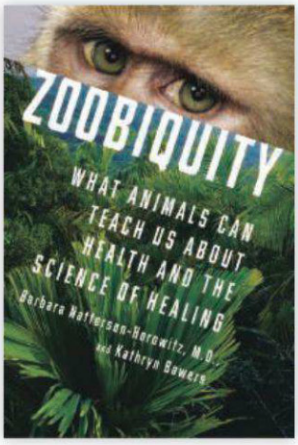

– Laura M. Zahn

The Violinist's Thumb: And Other Lost Tales of Love, War, and Genius, as Written by Our Genetic Code/And Other Extraordinary True Tales As Written by Our DNA. Sam Kean. Little, Brown, New York, 2012. 413 pp. $25.99, C$28.99. ISBN 9780316182317. Doubleday, London. £20. ISBN 978-0857520289.

An excellent storyteller, Kean weaves together history, science, and (sometimes scandalous) tales of the lives of the researchers involved in understanding the genetic code. His informative and entertaining descriptions of such topics as DNA structure and replication, natural selection and evolution, transposable elements, paleovirology, the information content of DNA, and genetics and diseases provide details that will occasionally surprise even investigators in the field. Although his colloquialisms will sometimes jar conservative readers, his creativity—such as in depicting hydrogen bonding in terms of a proton's "exposed derriere" or noting the ability of genes like *hox* to map out body plans with "GPS-like precision"—keep this fact-filled book from becoming dry. Like any good raconteur, Kean takes his audience on interesting digressions. For example, he enlivens a discussion of the role of vitamin A in cell differentiation with the adventures of sailors in 1594 who, while searching for a passage to Asia, became violently ill after gorging on polar bear liver. Notes at the back offer references for (or, occasionally, tone down) some of his statements. On balance, Kean does justice to the actors in this extraordinary saga and to the investigations themselves.

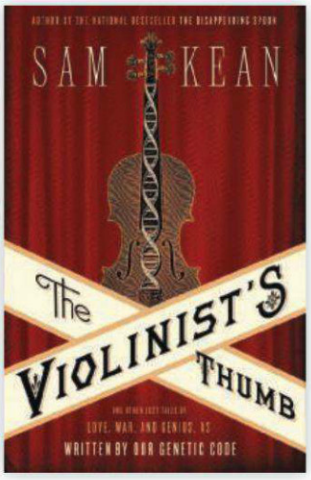

– Barbara R. Jasny

10.1126/science.1232263

FOR YOUNGER READERS

Finalists for the Royal Society's Young People's Book Prize

With its Young People's Book Prize, the Royal Society celebrates books that effectively communicate science to readers up to age 14. In April, publishers were invited to submit for consideration titles that first appeared in English in 2011 and that weave substantial science into their content, narrative, or theme.

A jury of adults—neuroscientist Andrea Brand (University of Cambridge), inventor Mark Champkins (Science Museum, London), science presenter Greg Foot (British Broadcasting Corportation), science teacher Anna Parrish (Coloma Convent Girls School, Croydon) and astrophysicist Angela Taylor (Oxford University)—trimmed the list of nominations down to six finalists. Although these differ in terms of the topics covered and the age group targeted, each succeeds at combining text and design to effectively present science.

The shortlisted titles were distributed to 100 judging panels in schools and youth groups from around the United Kingdom. On the basis of the combined decisions of these panels of young readers, the £10,000 prize was awarded last month to Robert Winston and Ian Graham for Science Experiments. (The other finalists each received £1000.) Your young readers may have their own preferences, but all six books clearly further the Royal Society's goal to "inspire an interest in the joy, wonder and excitement of scientific discovery."

How the Weather Works: A Hands-On Guide to Our Changing Skies and Climate/A Hands-On Guide to Our Changing Climate. Christiane Dorion, illustrated by Beverley Young. Templar, Dorking, Surrey, UK, 2012. 18 pp. £14.99. ISBN 9781848771956. Candlewick, Somerville, MA. $17.99, C$20. ISBN 9780763652623.

Dorion and Young pack a great deal of information about weather and climate into nine hands-on spreads. They describe the fundamental role of the Sun, the cycling of water (through evaporation, condensation, precipitation, and infiltration or run-off), weather fronts, and wind patterns. Their introduction to weather prediction includes folklore (some reliable, such as low-flying birds before rains and a blow), meteorologists' instruments, and weather maps. They discuss climates and the factors responsible for them, and they chart the occurrence of cold, cool, warm, and hot times through Earth's past. They end by considering the current warming and ways in which human activities can affect climate. Pop-ups illustrate the patterns of global winds, the structure of hurricanes, and how we add greenhouse gases to the atmosphere. Readers can lift flaps or pull tabs to reveal details such as the behavior of monsoon winds and the cause of convectional rainfall. The previous title in the series won last year's prize, and children (and their parents) are likely to find this book as stimulating and hard to put down.

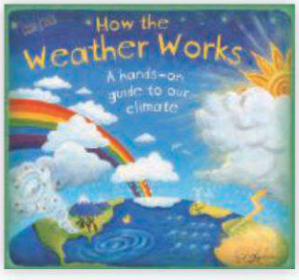

– Sherman J. Suter

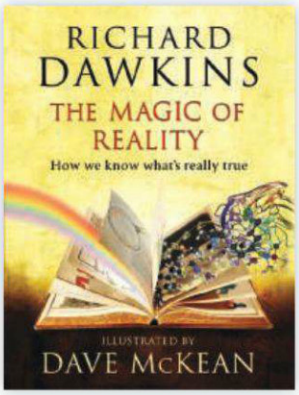

The Magic of Reality: How We Know What's Really True. Richard Dawkins, illustrated by Dave McKean. Bantam, London, 2011. 272 pp. £20. ISBN 9780593066126. Free Press, New York, 2012. Paper, $19.99, C$22.99 ISBN 978-1451690217.
Despite some resemblance to a textbook, Dawkins's latest work reads more like a novel with science cast as the heroine. In an opening discussion that contrasts science with magic, the author notes that it is at least as thrilling. He demonstrates this through a comparison of traditional creation stories with scientific accounts for the origin and evolution of life on Earth. As in his subsequent discussions of topics such as why there are so many different kinds of animals and what things are made of, Dawkins does not simply provide the answers. Instead, he walks readers through detailed descriptions of how we know those answers. McKean complements Dawkins's explanations by providing easier-to-grasp illustrations of complex ideas found in the text. Although Dawkins does not go into great depth on the many topics he covers, the book offers enough comprehensible science for middle- and high-school students to engage in constructive debates about such topics as the origin of life. **– Melissa McCartney**

Plagues, Pox and Pestilence. Richard Platt, illustrated by John Kelly. Kingfisher, London, 2011. 48 pp. £10.99, $15.99. ISBN 9780753431689 .
Four vectors (flea, rat, mosquito, and tsetse fly) guide readers through a whirlwind of facts about microbes and diseases. Nearly bursting with Kelly's amusing, colorful illustrations, the book covers pestilences such as cholera, bubonic plague, potato blight, malaria, and influenza. Platt also discusses how diseases spread and how they can be tackled. In addition to surveying histories of disease discoveries and treatments, he warns of modern threats, including the dangers of biological warfare, improper food handling, and global spread of diseases resulting from increased travel.

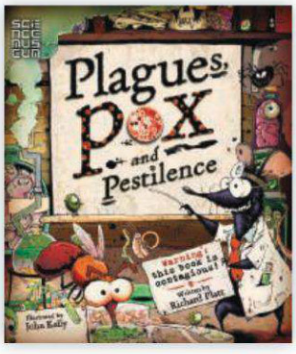

– Barbara R. Jasny

Science Experiments. Robert Winston and Ian Graham. Dorling Kindersley, London, 2011. 144 pp. £14.99. ISBN 9781405362863.
"Science starts with experiments," Winston notes in his introduction to this collection of hands-on activities. The 85 demonstrations reveal aspects of materials ("slime time"), forces and motion ("puzzling pendulums"), energy ("make a spectroscope"), electricity and magnetism ("tiny lightning"), and the natural world ("revive a carrot"). For each, the authors provide a list of materials needed (most of which can be found around the house), step-by-step instructions, and the expected results. They also offer short explanations of the underlying scientific principles. The individual experiments range from simple to quite tricky, and around half of them should be supervised by an adult. By making discovery fun, the experiments are likely to start some readers toward science. (Some of the demonstrations had that very effect on Winston himself.) **– Sherman J. Suter**

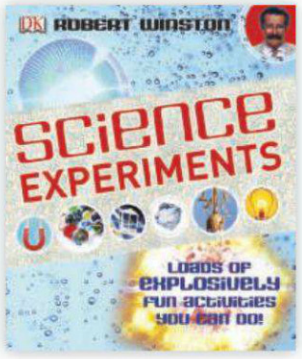

Out of This World: All the Cool Bits About Space. Clive Gifford, illustrated by Andrew Pinder. Buster Books, London, 2011. 128 pp. £7.99. ISBN 9781907151941.
Mars has the largest volcano in the solar system. A relatively nearby brown dwarf star runs at a temperature close to that of a cup of tea, a tepid contrast indeed to our own Sun. And signals from the first-discovered pulsar (1967) were named LGM-1 for "little green men." Gifford provides a trove of such facts, covering the standard fare of astronomy as well as entertaining with little bits of information that bring discovery to life. Historical notes provide context—reminding us, for example, that there can be little patience for getting things right (in ancient Greece, Anaxagoras was evicted from Athens for asserting that Earth orbits the Sun) and little patience for getting things wrong (in ancient China, astronomers His and Ho were executed for failing to predict a solar eclipse). The text can be approached as either a continuous read or a fact-finding mission. Line drawings with some levity put aliens to work explaining our universe, and diagrams explain difficult-to-grasp aspects of astronomical tools and features. Middle-school stargazers (practicing and prospective alike) will find themselves amused and informed.

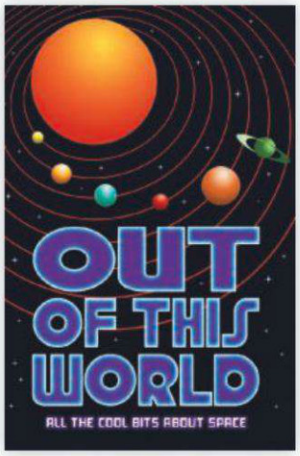

– Pamela J. Hines

See Inside Inventions. Alex Frith, illustrated by Colin King. Usborne, London, 2011. 16 pp. £10, $13.99. ISBN 9781409532729.
Some inventions, such as hook-and-loop fasteners (Velcro), are the quick result of a careful observation combined with a creative mind. Others, such as photography, develop over years (sometimes thousands of years) of refinement. This lift-the-flap book is filled with curious facts about the how, who, and why of inventions we now take as normal parts of our world. Each page highlights a particular concept (for example, engines, flying, or infectious disease). Raising flaps to reveal further vignettes and explanatory drawings makes reading the book an interactive experience. One flap hides a message sent through a very early telegraph machine. (Given that the message was limited to 23 letters, the operators could have used a lesson from today's tweeters and texters.) The final page of "crazy contraptions" that didn't quite work out reminds us that some concepts appear before their time. Altogether, this well-illustrated exploration of problem-solving creations should entertain and inform the elementary-school bracket. **– Pamela J. Hines**

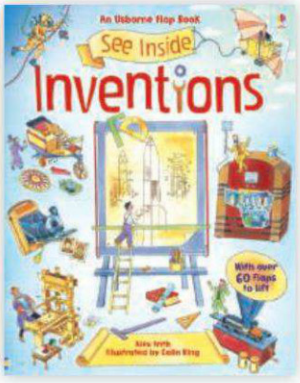

10.1126/science.1232264

Science Translational Medicine AAAS

Science Translational Medicine is pleased to announce the

AAAS Martin and Rose Wachtel Cancer Research Award

This new annual award will honor an early-career cancer researcher who has performed outstanding work in the field of cancer research. Nominees must have received their PhD or MD within the last 10 years. The award winner will be invited to deliver a public lecture on his or her research and will receive a cash award of $25,000. The award winner's Perspective will be published in *Science Translational Medicine*.

Call for Nominations

Due by Friday
February 1st, 2013

Nomination packages must include the following materials, written in English:

» A letter describing the nominee's significant contributions to cancer research, including supporting publications. The letter should explain how the candidate's research promises to make a lasting impact on the cancer field.

» Two letters of support from other individuals.

» The nominee's curriculum vitae.

» A Perspective (*1500 words maximum, 1 figure*) written by the nominee describing their research project and explaining how it advances our understanding of cancer. The research described in the Perspective must be in the field of cancer and the nominee must have performed or directed the work within the last 10 years.

Submit nominations to **WachtelPrize@aaas.org** and put "Wachtel Award Nomination" in the subject line.

This award is funded by an endowment established through a bequest from Martin Wachtel and is presented by Science Translational Medicine.

Produced by the *Science*/AAAS Custom Publishing Office

LIFE SCIENCE TECHNOLOGIES

Tissue Engineering

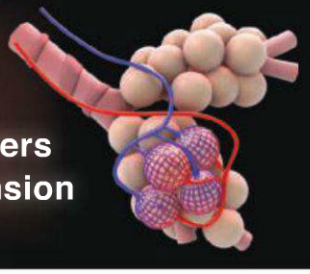

Cell Culture Enters the Third Dimension

In This Issue

Scientists have been culturing mammalian cells in flat petri dishes for decades, but a new generation of tools and techniques is now letting them grow three-dimensional cultures that more closely mimic the biology of real tissues.

See full story on page 1366.

Upcoming Features

The Connectome—January 18, 2013
Genomics—February 15, 2013
Proteomics—March 1, 2013

Lambda TLED™
Transmitted Light Source

High-output white light LED!

NEW!

FEATURES

- >10,000 hour lifetime
- >25µsecs on-off time
- TTL control (with polarity switch)
- Very stable output
- Compact stand-alone design
- Easy installation

SUTTER INSTRUMENT

PHONE: 415.883.0128 | FAX: 415.883.0572
EMAIL: INFO@SUTTER.COM | WWW.SUTTER.COM

STEM CELLS

U.S. Regulation of Stem Cells as Medical Products

Premarketing approval by the federal government should ensure not only safety, but efficacy as well.

Douglas Sipp,[1]* and Leigh Turner[2,3,4]

A recent decision by a U.S. District Court judge could have profound implications for the increasing number of U.S. clinics that advertise putative "stem cell treatments" for a wide range of clinical, rejuvenation, and aesthetic applications. In *United States* v. *Regenerative Sciences LLC* et al., the court upheld the authority of the Food and Drug Administration (FDA) to require the premarketing approval of human stem cell–derived products that meet any of several broad criteria (*1*). The court concluded that the cultured autologous mesenchymal stem cell–based product at issue in the case is subject to FDA regulatory oversight, as it meets criteria for classification as a biological drug, and its manufacture, distribution, and sale constitute interstate commerce. Although the court described the decision, which has been appealed, as "a close question," this new ruling reaffirming FDA authority has prompted heightened interest in the regulation of stem cells as medical products.

Safety, Efficacy, Commerce, and Practice

The relevant federal regulations in Title 21, part 1271 of the Code of Federal Regulations (C.F.R.) call for establishments engaged in the manufacture of human cell and tissue products that meet any one of certain criteria to comply with registration, donor-eligibility, good-manufacturing, and quality-assurance requirements (*2*). These criteria include "more than minimal manipulation" of cells (such as by extended ex vivo culture or treatment with growth factors) and nonhomologous uses (such as the use of blood-forming stem cells in heart or brain tissue). This regulatory framework subjects all such stem cells and other cell-based products to regulatory review as biologics (drugs derived from living materials, rather than by chemical synthesis).

Also at issue in the recent case was the question of whether administering autologous cells to patients solely on an intrastate basis constitutes interstate commerce. The court followed precedent in ruling that any drug containing a component from out of state triggers the interstate commerce clause, which is crucial, as the FDA only has authority over commercial activities that involve the crossing of state lines. The defendants had contested this point, and it seems likely that FDA authority to regulate stem cell–based interventions delivered within the borders of a state will remain a point of contention.

Mesenchymal stem cells.

Analyses of the FDA framework for regulating human cell and tissue products have largely focused on safety issues associated with pluripotent stem cells, such as embryonic stem cells and induced pluripotent stem cells (*3*, *4*), which have not been extensively tested in clinical trials. In contrast, the overwhelming majority of clinical studies involving administration of stem cells test the use of somatic stem cells. In randomized controlled trials, such cells have generally been well tolerated (*5*–*7*). In settings with poor oversight, however, the use of putative stem cells has been accompanied by severe adverse reactions, including death (*8*, *9*). In addition, regulatory approaches to evaluation of the efficacy of stem cell products also remain little discussed.

Critics of the current federal regulations have proposed that, once safety is established, new treatments should be allowed to enter the health-care market and that efficacy should be evaluated through postmarketing reporting; some commentators think that premarketing requirements should be relaxed for stem cell treatments (*10*). Such critics believe the existing regulatory framework delays the movement of these interventions to market and impedes access to a potentially revolutionary form of medicine (*11*).

Arguments opposed to the present regulatory framework in the United States further assert that channeling stem cell interventions down the same regulatory pathway as the premarket review process for other types of drugs imposes a mass-production manufacturing model on individually "customized" autologous stem cell procedures. But the notion that a custom intervention can be marketed wholesale and directly to consumers is problematic and does not, in any case, appear to apply to apparently indistinguishable ex vivo–manipulated products marketed for wide ranges of conditions. Also, the mere fact that a product uses processed autologous cells does not mean that it is therefore customized.

Legal, ethical, and scientific questions concerning the optimal system for regulatory governance over stem cells also surrounded a policy approved by the Texas Medical Board in April 2012 (*12*, *13*). The policy permits physicians in Texas to administer human stem cells as investigational agents if patients consent to such procedures, the cells are provided as part of a clinical study, and the study protocols are approved by an institutional review board (IRB) or what the Texas Medical Board confusingly describes as "FDA/National Institutes of Health." The policy is controversial because it appears to challenge the regulatory authority of the FDA by stating that researchers can choose between submitting their research protocols to the FDA or local IRBs. Commentators have been sharply divided over the meaning, scope, internal consistency, and legal status of this policy. Whether it was intended to supplement or challenge federal oversight of stem cells remains unclear.

Whatever the intended purpose of the policy, it seems likely that in the event that stem cell clinics and banks in Texas are inspected by FDA investigators, they will draw upon these new rules should they decide to challenge the FDA's authority by claiming that administration of stem cells to patients on an intrastate basis falls within the scope of medical practice and the Texas Medical Board's purview and is therefore not subject to FDA oversight. This view was echoed by Texas Governor Perry at a recent meeting sponsored by one such company, Celltex Therapeutics (*14*). As noted above, the recent District Court ruling hinged in part on a close analysis of what constitutes interstate com-

CREDIT: C. MAHAPATRA/WIKIPEDIA

[1]RIKEN Center for Developmental Biology, Kobe 12345 Japan. [2]University of Minnesota Center for Bioethics, Minneapolis, MN 55455, USA. [3]School of Public Health, Minneapolis, MN 55455, USA. [4]College of Pharmacy, Minneapolis, MN 55455, USA.

*Author for correspondence. E-mail: sipp@cdb.riken.jp

merce and what distinguishes state regulation of the practice of medicine from federal regulation of interstate commerce.

Efficacy, Ethics, and Law

Would allowing the sale of products of unknown effectiveness provide a reasonable, ethical, scientifically credible alternative to the current standard of requiring rigorous premarketing trials to establish safety and efficacy? The history of medicine suggests that it would not. In 1905, more than 28,000 so-called "patent medicines" were sold freely on the U.S. market without any requirement to show efficacy or, for that matter, safety (as the Pure Food and Drugs Act was not passed until the following year). Essentially, none of these products remains available or in demand today; this is presumably because many of them did not work (*15*). Similarly, after the 1962 Kefauver-Harris amendment expanded premarket requirements to include establishing efficacy, post hoc studies resulted in the withdrawal from the market of nearly 40% of products tested.

Furthermore, obtaining informed consent from patients requires describing both risks and benefits to prospective treatment recipients. Valid efficacy data are needed if clinicians are to responsibly describe benefits and risks, compare stem cell–based interventions with alternative procedures, and help patients make informed decisions. It seems clear that patients agree to pay for treatment, even when it is described as "experimental," because they believe that they can expect meaningful benefit from receiving stem cells and that the likelihood and degree of potential benefit outweighs that of potential harm. Without convincing evidence for efficacy, stem cell interventions to are not likely become part of the science-based practice of medicine, particularly in commercial form.

Controlled, randomized clinical trials of any intervention are needed to assess toxicity, to establish safety and dose, and to determine whether a given intervention is efficacious in treating a particular condition (*16*). Postmarketing studies typically do not produce the same quality of evidence, because the agent being studied is not compared against a placebo or alternative in a control group; recipients and health-care providers are not blinded, and there is no effort to address well-known biases; and randomization does not occur. In short, for scientific and ethical reasons, both safety and efficacy need to be studied in registered controlled trials, and data should have to be presented to a competent regulatory authority and reviewed before stem cell interventions enter the marketplace.

Are stem cells truly safe and efficacious when used in the treatment of human medical conditions? Rigorous scientific testing and decades of clinical experience with bone marrow and other tissues rich in hematopoietic stem cells has shown their great utility as a component of treatments for cancers and other diseases of the blood and immune systems (*17*), and the FDA has already approved three allogeneic cord blood–derived products for such uses. The use of bone marrow—and, later, peripheral and umbilical cord blood—to reconstitute the blood system after cancer treatment was introduced in academic settings before the current requirements and only entered standard of care for certain indications after years of clinical testing. Many other types of stem cells are currently being tested for use as therapies for particular conditions; however, the FDA is right to keep the gateway to the American medical market closed until well-designed clinical trials find evidence of both safety and, crucially, efficacy.

Global Challenges

Whereas the European Union and Canada—which have established regulatory frameworks similar to those in the United States—have been broadly effective in preventing clinics from selling unapproved stem cell interventions, several other countries have struggled when faced with the challenge of addressing domestic proliferation of clinics marketing stem cell "therapies." In Japan and Australia, for example, current legislation provides enormous latitude for individual physicians to market autologous stem cells directly to patients without first obtaining approval from national regulatory bodies. As a result, both countries have numerous clinics that advertise purported autologous stem cell treatments for an astonishingly wide array of unrelated medical conditions and do so with virtual impunity, as has been noted with concern by scientists working in those countries (*18*, *19*).

Similarly, China (*20*) and India (*21*) have yet to establish legally binding regulations over stem cell interventions, enabling a great many spurious stem cell clinics to operate openly, and enticing large numbers of domestic and international patients to pay thousands of dollars for treatments of doubtful safety and medical value. Both countries are now working to develop stricter regulations intended to close this gap. Ironically, despite its stringent regulatory requirements, the United States is also home to numerous companies that offer ostensible stem cell–based treatments in apparent violation of the law (*22*).

Regulatory systems that require extensive independent oversight and premarket scientific testing of drugs and devices for safety and efficacy are undeniably confronted with issues of high costs, long development times, and the potential for public frustration when interventions once viewed as promising fail to demonstrate their worth. But if patients are to have confidence that marketed health-care products, including cell-based ones, are not only safe to take but are worth taking at all, then conformity with scientific and regulatory standards is essential.

Much of the contemporary debate concerning federal regulation of stem cells and other emerging biomedical technologies focuses on whether hurdles to market entry should be lowered. Given the efforts by various companies to bypass efficacy requirements and to promote their inadequately tested products directly to consumers, perhaps the more meaningful question is whether the regulation of stem cell–based interventions in the United States needs to be more rigorously enforced through injunctions and seizures with significant consequences for violators who, by their actions, jeopardize public health and patient safety; undermine trust in the integrity of the health-care system; and risk damaging the field of stem cell research.

References and Notes

1. *United States of America* v. *Regenerative Sciences, LLC et al.*, Civil Action No. 2010-1327 (RMC) US District Court DC (2012); https://ecf.dcd.uscourts.gov/cgi-bin/show_public_doc?2010cv1327-47=.
2. U.S. C.F.R., Title 21, Part 1271 (2012); www.accessdata.fda.gov/scripts/cdrh/cfdocs/cfcfr/CFRSearch.cfm?CFRPart=1271.
3. D. G. Halme, D. A. Kessler, *N. Engl. J. Med.* **355**, 1730 (2006).
4. D. W. Fink Jr., *Science* **324**, 1662 (2009).
5. D. J. Prockop *et al.*, *Cytotherapy* **12**, 576 (2010).
6. A. Giannakopoulou *et al.*, *Exp. Neurol.* **230**, 16 (2011).
7. M. M. Lalu *et al.*, *PLoS ONE* **7**, e47559 (2012).
8. D. Thirabanjasak, K. Tantiwongse, P. S. Thorner, *J. Am. Soc. Nephrol.* **21**, 1218 (2010).
9. Y. J. Alderazi *et al.*, *J. Child Neurol.* **27**, 632 (2012).
10. A. von Eschenbach, *Wall Street Journal*, 14 February 2012, p. A19.
11. S. Gottlieb, C. Klasmeier, *Wall Street Journal*, 8 August 2012, p. A13.
12. J. Kaiser, *Science* **336**, 284 (2012).
13. A. D. Levine, *Regen. Med.* **7**, 451 (2012).
14. L. Johnson, Governor Perry wants more stem cell research in Texas, Houston Public Radio, 26 October 2012.
15. D. P. Carpenter, *Reputation and Power: Organizational Image and Pharmaceutical Regulation at the FDA* (Princeton Univ. Press, Princeton, NJ, 2010), p. 77.
16. J. D. Steeves, J. Zariffa, J. L. Kramer, *Yonsei Med. J.* **52**, 701 (2011).
17. G. Q. Daley, *Cell Stem Cell* **10**, 740 (2012).
18. H. Ikegaya, *Nature* **489**, 33 (2012).
19. M. F. Pera, M. Munsie, Submission to the NHMRC Public Consultation—Stem cell treatments: A quick guide for medical practitioners, and Frequently asked questions: A resource for patients (National Health and Medical Research Council, Canberra, Australian Capital Territory, 2012).
20. D. Cyranoski, *Nature* **484**, 149 (2012).
21. P. K. Patra, M. Sleeboom-Faulkner, SCRIPTed J. *Law Technol. Sci.* **7**, 295 (2010).
22. D. Cyranoski, *Nature* **477**, 377 (2012).

10.1126/science.1229918

CHEMISTRY

Putting a Greenhouse Gas to Work

Fluoroform (CHF_3), a waste product that has been destroyed, can now be used to synthesize a wide variety of fluorinated compounds.

Günter Haufe

In 2011, 3 of the 10 best-selling pharmaceuticals and 7 of the 35 newly approved active ingredients were compounds bearing organofluorine groups such as trifluoromethyl (CF_3) (*1*). Similar statistics hold for agrochemicals. Organofluorine groups confer useful properties such as high lipophilicity (and membrane permeability) and enhanced metabolic stability. The vast majority of methods for the introduction of CF_3 groups are based on $CBrF_3$ (either directly or as a starting material) and similar ozone-depleting substances that have their atmospheric emission strictly regulated by the Montreal protocol. Thus, new trifluoromethylating reagents are highly desirable. On page 1324 of this issue, Prakash *et al.* (*2*) report on direct nucleophilic trifluoromethylation reactions of a variety of silicon, boron, sulfur, and, most interestingly, carbon electrophiles using only stoichiometric amounts of CHF_3 (fluoroform) facilitated by optimizing the base and solvent used in the reaction. This compound is actually an unwanted greenhouse-gas byproduct from the production of fluoropolymers and refrigerants (see the figure).

The synthesis of a particular organofluorine molecule is still challenging because an organic reaction that normally would proceed smoothly might not work as well once parts of the molecule are fluorinated. The extent of fluorination desired is often not high; most pharmaceuticals contain either a single aliphatic or aromatic fluorine atom or a CF_3 group attached to aliphatic, aromatic, or heteroaromatic positions (*3*, *4*). A most promising source for a fluorinating agent is CHF_3 (trifluoromethane, also known as fluoroform, Freon 23, HFC 23, and R-23) because it is available at a rate of thousands of tons per year. Its global warming potential is up to 15,000 times that of carbon dioxide, and it has an atmospheric lifetime of 264 years (*5*), but there has been no major use for CHF_3. Instead, it is decomposed at great costs by thermal oxidation, catalytic hydrolysis, plasma destruction, or conversion to environmentally benign compounds (*5*).

The problem with using CHF_3 versus $CBrF_3$ is that the C-H bond is much stronger than the C-Br bond, and it requires activation by a strong base. CHF_3 is a weak carbon acid with an acidity constant or pK_a of 25 to 28 in water, intermediate between esters and amine. The development of bases to activate dates back more than 20 years, although the methods have had limited scope. The electrochemically generated anion of pyrrolidone deprotonates CHF_3, and the CF_3 anion formed can add to carbonyl groups efficiently in dimethylformamide (DMF) in the presence of hexamethyldisilazane (*6*). Furthermore, treatment of CHF_3 with strong organic bases in the presence of DMF provided a form of the CF_3 anion stabilized as a hemiaminolate species, which reacted with carbonyl compounds (*7*). Recent studies demonstrated the direct transition-metal–mediated substitutive trifluoromethylations of aromatic and heteroaromatic halides, including those applying fluoroform as starting material, as highlighted recently (*8*).

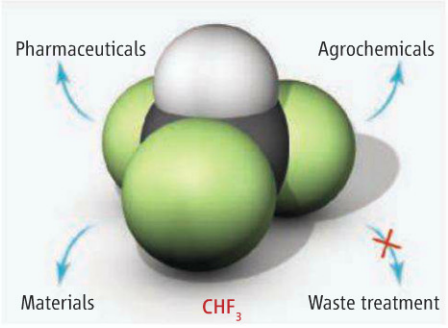

Repurposing fluoroform. A major by-product of the industrial synthesis of fluoropolymers and refrigerants, CHF_3 is a powerful greenhouse gas that must be destroyed as a waste. Its use as a common fluorinated building block, as developed by Prakash *et al.*, should allow its use in synthesis of pharmaceuticals, agrochemicals, and materials.

In general, CF_3 groups can be transferred to organic substrates by C-C bond formation using three different strategies. In addition to nucleophilic, radical and electrophilic trifluoromethylations also were extensively used (*9*), and asymmetric variations to trifluoromethylate carbonyl compounds were developed (*10*). Recently, both electrophilic (*11*) and radical trifluoromethylations (*1*) have undergone a renaissance.

Alternatively to the C-C bond-forming methods, the CF_3 group can also be prepared from the corresponding CCl_3 unit by treatment with different inorganic fluoride sources such as KF or HF (*12*), from carboxylic acids by treatment with SF_4 in HF, or by oxidative desulfurization-fluorination by treatment of dithiocarboxylic acid esters (*13*) or even aryl thioethers (*14*) with electrophiles in the presence of fluoride sources.

All these pathways do serve perfectly for particular applications but lack general applicability, are based on potentially dangerous and expensive reagents, or suffer from both drawbacks. In contrast, the method developed by Prakash *et al.*, in which the use of potassium hexamethyldisilazide (KHMDS) as the base in common organic solvents such as THF or toluene was carefully optimized, provides smooth access to reagents such as trifluoromethyl trialkylsilanes or trifluoromethyl trialkylborates. The latter can be transformed to the increasingly important trifluoromethyl trifluoroborate anion. Furthermore, aromatic nonenolizable ketones, aldehydes, chalcones, formate esters, benzyl bromide, and methylbenzoate were successfully trifluoromethylated in moderate to good yields. Thus, this method is a welcome extension of the toolbox for trifluoromethylation of various silicon, boron, sulfur, and carbon compounds. In the future, additional—preferably atom-economic and environmentally benign—methods will be desired.

Organisch-Chemisches Institut, Universität Münster, D-48149 Münster, Germany. E-mail: haufe@uni-muenster.de

References

1. A. Studer, *Angew. Chem. Int. Ed.* **51**, 8950 (2012).
2. G. K. S. Prakash, P. V. Jog, P. T. D. Batamack, G. A. Olah, *Science* **338**, 1324 (2012).
3. S. Swallow, in *Fluorine in Pharmaceutical and Medicinal Chemistry. From Biophysical Aspects to Clinical Applications*, V. Gouverneur, K. Müller Eds. (Imperial College Press, London, 2012), pp. 141–174.
4. E. P. Cormier, M. Das, I. Ojima, in *Fluorine in Medicinal Chemistry and Chemical Biology*, I. Ojima, Ed. (Wiley-Blackwell, Chichester, 2009), pp. 525–603.
5. W. Han, Y. Li, H. Tang, H. Liu, *J. Fluor. Chem.* **140**, 7 (2012).
6. T. Shono, M. Ishifune, T. Okada, S. Kashimura, *J. Org. Chem.* **56**, 2 (1991).
7. B. R. Langlois, T. Billard, *ACS Symp. Ser.* **911**, 57 (2005).
8. O. A. Tomashenko, V. V. Grushin, *Chem. Rev.* **111**, 4475 (2011).
9. J.-A. Ma, D. Cahard, *J. Fluor. Chem.* **128**, 975 (2007).
10. J.-A. Ma, D. Cahard, *Chem. Rev.* **108**, PR1 (2008).
11. N. Shibata, A. Matsnev, D. Cahard, *Beilstein J. Org. Chem.* **6**, 65 (2010).
12. M. A. McClinton, D. A. M. McClinton, *Tetrahedron* **48**, 6555 (1992).
13. M. Shimizu, T. Hiyama, *Angew. Chem. Int. Ed.* **44**, 214 (2005).
14. V. Hugenberg, G. Haufe, *J. Fluor. Chem.* **143**, 238 (2012).

10.1126/science.1231092

BIOCHEMISTRY

Redder Than Red

Molecular engineering of a retinol binding protein defies prediction.

Thomas P. Sakmar

A chromophore is the part of a molecule that imparts its color. Arguably the most common chromophores in biology are carotenoids such as retinoids. Their absorption spectra can be tuned across a wide range of light energy by modulating the electronic environment within the protein to which they are attached. On page 1340 of this issue, Wang *et al.* (*1*) report a systematic study of the spectral tuning of an engineered all-*trans*-retinal pigment within a protein environment. Using protein engineering and x-ray crystallography, they create a palette of retinal-based pigments that reveal how electrostatics dominates spectral tuning (see the figure).

The physicochemical basis of retinoid chromophore spectral tuning is embodied in the term "opsin shift" (*2*). A model retinal chromophore compound absorbs maximally at 440 nm in methanol solution, but its absorption can be red-shifted to ~600 nm. The energy difference between 440 nm and the absorption of the pigment in question is the opsin shift. Factors that may affect the opsin shift include the presence of charged or polar amino acids in the chromophore-binding pocket, as well as protein-induced twisting of the normally planar polyene system. Just how a protein alters the electronic structure of the chromophore to cause dramatic spectral changes has been a matter of debate.

Knowledge of the opsin shift mechanism is important for understanding color vision (*3*). Most humans have three separate visual pigments—blue, green, and red—that absorb light maximally at ~420, ~530, and ~560 nm, respectively (*4*–*6*). In each case, the chromophore is the same: a vitamin A aldehyde linked to a lysine residue by a Schiff base (a carbon-nitrogen double bond). Spectral tuning is achieved by genetic differences in the opsin genes that encode different amino acid sequences in the binding pocket of the chromophore. Other animals are much more spectrally endowed than humans. The mantis shrimp, for example, has 12 spectral channels from ultraviolet to deep red (*7*). But in all cases, the visual chromophore is retinal (vitamin A aldehyde), or a very closely related hydroxyl or dihydro form of vitamin A.

Light-activated channelrhodopsins from the green alga *Chlamydomonas* also contain retinal and are used as tools in optogenetics (in which optics and genetics are integrated at the cellular level to control an organism's physiology and behavior). In these channelrhodopsins, desirable spectral properties such as red-shifted absorption can be engineered by site-directed mutagenesis.

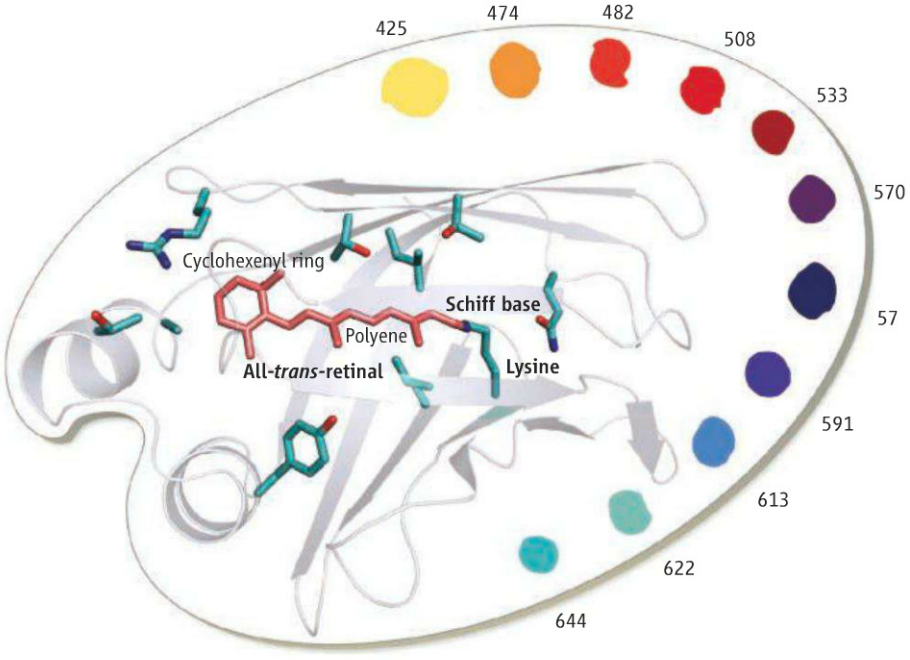

Expanding the color palette of a retinal-based pigment. Wang *et al.* have engineered the CRBPII binding pocket for the all-*trans*-retinal chromophore to tune its absorption. They introduced a lysine residue to facilitate a Schiff base linkage of the chromophore to the protein, and replaced other amino acid residues by site-directed mutagenesis to create pigments with increasing red shifts. Shown along the edge are the maximal absorption wavelengths of the mutant pigments in nanometers.

As a model system to study spectral tuning and the opsin shift mechanism, Wang *et al.* used a rationally engineered version of human cellular retinol binding protein II (CRBPII), a soluble retinol transport protein found mainly in the gut. The crystal structures of the retinol-bound and retinol-free forms of this protein are virtually identical, creating a scaffold where the effects of amino acid side chain substitutions might be revealed without significant secondary effects (*8*). The key enabling mutation was to introduce a lysine residue in the proper position so that retinal could replace retinol (the usual ligand for CRBPII) and could form the covalent protonated Schiff base bond characteristic of all retinylidene pigments (*9*).

Once the stable pigment was formed, Wang *et al.* carried out systematic rational mutagenesis and solved crystal structures for several pigments to test their hypothesis that an electrostatic field completely dispersed along the polyene should allow a "super red" pigment. A key conceptual jump was to mutate the negative counterion that would normally compensate for the positive charge on the Schiff base imine.

To form a protonated Schiff base in the core of the protein without a compensatory negative counterion was counterintuitive. But in fact, the absence of a counteranion causes more charge delocalization along the polyene and facilitates red shifts. Further disruption of hydrogen bonding with the imine by replacing a glutamine with an arginine caused a massive red shift. Removal of hydroxyl-bearing amino acids along the polyene caused additional red shifts, as did the introduction of polarizable groups.

Laboratory of Chemical Biology and Signal Transduction, The Rockefeller University, New York, NY 10065, USA. E-mail: sakmar@rockefeller.edu

CREDIT: KARINA ÅBERG

Knowledge of the crystal structures of successively engineered pigments was crucial when Wang *et al*. tried to isolate the retinal binding pocket from the surrounding aqueous environment. They replaced an arginine residue at the entrance of the binding pocket by a tryptophan residue to plug the aqueous opening. Replacement of an alanine with another tryptophan further dehydrated and encapsulated the binding pocket.

The crystal structures of the most red-shifted mutants showed almost no twisting of the retinal polyene, with the cyclohexenyl ring and polyene almost coplanar. Thus, extreme red shifts were achieved with almost no apparent contribution from conformational effects. Once the binding pocket of the chromophore was dry and insulated, it was possible to distribute the electrostatic potential uniformly along the polyene, and the positive charge from the Schiff base imine became completely delocalized. The most highly engineered pigment absorbed maximally at 644 nm (see the figure), redder than any retinal-based pigment previously reported and even redder than predicted to be possible for that chromophore (*10*).

The theoreticians will have a field day with the redder-than-red structures reported by Wang *et al*. And although it is not likely that transmembrane proteins such as visual pigments and channelrhodopsins can be engineered analogously because they are more dynamic and flexible, molecular and chemical biologists will certainly try. It will be interesting to see how the principles elucidated here might be applied to other systems with the aim of expanding the color palette in photoactive biological systems.

References

1. W. Wang *et al*., *Science* **338**, 1340 (2012).
2. K. Nakanishi, V. Balogh-Nair, M. Arnaboldi, K. Tsujimoto, B. Honig, *J. Am. Chem. Soc.* **102**, 7945 (1980).
3. G. G. Kochendoerfer, S. W. Lin, T. P. Sakmar, R. A. Mathies, *Trends Biochem. Sci.* **24**, 300 (1999).
4. J. Nathans *et al*., *Science* **232**, 193 (1986).
5. D. D. Oprian, A. B. Asenjo, N. Lee, S. L. Pelletier, *Biochemistry* **30**, 11367 (1991).
6. S. L. Merbs, J. Nathans, *Nature* **356**, 433 (1992).
7. J. Marshall, J. Oberwinkler, *Nature* **401**, 873 (1999).
8. M. Tarter *et al*., *Proteins* **70**, 1626 (2008).
9. C. Vasileiou *et al*., *J. Am. Chem. Soc.* **129**, 6140 (2007).
10. R. Rajamani, Y. L. Lin, J. Gao, *J. Comput. Chem.* **32**, 854 (2011).

10.1126/science.1231589

CHEMISTRY

Atomic Layer Electrodeposition

An electrochemical process provides a cheap and simple route to layer-by-layer growth of metal films.

Jay A. Switzer

The growth of ultrathin films is generally hindered by roughening and three-dimensional mound formation. Atomic layer deposition (ALD), in which atomic layer control and conformal growth are achieved through sequential, self-limiting surface reactions (*1*), can eliminate or reduce such roughening. One application of ALD is to deposit ultrathin layers of expensive metals such as Pt that are used, for example, as the catalyst in proton-exchange membrane fuel cells (*2*). Besides the economic incentives to produce ultrathin films (*3*), there are also scientific payoffs—they often have catalytic, electronic, or magnetic properties that are not found in the bulk material (*4*–*6*). Although ALD processes are usually conducted in the vapor phase, Liu *et al*. (*7*) show on page 1327 of this issue that they can sequentially electrodeposit two-dimensional Pt layer by layer by simply pulsing the applied electrochemical potential in a single plating bath. The process is inexpensive and rapid. Because each layer is produced by cycling the potential rather than by exchange of reactants, electrochemical ALD could be orders of magnitude faster than vapor-phase ALD.

Electrodeposition is a bottom-up processing method, because the solid is assembled from ionic or molecular precursors in solution. It is similar in many ways to biomineralization, because solution additives and pH can be used to control the growth. Hence, the size, shape (*8*), crystallographic orientation, and even chirality (*9*) can be tuned. Compared with deposition from ultrahigh vacuum, electrodeposition is inexpensive, and the deposition rates can be much higher. It is not a line-of-sight process, so conformal films can be grown on complex shapes—for instance, in the on-chip deposition of copper interconnects into submicrometer-sized features of semiconductor devices.

What distinguishes electrodeposition from other deposition techniques is the applied potential, a single parameter that controls the departure from equilibrium and, therefore, the rate of the reaction. The electrodeposition of metals requires only that the electrode potential be driven negative of the equilibrium potential. The difference between the applied potential and the equilibrium potential is called the over-

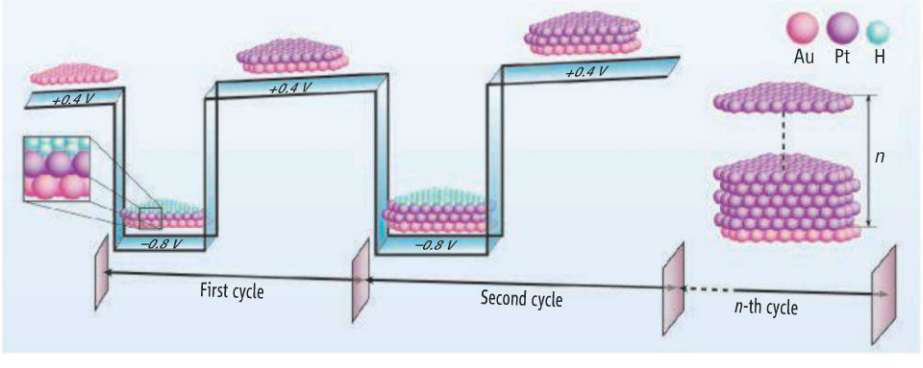

One step at a time. Electrochemical atomic layer deposition of ultrathin Pt films (*7*) deposited one monolayer at a time by simply pulsing the electrode potential between +0.4 and −0.8 V. A capping layer of hydrogen is produced at −0.8 V that blocks the deposition of more than one monolayer of Pt. When the potential is stepped to +0.4 V, the hydrogen layer is desorbed and the cycle can begin again. The self-limiting processing method is fast because it is performed in a single plating bath, so it is not necessary to exchange reactants. The ultrathin Pt films could lower the costs of the Pt catalyst in fuel cells and provide a platform to study how the catalytic, electronic, and magnetic properties of ultrathin films evolve with film thickness (*4*–*6*).

CREDIT: C. SMITH/SCIENCE

Department of Chemistry and Materials Research Center, Missouri University of Science and Technology, Rolla, MO 65409–1170, USA. E-mail: jswitzer@mst.edu

potential. Because the electrode must be poised at a potential for deposition to occur, the substrate must be a conductor or semiconductor. In contrast, vapor-phase ALD does not require a conducting substrate.

It is also possible by underpotential deposition (UPD) to produce a highly ordered monolayer or submonolayer of a metal at potentials positive of the equilibrium potential (*10*, *11*). The substrate can be single crystalline or polycrystalline. UPD occurs because the binding of the monolayer to the foreign substrate is stronger than the binding of the monolayer to a substrate of the same material. This phenomenon is a surface-limited reaction, because only a monolayer will be deposited, regardless of how long the UPD potential is held. The self-limiting action of metal UPD allows electrochemical deposition to function as an ALD method. Electrochemical ALD has been used, for instance, to grow compound semiconductors by sequentially depositing each element in a UPD cycle (*12*).

Previous work on the atomic layer deposition of metals used a process called surface-limited redox replacement to produce ultrathin layers of metals such as Pt, Pd, and Ag (*13*, *14*). The atomic layer deposition is realized by galvanic replacement of underpotentially deposited metal monolayers of less noble metals such as Pb or Cu. The surface-limited redox replacement occurs spontaneously, because the reduction potential of the less noble metal is more negative than that of the subsequent ALD layer. The two deposition steps in the surface-limited redox replacement of metals must be performed in separate solutions, so it is necessary to exchange reactants, much like the case of ALD by vapor deposition methods.

Conventional wisdom would suggest that the best way to electrodeposit ultrathin metal films would be to apply either an underpotential or a very small overpotential. Liu *et al*. report the surprising result that a monolayer of Pt is deposited at an overpotential of 1 V, a value at which the deposition rate of Pt should be very large. At this high overpotential, a monolayer of hydrogen is formed on the Pt surface, which completely blocks the deposition of additional Pt, thereby making the process self-limiting. Liu *et al*. attribute this blocking to the disruption of the electrical double layer. The trick to producing multilayers of Pt comes from the fact that the hydrogen that is deposited at –0.8 V can be desorbed at +0.4 V. By pulsing the potential between –0.8 and +0.4 V in a single plating bath, Pt is deposited on the surface monolayer by monolayer (see the figure). The deposition of a Pt monolayer is fast (complete in 1 s) and may also lead to less carryover of contaminants that occur when the reactants are exchanged in the surface-limited redox replacement scheme.

If the self-limiting growth is observed in alloys of Pt, magnetism could be imparted in the films by incorporation of magnetic metals. It would also be intriguing to deposit compositionally modulated superlattices (*15*) one monolayer at a time. As other metals have well-defined hydrogen adlayers, the prospects of this as a general processing method are encouraging. What about deposition of materials other than metals? Is there some potential-controlled process that can make the growth of metal oxides (*8*, *9*, *15*) or semiconductors (*12*) self-limiting? Ultrathin films deposited layer by layer onto single-crystalline substrates should be epitaxial. Electrochemical ALD would be ideal for in situ studies of the effect of lattice mismatch on the transition from two-dimensional to three-dimensional growth in epitaxial films. The beauty of this new electrochemical route to ALD is that it blends basic electrochemistry and surface science to unlock an important new technology.

References

1. S. M. George, *Chem. Rev.* **110**, 111 (2010).
2. L. Baker *et al*., *Appl. Phys. Lett.* **101**, 111601 (2012).
3. M. K. Debe, *Nature* **486**, 43 (2012).
4. M. S. Chen, D. W. Goodman, *Science* **306**, 252 (2004).
5. X. Jiang, T. M. Gür, F. B. Prinz, S. F. Bent, *Chem. Mater.* **22**, 3024 (2010).
6. P. Allongue, F. Maroun, *MRS Bull.* **35**, 761 (2010).
7. Y. Liu, D. Gokcen, U. Bertocci, T. P. Moffat, *Science* **338**, 1327 (2012).
8. M. J. Siegfried, K.-S. Choi, *Angew. Chem. Int. Ed.* **44**, 3218 (2005).
9. J. A. Switzer, H. M. Kothari, P. Poizot, S. Nakanishi, E. W. Bohannan, *Nature* **425**, 490 (2003).
10. D. M. Kolb, M. Przasnyski, H. Gerischer, *J. Electroanal. Chem.* **54**, 25 (1974).
11. E. Herrero, L. J. Buller, H. D. Abruña, *Chem. Rev.* **101**, 1897 (2001).
12. B. W. Gregory, J. L. Stickney, *J. Electroanal. Chem.* **300**, 543 (1991).
13. S. R. Brankovic, J. X. Wang, R. R. Adzic, *Surf. Sci.* **474**, L173 (2001).
14. N. Jayaraju, D. Vairavapandian, Y. G. Kim, D. Banga, J. L. Stickney, *J. Electrochem. Soc.* **159**, D616 (2012).
15. J. A. Switzer *et al*., *J. Am. Chem. Soc.* **132**, 1258 (2010).

10.1126/science.1231853

CANCER

The Utility of Mouse Models in Post-GWAS Research

Annabelle Lewis and Ian Tomlinson

Functional validation of a noncoding genetic variant linked to cancer risk is encouraging for genome-wide association studies.

Genome-wide association studies (GWAS) have discovered over 100 haplotype-tagging single-nucleotide polymorphisms (SNPs) that are associated with cancer risk. The small region between 128 and 129 Mb on the long arm of human chromosome 8 (Human Genome Build 37) notably contains a number of uncorrelated cancer predisposition SNPs (see the figure) (*1*–*6*). There are probably five or more different causal genetic variants in the region, and each is independently associated with the risk of one or more common cancers. Perhaps the most promiscuous variant is rs6983267—a common SNP in which guanine (G) is replaced by thymine (T)—at which the G allele is associated with increased risk of cancers of the prostate, large bowel, and thyroid. On page 1360 in this issue, Sur *et al*. (*7*) use a loss-of-function animal model to confirm that the region around the noncoding rs6983267 SNP identified using human GWAS probably has direct functional effects on tumorigenesis.

Tuupanen and colleagues previously refined the association between colorectal cancer and polymorphisms in the region around rs6983267, and concluded that rs6983267 may itself be the functional variation responsible for the differential cancer risk (*8*). Of the genes and noncoding transcripts near rs6983267, the *MYC* oncogene is a priori the best candidate for influencing tumorigenesis, despite the *MYC* coding region being several hundred kilobases away. *MYC* potentially plays a role in almost

Wellcome Trust Center for Human Genetics, University of Oxford, Roosevelt Drive, Oxford OX3 7BN, UK. E-mail: iant@well.ox.ac.uk

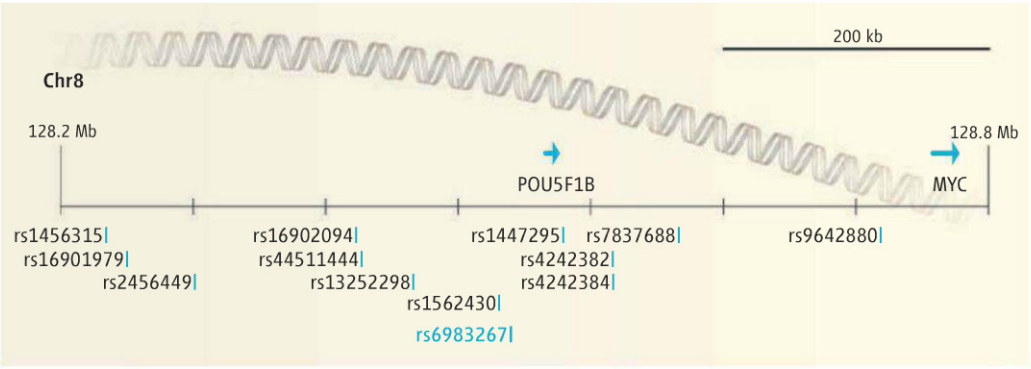

Genetic variants and risk. The cancer predisposition SNPs upstream of the *MYC* oncogene.

all cancers (*9*) and is a downstream target of several signaling pathways, including Wnt and Hedgehog. Tuupanen *et al*. showed that rs6983267 lies within an atypical binding site for the Wnt pathway effector β-catenin and the transcription factor TCF4 (TCF7L2) (*8*). TCF7L2 binds to the region surrounding rs6983267 (MYC-335), with stronger binding to the high-risk (G) allele. In a LacZ reporter mouse, MYC-335 drives transcription in a pattern similar to that of endogenous Myc expression. Others then showed that the region around rs6983267 physically interacts with *MYC* (*10*) and that the rs6983267-heterozygous colorectal cancer cell line DLD1 shows imbalanced expression of *MYC* alleles (*11*).

Unlike many polymorphisms associated with cancer risk, rs6983267 lies in a region that is conserved in mammals. Sur *et al*. tested the effects of germline MYC-335 deletion in mice, focusing on the intestinal phenotype. MYC-335–deficient ($Myc\text{-}335^{-/-}$) animals showed no abnormalities during development or as adults, and intestinal MYC expression was normal. *Myc* mRNA expression was not affected in the small bowel, but $Myc\text{-}355^{-/-}$ mice showed lower expression in whole colons compared with three paired wild-type animals. More dramatic differences were seen in $Myc\text{-}355^{-/-}$ animals when intestinal tumorigenesis was assessed with the commonly used Apc^{R850X} (*Min*) model. $Apc^{Min/+}; Myc\text{-}355^{-/-}$ animals showed a fourfold reduction in intestinal tumor numbers compared with their $Apc^{Min/+}; Myc\text{-}355^{+/-}$ and $Apc^{Min/+}; Myc\text{-}355^{+/+}$ littermates.

The findings of Sur *et al*. add to the evidence for rs6983267 being functional and for that function being mediated through *MYC*. This may seem an incremental advance, but the study provides the strongest evidence yet that the region around rs6983267 plays an important role in tumorigenesis. The authors suggest that MYC-335 could be a target for cancer prevention, given that the region surrounding *MYC* may be responsible for more cancer deaths than any other genetic region or unavoidable environmental risk factor.

This is unlikely, however, to be the end of the rs6983267 story. Questions remain. For example, although Sur *et al*. provide solid evidence for the importance of the MYC-335 region, the relevance of *MYC* itself in this context is still in question. Most studies have supported the importance of *Myc* in intestinal tumorigenesis—for example, $Apc^{Min/+}; Myc^{+/-}$ mice develop fewer polyps than $Apc^{Min/+}; Myc^{+/+}$ littermates (*12*)—but these studies used animals that had large differences in *Myc* expression. By contrast, Sur *et al*. did not find differential *Myc* expression in the normal small bowel between the $Myc\text{-}355^{-/-}$ and wild-type mice that they studied, yet most mouse tumors occur in the small intestines. Allele-specific *Myc* mRNA expression was not assessed in $Myc\text{-}355^{+/-}$ animals, and *Myc* expression in tumors was not reported. It is hard, therefore, formally to exclude the possibility that the critical gene (or genes) targeted by MYC-355 is not *MYC*. Observations in other transgenic mice have shown that gene targeting can have long-range effects that are not restricted to the sequence removed or altered, and this is a critical issue for models of the regulation of gene expression. Moreover, the possibility exists that MYC-335 additionally interacts with genes other than *MYC* in cis or in trans, and acts through them in modulating tumor growth.

If rs6983267 is truly a functional polymorphism, an additional interesting experiment would be to delete only the essential TCF4 binding motif within which the SNP lies. Sur *et al*. understandably rejected the construction of "SNP-mimic" mouse models—in which the two human alleles are directly compared—on the grounds that hundreds or thousands of mice, similar to human GWAS, might be required. Such a comparison would, however, have provided a more direct test of the effects of rs6983267 on human disease and would also have overcome the hypothetical effects of the MYC-335 deletion on nearby genes other than *Myc*. Moreover, a sample size of only 100 mice would probably have been sufficient to detect an effect of a "mouse rs6983267," assuming a modest 25% increase in tumor burden. It would also be interesting to compare tumor numbers in $Apc^{Min/+}; Myc\text{-}355^{+/-}$ and $Apc^{Min/+}; Myc\text{-}355^{+/+}$ animals, because this might provide a more apposite comparison with the human polymorphism.

The work of Sur *et al*. in the context of human disease illustrates some emerging lessons from post-GWAS science. One is that accumulation of functional evidence is likely to be time-consuming and stepwise for the time being, and high-quality studies are required. In addition, more sensitive assays of gene expression, interaction, and downstream function are needed, if all but a few exemplar polymorphisms are to be assessed. No group has yet demonstrated that the rs6983267 alleles or genotypes are associated with differential *MYC* expression in a large sample set. Further, appropriate mouse models have advantages in allowing assessment of tissue-specific effects and influences of polymorphisms on tumorigenesis, although the analysis of nonconserved regions may be more challenging in this respect. In the absence of new, inexpensive techniques or resources, "post-GWAS" functional analysis is increasingly likely to be restricted to the most interesting or famous loci, such as *MYC* and *CDKN1A*. However, should any of the cancer SNPs be shown to have importance in disease prevention, all of that might change.

References

1. C. A. Haiman *et al*., *Nat. Genet.* **39**, 954 (2007).
2. A. M. Jones *et al*., *J. Med. Genet.* **49**, 158 (2012).
3. I. Tomlinson *et al*., *Nat. Genet.* **39**, 984 (2007).
4. D. Wokolorczyk *et al*., *Cancer Res.* **68**, 9982 (2008).
5. M. Yeager *et al*., *Nat. Genet.* **39**, 645 (2007).
6. B. W. Zanke *et al*., *Nat. Genet.* **39**, 989 (2007).
7. I. K. Sur *et al*., *Science* **338**, 1360 (2012); 10.1126/science.1228606.
8. S. Tuupanen *et al*., *Nat. Genet.* **41**, 885 (2009).
9. N. M. Sodir, G. I. Evan, *Oncotarget* **2**, 1307 (2012).
10. M. M. Pomerantz *et al*., *Nat. Genet.* **41**, 882 (2009).
11. J. B. Wright, S. J. Brown, M. D. Cole, *Mol. Cell. Biol.* **30**, 1411 (2010).
12. K. Yekkala, T. A. Baudino, *Mol. Cancer Res.* **5**, 1296 (2007).

10.1126/science.1231733

NEUROSCIENCE

Inflammation to Rebuild a Brain

Inflammation in the zebrafish brain stimulates neurogenesis and tissue regeneration.

Nephi Stella

The overarching strategy of all immune systems is as predictable as the plot of an episode of *Mission: Impossible*. A short-lived message describing the problem reaches commanding immune cells. A team of specialized expert cells is then dispatched to deal with the problem. Once successfully addressed, the team disappears without leaving a trace. On page 1353 of this issue, Kyritsis *et al.* (*1*) characterize an astonishing type of immune response—a new team of "executioner" cells—that is implemented when the zebrafish brain is injured. By tricking the immune system into believing neuronal injury had occurred, the authors discovered that inflammation alone is sufficient to switch on neurogenesis. The molecular components used by the highly specialized immune cells that promote neurogenesis represent potential novel therapeutic targets that could promote brain repair.

What type of specialized effector cells ("executioner" cells) are recruited in response to tissue damage, stress, or infection? Immunologists refer to two general characters adopted by these cells: pro- and anti-inflammatory phenotypes, or M1 and M2 phenotypes when referring to macrophages (*2*). These are distinguished by increased release of free radicals (nitric oxide) or anti-inflammatory cytokines [interleukin-4 (IL-4) and IL-10], respectively. However, macrophages can adopt other phenotypes that cannot be assigned to this simplistic binary fate. For example, those that invade tissue afflicted by neurodegeneration or brain tumors adopt qualities that do not correspond to the classical M1 and M2 definitions (*3*, *4*). This implies that a more complex, multidimensional range of change in macrophage exists, allowing for the recruitment of cells that have more specialized skills than previously recognized.

Microglia, the macrophages of the brain, patrol a privileged environment that dictates their phenotypic diversity and shapes their response to specific types of neuronal damage (*5*). The brain is isolated from the rest of the body by the so-called "blood-brain barrier," which protects it from circulating toxins and peripheral immune cells. It was long thought that mammalian microglia adopt an M1 phenotype in response to neuronal damage and produce proinflammatory mediators. It is now known that microglia adopt an M2 phenotype that counterbalances and resolves the preceding M1 response. Still, this dichotomy fails to capture microglia's true phenotypic diversity. These cells can produce entirely different classes of secreted effector signals, some of which are involved in tissue repair, including growth factors (brain-derived neurotrophic factor, vascular endothelial growth factor, and transforming growth factor–β), immune response modulators (interferon-γ, monocyte chemoattractant protein–1, and C5a), and signaling lipids (prostaglandins and endocannabinoids) (*6*, *7*). Accordingly, microglia phenotype is more plastic than previously thought.

Kyritsis *et al.* show that an archetypal signaling lipid, leukotriene C4 (LTC4), singlehandedly promotes regenerative neurogenesis in the zebrafish brain (see the figure). The plethora of lipid signals that are steadily released by both injured cells within affected tissues and the invading immune cells form a dynamic network of information that fine-tunes and orchestrates the tactics implemented by immune executioner cells in mammals (*8*). How does this regenerative pathway work in zebrafish, and why doesn't it work in mammals? What other molecular components are involved? Is it necessary for executioner cells to reach a critical mass at the lesion site? If so, cell migration would be a critical feature of this inflammatory response. Kyritsis *et al.* found that production of the secreted protein S100β by glia in the zebrafish brain increased during this particular response. S100β promotes neuronal differentiation and survival in response to neuronal injury in the mammalian brain, but may promote a persistent damaging neuroinflammatory state when produced in high amounts (*9*). This protein is a predictive clinical serum marker of brain injury and increased blood-brain barrier permeability (*10*). Whether the beneficial and/or detrimental effects of S100β depend on the type of injury remains an open question.

Kyritsis *et al.* also identified the transcription factor Gata3 in both the immune executioner cells and the neuronal progenitor cells as a likely molecular switch that controls the repair phenotype of the inflammation. Could this switch be targeted by therapeutics

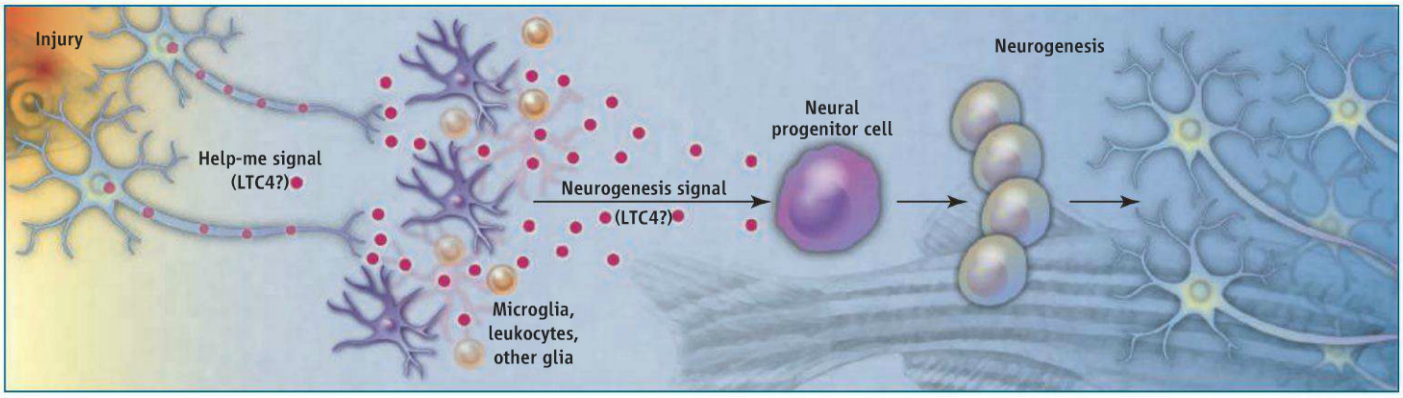

Brain regeneration. In the zebrafish brain, injured neurons release a signal (LTC4) that stimulates resident immune cells (microglia, leukocytes, and other glia) to release a signal (LTC4) that promotes neurogenesis. The transcription factor Gata3 in both the immune cells and the neuronal progenitor cells may operate as a molecular switch that controls the repair phenotype of the inflammation.

CREDIT: K. SUTLIFF/*SCIENCE*

Department of Pharmacology, University of Washington, 1959 NE Pacific Street, Seattle, WA 98195, USA. E-mail: nstella@u.washington.edu

to promote neuronal repair? Further studies are needed to establish where the inflammatory repair program diverges between zebrafish and mammals. It may be convenient to think of the point of divergence as positioned upstream or downstream of the zebrafish and mammalian glia cell response. Upstream differences may include the phenotype of respective glia at the site of injury and the types of molecules that they release. Downstream differences may include differences in LTC4 signaling or impaired ability of mammalian neuronal progenitor cells to respond to LTC4.

Mammalian neurogenesis can be turned on in the adult hippocampus, olfactory bulb, and other areas throughout the central nervous system, albeit at lower levels (*11*). Some mammalian brain injuries are associated with an inflammatory response, an increase in the proliferation of neuronal progenitor cells within the neurogenic areas, and sometimes the migration of these newborn neurons to the sites of injury (*6*). In humans, the positive correlation between the induction of inflammation and neurogenesis occurs during acute injuries induced by ischemia and epilepsy, and also in certain neurodegenerative diseases, such as Parkinson's disease and amyotropic lateral sclerosis, although with much lower incidence. Perhaps some of these immune functions are deregulated in the brain and peripheral tissue of patients with neurodegenerative diseases (*4*) and thereby contribute to the development of slow-progressing neurodegeneration.

There is clear strength in combining genetics and pharmacology in a model organism to study the complex cellular interactions implemented by the immune system. Our mission (should we choose to accept it) is to validate these findings in the mammalian brain and to search for new therapeutic venues that will control this particular arm of the immune system to swiftly temper and repair neuronal injuries and slowly progressing chronic neurodegeneration.

References

1. N. Kyritsis *et al.*, *Science* **338**, 1353 (2012); 10.1126/science.1228773.
2. F. O. Martinez *et al.*, *Front. Biosci.* **13**, 453 (2008).
3. Y. Komohara *et al.*, *J. Pathol.* **216**, 15 (2008).
4. M. Björkqvist *et al.*, *J. Exp. Med.* **205**, 1869 (2008).
5. G. A. Garden, T. Möller, *J. Neuroimmune Pharmacol.* **1**, 127 (2006).
6. S. Das, A. Basu, *J. Neurosci. Res.* **86**, 1199 (2008).
7. N. Stella, *Glia* **58**, 1017 (2010).
8. N. Stella, *Science* **334**, 768 (2011).
9. R. Bianchi, E. Kastrisianaki, I. Giambanco, R. Donato, *J. Biol. Chem.* **286**, 7214 (2011).
10. P. E. Vos *et al.*, *Neurology* **75**, 1786 (2010).
11. D. C. Lie, H. Song, S. A. Colamarino, G. L. Ming, F. H. Gage, *Annu. Rev. Pharmacol. Toxicol.* **44**, 399 (2004).

10.1126/science.1232331

IMMUNOLOGY

Platelets Kill the Parasite Within

Platelets destroy *P. falciparum* by secreting a factor that enters infected blood cells and destroys the parasite.

Christian R. Engwerda[1] and Michael F. Good[2]

The estimated 216 million cases of malaria in 2010 resulted in about 655,000 deaths, around 86% of which were children under the age of 5 (*1*), mainly in sub-Saharan Africa. Most of these deaths are caused by the protozoan parasite *Plasmodium falciparum*. Our poor understanding of innate resistance and the development of immunity to *P. falciparum* is an obstacle to developing vaccines and new therapeutics. The human body has numerous defenses to protect itself against severe forms of malaria. One such strategy, previously underappreciated, involves platelets—unnucleated fragments of megakaryocytes normally thought of as being critical solely to prevent hemorrhage. On page 1348 in this issue, McMorran *et al.* (*2*) reveal a mechanism by which platelets can recognize infected red blood cells and kill the parasite within (see the figure).

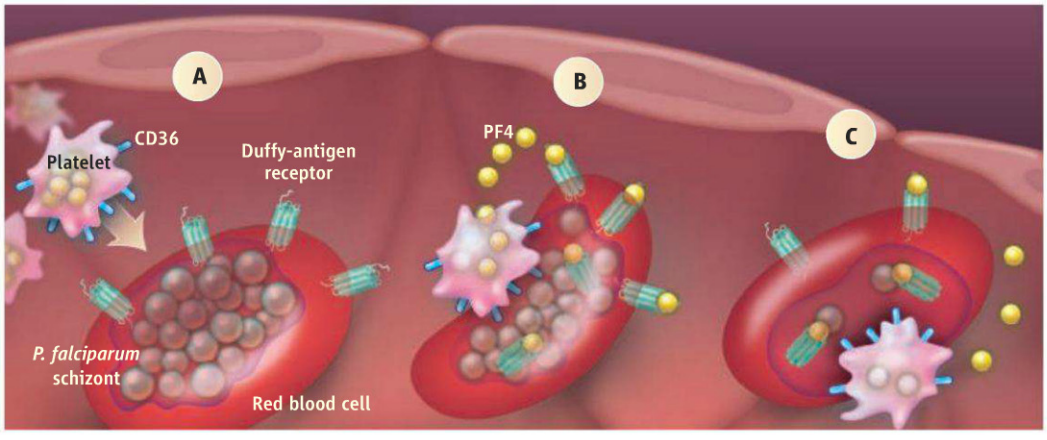

Destroying *P. falciparum*. (**A**) Activated platelets containing PF4-laden granules bind to parasitized red blood cells that express the Duffy-antigen receptor. (**B**) Upon binding [through CD36 on platelets and a parasite receptor on the red blood cell, possibly *P. falciparum* erythrocyte membrane protein 1 (PfEMP-1) (*15*)], PF4 is released and binds to the Duffy-antigen receptor on red blood cells. (**C**) The PF4–Duffy-antigen receptor complex translocates into the cell, colocalizes with intracellular parasites, and then kills the parasites.

The six *Plasmodium* parasite species that cause disease in humans (*P. falciparum*, *P. vivax*, *P. malariae*, *P. ovale wallickerie*, *P. ovale curtisii*, *and P. knowlesi*) appear to have independently colonized hominids and influenced the genetic composition of different human populations (*3*). For example, the genes responsible for sickle cell anemia, thalassemia, and glucose-6-phosphate dehydrogenase deficiency have a higher frequency in populations where malaria is, or was once, endemic. These genes provide protection against severe malaria syndromes and likely evolved in response to the disease by providing a survival advantage (*4*). Another of these genes encodes the Duffy-antigen receptor for chemokines (DARC/Fy glycoprotein/CD234) found on red blood cells. This protein also acts as a receptor for *P. vivax* (*5*), and human red blood cells lacking this receptor are resistant to invasion by this species and by *P. knowlesi* (*6*, *7*). The impact of this genetic selection can be seen in the geographical distribution of *P. vivax*. This parasite is spread throughout tropi-

CREDIT: K. SUTLIFF/*SCIENCE*

[1]Queensland Institute of Medical Research, Brisbane, QLD Australia. [2]Institute for Glycomics, Griffith University, Gold Coast, QLD Australia. E-mail: michael.good@griffith.edu.au

cal regions of the world, but is rare in large areas of central and western Africa where many individuals lack Duffy-antigen receptor expression on red blood cells. Thus, this "Duffy-negative" phenotype appears to have evolved as an innate resistance mechanism to *P. vivax* infection.

McMorran *et al*. extend previous work that demonstrated an important role for platelets in resistance to malaria (*8*) by identifying platelet factor 4 (PF4) as a key molecule in platelet-mediated killing of *P. falciparum*. PF4 is released from α granules in activated platelets to promote blood coagulation (*9*). It binds the Duffy-antigen receptor, along with several other chemokines (*10*). McMorran *et al*. found that a functional Duffy-antigen receptor is required for the antiparasitic activity of PF4.

The implications of lacking this antiparasitic mechanism for Duffy-negative individuals living in *P. falciparum* malaria endemic regions are not yet clear. One might predict that these individuals will be more prone to episodes of severe malaria. Indeed, mortality among African children with malaria-induced coma is higher than in children with the same condition from Papua New Guinea, where Duffy-negative individuals are less common (*11*). However, further evidence is required to support this proposition. Alternatively, compensatory antiparasitic mechanisms may have evolved in Duffy-negative individuals to help control parasite growth and/or reduce pathology following infection. The identification of other such mechanisms will offer further insights into innate immune responses to infection, and potentially identify vulnerable aspects of parasite biology.

Platelets decrease in number (thrombocytopenia) during acute malaria. McMorran *et al*. suggest that this is not to the host's advantage, limiting this innate form of resistance. However, other data show that platelets can contribute to cerebral malaria, a major cause of mortality. Platelets at normal physiological concentrations cause clumping of parasitized red blood cells from African children, a phenomenon associated with cerebral malaria (*12*). Thrombocytopenia may therefore reduce pathology by protecting the host against cerebral malaria, which may explain in part why there has been less pressure to maintain platelet-associated parasite killing mechanisms in Africans. The Duffy-negative phenotype to prevent *P. vivax* invasion of red blood cells seems to have been under stronger selective pressure than the maintenance of a PF4-dependent antiparasitic mechanism in central and western Africa. However, given the potentially different origins and timelines of *P. falciparum* and *P. vivax* adaptations to humans (*13*, *14*), another possibility is that the Duffy-negative phenotype has simply been under selective pressure in this part of Africa for longer. In addition, nonmalaria pressures may also have influenced this selection over time.

Cells of the innate immune system—macrophages, natural killer cells, dendritic cells, and γδ T cells—play an important role in defending against parasites, often providing a first line of defense and augmenting acquired (adaptive) immunity. By understanding how innate mechanisms of protection against malaria have been under strong selective pressure during evolution, we may better understand how to protect people from malaria. For example, how PF4 kills *P. falciparum* is not yet clear, but when this knowledge is available, vulnerable features of parasites will be identified that could be targeted with appropriate drugs. Understanding new antiparasitic mechanisms selected by evolution will enable us not only to complement existing cellular and molecular approaches to identifying drug targets to kill parasites, but also to select safer targets that have less effect on the host.

References

1. World Health Organization, "World Malaria Report" WHO Press, Geneva, 2011.
2. B. McMorran *et al*., *Science* **338**, 1348 (2008).
3. A. A. Escalante, F. J. Ayala, *Proc. Natl. Acad. Sci. U.S.A.* **92**, 5793 (1995).
4. D. P. Kwiatkowski, *Am. J. Hum. Genet.* **77**, 171 (2005).
5. R. Horuk *et al*., *Science* **261**, 1182 (1993).
6. J. D. Haynes *et al*., *J. Exp. Med.* **167**, 1873 (1988).
7. L. H. Miller, S. J. Mason, D. F. Clyde, M. H. McGinniss, *N. Engl. J. Med.* **295**, 302 (1976).
8. B. J. McMorran *et al*., *Science* **323**, 797 (2009).
9. R. Eisman, S. Surrey, B. Ramachandran, E. Schwartz, M. Poncz, *Blood* **76**, 336 (1990).
10. A. Chaudhuri *et al*., *J. Biol. Chem.* **269**, 7835 (1994).
11. S. J. Allen *et al*., *QJM* **89**, 779 (1996).
12. S. C. Wassmer *et al*., *J. Infect. Dis.* **197**, 72 (2008).
13. F. Prugnolle *et al*., *PLoS Pathog.* **7**, e1001283 (2011).
14. R. Culleton, R. Carter, *Int. J. Parasitol.* **42**, 1091 (2012).
15. D. I. Baruch *et al*., *Blood* **90**, 3766 (1997).

10.1126/science.1232439

ECOLOGY

Global Decline in Large Old Trees

The loss of large old trees in many ecosystems around the world poses a threat to ecosystem integrity.

David B. Lindenmayer,[1] William F. Laurance,[2] Jerry F. Franklin[3]

Large old trees are among the biggest organisms on Earth. They are keystone structures in forests, woodlands, savannas, agricultural landscapes, and urban areas, playing unique ecological roles not provided by younger, smaller trees. However, populations of large old trees are rapidly declining in many parts of the world, with serious implications for ecosystem integrity and biodiversity.

The definition of "large and old" trees depends on the ecosystem, tree species, and environmental conditions under consideration. Both the size and the age of a tree affect characteristics such as the large internal cavities, complex branching patterns, and idiosyncratic canopy architectures that distinguish large old trees from younger and smaller trees (*1*).

Large old trees (see the figure, panels A to C) play critical ecological roles. They provide nesting or sheltering cavities for up to 30% of all vertebrate species in some ecosystems (*2*). Large old trees also store large quantities of carbon, create distinct microenvironments characterized by high levels of soil nutrients and plant species richness, play crucial roles in local hydrological regimes, and provide abundant food for numerous animals in the form of fruits, flowers, foliage, and nectar. In agricultural landscapes, large old trees can be focal points for vegetation restoration, facilitate ecosystem connectivity by attracting mobile seed dispersers and pollinators, and act as stepping stones for many animals.

Younger and smaller trees cannot provide most of the distinctive ecological roles played by large old trees (*3*). For instance, large old trees in Mountain Ash (*Eucalyptus regnans*) forests of mainland Australia provide irreplaceable shelter and nesting sites for more

[1]Fenner School of Environment and Society, The Australian National University, Canberra, ACT 0200, Australia. [2]Centre for Tropical Environmental and Sustainability Science, and School of Marine and Tropical Biology, James Cook University, Cairns, Queensland 4878, Australia. [3]School of Environmental and Forest Science, University of Washington, Seattle, WA 98195, USA. E-mail: david.lindenmayer@anu.edu.au

than 40 species of cavity-using vertebrates (*4*). For many dependent species, the keystone roles of large old trees continue for decades or even centuries after tree death, when they become standing dead trees or large logs (*1*).

The loss of large old trees is a recognized concern in many ecosystems worldwide. For example, populations of large old trees are plummeting in intensively grazed landscapes in California, Costa Rica, and Spain, where such trees are predicted to disappear within 90 to 180 years (*5*). In southeastern Australia, millions of hectares of grazing lands are projected to support less than 1.3% of the historical densities of large old trees within 50 to 100 years (*6*).

Large old trees are declining in forests at all latitudes. Larger trees (>45 cm in diameter) throughout southern Sweden have declined from historical densities of ~19 per hectare to 1 per hectare (*7*). In California's Yosemite National Park, the density of the largest trees (see the figure, panel A) declined by 24% between the 1930s and 1990s (*8*). Large old *E. regnans* trees—Earth's tallest flowering plants (see the figure, panel B)—are predicted to decline from 5.1 in 1997 to 0.6 trees per hectare by 2070 (*4*). Fragmented Brazilian rainforests are likely to lose half of their original large trees (≥60 cm diameter) in the first three decades after isolation (*9*).

Large old trees are exceptionally vulnerable to intentional removal, elevated mortality, reduced recruitment, or combinations of these drivers (see the figure, panel C). They are removed during logging, land clearing, agricultural intensification, fire management, and for human safety. Droughts, repeated wildfires, competition with invasive plants, edge effects, air pollution, disease, and insect attack (*10*) can all increase tree mortality. The likelihood of new trees growing into large old trees can be diminished by overgrazing or browsing by native herbivores (*11*) and domestic livestock (*6*), by competition with exotic plants, and by altered fire regimes.

Drivers of large old tree loss often interact to create ecosystem-specific threats (*12*). In agricultural landscapes, chronic livestock overgrazing, excessive nutrients from fertilizers, and deliberate removal for firewood and land clearing combine to severely reduce large old trees (*6*). Populations of large old pines in the dry forests of western North America declined dramatically in the last century because of selective logging, uncharacteristically severe wildfires, and other causes, although efforts are now made to reduce the density of the stands so that high-severity fires do not occur and large trees are saved (see the figure, panel D). Salvage logging is equally damaging, whereby natural disturbances, such as fire or insect attack, are followed by removal of all remaining live and dead trees (see the figure, panel E). In certain tropical savannas and temperate forests, interactions among drivers occur over vast areas and result in entire landscapes supporting few large old trees (*13*). Modeling suggests that even modest increases in adult mortality can seriously erode populations of long-lived organisms such as large old trees (*14*).

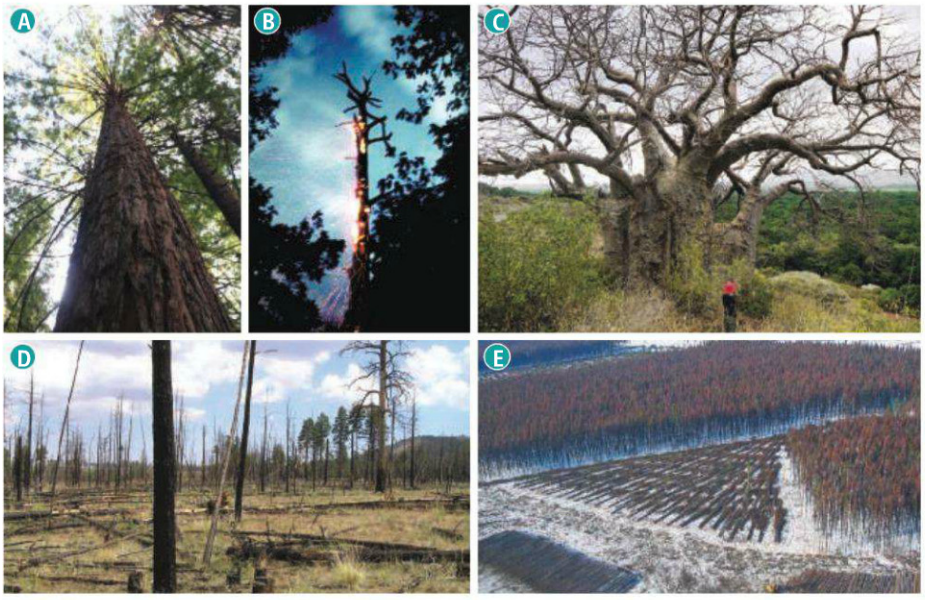

Global decline. **(A)** Over 95% of California's majestic coastal redwoods have been lost to logging and forest clearing (*8*). **(B)** Large old Mountain Ash (*E. regnans*) trees in mainland southern Australia are critical habitats for many elements of the biota but are also readily killed and often consumed by wildfires (*4*). **(C)** Baobab trees, like this giant in Tanzania, are under threat from land clearing, droughts, fungal pathogens, and overharvesting of their bark for mat-weaving (*3*). **(D)** Efforts to conserve large old Ponderosa Pine (*Pinus ponderosa*) trees include reducing the risk of stand-replacing fire by removing small trees and applying low-severity prescribed fire. **(E)** During post-insect attack salvage logging operations in British Columbia, Canada, all large trees are removed.

Although large old trees are declining across much of the planet, not all ecosystems are losing such trees. Elevated plant-growth rates in tropical forests, possibly in response to rising concentrations of atmospheric carbon dioxide, might result in larger numbers of large old trees, at least where such forests escape other human disturbances.

Large old trees are more likely to persist in particular parts of landscapes such as disturbance refugia. Research is needed to determine the locations and causes of such refugia and to devise strategies to protect them (*15*). For example, timber or other commodity extraction (e.g., cropping) in managed landscapes might be concentrated where large old trees are least likely to persist or develop. Maintenance of appropriate population age structures can help to ensure the perpetual supply of large old trees. This requires policies and management practices that intentionally grow such trees and reduce their mortality rates (*5*).

Just as large-bodied animals such as elephants, tigers, and cetaceans have declined drastically in many parts of the world, a growing body of evidence suggests that large old trees could be equally imperiled. Targeted research is needed to better understand their key threats and devise strategies to counter them. Without such initiatives, these iconic organisms and the many species dependent on them could be lost or greatly diminished.

References

1. R. van Pelt, *Identifying Mature and Old Forests in Western Washington* (Washington State Department of Natural Resources, Olympia, WA, 2007).
2. J. Remm, A. Lohmus, *For. Ecol. Manage.* **262**, 579 (2011).
3. D. B. Lindenmayer, *Forest Pattern and Ecological Process: A Synthesis of 25 Years of Research* (CSIRO Publishing, Melbourne, 2009).
4. W. F. Laurance, *New Sci.* **213**, 39 (2012).
5. P. Gibbons *et al.*, *Conserv. Biol.* **22**, 1309 (2008).
6. J. Fischer *et al.*, *Proc. Natl. Acad. Sci. U.S.A.* **107**, 19597 (2010).
7. M. T. Jönsson *et al.*, *J. Veg. Sci.* **20**, 91 (2009).
8. J. A. Lutz, J. W. van Wagtendonk, J. F. Franklin, *For. Ecol. Manage.* **257**, 2296 (2009).
9. W. F. Laurance *et al.*, *Nature* **404**, 836 (2000).
10. W. R. Anderegg *et al.*, *Nat. Climate Change*, 10.1038/nclimate1635 (2012).
11. A. T. Vanak *et al.*, *Ecography* **35**, 315 (2012).
12. G. P. Asner, S. R. Levick, *Ecol. Lett.* **15**, 1211 (2012).
13. B. J. Palik *et al.*, *For. Ecol. Manage.* **261**, 128 (2011).
14. S. L. Lewis *et al.*, *Nature* **457**, 1003 (2009).
15. B. Mackey *et al.*, *Ecol. Appl.* **22**, 1852 (2012).

10.1126/science.1231070

PHOTO CREDITS: (A) R. BUTLER; (B) W. INCOLL; (C) W. LAURANCE; (D) R. NOSS; (E) K. HODGES

Drought in Africa Caused Delayed Arrival of European Songbirds

A. P. Tøttrup,[1]* R. H. G. Klaassen,[2,3] M. W. Kristensen,[4] R. Strandberg,[2] Y. Vardanis,[2] Å. Lindström,[2] C. Rahbek,[1] T. Alerstam,[2] K. Thorup[4]

Advancement in phenological events such as spring arrival of songbirds at their breeding grounds is well documented (*1*). Despite this, the arrival in 2011 at northern European breeding grounds of several trans-Saharan migratory bird species was among the latest documented since 1950 (Fig. 1A). Local nonbreeding conditions can affect subsequent life-cycle stages at the level of individual birds (*2*). Here, we confirm this by showing a link of causality between the drought at the Horn of Africa (*3*) and the migratory behavior of individual birds resulting in subsequent delayed arrival at breeding grounds thousands of km away.

Photoperiod (*4*) and local environmental conditions (*5*) control timing of life-history events in migratory animals. Timing may also be affected by events during migration, e.g., on stopover sites. We followed individual movements of two long-distance migratory songbird species [18 red-backed shrikes (RS) and eight thrush nightingales (TN)] during three consecutive annual cycles (2009 to 2012) by miniature light-level geolocators (*6*) with the purpose of assessing the impacts of environmental conditions at different life-history stages. Breeding area arrival was documented by using 63 years of monitoring data and related to en route conditions by using remote-sensing data (31-year vegetation index series).

The exceptional 2011 delay in spring arrival could be traced back to a significant prolongation of stopover time during northward migration at the Horn of Africa, which was at that time affected by extreme drought (Fig. 1C). Mean stopover time in this region was longer during the drought year 2011 (18 days, SE = 1.72, $n = 5$ for RS and 29 days, SE = 4, $n = 3$ for TN) compared with the mean stopover time for the adjoining years, 2010 and 2012, combined (9 days, SE = 0.90, $n = 13$ for RS and 21 days, SE = 5, $n = 5$ for TN). This carried over to a corresponding delay in spring arrival and breeding start in Europe (Fig. 1A and fig. S1) even apparent at the individual level (two individuals tracked during two consecutive years; supplementary materials). There was no significant difference in the timing of migration between 2010/2012 and 2011 up to the spring stopover period in northeast Africa.

The extent of the catastrophic drought (*3*) at the refueling area (*6*) is illustrated by vegetation indices (Fig. 1C and fig. S2). The drought probably caused food shortage, which slowed down refueling rate and increased time needed to reach the necessary fuel loads. Other southeast African migrants were also delayed, whereas species not relying on the Horn of Africa for refueling were not (table S1). Thus, this demonstrates cross-season interactions in individual migratory animals (*2*).

Advances in tracking technology currently revolutionize migration research. Our results elucidate how new technology helps establish a direct link between local climate during migration and arrival/breeding conditions. Still, improvements in small-animal tracking are required to provide better precision globally (*7*).

Migration delay may have cascading effects on breeding success, mortality, and timing of later life-history stages. Start of breeding of RS was delayed in 2011, but population sizes and reproductive success were reported to be close to average (supplementary materials). However, the implications of our results are that even very local stopover conditions during short time periods have crucial importance for the entire migration system, emphasizing the challenges in conserving migration routes and systems (*8*).

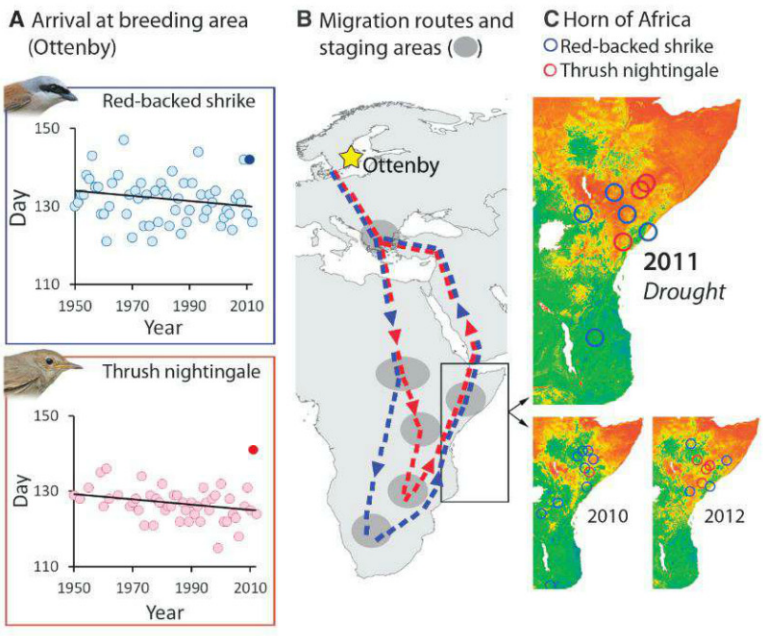

Fig. 1. (**A**) Trends in first-arrival day of RS and TN at Ottenby, Sweden, during 1950 to 2012 (solid dots are 2011 arrivals). (**B**) Migration revealed by year-round tracking of individuals during 2009 to 2012. (**C**) Horn of Africa staging positions of individual RS (blue; $n = 9$ in 2010, $n = 5$ in 2011, $n = 4$ in 2012) and TN (red; $n = 1$ in 2010, $n = 3$ in 2011, $n = 4$ in 2012). Background maps show eMODIS normalized difference vegetation index (NDVI) (15 to 30 April); color range (red to green) indicates increasing presence of green vegetation. The difference in number of northeast African staging days between 2010/12 and 2011 was significant for both species combined ($P = 0.006$, $n = 26$) as well as RS alone ($P < 0.002$, $n = 18$), but not the small sample of TN ($P = 0.46$, $n = 8$; Kruskal-Wallis).

References and Notes

1. C. Parmesan, *Annu. Rev. Ecol. Evol. Syst.* **37**, 637 (2006).
2. P. P. Marra, K. A. Hobson, R. T. Holmes, *Science* **282**, 1884 (1998).
3. C. Wolff *et al.*, *Science* **333**, 743 (2011).
4. E. Gwinner, W. Wiltschko, *J. Comp. Physiol.* **125**, 267 (1978).
5. C. E. Studds, P. P. Marra, *Proc. Biol. Sci.* **278**, 3437 (2011).
6. A. P. Tøttrup *et al.*, *Proc. Biol. Sci.* **279**, 1008 (2012).
7. M. Wikelski *et al.*, *J. Exp. Biol.* **210**, 181 (2007).
8. D. S. Wilcove, *No Way Home* (Island, Washington, DC, 2008).

Acknowledgments: Danish Nature Agency (J.nr.SN 302-009) and ethical committees in Malmö/Lund (M112-09) approved the studies. Swedish Research Council, Centre for Animal Movement Research, Villum Foundation, Swedish Environmental Protection Agency and Danish National Research Foundation financed this study. Contribution no. 259 from Ottenby Bird Observatory. Tracking data are available at www.movebank.org (digital object identifier: 10.5441/001/1.8jg3h6n7).

Supplementary Materials

www.sciencemag.org/cgi/content/full/338/6112/1307/DC1
Materials and Methods
Supplementary Text
Figs. S1 and S2
Table S1
References (*9*–*17*)

17 July 2012; accepted 23 October 2012
10.1126/science.1227548

[1]Center for Macroecology, Evolution, and Climate, University of Copenhagen, Universitetsparken 15, DK-2100 Copenhagen, Denmark. [2]Department of Biology, Lund University, Ecology Building, SE-22362 Lund, Sweden. [3]Montagu's Harrier Foundation and Animal Ecology Group, Centre for Ecological and Evolutionary Studies, Post Office Box 11103, Groningen University, NL-9700 CC Groningen, Netherlands. [4]Natural History Museum, Center for Macroecology, Evolution and Climate, University of Copenhagen, Universitetsparken 15, DK-2100 Copenhagen, Denmark.

*To whom correspondence should be addressed. E-mail: aptottrup@bio.ku.dk

Crystal Structure of the Calcium Release–Activated Calcium Channel Orai

Xiaowei Hou, Leanne Pedi, Melinda M. Diver, Stephen B. Long*

The plasma membrane protein Orai forms the pore of the calcium release–activated calcium (CRAC) channel and generates sustained cytosolic calcium signals when triggered by depletion of calcium from the endoplasmic reticulum. The crystal structure of Orai from *Drosophila melanogaster*, determined at 3.35 angstrom resolution, reveals that the calcium channel is composed of a hexameric assembly of Orai subunits arranged around a central ion pore. The pore traverses the membrane and extends into the cytosol. A ring of glutamate residues on its extracellular side forms the selectivity filter. A basic region near the intracellular side can bind anions that may stabilize the closed state. The architecture of the channel differs markedly from other ion channels and gives insight into the principles of selective calcium permeation and gating.

In many cell types, the depletion of calcium ions (Ca^{2+}) stored within the endoplasmic reticulum (ER) causes the opening of Ca^{2+}-selective channels in the plasma membrane (*1*). The resulting influx of Ca^{2+} through these calcium release–activated calcium (CRAC) channels generates sustained intracellular Ca^{2+} signals, the roles of which are well appreciated in cells of the immune system, where they mediate signaling through B cell, T cell, and Fc receptors (*1*). Although this process of "store-operated Ca^{2+} entry" has been recognized for decades, Orai and stromal interaction molecule (STIM), the CRAC channel pore and its regulator, were identified fairly recently (*2*–*7*). Orai, located in the plasma membrane, forms the Ca^{2+} pore (*8*–*10*). Humans have three Orai proteins (Orai1 to -3). A mutation in Orai1 that renders the channel nonconductive [Arg^{91}→Trp^{91} (R91W) (*11*)] causes a form of immune deficiency, underscoring its importance in the immune system (*5*). STIM is a single-pass membrane protein in the ER that senses the luminal Ca^{2+} concentration. It opens the pore of Orai following Ca^{2+} store depletion, probably via interaction between the cytosolic portions of STIM and Orai, which accumulate at ER-plasma membrane junctions (*1*, *12*).

Orai proteins constitute a highly conserved ion-channel family and have no discernible sequence homology with other ion channels (*5*–*7*), suggesting distinctive architecture and mechanisms for selective ion permeation and gating. From sequence analysis, Orai is predicted to have four transmembrane helices (M1 to M4). The chemical accessibility and intersubunit cross-linking of cysteine residues introduced into the channel by mutagenesis predict that residues on the M1 helix contribute to the ion-conduction pore (*13*, *14*). Several lines of evidence indicate that Orai channels are multimers, but studies have led to differing conclusions about the oligomeric state. Some studies suggest a tetrameric assembly (*15*–*18*), whereas others hint at a higher-order oligomer (*14*) or raise the possibility that the oligomeric state of the channel might change when it is activated by STIM (*15*, *18*).

Under physiological conditions, in which the extracellular Ca^{2+} concentration is 1 to 2 mM, CRAC channels select for Ca^{2+} over monovalent cations such as sodium (Na^+) or potassium (K^+) by more than 1000:1, placing them among the most highly-selective Ca^{2+} channels known (*19*). However, as is the case for many Ca^{2+}-selective channels, when divalent cations are removed from the extracellular solution, CRAC channels become permeant to monovalent cations, including K^+ and Na^+ (*19*, *20*). Both the Ca^{2+} and monovalent cation currents through CRAC channels require activation by STIM and are blocked by gadolinium (Gd^{3+}) and lanthanum (La^{3+}) ions from the extracellular side (inhibition constant K_i < 100 nM) (*8*, *21*, *22*).

To better understand ion permeation, ion selectivity, and gating in CRAC channels, we have determined the crystal structure of Orai from *Drosophila melanogaster*, which shares 73% sequence identity with human Orai1 within its transmembrane region. We have also determined the structure of the nonconductive K163W mutant, corresponding to the R91W mutant in Orai1 that causes immune deficiency in humans. The structures define the architecture of a Ca^{2+} channel, establish principles of its Ca^{2+} selectivity, and give insight into the mechanism of activation by STIM.

Structure determination and channel reconstitution. To obtain well-diffracting crystals of Orai, we evaluated the biochemical behavior of

Structural Biology Program, Memorial Sloan-Kettering Cancer Center (MSKCC), 1275 York Avenue, New York, NY 10065, USA.

*To whom correspondence should be addressed. E-mail: longs@mskcc.org

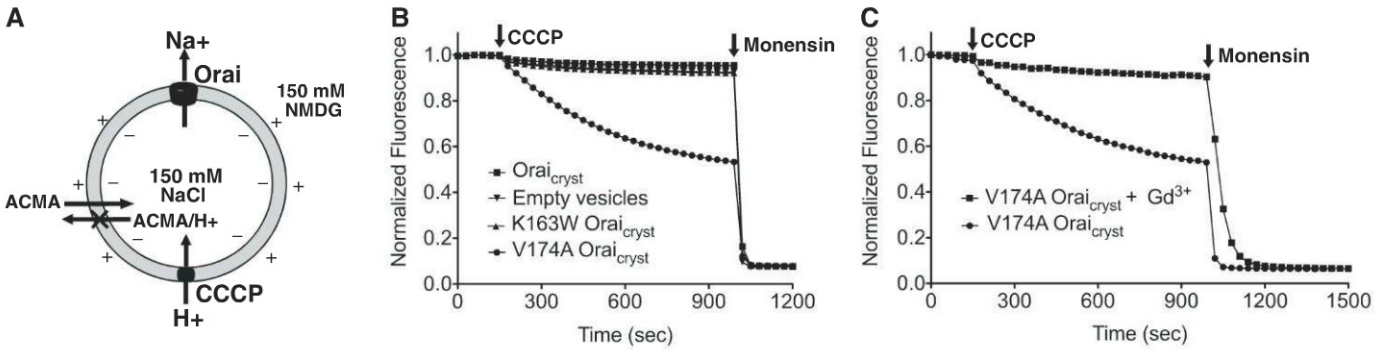

Fig. 1. Channel reconstitution in liposomes. (**A**) Schematic of the fluorescence-based flux assay. Vesicles containing Orai or those prepared without protein (empty vesicles) were loaded with 150 mM NaCl and diluted 100-fold into flux buffer containing a fluorescent pH indicator (ACMA) and 150 mM *N*-methyl-D-glucamine (NMDG) to establish a Na^+ gradient. After stabilization of the fluorescence signal (150 s), a proton ionophore (CCCP) was added to the sample, and an electrical potential arising from Na^+ efflux was used to drive the uptake of protons into the vesicles, which quenches the fluorescence of ACMA. The "X" indicates that ACMA is no longer membrane-permeable in the protonated form. (**B**) Fluorescence measurements for the indicated protein constructs of Orai. Monensin, a Na^+ ionophore, was added after 990 s to render all vesicles permeable to Na^+ and establish a minimum fluorescence baseline. Fluorescence was normalized by dividing by the initial value. (**C**) Fluorescence trace observed for V174A $Orai_{cryst}$ in the absence and presence of Gd^{3+}.

~50 orthologs and engineered a variety of protein forms, including truncations and fusions. Crystals that diffracted to 3.35 Å resolution were obtained from a construct (termed $Orai_{cryst}$) spanning residues 132 to 341 of Orai from *Drosophila melanogaster* in which two nonconserved cysteine residues and two residues in the hypervariable M3-M4 loop were mutated (see the supplementary materials and methods). The construct corresponds to the conserved region of Orai and contains all regions necessary for activation by STIM (fig. S1) (*23*–*25*).

We tested the function of the purified channel protein by reconstituting it into liposomes and using a fluorescence-based assay to monitor ion flux under divalent ion-free conditions (Fig. 1). As would be expected for a closed channel before activation by STIM, ion flux was not detected for $Orai_{cryst}$ or for the K163W mutant. Introduction of the mutation V174A (V102A in Orai1), which creates channels that are open in the absence of STIM (*26*), yielded a robust decrease in fluorescence, indicative of ion flux (Fig. 1B). We confirmed that the fluorescence decrease was due to ion flux through Orai by adding the pore-blocker Gd^{3+}, which eliminated the observed flux through the pore but had no effect on the baseline fluorescence induced by the Na^{+}-ionophore monensin (Fig. 1C). Therefore, the reconstituted protein recapitulated known properties of Orai.

The crystals form in the space group $P2_13$ and contain two Orai subunits (referred to as subunits A and B of the channel) within the asymmetric unit. Experimental phases were derived from diffraction data collected from crystals containing mercury, iridium, and gadolinium heavy atoms. The phases, which were improved by noncrystallographic symmetry averaging, yielded an electron-density map that allowed placement of the majority of the amino acid side chains (fig. S2). The atomic model contains amino acids 144 to 334 of Orai, except for the M1-M2 loop (amino acids 181 to 190), the M2-M3 loop (amino acids 220 to 235), and amino acids 330 to 334 of subunit B, which are disordered. Anomalous-difference electron-density peaks for sulfur atoms of methionine and cysteine residues confirm the correct assignment of amino acids in the atomic model (fig. S2E), which is refined to a free residual (R_{free}) of 28% (table S1).

Architecture of Orai. The crystal structure shows that the channel is formed from a hexamer of six Orai subunits arranged around a central axis (Fig. 2). Cross-linking and light-scattering data are consistent with a hexameric assembly for both purified Orai in detergent and Orai expressed in cell membranes (fig. S3). Each subunit contains four transmembrane α helices (M1 to M4) and a helix following M4 that extends into the cytosol (termed the M4 extension helix). The M4 extension helices of neighboring subunits adopt one of two alternating conformations and pack with each other in pairs, giving this region of the channel threefold symmetry (Fig. 2). Within the channel's transmembrane region, there is sixfold symmetry.

The ion pore is located at the center of the channel along the sixfold axis, and the transmembrane helices are arranged in three concentric rings (Fig. 2B). Six M1 helices, one from each subunit, make up an inner ring of helices and line the ion pore. The M2 and M3 helices constitute a middle ring that surrounds the transmembrane portion of the M1 helices and separates them from M4 helices, which are arranged in an outer ring and located at the periphery of the channel. The channel extends just beyond the extracellular side of the membrane, and the M1 helix and the M4 extension helix protrude 20 to 25 Å into the cytosol.

The M1 helices extend from Thr^{144} to Gln^{180} and are ~55 Å long. The region of M1 that extends into the cytosol was not expected to be part of M1 from sequence analysis and includes four helical turns at its N terminus (residues 144 to 157). As this region does not make contacts with other parts of the channel in the structure, it could conceivably interact with cellular factors such as STIM.

The M2 helix traverses just beyond the thickness of a lipid bilayer, and the M3 helix extends about two helical turns further into the cytosol. The arrangement of the M2 and M3 helices in a ring surrounding the transmembrane portion of the M1 helices, while leaving the cytosolic portion of M1 free, suggests that M2 and M3 help provide structural integrity to the transmembrane region of the pore but would permit widening of the intracellular region of the pore.

The M4 helices are located furthest away from the ion pore. In comparison to the M1 to M3 helices, the M4 helices have fewer contacts with other parts of the channel, and their peripheral location may allow mobility (Fig. 2A). A bend near the middle of the transmembrane region (Pro^{288}) means that approximately half of M4 (within the outer leaflet) is roughly perpendicular to the plane of the membrane, whereas the other half is oriented diagonally (Fig. 2A). Connected to M4 by a highly conserved hinge region (residues 305 to 308), the M4 extensions of subunit A and subunit B pair with one another through an antiparallel coiled-coil helix packing arrangement (Fig. 2C). The interaction involves two residues from each subunit (Ile^{316} and Leu^{319}) that form a hydrophobic patch on the M4 extension, which is otherwise predominantly decorated with hydrophilic amino acids. Mutation of either residue (L273S or L276D mutants of Orai1) disrupts interaction with STIM and its ability to open the channel (*27*–*29*).

Chemical composition of the pore. The chemical environment along the length of the ion pore

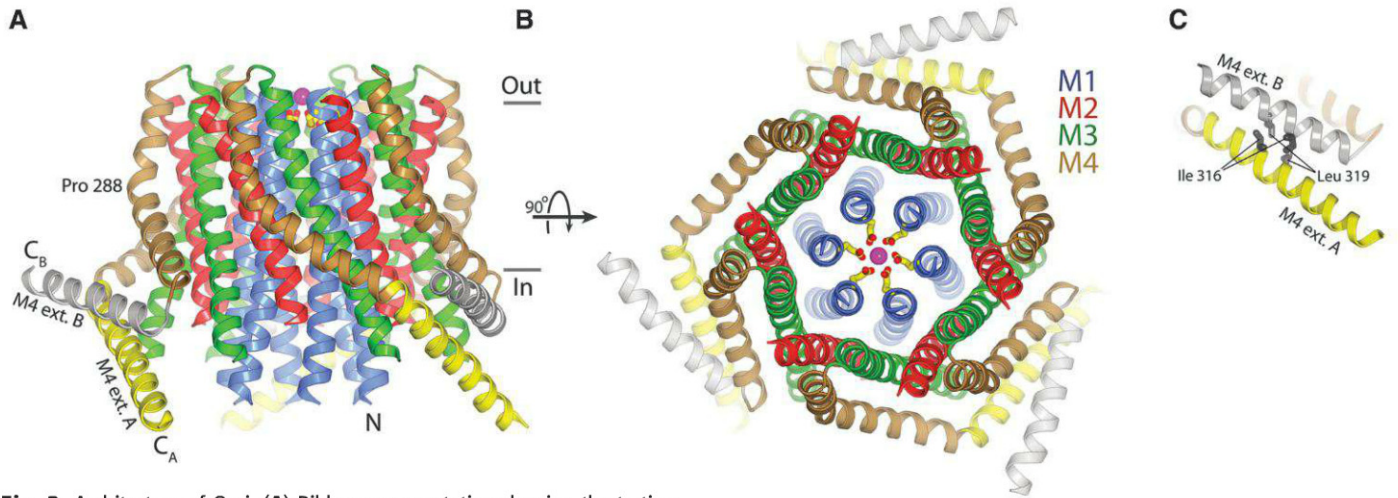

Fig. 2. Architecture of Orai. (**A**) Ribbon representation showing the tertiary structure of the channel from the side. The helices are colored: M1 (blue), M2 (red), M3 (green), M4 (brown), M4 extension (yellow in subunit A and gray in subunit B). Also shown are a Ca^{2+} ion (magenta sphere) and the nearby Glu^{178} residues (yellow sticks). Based on the hydrophobic region of the channel's surface, horizontal lines (~30 Å apart) suggest approximate boundaries of the inner (In) and outer (Out) leaflets of the membrane. (**B**) Orthogonal view of the channel from the extracellular side. (**C**) Close-up view showing the interaction between the M4 extension helices.

is determined by side chains of the amino acids of M1 that line the pore. This is in marked contrast to the pore of K^+ channels, where a substantial part of it is formed by an extended conformation of the polypeptide backbone (*30*). The pore of Orai has four distinct sections (Fig. 3, A and B): (i) a ring of glutamates at its extracellular end (termed the glutamate ring and composed of six Glu^{178} side chains), (ii) a hydrophobic section spanning three helical turns of M1 within the transmembrane region, (iii) a basic section spanning three helical turns near the intracellular side, and (iv) a wider section that extends into the cytosol.

The pore is ~55 Å long, and its diameter varies along its distance (Fig. 3B). In the glutamate ring, the Glu^{178} side chains point toward the center of the pore with their side chain oxygen atoms separated by ~6 Å across the pore, giving the extracellular entrance to the pore negative electrostatic potential (Fig. 3, B and C). Glu^{178}, which is conserved in Orai channels, is the only acidic residue lining the pore (*31*).

The side chains of Val^{174}, Phe^{171}, and Leu^{167} are separated by 8 to 10 Å across the pore and line the walls of the hydrophobic section, which is roughly tube-shaped and ~18 Å long (Fig. 3B). The hydrophobic side chains are well packed in the pore, make extensive van der Waals interactions with one another, and are strictly conserved among Orai channels. This region also has well-defined electron density (fig. S2) and the lowest temperature factors of the structure, suggesting that it is relatively rigid. In addition to lining the pore, the hydrophobic residues form a core of the protein that likely contributes to the channel's structural integrity. Mutations of amino acids in the hydrophobic region have yielded channels with dramatically altered ion-conduction properties. For instance, mutations of Val^{174} (Orai1 mutants V102C, V102A, V102T, or V102S) or Gly^{170} (Orai1 mutants G98P and G98D), which closely packs its Cα carbon with the side chain of Phe^{171}, result in channels that are constitutively conductive and demonstrate altered ion selectivity (*26*, *32*). The close packing in the hydrophobic region suggests that the functional abnormalities of these mutants may be due to reduced structural integrity and/or slightly altered packing in the pore.

Below the hydrophobic region in Fig. 3B and near the intracellular side of the membrane, the pore is lined by three basic residues from each subunit (Lys^{163}, Lys^{159}, and Arg^{155}) that are conserved as lysine or arginine among Orai orthologs (fig. S1). The 18 lysine or arginine residues that line this portion of the pore create an unexpected environment for the pore of a channel that conducts cations (Fig. 3D). The M1 helix is slightly bent at Ser^{162} and is enriched for residues that are often associated with bends in helices (serine, threonine, and glycine) in the region that spans the junction between the hydrophobic and basic portions of the pore (Fig. 3A and fig. S4). This raises the possibility that the conformation of the basic region could change, perhaps as part of the gating process, while the hydrophobic section and glutamate ring remain fairly fixed.

External Ca^{2+} binding and ion selectivity. In crystals soaked in Ca^{2+}, electron density consistent with a Ca^{2+} ion is observed on the extracellular side of the glutamate ring (in what we term the external site) (Fig. 4A). Because it is difficult to distinguish Ca^{2+} from other ions or water molecules in electron-density maps, we collected diffraction data from a crystal soaked in barium (Ba^{2+}), which permeates through the CRAC channel (*22*, *33*) and can be identified in electron-density maps from its anomalous diffraction signal. The anomalous-difference electron-density map contained a 10σ peak for Ba^{2+} in the external site, consistent with the assessment that it is a binding site for Ca^{2+} (Fig. 4A). Ba^{2+} is positioned slightly farther away from the glutamate ring than Ca^{2+}, and this correlates with the ionic radii of the ions (1.35 Å for Ba^{2+} and 0.99 Å for Ca^{2+}). It is possible that the ion coordination, which could be either direct or water-mediated, is not sixfold symmetric due to the flexibility of glutamate side chains. The backbone carbonyl oxygen of Glu^{178} at the C-terminal end of M1 might also contribute to Ca^{2+} binding (Fig. 4A). To investigate if Gd^{3+} blocks the channel by binding to the same site, we collected diffraction data from crystals soaked in Gd^{3+}, which also has a strong anomalous diffraction signal. The anomalous-difference electron-density map showed a 14σ peak for Gd^{3+} in the external site (Fig. 4B). The density is positioned closer to the glutamate ring than for Ca^{2+}; this

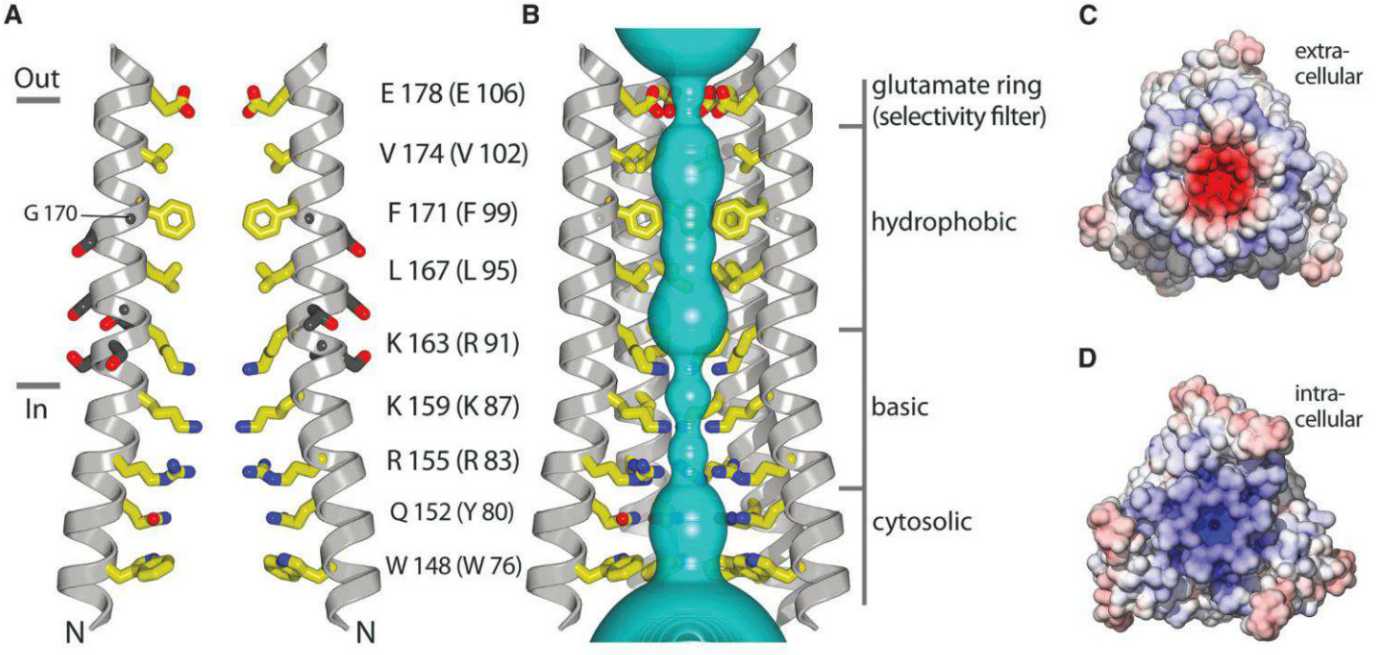

Fig. 3. Ion pore. (**A**) Two M1 helices are drawn (four are omitted for clarity), showing the amino acids lining the pore in yellow. The approximate boundaries of the membrane-spanning region are shown as horizontal lines. The corresponding amino acids in human Orai1 are shown in parentheses. Ser^{161}, Ser^{162}, Thr^{164}, Ser^{165}, Ser^{169}, and Gly^{170} are drawn as gray sticks. (**B**) View of the pore. Within a ribbon representation of four M1 helices (two in the foreground are removed for clarity) is a representation (teal) of the minimal radial distance from the center to the nearest van der Waals protein contact. The sections of the pore discussed in the text are labeled. (**C** and **D**) Molecular surface of Orai viewed from the extracellular (C) and intracellular (D) sides and colored according to the electrostatic potential contoured from −10 kT (red) to +10 kT (blue) (dielectric constant: 80).

may be indicative of the high affinity of Gd^{3+} and its +3 charge. Notably, the single Ca^{2+} binding site identified is located just outside the pore rather than within it. This configuration of ion binding distinguishes Orai from K^+ channels, which have multiple ions present within the pore in their structures (*34*), and this probably reflects differences in the mechanisms for ion permeation and selectivity.

CRAC channels may achieve their exquisite Ca^{2+} selectivity by high-affinity binding of Ca^{2+} to the glutamate ring that probably constitutes the ion selectivity filter. Accordingly, mutation of the glutamate (Glu^{178} in Orai or Glu^{106} in Orai1) to aspartic acid dramatically increases the channel's permeability to monovalent cations (*8–10*, *13*). Because the ionic radii of Ca^{2+} and Na^+ are nearly identical (0.99 and 0.95 Å, respectively), selectivity for Ca^{2+} is most likely due to the ion's greater positive charge. Consistent with this trend, we observe that high-affinity blockage of Orai by the trivalent lanthanide Gd^{3+} is due to binding in the external site.

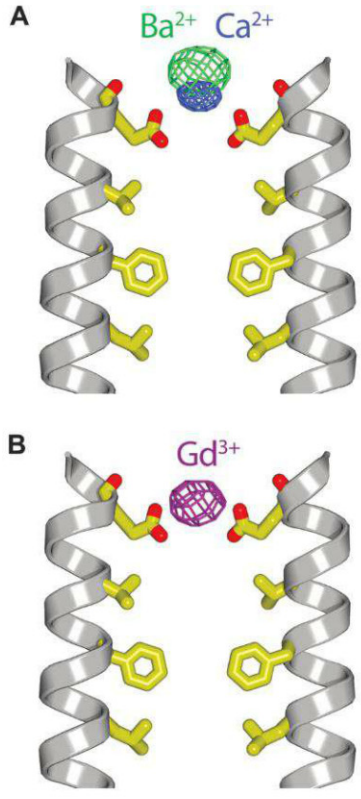

Fig. 4. Cation binding in the external site. (**A**) Ba^{2+} and Ca^{2+} binding. The glutamate ring and hydrophobic section of the pore are depicted as in Fig. 3A. Anomalous-difference electron density for Ba^{2+} is shown in green mesh (calculated from 20 to 5 Å resolution using phases derived from the final model and contoured at 6σ from a diffraction data set collected from a crystal soaked in 50 mM $BaCl_2$ using x-rays with λ = 1.70 Å. Electron density corresponding to Ca^{2+} is shown from a simulated annealing F_o-F_c omit map (blue mesh, calculated from 20 to 3.8 Å resolution and contoured at 4σ) from a crystal soaked in 50 mM $CaCl_2$ (table S1). The backbone carbonyl oxygen of Glu^{178} is also shown in stick representation. (**B**) Gd^{3+} binding. Anomalous-difference electron density is shown in purple mesh from a crystal soaked in 1 mM $GdCl_3$ (calculated from 20 to 5 Å resolution using model phases and contoured at 11σ from a diffraction data set collected using λ = 1.70 Å x-rays).

Identification of the external site raises the question of whether there is only one Ca^{2+} binding site or if there are other site(s) that are occupied during permeation. In Orai, the Ca^{2+} permeation rate [up to ~10^4 ions per second (*35*, *36*)] is much slower than the rate at which Ca^{2+} ions would diffuse to the extracellular mouth of the pore [~10^6 ions per second at physiological Ca^{2+} concentration (*37*)], so a single high-affinity Ca^{2+} binding site with a fast on-rate (from the extracellular solution) and a slow off-rate (into the pore) might be able to account for Ca^{2+}-selective permeation. However, some evidence, including an anomalous mole fraction effect (*33*), suggests that there may be more than one Ca^{2+} binding site. A second binding site might account for the property that, although Na^+ currents through CRAC channels are blocked by micromolar concentrations of Ca^{2+}, Ca^{2+} does not appreciably flow until the external solution contains millimolar concentrations of it (*19*, *20*). Additionally, the extent of blockage of Na^+ current at micromolar levels of Ca^{2+} is dependent on the voltage applied across the membrane (~10% block at –20 mV and ~50% block at –80 mV with 20 μM external Ca^{2+}) (*36*, *38*), which suggests that an ion binding site is located within the voltage gradient, whereas the external site would probably be located outside of it.

If a second binding site for Ca^{2+} in the selectivity filter exists, we expect that it would be located just below the glutamate ring. This hypothetical internal site, which might only be occupied transiently during permeation, would reside within a voltage field across the membrane and may explain the voltage-dependence for blockage of Na^+ current by Ca^{2+}. The binding of a Ca^{2+} ion in the external site could displace a Ca^{2+} ion from the internal site due to electrostatic repulsion between the ions, thereby allowing selective Ca^{2+} permeation.

Anion binding in the basic region of the pore. Electron-density maps have strong density in the basic region of the pore that appears to plug it. The anomalous-difference electron density was also strong in this site (up to 20σ), aiding the identification of the bound atom(s) (Fig. 5A). The density cannot be due to the surrounding protein side chains because they would have negligible anomalous scattering, and the components of the crystallization solution did not contain elements that would give a strong anomalous signal. To identify possible metal ions that might have copurified with Orai, purified protein was analyzed by inductively coupled plasma mass spectrometry (ICP-MS) and found to contain ~0.6 molar equivalents of iron and ~0.1 molar equivalents of zinc (table S2), both of which have anomalous scattering properties. Diffraction data collected using x-rays with a wavelength (λ) of 1.735 Å, slightly shorter than an absorption edge for iron (1.7433 Å) where the anomalous signal from iron would be strong (the imaginary component of the anomalous scattering factor f'' for iron is approximately 3.9 electrons at λ = 1.735 Å), yielded a 20σ peak in the anomalous-difference map (Table 1). Using λ = 1.900 Å x-rays, where the anomalous signal from iron would be weaker (f'' ~ 0.5 electrons), the peak was 5σ. F_o-F_c electron-density maps calculated from these data sets had comparable (~10σ) peaks, indicating that the difference in the strength of the anomalous signal was not due to differing occupancies of the bound entity between the crystals. Data sets collected above and below an absorption edge for zinc (λ = 1.284 Å) yielded comparable anomalous-difference density in the pore, but indicated that zinc was bound in a crystal contact (fig. S6). We therefore conclude that a major species bound in the basic region of the pore contains iron, which was present in the media used for cell growth.

Because this region of the pore is highly basic, we tested whether it could bind anions by soaking crystals in the complex anion iridium hexachloride, $(IrCl_6)^{3-}$. Diffraction data were collected using λ = 1.1033 Å x-rays to optimize the anomalous diffraction signal from iridium (f'' ~ 10.1 electrons), where it would be stronger than that for iron (f'' ~ 1.8 electrons) (Table 1). The anomalous-difference electron-density map contained two peaks in the basic region: (i) a 29σ peak for $(IrCl_6)^{3-}$ between Lys^{163} and Lys^{159} and (ii) an 8σ peak adjacent to Arg^{155} (Fig. 5B). Otherwise, the overall structure of Orai complexed with $(IrCl_6)^{3-}$ was indistinguishable from the native structure. We conclude that the basic region can bind anion(s). Because we observe iron in this anion binding site, we speculate that it is also bound in the form of a complex anion or mediated by counter ions. In support of this, hexachloroferrate anions, $(FeCl_6)^{3-}$, are known to be stabilized by hydrogen-bond interactions with amines (*39*). Although possible, it seems unlikely that iron binds within the pore in a physiological setting because of the limited amount of iron freely available within cells. More likely, the basic region of the pore binds available intracellular anion(s), with possible candidates being a sulfate or phosphate species (phosphate, pyrophosphate, etc.).

The K163W mutant. The crystal structure of the nonconductive K163W mutant gives further insight into the basic region of the pore. The overall structure of the K163W mutant is indistinguishable (at the current resolution) from the structure with the wild-type (WT) pore (root mean square deviation for Cα atoms is 0.1 Å). The only discernible difference with regard to the protein is that the side chain of the tryptophan residue at position 163 projects into the pore (Fig. 5C). The

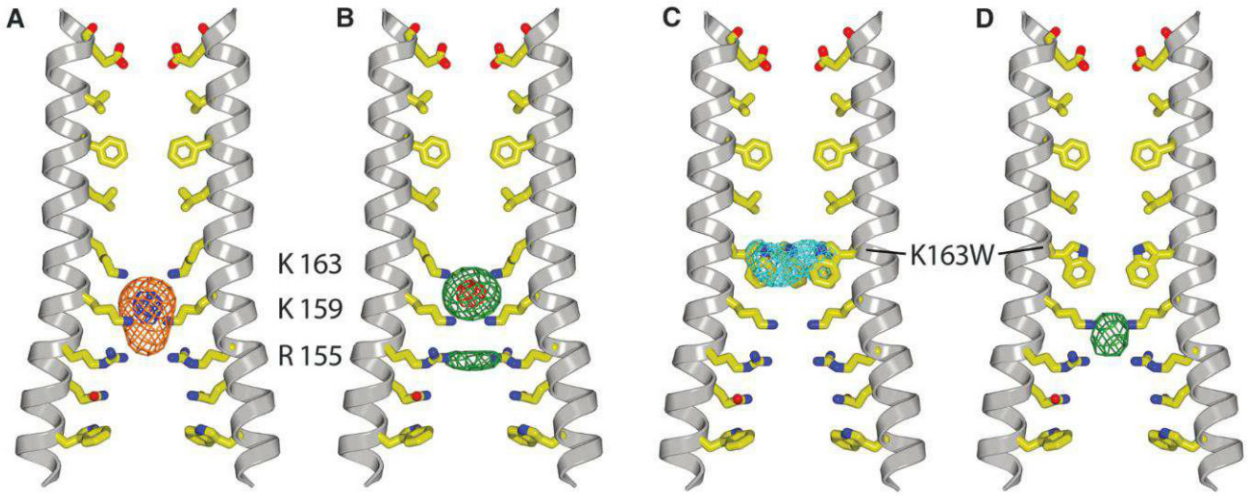

Fig. 5. Anion binding and the K163W mutant. (**A**) Anomalous-difference electron density in the basic region of the WT pore contoured at 7σ (orange mesh) and 14σ (blue mesh) from a native unsoaked crystal. The M1 helices are x-rays). (**C** and **D**) The K163W mutant. Two M1 helices of the K163W mutant are depicted in the same manner as in (A). (C) Electron density (cyan mesh) is shown for the tryptophan side chains at residue 163 (represented as sticks). The density

Binary Millisecond Pulsar Discovery via Gamma-Ray Pulsations

H. J. Pletsch,[1,2]* L. Guillemot,[3] H. Fehrmann,[1,2] B. Allen,[1,2,4] M. Kramer,[3,5] C. Aulbert,[1,2] M. Ackermann,[6] M. Ajello,[7] A. de Angelis,[8] W. B. Atwood,[9] L. Baldini,[10] J. Ballet,[11] G. Barbiellini,[12,13] D. Bastieri,[14,15] K. Bechtol,[7] R. Bellazzini,[16] A. W. Borgland,[7] E. Bottacini,[7] T. J. Brandt,[17,18] J. Bregeon,[16] M. Brigida,[19,20] P. Bruel,[21] R. Buehler,[7] S. Buson,[14,15] G. A. Caliandro,[22] R. A. Cameron,[7] P. A. Caraveo,[23] J. M. Casandjian,[11] C. Cecchi,[24,25] Ö. Çelik,[26,27,28] E. Charles,[7] R. C. G. Chaves,[11] C. C. Cheung,[29] J. Chiang,[7] S. Ciprini,[25,30] R. Claus,[7] J. Cohen-Tanugi,[31] J. Conrad,[32,33] S. Cutini,[34] F. D'Ammando,[24,35,36] C. D. Dermer,[37] S. W. Digel,[7] P. S. Drell,[7] A. Drlica-Wagner,[7] R. Dubois,[7] D. Dumora,[38] C. Favuzzi,[19,20] E. C. Ferrara,[26] A. Franckowiak,[7] Y. Fukazawa,[39] P. Fusco,[19,20] F. Gargano,[20] N. Gehrels,[26] S. Germani,[24,25] N. Giglietto,[19,20] F. Giordano,[19,20] M. Giroletti,[40] G. Godfrey,[7] I. A. Grenier,[11] M.-H. Grondin,[41,42] J. E. Grove,[37] S. Guiriec,[26] D. Hadasch,[22] Y. Hanabata,[39] A. K. Harding,[26] P. R. den Hartog,[7] M. Hayashida,[7,43] E. Hays,[26] A. B. Hill,[7,44] X. Hou,[45] R. E. Hughes,[46] G. Jóhannesson,[47] M. S. Jackson,[33,48] T. Jogler,[7] A. S. Johnson,[7] W. N. Johnson,[37] J. Kataoka,[49] M. Kerr,[7] J. Knödlseder,[17,18] M. Kuss,[16] J. Lande,[7] S. Larsson,[32,33,50] L. Latronico,[51] M. Lemoine-Goumard,[38] F. Longo,[12,13] F. Loparco,[19,20] M. N. Lovellette,[37] P. Lubrano,[24,25] F. Massaro,[7] M. Mayer,[6] M. N. Mazziotta,[20] J. E. McEnery,[26,52] J. Mehault,[31] P. F. Michelson,[7] W. Mitthumsiri,[7] T. Mizuno,[53] M. E. Monzani,[7] A. Morselli,[54] I. V. Moskalenko,[7] S. Murgia,[7] T. Nakamori,[49] R. Nemmen,[26] E. Nuss,[31] M. Ohno,[55] T. Ohsugi,[53] N. Omodei,[7] M. Orienti,[40] E. Orlando,[7] F. de Palma,[19,20] D. Paneque,[7,56] J. S. Perkins,[26,27,28,57] F. Piron,[31] G. Pivato,[15] T. A. Porter,[7] S. Rainò,[19,20] R. Rando,[14,15] P. S. Ray,[37] M. Razzano,[9,16] A. Reimer,[7,58] O. Reimer,[7,58] T. Reposeur,[38] S. Ritz,[9] R. W. Romani,[7] C. Romoli,[15] D. A. Sanchez,[41] P. M. Saz Parkinson,[9] A. Schulz,[6] C. Sgrò,[16] E. do Couto e Silva,[7] E. J. Siskind,[59] D. A. Smith,[38] G. Spandre,[16] P. Spinelli,[19,20] D. J. Suson,[60] H. Takahashi,[39] T. Tanaka,[7] J. B. Thayer,[7] J. G. Thayer,[7] D. J. Thompson,[26] L. Tibaldo,[14,15] M. Tinivella,[16] E. Troja,[26] T. L. Usher,[7] J. Vandenbroucke,[7] V. Vasileiou,[31] G. Vianello,[7,61] V. Vitale,[54,62] A. P. Waite,[7] B. L. Winer,[46] K. S. Wood,[37] M. Wood,[7] Z. Yang,[32,33] S. Zimmer[32,33]

Millisecond pulsars, old neutron stars spun up by accreting matter from a companion star, can reach high rotation rates of hundreds of revolutions per second. Until now, all such "recycled" rotation-powered pulsars have been detected by their spin-modulated radio emission. In a computing-intensive blind search of gamma-ray data from the Fermi Large Area Telescope (with partial constraints from optical data), we detected a 2.5-millisecond pulsar, PSR J1311−3430. This unambiguously explains a formerly unidentified gamma-ray source that had been a decade-long enigma, confirming previous conjectures. The pulsar is in a circular orbit with an orbital period of only 93 minutes, the shortest of any spin-powered pulsar binary ever found.

Almost exactly 30 years ago, radio observations detected the first neutron star with a millisecond spin period (*1*). Launched in 2008, the Large Area Telescope (LAT) on the Fermi Gamma-ray Space Telescope (*2*) confirmed that many radio-detected millisecond pulsars (MSPs) are also bright gamma-ray emitters (*3*). In each case, gamma-ray (0.1 to 100 GeV) pulsations were revealed by using rotation parameters obtained from radio telescopes (*4*) to assign rotational phases to LAT-detected photons.

The Fermi LAT also provides sufficient sensitivity to detect pulsars via direct searches for periodicity in the sparse gamma-ray photons. Such blind searches (*5*) of LAT data for solitary pulsars have so far unveiled 36 younger gamma-ray pulsars (*6*–*9*) with rotation rates between 2 and 20 Hz. In the radio band, all but four of these objects remain completely undetected despite deep follow-up radio searches (*10*). This is a large fraction of all young gamma-ray–emitting neutron stars and shows that such blind-search gamma-ray detections are essential for understanding the pulsar population (*11*). However, no MSP has been detected via gamma-ray pulsations until now, and so we have not been able to see whether a similar population of radio-quiet MSPs exists.

The blind-search problem for gamma-ray pulsars is computationally demanding, because the relevant pulsar parameters are unknown a priori and must be explicitly searched. For observation times spanning several years, this requires a dense grid to cover the multidimensional parameter space, with a tremendous number of points to be individually tested. Blind searches for MSPs in gamma-ray data are vastly more difficult than for slower pulsars, largely because the search must extend to much higher spin frequencies [to and beyond 716 Hz (*12*)]. Furthermore, most MSPs are in binary systems, where the additionally unknown orbital parameters can increase the computational complexity by orders of magnitude. Thus, blind searches for binary MSPs were hitherto virtually unfeasible.

We have now broken this impasse, detecting a binary MSP, denoted PSR J1311−3430, in a direct blind search of the formerly unidentified gamma-ray source 2FGL J1311.7−3429, one of the brightest listed in the Fermi-LAT Second Source Catalog [2FGL (*13*)]. This source also had counterparts in several earlier gamma-ray catalogs and was first registered in data from the Energetic Gamma Ray Experiment Telescope [EGRET (*14*)] on the Compton Gamma Ray Observatory.

In a search for potential optical counterparts of 2FGL J1311.7−3429, Romani (*15*) identified a quasi-sinusoidally modulated optical flux with a period of 93 min and conjectured this to be a "black-widow" pulsar binary system (*16*). In this interpretation, an MSP strongly irradiates what is left of the donor companion star to eventually evaporate it. This plausibly explained the observed brightness variation resulting from strong heating of one side of the companion by the pulsar radiation. Associating this optical variation with the orbital period of the putative binary system constrained the ranges of orbital search parameters and also confined the sky location for the search. Thus, these constraints made a blind binary-MSP search in LAT data feasible; however, the computational challenge involved remained enormous. To test the binary-MSP hypothesis as the possible nature of 2FGL J1311.7−3429, we developed a method to search the LAT data for pulsations over the entire relevant parameter space.

Under the black-widow interpretation, the search is confined toward the sky location of the potential optical counterpart and the orbit is expected to be circular, leaving a five-dimensional search space. The individual dimensions are spin frequency f, its rate of change $\dot{f}$, the orbital period P_{orb}, time of ascending node T_{asc}, and $x = a_{\mathrm{p}} \sin \iota$, the projection of the pulsar semimajor axis a_{p} onto the line of sight with orbital inclination angle ι. We designed the blind search to maintain sensitivity to very high pulsar spin frequencies, $f < 1.4$ kHz, and values of $\dot{f}$ typical for MSPs, $-5 \times 10^{-13}\ \mathrm{Hz\,s^{-1}} < \dot{f} < 0$. Although the optical data constrain P_{orb} and T_{asc}, the uncertainties are by far larger than the precision necessary for a pulsar detection. This required us to search ranges of $P_{\mathrm{orb}} = 5626.0 \pm 0.1$ s and $T_{\mathrm{asc}} = 56009.131 \pm 0.012$ MJD (modified Julian days) around the nominal values (*15*), and $0 < x < 0.1$ lt-s (light-seconds).

Searching this five-dimensional parameter space fully coherently given a multiple-year data time span is computationally impossible. To solve this problem, we used the hierarchical (three-staged) search strategy that previously enabled the detection of 10 solitary, younger (i.e., non-MSP)

pulsars in blind searches of LAT data (*8*, *9*), exploiting methods originally developed to detect gravitational waves from pulsars (*17*–*20*). Here, we expanded this approach to also search over binary orbital parameters. The first stage of the hierarchical scheme is the most computing-intensive and uses an efficient "semicoherent" method (*8*), extending the method of Atwood *et al.* (*21*). This step involves (incoherently) combining coherent Fourier power computed using a window of 2^{20} s (~12 days) by sliding the window over the entire LAT data set (hence the term "semicoherent"). In a second stage, significant semicoherent candidates are automatically followed up through a fully coherent analysis made possible because only a small region of parameter space around the candidate is explored. A third stage further refines coherent pulsar candidates by including higher signal harmonics [using the *H*-test (*22*, *23*)]. The computing cost to coherently follow up a single semicoherent candidate is negligible relative to the total cost of the first stage. Therefore, constructing the search grid of the semicoherent stage as efficiently as possible is of utmost importance.

The key element in constructing an optimally efficient grid for the semicoherent search is a distance metric on the search space (*17*–*19*, *24*). The metric provides an analytic geometric tool measuring the expected fractional loss in signal-to-noise ratio (S/N) squared for any given pulsar-signal location at a nearby grid point. The metric is obtained from a Taylor expansion of the fractional loss to second order around the parameter-space location of a given signal. In contrast to searching for solitary pulsars, a difficulty in the binary case is that the metric components explicitly depend on the search parameters (*24*). Thus, the metric (and so the grid point density required to not miss a signal) changes across orbital parameter space. Constructing a simple lattice with constant spacings would be highly inefficient, resulting in either vast over- or under-covering of large parameter-space regions. We developed a grid construction algorithm (*25*) that effectively uses the metric formalism. Orbital grid points were first placed at random; then, those that were either too close together or too far apart according to the metric were moved (barycentric shifts), minimizing the maximum possible loss in S/N for any pulsar signal across the entire search parameter space. By design, the resulting grid (*25*) ensured never losing more than 30% in S/N for any signal parameters.

The input LAT data we prepared for this search spanned almost 4 years (1437 days) and include gamma-ray photons with LAT-reconstructed directions within 15° around the targeted sky position (*25*). To improve the S/N of a putative pulsar signal, we assigned each photon a weight (*23*) measuring the probability of originating from the conjectured pulsar, computed with a spectral likelihood method (*25*). The gamma-ray spectrum of 2FGL J1311.7−3429 is best modeled by an exponentially cut-off power law (fig. S1), with spectral parameters reminiscent of other gamma-ray pulsars (Table 1). The computational work of the search was done on the ATLAS cluster in Hannover, Germany. Soon after initiation, the searching procedure convincingly detected PSR J1311−3430.

Following the blind-search detection, we refined the pulsar parameters further in a timing analysis (*26*). We obtained pulse times of arrival (TOAs) from subdividing the LAT data into 40 segments of about equal length. We produced a pulse profile for each segment using the initial pulsar parameters, and cross-correlated each pulse profile with a multi-Gaussian template derived from fitting the entire data set to determine the TOAs. We used the Tempo2 software (*27*) to fit the TOAs to a timing model including sky position, f, $\dot{f}$, and binary-orbit parameters (Fig. 1 and Table 1). We found no statistically significant evidence for orbital eccentricity at the $e < 10^{-3}$ level. We measured a marginal evidence for a total proper motion of 8 ± 3 milliarcseconds per year. Generally, the observed value of $\dot{f} = -3.198\ (\pm 0.002) \times 10^{-15}$ Hz s^{-1} is only an upper limit of the intrinsic frequency change $\dot{f}_{\rm in}$, because of the Shklovskii effect in which Doppler shifts caused by the proper motion can account for part of $\dot{f}$. Under the assumption that the proper motion of PSR J1311−3430 is small enough to approximate $\dot{f} \approx \dot{f}_{\rm in}$, we derived further quantities from the pulsar rotational parameters (Table 1).

The rotational ephemeris of PSR J1311−3430 also provided constraints on the companion mass $m_{\rm c}$ through the binary mass function that combines x, $P_{\rm orb}$, and the gravitational constant G,

$$f(m_{\rm p}, m_{\rm c}) = \frac{4\pi^2}{G}\frac{x^3}{P_{\rm orb}^2} = \frac{(m_{\rm c}\sin\iota)^3}{(m_{\rm c}+m_{\rm p})^2} = 2.995\ (\pm 0.003) \times 10^7 M_\odot$$

where $m_{\rm p}$ is the pulsar mass and $M_\odot$ is the mass of the Sun. Typical MSP masses are 1.35 to 2.0 $M_\odot$. Assuming $m_{\rm p} = 1.35\ M_\odot$ and $\iota = 90°$ (orbit is

[1]Max-Planck-Institut für Gravitationsphysik (Albert-Einstein-Institut), D-30167 Hannover, Germany. [2]Institut für Gravitationsphysik, Leibniz Universität Hannover, D-30167 Hannover, Germany. [3]Max-Planck-Institut für Radioastronomie, Auf dem Hügel 69, D-53121 Bonn, Germany. [4]Department of Physics, University of Wisconsin, Milwaukee, WI 53201, USA. [5]Jodrell Bank Centre for Astrophysics, School of Physics and Astronomy, University of Manchester, Manchester M13 9PL, UK. [6]Deutsches Elektronen Synchrotron DESY, D-15738 Zeuthen, Germany. [7]W. W. Hansen Experimental Physics Laboratory, Kavli Institute for Particle Astrophysics and Cosmology, Department of Physics, and SLAC National Accelerator Laboratory, Stanford University, Stanford, CA 94305, USA. [8]Dipartimento di Fisica, Università di Udine and Istituto Nazionale di Fisica Nucleare, Sezione di Trieste, Gruppo Collegato di Udine, I-33100 Udine, Italy. [9]Santa Cruz Institute for Particle Physics, Department of Physics, and Department of Astronomy and Astrophysics, University of California, Santa Cruz, CA 95064, USA. [10]Università di Pisa and Istituto Nazionale di Fisica Nucleare, Sezione di Pisa, I-56127 Pisa, Italy. [11]Laboratoire AIM, CEA-IRFU/CNRS/Université Paris Diderot, Service d'Astrophysique, CEA Saclay, F-91191 Gif sur Yvette, France. [12]Istituto Nazionale di Fisica Nucleare, Sezione di Trieste, I-34127 Trieste, Italy. [13]Dipartimento di Fisica, Università di Trieste, I-34127 Trieste, Italy. [14]Istituto Nazionale di Fisica Nucleare, Sezione di Padova, I-35131 Padova, Italy. [15]Dipartimento di Fisica e Astronomia "G. Galilei," Università di Padova, I-35131 Padova, Italy. [16]Istituto Nazionale di Fisica Nucleare, Sezione di Pisa, I-56127 Pisa, Italy. [17]CNRS, IRAP, F-31028 Toulouse Cedex 4, France. [18]GAHEC, Université de Toulouse, UPS-OMP, IRAP, Toulouse, France. [19]Dipartimento di Fisica "M. Merlin" dell'Università e del Politecnico di Bari, I-70126 Bari, Italy. [20]Istituto Nazionale di Fisica Nucleare, Sezione di Bari, I-70126 Bari, Italy. [21]Laboratoire Leprince-Ringuet, École Polytechnique, CNRS/IN2P3, Palaiseau, France. [22]Institut de Ciències de l'Espai (IEEE-CSIC), Campus UAB, 08193 Barcelona, Spain. [23]INAF–Istituto di Astrofisica Spaziale e Fisica Cosmica, I-20133 Milano, Italy. [24]Istituto Nazionale di Fisica Nucleare, Sezione di Perugia, I-06123 Perugia, Italy. [25]Dipartimento di Fisica, Università degli Studi di Perugia, I-06123 Perugia, Italy. [26]NASA Goddard Space Flight Center, Greenbelt, MD 20771, USA. [27]Center for Research and Exploration in Space Science and Technology (CRESST) and NASA Goddard Space Flight Center, Greenbelt, MD 20771, USA. [28]Department of Physics and Center for Space Sciences and Technology, University of Maryland Baltimore County, Baltimore, MD 21250, USA. [29]National Research Council Research Associate, National Academy of Sciences, Washington, DC 20001, resident at Naval Research Laboratory, Washington, DC 20375, USA. [30]ASI Science Data Center, I-00044 Frascati (Roma), Italy. [31]Laboratoire Univers et Particules de Montpellier, Université Montpellier 2, CNRS/IN2P3, Montpellier, France. [32]Department of Physics, Stockholm University, AlbaNova, SE-106 91 Stockholm, Sweden. [33]Oskar Klein Centre for Cosmoparticle Physics, AlbaNova, SE-106 91 Stockholm, Sweden. [34]Agenzia Spaziale Italiana (ASI) Science Data Center, I-00044 Frascati (Roma), Italy. [35]IASF Palermo, I-90146 Palermo, Italy. [36]INAF–Istituto di Astrofisica Spaziale e Fisica Cosmica, I-00133 Roma, Italy. [37]Space Science Division, Naval Research Laboratory, Washington, DC 20375, USA. [38]Université Bordeaux 1, CNRS/IN2p3, Centre d'Études Nucléaires de Bordeaux Gradignan, F-33175 Gradignan, France. [39]Department of Physical Sciences, Hiroshima University, Higashi-Hiroshima, Hiroshima 739-8526, Japan. [40]INAF Istituto di Radioastronomia, I-40129 Bologna, Italy. [41]Max-Planck-Institut für Kernphysik, D-69029 Heidelberg, Germany. [42]Landessternwarte, Universität Heidelberg, Königstuhl, D-69117 Heidelberg, Germany. [43]Department of Astronomy, Graduate School of Science, Kyoto University, Sakyo-ku, Kyoto 606-8502, Japan. [44]School of Physics and Astronomy, University of Southampton, Highfield, Southampton SO17 1BJ, UK. [45]Centre d'Études Nucléaires de Bordeaux Gradignan, IN2P3/CNRS, Université Bordeaux 1, BP120, F-33175 Gradignan Cedex, France. [46]Department of Physics, Center for Cosmology and Astro-Particle Physics, Ohio State University, Columbus, OH 43210, USA. [47]Science Institute, University of Iceland, IS-107 Reykjavik, Iceland. [48]Department of Physics, Royal Institute of Technology (KTH), AlbaNova, SE-106 91 Stockholm, Sweden. [49]Research Institute for Science and Engineering, Waseda University, 3-4-1, Okubo, Shinjuku, Tokyo 169-8555, Japan. [50]Department of Astronomy, Stockholm University, SE-106 91 Stockholm, Sweden. [51]Istituto Nazionale di Fisica Nucleare, Sezione di Torino, I-10125 Torino, Italy. [52]Department of Physics and Department of Astronomy, University of Maryland, College Park, MD 20742, USA. [53]Hiroshima Astrophysical Science Center, Hiroshima University, Higashi-Hiroshima, Hiroshima 739-8526, Japan. [54]Istituto Nazionale di Fisica Nucleare, Sezione di Roma "Tor Vergata," I-00133 Roma, Italy. [55]Institute of Space and Astronautical Science, JAXA, 3-1-1 Yoshinodai, Chuo-ku, Sagamihara, Kanagawa 252-5210, Japan. [56]Max-Planck-Institut für Physik, D-80805 München, Germany. [57]Harvard-Smithsonian Center for Astrophysics, Cambridge, MA 02138, USA. [58]Institut für Astro- und Teilchenphysik and Institut für Theoretische Physik, Leopold-Franzens-Universität Innsbruck, A-6020 Innsbruck, Austria. [59]NYCB Real-Time Computing Inc., Lattingtown, NY 11560, USA. [60]Department of Chemistry and Physics, Purdue University Calumet, Hammond, IN 46323, USA. [61]Consorzio Interuniversitario per la Fisica Spaziale (CIFS), I-10133 Torino, Italy. [62]Dipartimento di Fisica, Università di Roma "Tor Vergata," I-00133 Roma, Italy.

*To whom correspondence should be addressed. E-mail: holger.pletsch@aei.mpg.de

edge-on) yields the minimum companion mass, $m_c > 8.2 \times 10^{-3}\ M_\odot$, which is only about eight times the mass of Jupiter. By means of Kepler's third law and typical MSP masses ($m_p >> m_c$), the binary separation $a = a_p + a_c$ is accurately approximated by $a = 0.75\ R_\odot (m_p/1.35\ M_\odot)^{1/3}$, where $R_\odot$ is the radius of the Sun. Thus, PSR J1311−3430 is likely the most compact pulsar binary known.

The compact orbit and the optical flaring events (*15*) suggest that the pulsar heating is driving a strong, possibly variable, stellar wind of ablated material of the companion. Interactions with the companion wind could affect the gamma-ray flux observed. In a dedicated analysis (*25*), we found no evidence for a modulation at the orbital period of the gamma-ray flux or its spectrum.

We also examined the gamma-ray spectral parameters of PSR J1311−3430 as a function of rotational phase (*25*). Dividing the data into 10 segments according to different rotational-phase intervals, we spectrally analyzed each segment separately. In line with the background estimation in the pulse profile (Fig. 1), we detected significant gamma-ray emission at all phases. The gamma-ray spectrum in the off-pulse phase interval (fig. S2) is better modeled by an exponentially cut-off power law, potentially indicative of magnetospheric origin from the pulsar, rather than by a simple power law, which would more likely suggest intrabinary wind shock emission.

Repeated, sensitive radio searches of the previously unidentified gamma-ray source, including Green Bank Telescope observations at 820 MHz, gave no pulsar detection (*28*). However, material ablated from the companion by the pulsar irradiation might obscure radio pulses. At higher radio frequencies, decreased scattering and absorption resulting in shorter eclipses are observed for other black-widow pulsars (*12*).

The optical observations provide evidence for strong heating of the pulsar companion that is near filling its Roche lobe (*15*). With $m_p = 1.35\ M_\odot$ and $\iota = 90°$, the Roche lobe radius of the companion is, to good approximation (*29*), $R_L = 0.063\ R_\odot$. The minimum mean density of the Roche lobe–filling companion directly follows from the orbital period (*30*), $\bar{\rho} = 45\ \mathrm{g\ cm^{-3}}$. This is twice the density of the planetary-mass companion of PSR J1719−1438 (*31*). One scenario for the formation of that system posits an ultracompact x-ray binary with a He or C degenerate donor transferring mass to the neutron star. However, van Haaften *et al*. (*32*) argue that angular momentum losses through gravitational-wave emission are insufficient to reach the low masses and short period of the PSR J1719−1438 system within the age of the universe. Instead, strong heating to bloat the companion or extra angular momentum loss from a companion evaporative wind are required. An alternative scenario (*33*) proposes that a combination of angular momentum loss and wind evaporation from an initial companion mass of 2 $M_\odot$ in a 0.8-day orbit can bring the system to low masses and short orbital

Table 1. Measured and derived parameters for PSR J1311−3430, with formal 1σ uncertainties (dd, days; hh, hours; mm, minutes; ss, seconds). Spectral parameters are averages over pulse phase.

Parameter	Value
Right ascension (J2000.0) (hh:mm:ss)	13:11:45.7242 ± 0.0002
Declination (J2000.0) (dd:mm:ss)	−34:30:30.350 ± 0.004
Spin frequency, f (Hz)	390.56839326407 ± 0.00000000004
Frequency derivative, $\dot{f}$ (10^{-15} Hz s^{-1})	−3.198 ± 0.002
Reference time scale	Barycentric Dynamical Time (TDB)
Reference time (MJD)	55266.90789575858
Orbital period P_{orb} (d)	0.0651157335 ± 0.0000000007
Projected pulsar semimajor axis x (lt-s)	0.010581 ± 0.000004
Time of ascending node T_{asc} (MJD)	56009.129454 ± 0.000007
Eccentricity e	<0.001
Data span (MJD)	54682 to 56119
Weighted root mean square residual (μs)	17
Derived Quantities	
Companion mass m_c ($M_\odot$)	>0.0082
Spin-down luminosity $\dot{E}$ (erg s^{-1})	4.9×10^{34}
Characteristic age τ_c (years)	1.9×10^{9}
Surface magnetic field B_S (G)	2.3×10^{8}
Gamma-Ray Spectral Parameters	
Photon index, Γ	1.8 ± 0.1
Cutoff energy, E_c (GeV)	3.2 ± 0.4
Photon flux above 0.1 GeV, F (10^{-8} photons cm^{-2} s^{-1})	9.2 ± 0.5
Energy flux above 0.1 GeV, G (10^{-11} erg cm^{-2} s^{-1})	6.2 ± 0.2

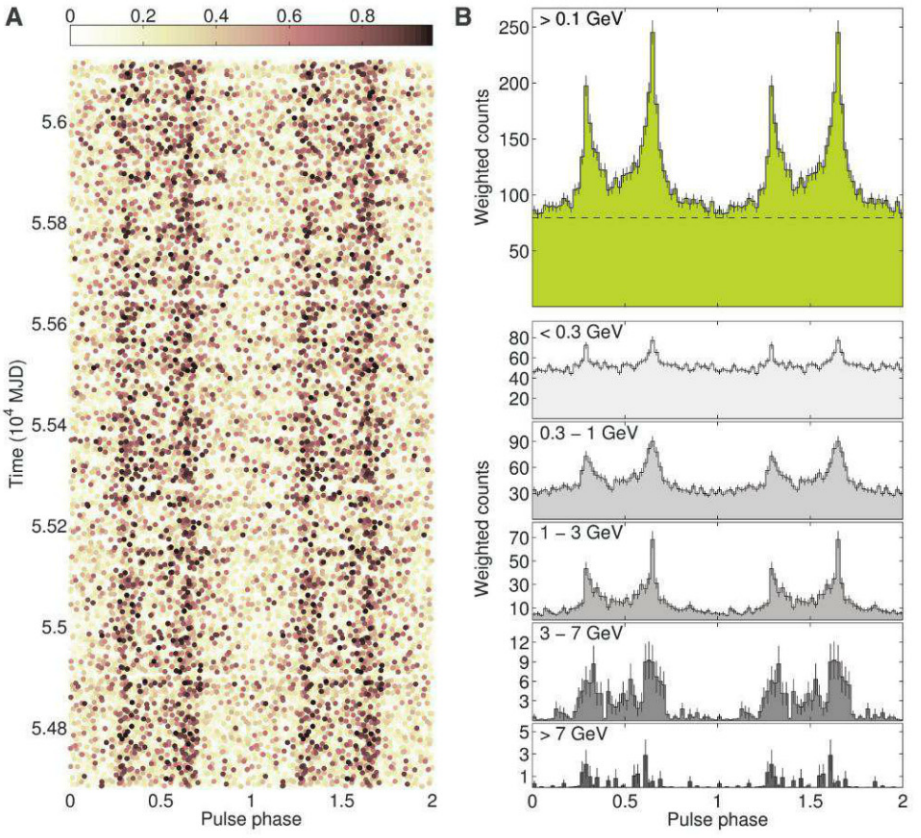

Fig. 1. Phase-time diagram and gamma-ray pulse profiles for PSR J1311−3430. Two pulsar rotations are shown for clarity. (**A**) The pulsar rotational phase for each gamma-ray photon arrival time; probability weights are shown in color code. (**B**) The pulse profiles in different energy bands. Each bin is 0.02 in phase, and photon weights are used. The dashed line indicates the estimated background level from a surrounding annular region.

periods in ~6 billion years. Indeed, their scenario produces a good match to the $m_c \sim 0.01\ M_\odot$, $P_{orb} \sim 0.065$ days seen for PSR J1311−3430. At this point in the evolution the system is detached, the companion is He-dominated, and irradiation has taken over the evolution. Presumably, continued irradiation can drive the system toward PSR J1719−1438-type companion masses, or produce an isolated MSP.

The direct detection of an MSP in a blind search of gamma-ray data implies that further MSPs, including other extreme binary pulsars, may exist among the bright, as yet unidentified 2FGL gamma-ray sources [e.g., (*34*, *35*)], which are too radio-faint or obscured by dense companion winds to be found in typical radio searches.

References and Notes

1. D. C. Backer, S. R. Kulkarni, C. Heiles, M. M. Davis, W. M. Goss, *Nature* **300**, 615 (1982).
2. W. B. Atwood *et al.*, *Astrophys. J.* **697**, 1071 (2009).
3. A. A. Abdo *et al.*, *Science* **325**, 848 (2009).
4. D. A. Smith *et al.*, *Astron. Astrophys.* **492**, 923 (2008).
5. The term "blind search" is used to reflect the fact that the pulsar parameters are unknown a priori, implying that a wide range of pulsar parameters must be explicitly searched.
6. A. A. Abdo *et al.*, *Science* **325**, 840 (2009).
7. P. M. Saz Parkinson *et al.*, *Astrophys. J.* **725**, 571 (2010).
8. H. J. Pletsch *et al.*, *Astrophys. J.* **744**, 105 (2012).
9. H. J. Pletsch *et al.*, *Astrophys. J.* **755**, L20 (2012).
10. P. S. Ray *et al.*, http://arxiv.org/abs/1205.3089 (2012).
11. K. P. Watters, R. W. Romani, *Astrophys. J.* **727**, 123 (2011).
12. J. W. T. Hessels *et al.*, *Science* **311**, 1901 (2006).
13. P. L. Nolan *et al.*, *Astrophys. J.* **199** (suppl.), 31 (2012).
14. C. E. Fichtel *et al.*, *Astrophys. J.* **94** (suppl.), 551 (1994).
15. R. W. Romani, *Astrophys. J.* **754**, L25 (2012).
16. A. S. Fruchter, D. R. Stinebring, J. H. Taylor, *Nature* **333**, 237 (1988).
17. P. R. Brady, T. Creighton, *Phys. Rev. D* **61**, 082001 (2000).
18. H. J. Pletsch, B. Allen, *Phys. Rev. Lett.* **103**, 181102 (2009).
19. H. J. Pletsch, *Phys. Rev. D* **82**, 042002 (2010).
20. H. J. Pletsch, *Phys. Rev. D* **83**, 122003 (2011).
21. W. B. Atwood, M. Ziegler, R. P. Johnson, B. M. Baughman, *Astrophys. J.* **652**, L49 (2006).
22. O. C. de Jager, B. C. Raubenheimer, J. W. H. Swanepoel, *Astron. Astrophys.* **221**, 180 (1989).
23. M. Kerr, *Astrophys. J.* **732**, 38 (2011).
24. C. Messenger, *Phys. Rev. D* **84**, 083003 (2011).
25. See supplementary materials on *Science* Online.
26. P. S. Ray *et al.*, *Astrophys. J.* **194** (suppl.), 17 (2011).
27. G. B. Hobbs, R. T. Edwards, R. N. Manchester, *Mon. Not. R. Astron. Soc.* **369**, 655 (2006).
28. S. M. Ransom *et al.*, *Astrophys. J.* **727**, L16 (2011).
29. B. Paczyński, *Annu. Rev. Astron. Astrophys.* **9**, 183 (1971).
30. J. Frank, A. R. King, D. J. Raines, *Accretion Power in Astrophysics* (Cambridge Univ. Press, Cambridge, 1985).
31. M. Bailes *et al.*, *Science* **333**, 1717 (2011).
32. L. M. van Haaften, G. Nelemans, R. Voss, P. G. Jonker, *Astron. Astrophys.* **541**, A22 (2012).
33. O. G. Benvenuto, M. A. De Vito, J. E. Horvath, *Astrophys. J.* **753**, L33 (2012).
34. R. W. Romani, M. S. Shaw, *Astrophys. J.* **743**, L26 (2011).
35. M. Ackermann *et al.*, *Astrophys. J.* **753**, 83 (2012).

Acknowledgments: This work was supported by the Max-Planck-Gesellschaft. The Fermi LAT Collaboration acknowledges support from several agencies and institutes for both development and the operation of the LAT as well as scientific data analysis. These include NASA and Department of Energy (United States), CEA/Irfu and IN2P3/CNRS (France), ASI and INFN (Italy), MEXT, KEK, and JAXA (Japan), and the K. A. Wallenberg Foundation, the Swedish Research Council, and the National Space Board (Sweden). Additional support from INAF in Italy and CNES in France for science analysis during the operations phase is also gratefully acknowledged. Fermi LAT data are available from the Fermi Science Support Center (http://fermi.gsfc.nasa.gov/ssc).

Supplementary Materials

www.sciencemag.org/cgi/content/full/science.1229054/DC1
Materials and Methods
Figs. S1 and S2
References (*36*–*38*)

20 August 2012; accepted 17 October 2012
Published online 25 October 2012;
10.1126/science.1229054

Mapping Local Charge Recombination Heterogeneity by Multidimensional Nanospectroscopic Imaging

Wei Bao,[1,2]* M. Melli,[1]* N. Caselli,[3,4] F. Riboli,[3,4] D. S. Wiersma,[3,5] M. Staffaroni,[6] H. Choo,[7] D. F. Ogletree,[1] S. Aloni,[1] J. Bokor,[1,6] S. Cabrini,[1]† F. Intonti,[3,4] M. B. Salmeron,[1,2] E. Yablonovitch,[6] P. J. Schuck,[1]† A. Weber-Bargioni[1]†

As materials functionality becomes more dependent on local physical and electronic properties, the importance of optically probing matter with true nanoscale spatial resolution has increased. In this work, we mapped the influence of local trap states within individual nanowires on carrier recombination with deeply subwavelength resolution. This is achieved using multidimensional nanospectroscopic imaging based on a nano-optical device. Placed at the end of a scan probe, the device delivers optimal near-field properties, including highly efficient far-field to near-field coupling, ultralarge field enhancement, nearly background-free imaging, independence from sample requirements, and broadband operation. We performed ~40-nanometer–resolution hyperspectral imaging of indium phosphide nanowires via excitation and collection through the probes, revealing optoelectronic structure along individual nanowires that is not accessible with other methods.

In the study of materials, optical microscopy maps the spatial distribution of a specific quantity (such as morphology), whereas optical spectroscopy provides physical and chemical material properties (such as electronic structure). An ongoing challenge to understanding matter at the nanoscale is the difficulty in carrying out local optical spectroscopy. On a fundamental level, this should be possible by squeezing light beyond the diffraction limit (*1*–*4*). Optical antenna–based geometries have been designed to address this nanospectroscopy imaging problem by transforming light from the far field to the near field, but with limitations on sensitivity, bandwidth, resolution, and/or sample types (*5*).

We report a strategy that overcomes these limitations, based on a geometry that is capable of efficiently coupling far-field light to the near field and vice versa, without background illumination over a wide range of wavelengths. The geometry consists of a three-dimensional (3D) tapered structure terminating in a nanometer-sized gap (Fig. 1A), with a shape resembling that of a "campanile" bell tower (hereafter referred to as campanile). We demonstrated with the campanile probe hyperspectral imaging of local optoelectonic properties in indium phosphide nanowires (InP NWs) by exciting and collecting signal through the probe tip. InP NWs, with their direct solar spectrum–matched bandgap and presumed low surface recombination velocity, are expected to be the central functional elements of next-generation light-harvesting devices. With the campanile probe, we collect full spectra at each pixel in a scan image, revealing photoluminescence (PL) heterogeneity along individual NWs by mapping local charge recombination originating from trap states: critical optoelectronic information that was unobtainable with previous methods.

Various near-field probe geometries have been engineered with extraordinary optical transmission (*6*) or with coupled optical antenna structures (*7*, *8*) directly on the scanning-probe apex, greatly improving coupling efficiencies as compared to conventional aperture-based probes (*9*)

[1]Molecular Foundry, Lawrence Berkeley National Laboratory, Berkeley, CA 94720, USA. [2]Department of Materials Science and Engineering, University of California Berkeley, Berkeley, CA 94720, USA. [3]European Laboratory for Non-Linear Spectroscopy, 50019 Sesto Fiorentino, Firenze, Italy. [4]Dipartimento di Fisica e Astronomia, Università di Firenze, 50019 Sesto Fiorentino, Firenze, Italy. [5]Istituto Nazionale di Ottica (CNR-INO), 50125 Firenze, Italy. [6]Department of Electrical Engineering and Computer Sciences, University of California Berkeley, Berkeley, CA 94720–1770, USA. [7]Department of Electrical Engineering, California Institute of Technology, Pasadena, CA 91125, USA.

*These authors contributed equally to this work.
†To whom correspondence should be addressed. E-mail: afweber-bargioni@lbl.gov (A.W.-B.); scabrini@lbl.gov (S.C.); pjschuck@lbl.gov (P.J.S.)

(fig. S2). However, these rely on resonant structures with limited spectral bandwidth and have often used excitation modalities that are not background-free, in which a diffraction-limited (or larger) spot illuminates the optical antenna, but also excites portions of the sample not in the immediate vicinity of the tip, leading to unwanted background (*10*, *11*). Of note are recent approaches combining elements of apertureless near-field scanning optical microscopy (a-NSOM) tips with efficient photon-to-plasmon coupling structures that can be illuminated far from the sample (*11*, *12*). When designed correctly, these types of probes can be broadband because they exploit adiabatic plasmonic compression (*13*, *14*). There is, however, one primary drawback to these probes: A large enhancement is achieved only for very small tip/metallic-substrate gap modes. Therefore, only very thin samples (such as molecular monolayers) can be studied. Our work overcomes these problems, merging broadband field enhancement and confinement with efficient bidirectional coupling between far-field and near-field electromagnetic energy. We take advantage of the campanile concept to map optoelectronic properties of InP NWs.

The campanile probe is based on a 3D tapered metal-insulator-metal (MIM) structure ending in a nanogap (Fig. 1, A to C). Our simulations show that this geometry provides efficient coupling between far and near fields (Fig. 1D), because the fundamental mode in an MIM structure is supported without any cutoff frequency, no matter how thin the insulating layer (*13*). In the optical regime, where plasmonic effects become important at small length scales, it has been shown that efficient delivery of far-field light to a confined ultrasmall region is possible in two dimensions, using a tapered planar MIM structure [>70% conversion efficiency (*15*)], and in three dimensions with a dimple lens structure (*16*). The bidirectional coupling of the campanile probe is efficient over a large bandwidth (Fig. 1G), taking advantage of an adiabatically tapered (*13*, *14*) geometry used at longer wavelengths [such as the microwave and terahertz regimes (*17*)] to provide one of the simplest broadband methods for effectively overcoming the diffraction limit. The bandwidth is limited only by metal absorption at short wavelengths and can be extended well into the infrared region and beyond.

The plasmonic mode in the campanile is confined to the gap region, which thus defines the spatial resolution as well as the field enhancement [the ratio of electric field strength ($|E|$) in the gap to the incoming field strength ($|E_0|$)]. This ratio is greater than that from a bowtie antenna with the same-sized gap (Fig. 1G and fig. S1).

The highly confined field in the gap region avoids the illumination of large areas of the sample that is characteristic of other near-field methods: an important goal for nano-optical imaging and spectroscopy (*10*, *11*). Also, in the taper region, only a few photons leave the tip because of edge scattering and leakage before reaching the apex. Considering that we operate in a mode where signal is collected back through the antenna gap, the background from the sample arising from the edge-scattered light is insignificant and below the noise threshold in the PL images shown here. As with all near-field probes, the campanile tips interrogate only material located within a few nanometers of the apex (Fig. 1F), eliminating most background spectroscopic signal arising from bulk material or surrounding fluid.

Using standard nanofabrication techniques, the antenna design illustrated in Fig. 1A can be integrated into the apex of a number of scanning probes such as the cantilevers used in atomic force microscopy or into the tapered optical fibers used in conventional aperture-based NSOM. Representative images of a campanile tip used in this work are shown in Fig. 1, B and C. For a linearly tapered 3D MIM structure, the optimal taper angle is around 20° to 40°, over which range the transfer efficiency shows only minor changes (*13*). Similar properties could be obtained in a tapered cylindrical coaxial structure.

To demonstrate the utility of this concept, campanile tips with ~40-nm-wide gaps were used

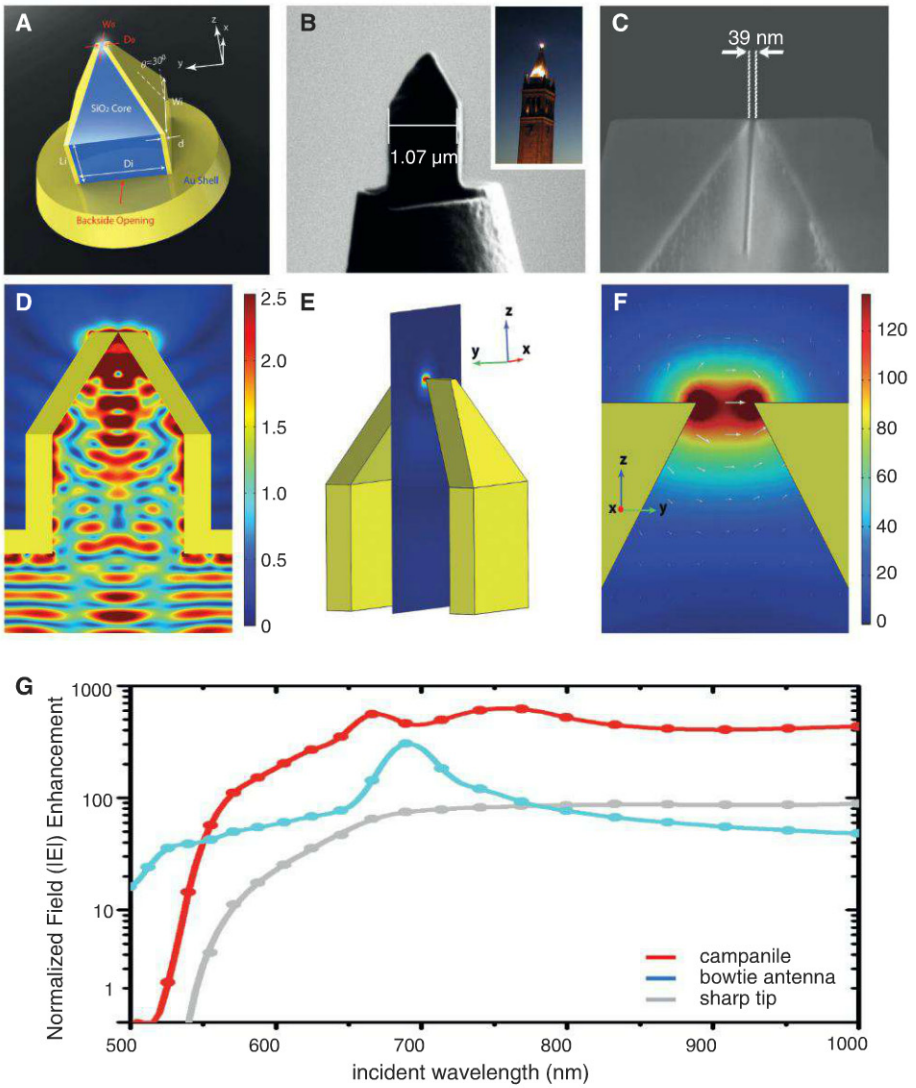

Fig. 1. Structure and optical properties of the 3D tapered (campanile) far-field to near-field transformer. The campanile geometry (**A**) is composed of a tapered metal insulator–metal waveguide fabricated at the end of a tapered glass fiber (**B**) by focused ion beam milling. Its shape resembles that of a bell tower of the same name (inset: photo of the Berkeley campanile), with a 39-nm (±2 nm) gap between the 3D tapered Au plates (**C**). (**D**) Finite element simulations reveal the highly efficient bidirectional coupling between macro and nano length scales (the electric field strength color-scale contrast is saturated to show the much weaker photonic and weakly confined plasmonic modes). Extending the contrast over the full color scale shows the nearly background-free near-field enhancement at the tip apex (**E**), while maintaining the linear polarization of the far field (**F**) (gap size = 10 nm; wavelength = 666 nm). (**G**) The ultralarge field ($|E|$) enhancement for a campanile with a 2-nm gap extends over larger bandwidth (red curve) than does a coupled optical bowtie antenna (blue curve) with a 2-nm gap or a sharp Au tip with a 20-nm radius of curvature (gray curve; assuming 100% light-coupling efficiency to the Au tip).

to map out the inhomogeneous radiative recombination in individual InP NWs, chosen because of their PL emission properties and potential as an ideal nanomaterial for light-harvesting due to the 1.4-eV bandgap and presumed low surface recombination rates (*18*–*20*). Trap states are believed to be responsible for many optical phenomena in nanocrystals and wires (*21*, *22*), including surface state–mediated luminescence modification in InP NWs (*23*), but are not well understood because of optical resolution limitations. Gaining this crucial insight requires both local optical excitation and local luminescence collection.

The glass fiber with the campanile tip was mounted in a shear-force scanner and coupled to a 633-nm laser. The near-field spot was scanned over the sample to locally excite and collect PL from InP NWs. Because of the huge field enhancement, only 100 μW of pre–fiber-coupled laser excitation power was needed to obtain a full emission spectrum between 760 and 900 nm. With a 100-ms integration time, a signal-to-noise ratio >60/1 was achieved.

Topography and a full spectrum were recorded at each image pixel, and PL maps were built by taking slices from the hyperspectral data set, which contains both amplitude and spectral variations. Figure 2 shows a 95-nm-wide InP NW imaged with a scanning electron microscope (Fig. 2A), with the campanile tip (Fig. 2B) and with a far-field confocal microscope (Fig. 2C). The confocal excitation power was the same as that used with the campanile tip. As can be seen, the campanile tip provides an optical resolution approximately equal to the gap size and much higher than the confocal resolution (Fig. 2D), as shown in the line scans in Fig. 2E, taken along the NW.

A typical PL spectrum from the center of a wire is shown in Fig. 3A, with the band-edge emission peak at 839 nm (1.47 eV) corresponding to the expected 100-meV blueshift relative to bulk InP NWs, independent of quantum confinement (*23*). Moreover, we observe various shoulders 40 to 100 meV above the band-edge emission that broaden the spectra considerably. With the campanile tip, we observed the spectral intensity and linewidth variations along individual NWs. PL emission intensities along the wire are mapped in Fig. 3, B to F, for wavelengths of 783, 802, 821, 839, and 857 nm. The first three maps represent the different shoulders above the band-edge emission and display considerable (300%) local variation of the PL intensity along an individual wire. For energies less than or equal to the band edge, the PL intensity remains fairly homogenous along the wire. In addition, for some of the studied wires, we observed PL hotspots located approximately 250 to 300 nm from one or both ends of the wire (compare Fig. 3, G and H, and fig. S1). The hot spots show spectral broadening toward the blue with additional luminescence 40 to 100 meV above the band edge, as seen in the waterfall plot of PL spectra from various points along the wire (Fig. 3I; PL peak intensity normalized to 1 for clarity). In contrast, confocal PL measurements of the same wire (Fig. 3J) also display two maxima but show no spectral variations along the NW (Fig. 3L), in agreement with previous confocal studies.

It was previously observed that strong PL enhancements and PL blueshifts result from passivated InP NW surfaces (*23*). This was attributed to Coulombic interactions between excitons and positively charged trap states on the NW surfaces (*21*). These studies proposed that trap states influence the optoelectronic properties of nanocrystals and NWs much more strongly than commonly assumed. The exciton diffusion length in these materials is hundreds of nanometers, and therefore individual trap states within the diffusion volume should strongly influence the local absorption energy and charge recombination rate.

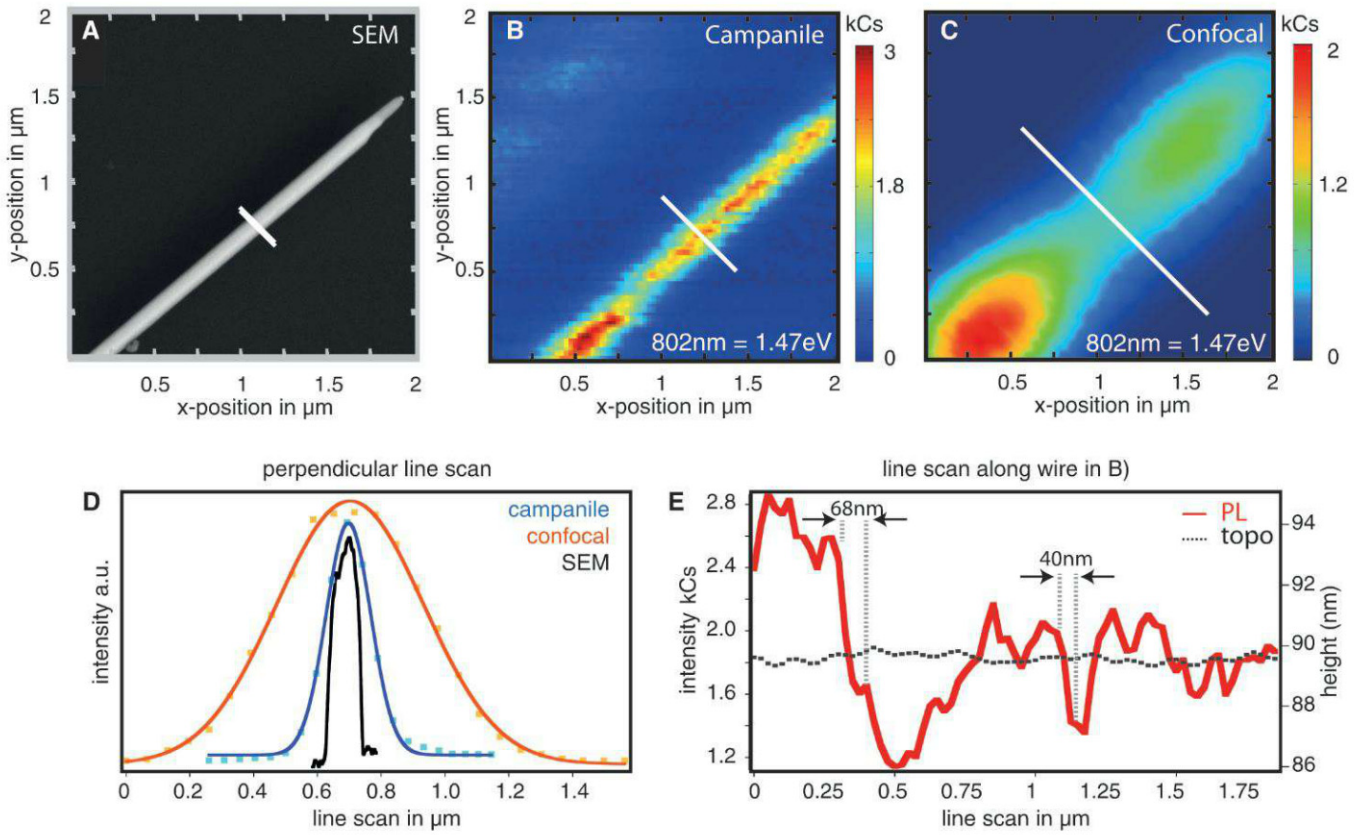

Fig. 2. Nano-optical hyperspectral PL mapping of InP NWs. (**A**) Scanning electron microscope (SEM) image of an InP NW that was hyperspectrally mapped with the campanile tip (**B**) (100 μW of excitation power, 100 ms per spectrum, map at 802 nm, intensity in kilocounts (kCs)), and confocally (**C**) (900 μW, 10 ms per spectrum, map at 802 nm). The near-field map (B) has considerably higher spatial resolution than the confocal map, as shown by the line scans across the wire (**D**) and strong local PL variations along the wire. a.u., arbitrary units. (**E**) A line scan along the wire length in (B) reveals a spatial resolution of ~40 nm (approximately equal to the gap size), whereas the topographic (topo) line scan shows negligible variations.

We believe that the heterogeneity observed along the wires (Figs. 2B and 3, B to F), on length scales well below the exciton diffusion length, are direct maps of trap-state modifications of the local exciton properties (*22*). The observed PL intensity hot spots (Fig. 3, G and J, and fig. S3) are probably due to an increase of trap-state densities (and changes in the native oxide layer) at the wire ends, resulting from the NW broken-end morphology. Their spectral characteristics are consistent with a trap-induced Stark shift, predicted to be ~60 to 70 meV above the band edge (*21*) for positive trap states (*23*), in accordance with our observations. Additionally, local trap states are known to cause Fermi level pinning and local band-bending in some cases (*21*), which would also affect local recombination rates. The absence of spectral variations in the confocal measurements is attributed to (i) lack of spatial resolution, and (ii) far-field PL measurement probing the entire NW thickness; i.e., surface-specific effects are obscured by bulk behavior. Cathodoluminesence measurements on InP NWs achieve a comparable resolution and provide complementary

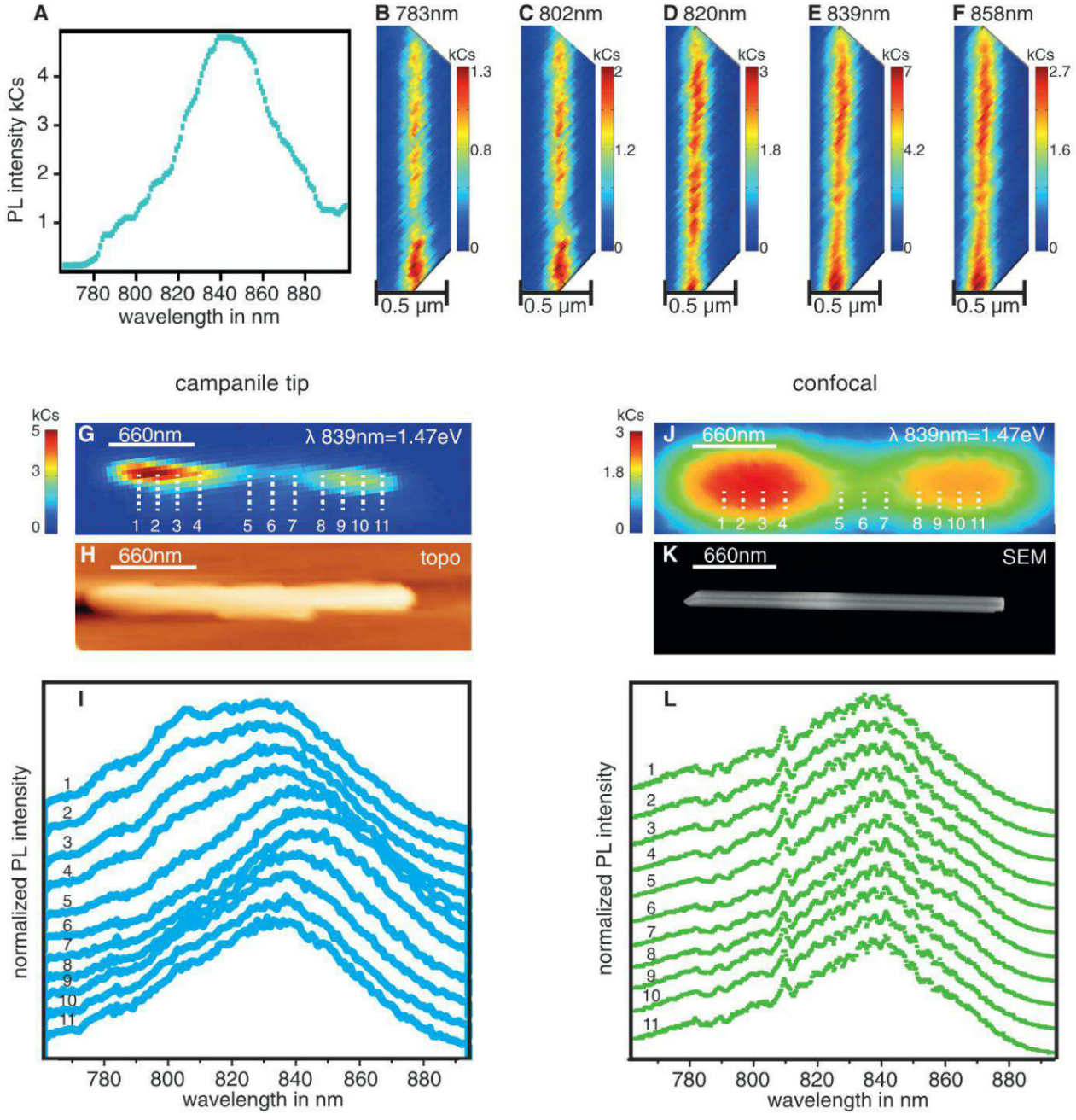

Fig. 3. Hyperspectral PL maps of InP NWs displaying local intensity (measured in kCs) and spectral variations. (**A**) Representative PL spectrum of the InP NW from Fig. 2, integrated over 10 ms. Various shoulders 40 to 100 nm above the band-edge emission at 839 nm are observed. Slices from the hyperspectral data at specific wavelengths are mapped (**B** to **F**), showing local intensity variations (up to a factor of 3) for the spectral components above the bandgap, whereas at bandgap energies and below, the PL is mostly homogenous. Images in (B) to (F) are raw data from a single hyperspectral scan. Other InP NWs displayed one (fig. S3) or two PL intensity hot spots (**G**) typically 250 to 300 nm from the wire ends as compared to topography (**H**) and SEM (**K**) images of the same NW. A waterfall plot of near-field spectra taken at positions 1 to 11 (peak emission intensity normalized to 1) shows strong local spectral variations, with the PL hot spots showing a band-edge blueshift as well as stronger contributions from trap-related spectral components above the bandgap (**I**). The same wire imaged confocally (**J**) displays two maxima but no spectral variations along the NW (**L**).

information. However, the large number of incident electrons fill the trap states and do not detect any spatial variation in emission from InP NWs (*24*).

We emphasize that the increased density of optical states at the tip apex will change the balance between various recombination pathways and may enable otherwise dark states to radiatively recombine (*25*–*27*). Finally, we note that measurements on NWs (and any sample thicker than ~2 nm) are not possible with NSOM in the tip-substrate gap mode, because that modality lacks the signal strength and sensitivity shown here, which is critical for investigating the majority of samples.

Campanile-style far-to-near–field transformers provide a pathway for understanding energy conversion processes at critical length scales, in our case yielding insights into the role of local trap states in radiative charge recombination in InP NWs. More generally, our study demonstrates the impact of the campanile geometry on a wide range of nano-optical measurements, because virtually all modes of optical imaging and spectroscopy are possible, including Raman and infrared/Fourier transform infrared hyperspectral imaging, as well as white-light nano-ellipsometry/interferometric mapping of dielectric functions. We expect that the combination of large bandwidth and enhancement makes them ideal for ultrafast pump-probe and/or nonlinear experiments down to molecular length scales (*28*–*31*). They also could be used for ultrasensitive medical detection, (photo) catalysis and quantum-optics investigations, as plasmonic optomechanics and circuitry elements, and as the cornerstone of tabletop high-harmonic/x-ray and photoemission sources.

References and Notes

1. R. Hillenbrand, T. Taubner, F. Keilmann, *Nature* **418**, 159 (2002).
2. L. Novotny, B. Hecht, *Principles of Nano-Optics* (Cambridge Univ. Press, Cambridge, 2006).
3. S. Kawata, Y. Inouye, P. Verma, *Nat. Photonics* **3**, 388 (2009).
4. D. Zhang *et al.*, *Phys. Rev. Lett.* **104**, 056601 (2010).
5. J. Stadler, T. Schmid, R. Zenobi, *Nanoscale* **4**, 1856 (2012).
6. Y. Wang, W. Srituravanich, C. Sun, X. Zhang, *Nano Lett.* **8**, 3041 (2008).
7. J. N. Farahani, D. W. Pohl, H. J. Eisler, B. Hecht, *Phys. Rev. Lett.* **95**, 017402 (2005).
8. A. Weber-Bargioni *et al.*, *Nano Lett.* **11**, 1201 (2011).
9. P. D. Yang *et al.*, *Adv. Funct. Mater.* **12**, 323 (2002).
10. D. Roy, J. Wang, C. Williams, *J. Appl. Phys.* **105**, 013530 (2009).
11. C. C. Neacsu *et al.*, *Nano Lett.* **10**, 592 (2010).
12. F. De Angelis *et al.*, *Nat. Nanotechnol.* **5**, 67 (2010).
13. M. Staffaroni, J. Conway, S. Vedantam, J. Tang, E. Yablonovitch, *Photonics Nanostructures Fundam. Appl.* **10**, 166 (2012).
14. M. I. Stockman, *Phys. Rev. Lett.* **93**, 137404 (2004).
15. P. Ginzburg, D. Arbel, M. Orenstein, *Opt. Lett.* **31**, 3288 (2006).
16. S. Vedantam *et al.*, *Nano Lett.* **9**, 3447 (2009).
17. E. Peytavit, J. F. Lampin, T. Akalin, L. Desplanque, *Electron. Lett.* **43**, 73 (2007).
18. J. F. Wang, M. S. Gudiksen, X. F. Duan, Y. Cui, C. M. Lieber, *Science* **293**, 1455 (2001).
19. J. M. Bao *et al.*, *Nano Lett.* **8**, 836 (2008).
20. K. Cho *et al.*, *Appl. Phys. Lett.* **98**, 203101 (2011).
21. A. Franceschetti, A. Zunger, *Phys. Rev. B* **62**, R16287 (2000).
22. S. A. Fischer, C. M. Isborn, O. V. Prezhdo, *Chem. Sci.* **2**, 400 (2011).
23. L. K. van Vugt, S. J. Veen, E. P. A. M. Bakkers, A. L. Roest, D. Vanmaekelbergh, *J. Am. Chem. Soc.* **127**, 12357 (2005).
24. N. Yamamoto, S. Bhunia, Y. Watanabe, *Appl. Phys. Lett.* **88**, 153106 (2006).
25. E. Shafran, B. D. Mangum, J. M. Gerton, *Phys. Rev. Lett.* **107**, 037403 (2011).
26. J. J. Greffet, *Science* **308**, 1561 (2005).
27. S. Kühn, U. Håkanson, L. Rogobete, V. Sandoghdar, *Phys. Rev. Lett.* **97**, 017402 (2006).
28. H. J. Maas *et al.*, *J. Opt. Soc. Am. B* **19**, 1295 (2002).
29. M. L. M. Balistreri, H. Gersen, J. P. Korterik, L. Kuipers, N. F. van Hulst, *Science* **294**, 1080 (2001).
30. P. Vasa, C. Ropers, R. Pomraenke, C. Lienau, *Laser Photon. Rev.* **3**, 483 (2009).
31. M. Seo *et al.*, *Nano Lett.* **10**, 2064 (2010).

Acknowledgments: The authors specifically thank E. Wong for fast and high-quality technical support, as well as our colleagues at the Molecular Foundry for stimulating discussion and assistance. We thank O. Yaghi, D. Milliron, M. Crommie, J. DeYoreo, and Y. D. Suh for valuable advice, discussions and reading of the manuscript. A provisional patent application regarding the fabrication of campanile-like structures on scan probes has been filed. Work at the Molecular Foundry was supported by the U.S. Department of Energy (DOE), Office of Basic Energy Sciences, Scientific User Facilities Division, under contract no. DE-AC02-05CH11231. Campanile tips were prepared by M. Melli, who was supported by the DOE, Office of Basic Energy Sciences, Materials Sciences and Engineering Division, under contract no. DE-AC02-05CH11231.

Supplementary Materials

www.sciencemag.org/cgi/content/full/338/6112/1317/DC1
Materials and Methods
Supplementary Text
Figs. S1 to S3
References (*32*, *33*)

26 July 2012; accepted 19 October 2012
10.1126/science.1227977

Robust Photogeneration of H_2 in Water Using Semiconductor Nanocrystals and a Nickel Catalyst

Zhiji Han,* Fen Qiu,* Richard Eisenberg,† Patrick L. Holland,† Todd D. Krauss†

Homogeneous systems for light-driven reduction of protons to H_2 typically suffer from short lifetimes because of decomposition of the light-absorbing molecule. We report a robust and highly active system for solar hydrogen generation in water that uses CdSe nanocrystals capped with dihydrolipoic acid (DHLA) as the light absorber and a soluble Ni^{2+}-DHLA catalyst for proton reduction with ascorbic acid as an electron donor at pH = 4.5, which gives >600,000 turnovers. Under appropriate conditions, the precious-metal–free system has undiminished activity for at least 360 hours under illumination at 520 nanometers and achieves quantum yields in water of over 36%.

Molecular hydrogen (H_2) is a clean-burning fuel that can be produced from protons (H^+) in the reductive half-reaction of artificial photosynthesis systems (*1*, *2*). One of the most prominent strategies for light-driven proton reduction features a multicomponent solution with a light-absorbing molecule (chromophore) that transfers electrons to a catalyst that reduces protons (*3*, *4*). However, these solution systems often use nonaqueous solvents and always have short lifetimes from decomposition of the chromophore over a period of hours (*5*). This difficulty has led to more-complicated architectures that separate the sites of light absorption and proton reduction (*2*).

Semiconductor nanocrystals (NCs) are promising alternative chromophores for light-driven proton reduction (*6*, *7*). Compared with traditional organic or organometallic chromophores, NCs have superior photostability, larger absorption cross-sections over a broad spectral range, orders of magnitude longer excited state lifetimes, electronic states and associated optical properties that vary with NC size, and the capacity to deliver multiple electrons with minimal structural perturbations (*6*, *7*). Heterostructures combining NCs with traditional precious-metal nanoparticle proton-reduction catalysts, or with iron hydrogenases, have produced efficient proton-reduction catalysis in solution (*8*–*10*). However, small-molecule catalysts in conjunction with NCs have given only modest H_2 production (*11*, *12*).

We report here a system that provides light-driven H_2 production with exceptional longevity, maintaining its high activity with no decrease for over 2 weeks using water as solvent. The system uses no precious metals and is based on light absorption and photoinduced electron transfer from semiconductor nanocrystals that are photochemically stable. Under optimal conditions, the system generates over 600,000 turnovers of H_2 (with respect to catalyst) without deterioration

Department of Chemistry, University of Rochester, Rochester, NY 14627, USA.

*These authors contributed equally to this work.
†To whom correspondence should be addressed. E-mail: eisenberg@chem.rochester.edu (R.E.); holland@chem.rochester.edu (P.L.H.); krauss@chem.rochester.edu (T.D.K.)

of activity and thus has promise for incorporation into full artificial photosynthesis (AP) systems.

Hydrophobic CdSe NCs with diameters varying from 2.5 to 5.5 nm [defined on the basis of the wavelength of the peak in their lowest energy excitonic absorption feature as NC(520) and NC(620) respectively, fig. S1] were synthesized by variations of literature methods (*13*, *14*). These NCs were subsequently rendered water soluble by capping with dihydrolipoic acid (DHLA, Fig. 1) (*14*). Photochemical experiments were performed in a custom-built 16-sample apparatus with excitation at 520 nm and a measurement uncertainty of 7.0% in the amount of H_2 produced (based on multiple-run experiments). Each 40-ml sample vessel contained 5.0 ml of solution, a cap with a sensor to allow real-time monitoring of head space pressure, and a port for quantitative analysis of H_2 production.

In a complete artificial photosynthesis system, two molecules of water are photochemically split into H_2 (reductive side) and O_2 (oxidative side) (*1*, *2*). Electrons from the oxidative side of the system are shuttled to the reductive side where they reduce protons to hydrogen. However, because of the complexity in building and optimizing such a complete artificial photosynthesis system, when studying the reductive half-reaction it is common for a sacrificial electron donor to be used to optimize catalysts for hydrogen production. Here, ascorbic acid (AA, 0.1 to 1.0 M) was used as the sacrificial electron donor, because reduction of protons by ascorbate is thermodynamically unfavorable (E) = –0.41 V] under these conditions (*15*) and therefore light energy is needed to bring about H_2 production (Fig. 1). Thus, this experiment provides a proof of principle regarding photochemical proton reduction.

In a typical experiment, production of hydrogen occurred upon irradiation (λ = 520 nm) of a solution formed from nickel(II) nitrate and NCs in water. Under appropriate conditions [10.0 μM $Ni(NO_3)_2$, 0.5 μM NC(570), and 1.0 M AA], the system continues to produce H_2 at a constant rate for over 360 hours (Fig. 2A). A control experiment without added Ni^{2+} yielded no substantial H_2 production (Fig. 2A). The unusual longevity is attributed to the use of NCs as the photosensitizer, because other systems using transition metal catalysis and small-molecule photosensitizers (organic dyes or Ru, Ir, Rh, or Re coordination compounds) cease activity in under 50 hours because of bleaching of the dye (*16*–*22*). Other recent reports have described NC photosensitizers in systems for H_2 production, but the activity and longevity were not comparable to those described here (*11*, *12*).

By using different concentrations of system components that were chosen to maximize catalyst activity [1.0 μM $Ni(NO_3)_2$, 5.0 μM NC(540), and 0.8 M AA, pH = 4.5 in water], this same system achieves a turnover number over 600,000 moles of H_2 per mole of catalyst after 110 hours and an initial turnover frequency of 7000 moles of H_2 per mole of catalyst per hour upon irradiation with 520-nm light (fig. S2). The slight decrease in H_2 production rate in fig. S2 results from depletion of AA as the electron donor and not from photochemical instability, as evidenced by the increasing lifetime of H_2 production with higher starting concentrations of AA (Fig. 2B). Even higher activity is obtained under the same irradiation conditions if the solvent is changed to 1:1 ethanol (EtOH):H_2O (fig. S3). The initial rate of H_2 production is saturated above [AA] = 0.3 M (Fig. 2B) and slows over time only upon depletion of the electron donor AA. Consistent with this interpretation, subsequent addition of AA restarts H_2 production (fig. S4).

We hypothesize that the catalytic system functions through light absorption by the CdSe nanocrystal, electron transfer to the catalyst, and then proton reduction by the catalyst. The oxidation of AA, which fills the photogenerated hole on the NC, leads to dehydroascorbic acid, $2e^-$, and $2H^+$. Ascorbic acid thus serves as both a potential source of hydrogen and as a buffer because of the production of the conjugate base, helping to maintain the acidic pH even as protons are reduced to hydrogen. The absorption wavelength maximum of the first excitonic state can be controlled by NC size, which correlates with the reduction potential of the excited state (*23*). In our photocatalytic H_2 production system, reducing NC size leads to an increase in the activity (Fig. 3A), which we attribute to an increase in NC reducing power. Conversely, there is no formation of H_2 with NC(620), presumably because the reduction potential for NC(620) is not reducing enough for catalyst activity (*12*). Because the NC absorption edge is to the blue of the light-emitting diode (LED) spectral emission profile, the system with NC(520) produces less H_2 than an identical one with NC(540).

Organic electron acceptors were also used as indicators for the reducing power of the CdSe NCs. When a 3.8 μM solution of NC(530) in 1:1 EtOH:H_2O was irradiated in the presence of methyl viologen dication (MV^{2+}) under N_2 for 5 min, a color change from orange to blue indicated formation of reduced viologen $MV^{+\bullet}$. A similar result was obtained by using a diquat acceptor DQ^{2+} [*N*,*N*′-(1,3-propylene)-5,5′-dimethylbipyridine], as indicated by the pink color of the reduced $DQ^{+\bullet}$ (fig. S5). Although the precise potential for each NC was not determined, the result for DQ^{2+} suggests that the reducing ability of NC(530) corresponds to a potential more negative than –0.7 V versus a normal hydrogen electrode (NHE), and thus the excited state is sufficiently reducing for H^+ reduction. These measurements agree with published cyclic voltammetric studies that indicate a reduction potential more negative than –1 V for CdSe NCs of this size (*23*).

The catalytic mechanism was evaluated by varying the concentrations of system components. When the Ni^{2+} concentration was varied, the rate of H_2 production reached a maximum at 20 μM Ni^{2+}, whereas when the concentration of NC(520) was varied, the rate leveled off above 4.0 μM NC (fig. S6). These results suggest that at a Ni^{2+} concentration of 20 μM or greater, the rate becomes limited by NC light absorption, whereas at a NC concentration of 4.0 μM, the system is limited by the H_2-forming reaction at Ni^{2+}. Similarly, the rate of H_2 production depends linearly on light intensity up to about 13 mW/cm^{-2} (fig. S7). Overall, it appears that photon absorption by NCs and catalysis by Ni^{2+} have similar enough rates that each can be rate-limiting under different conditions.

Quantum yields for H_2 generation were determined for the system at [Ni^{2+}] = 20 μM (where the rate of H_2 evolution is controlled by NC concentration) with NCs of different sizes. In water, the quantum yield ϕ based on two photons per H_2 evolved is 36 ± 10% at [NC(520)] = 1 to 2 μM, decreasing to 20 ± 2% at [NC(520)] = 4.0 μM (supplementary materials); similarly, ϕ(H_2) is 35 ±

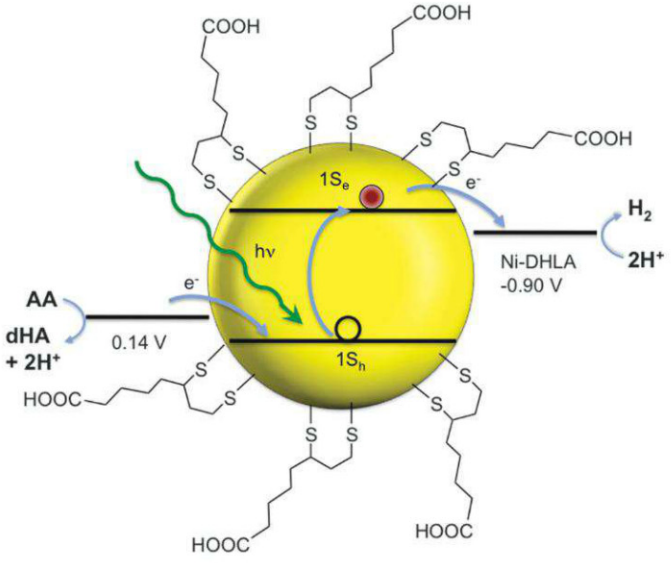

Fig. 1. Cartoon that illustrates the relevant energies for H_2 production. dHA indicates dehydroascorbic acid. Potentials are shown versus that of an NHE at pH = 4.5.

4% at [NC(540)] = 4.0 μM. The quantum yield reaches 59 ± 8% when using a 1:1 EtOH/H_2O mixture as the solvent (table S2). Complete conversion of all available light energy is presumably prevented by electron-hole recombination and/or fast nonradiative electronic relaxation.

We next sought to determine whether the active catalyst was on the NC surface or in solution during hydrogen photogeneration. After irradiation of a NC(540)-based H_2 generating system for 24 hours, the NCs were separated from the solution by centrifugation and filtration, and each component was examined separately for its H_2-generating activity with added AA. Neither the NCs nor the solution was found to have any substantial activity for photochemical H_2 generation. The chemical composition of the NCs and solution were each examined by atomic absorption spectroscopy (AAS), showing that >97% of the Ni and <3% of the Cd remained in solution whereas >97% of Cd and <3% of the Ni remained in the precipitated NCs (table S3). Additionally, transmission electron microscopy images of the separated NCs showed no substantial change in NC size, and energy dispersive x-ray analysis showed no evidence of colloidal Ni deposited on the NC surface (figs. S8 and S9). Addition of Ni^{2+} and AA to the NCs restored activity for H_2 production upon resuspension; likewise, when fresh NC(540) and AA were added to the Ni-containing solution, we observed activities that were similar to those during the initial irradiation (Fig. 3B). The results indicate that the active catalyst is a Ni species generated in solution and that the NCs maintain their ability to act as the photosensitizer during the catalytic process.

The use of different Ni^{2+} salts [$Ni(NO_3)_2$, $NiCl_2$, and Ni(acetate)$_2$] produced a similar level of H_2 production activity, suggesting that the actual catalyst is generated in situ. Because DHLA binds to Ni^{2+} with binding constants near or above 10^{10} (*24*) and nickel thiolates have previously been reported as catalysts for light-driven hydrogen production (*25*), we focused on the hypothesis that the catalyst is a nickel complex chelated by DHLA. Maintaining a solution of NC(520) at pH 4.5 under N_2 in the absence of light for 5 hours and centrifuging to precipitate the NCs gave a solution with 8 to 14 molecules of DHLA per NC, which had apparently dissociated from the NC. Due to the presence of free DHLA the formation of a Ni^{2+}-DHLA complex is both possible and favorable in the catalytic solutions. Adding up to 100 equivalents of excess DHLA gave similar activity toward H_2 production (fig. S10), but addition of EDTA (which prevents formation of a Ni^{2+}-DHLA complex) eliminated activity (fig. S11). Addition of colloidal Ni^0 (4 nm in diameter) in place of the nickel(II) salt gave no significant amount of H_2 under the standard catalytic conditions (fig. S11). Synthesizing the Ni^{2+}-DHLA catalyst ex situ and adding it to the NC solution (in place of Ni^{2+} salts) gives the same overall activity for H_2 production. All together, these experiments are consistent with a soluble nickel(II)-DHLA species being catalytically active. Lastly, electrochemical studies on independently prepared 1:1 Ni^{2+}:DHLA solutions (0.2 μM in 1:1 EtOH:H_2O) showed a cathodic feature at –0.9 V versus NHE that appears only upon addition of acid (fig. S12), indicating that Ni-DHLA can reduce protons catalytically and at a potential comparable to that produced by the excited NCs.

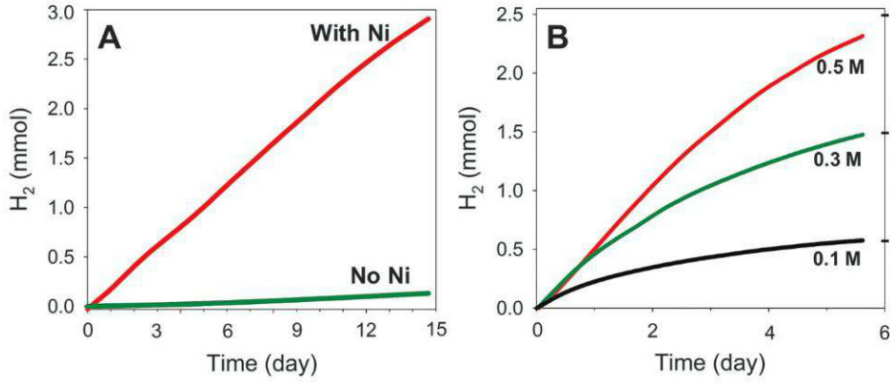

Fig. 2. (**A**) H_2 production over time from irradiation of an aqueous solution of $Ni(NO_3)_2$, NC(540), and AA. (**B**) Photoreductive H_2 production with different initial concentrations of AA in a system containing 20.0 μM $Ni(NO_3)_2$ and 1.0 μM NC(570). The marks on the right axis indicate the theoretical maximum of H_2 production on the basis of the amount of AA added. Hydrogen photogeneration experiments used a LED source (λ = 520 nm, 13 mW/cm^2) at 15°C and 1 atm initial pressure of N_2:CH_4 (79:21 mole %) with CH_4 as an internal standard for H_2 quantification by gas chromatography analysis.

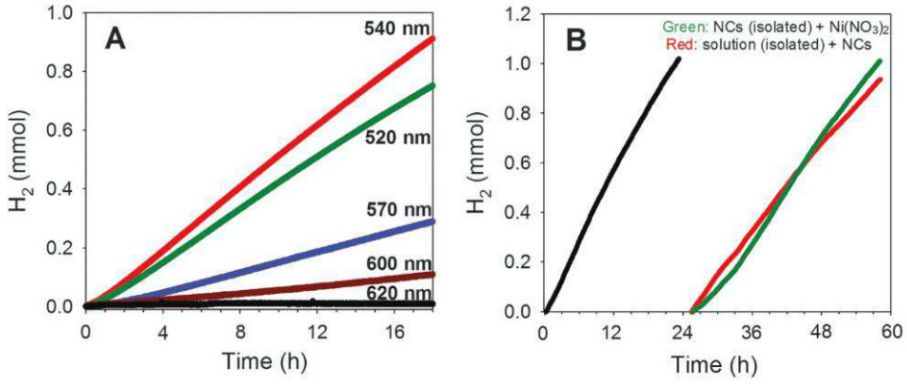

Fig. 3. (**A**) H_2 production from irradiation of aqueous solutions using different sizes of CdSe NCs (4.0 μM) labeled by the peak in their first excitonic absorption, 4.0 μM $Ni(NO_3)_2$, and 0.5 M AA. (**B**) After 24 hours, an active solution was filtered to separate the NCs from the solution and the nickel(II) catalyst. After the separation, each individual component was inactive but regained activity when the other was added.

Although we have not yet determined the structure of the catalytically active nickel species, spectroscopic studies on Ni^{2+}-DHLA help to understand the predominant forms of nickel in solution. The ultraviolet-visible spectrum of a 1:5 mixture of Ni^{2+} (50 μM) and DHLA (250 μM) at pH = 4.5 is very similar to that generated with a mixture of Ni^{2+} (50 μM) and 1,3-propanedithiol, suggesting that Ni^{2+} coordinates via the S donors of DHLA (fig. S13). The absorption maxima from a 1:1 Ni:DHLA solution follow Beer's Law between 5.0 and 500 μM, suggesting that nickel speciation does not change over the Ni^{2+} and DHLA concentrations used in the catalytic experiments (fig. S14). A Job plot of Ni^{2+} and DHLA in this concentration regime has a maximum at a metal:DHLA ratio of roughly 1:1, suggesting that the predominant complex has one DHLA per Ni^{2+} (fig. S14). X-ray crystal structures of nickel complexes with related dithiols (including 1,3-propanedithiol) have shown multimetallic structures containing square-planar nickel(II) centers bridged by thiolates, with stoichiometries such as 3:4, 4:4, 6:6, and 6:7 (*26*–*28*). Because nickel-thiolate species are labile in solution, many nickel species are accessible under the reaction conditions, and detailed mechanistic studies will be necessary to identify the one(s) responsible for proton reduction in this system.

A light-driven system for the photogeneration of hydrogen that consists of simple components containing only Earth-abundant elements could have a substantial impact on the sustainable production of chemical fuels. Further, the robustness of the system may be generalizable to other nanoparticle systems, such as type II NCs and dot-in-rod NCs (*6*, *10*), which are better engineered for charge separation. When considering the efficiency

of this system in a real-world context, further improvements could be made by adding light-harvesting components that absorb more of the solar spectrum, because with NC(540) only about 25% of the available solar flux is absorbed. Nonetheless, this particular NC-DHLA-Ni system exhibits high activity for proton reduction and impressive durability, which suggests that it could also serve as a valuable component in complete artificial photosynthetic water splitting systems for light-to-chemical energy conversion.

References and Notes

1. N. S. Lewis, D. G. Nocera, *Proc. Natl. Acad. Sci. U.S.A.* **103**, 15729 (2006).
2. J. H. Alstrum-Acevedo, M. K. Brennaman, T. J. Meyer, *Inorg. Chem.* **44**, 6802 (2005).
3. A. J. Bard, M. A. Fox, *Acc. Chem. Res.* **28**, 141 (1995).
4. A. J. Esswein, D. G. Nocera, *Chem. Rev.* **107**, 4022 (2007).
5. W. T. Eckenhoff, R. Eisenberg, *Dalton Trans.* **41**, 13004 (2012).
6. L. Amirav, A. P. Alivisatos, *J. Phys. Chem. Lett.* **1**, 1051 (2010).
7. K. A. Brown, S. Dayal, X. Ai, G. Rumbles, P. W. King, *J. Am. Chem. Soc.* **132**, 9672 (2010).
8. Y. Shemesh, J. E. Macdonald, G. Menagen, U. Banin, *Angew. Chem. Int. Ed.* **50**, 1185 (2011).
9. K. A. Brown, M. B. Wilker, M. Boehm, G. Dukovic, P. W. King, *J. Am. Chem. Soc.* **134**, 5627 (2012).
10. H. Zhu, N. Song, H. Lv, C. L. Hill, T. Lian, *J. Am. Chem. Soc.* **134**, 11701 (2012).
11. F. Wang *et al.*, *Angew. Chem. Int. Ed.* **50**, 3193 (2011).
12. M. A. Holmes, T. K. Townsend, F. E. Osterloh, *Chem. Commun. (Camb.)* **48**, 371 (2012).
13. D. V. Talapin *et al.*, *J. Phys. Chem. B* **108**, 18826 (2004).
14. Materials and methods are available in the online supplementary materials.
15. G. M. Brown, B. S. Brunschwig, C. Creutz, J. F. Endicott, N. Sutin, *J. Am. Chem. Soc.* **101**, 1298 (1979).
16. B. Probst, M. Guttentag, A. Rodenberg, P. Hamm, R. Alberto, *Inorg. Chem.* **50**, 3404 (2011).
17. B. F. DiSalle, S. Bernhard, *J. Am. Chem. Soc.* **133**, 11819 (2011).
18. T. M. McCormick *et al.*, *J. Am. Chem. Soc.* **132**, 15480 (2010).
19. W. R. McNamara *et al.*, *Proc. Natl. Acad. Sci. U.S.A.* **109**, 15594 (2012).
20. A. Fihri *et al.*, *Angew. Chem. Int. Ed.* **47**, 564 (2008).
21. D. Streich *et al.*, *Chemistry* **16**, 60 (2010).
22. T. A. White, B. N. Whitaker, K. J. Brewer, *J. Am. Chem. Soc.* **133**, 15332 (2011).
23. J. Jasieniak, M. Califano, S. E. Watkins, *ACS Nano* **5**, 5888 (2011).
24. F. Bonomi *et al.*, *Inorg. Chim. Acta* **192**, 237 (1992).
25. Z. Han, W. R. McNamara, M. S. Eum, P. L. Holland, R. Eisenberg, *Angew. Chem. Int. Ed.* **51**, 1667 (2012).
26. M. Köckerling, G. Henkel, *Inorg. Chem. Commun.* **3**, 117 (2000).
27. J. Sletten *et al.*, *Acta Chem. Scand.* **48**, 929 (1994).
28. W. Tremel, M. Kriege, B. Krebs, G. Henkel, *Inorg. Chem.* **27**, 3886 (1988).

Acknowledgments: Z.H. led the effort for hydrogen generation and catalysis, and F.Q. for nanocrystal synthesis and characterization. This work was supported by the Office of Basic Energy Sciences, U.S. Department of Energy, grant DE-FG02-09ER16121 and DE-SC0002106. The authors acknowledge the University of Rochester Medical Center and the Department of Environmental Medicine for the analytical support and R. M. Gelein for the cadmium and nickel AAS measurements.

Supplementary Materials

www.sciencemag.org/cgi/content/full/science.1227775/DC1
Materials and Methods
Figs. S1 to S16
Tables S1 to S3
References (*29*–*36*)

23 July 2012; accepted 10 October 2012
Published online 8 November 2012;
10.1126/science.1227775

Taming of Fluoroform: Direct Nucleophilic Trifluoromethylation of Si, B, S, and C Centers

G. K. Surya Prakash,* Parag V. Jog, Patrice T. D. Batamack, George A. Olah

Fluoroform (CF_3H), a large-volume by-product of the manufacture of Teflon, refrigerants, polyvinylidene fluoride (PVDF), fire-extinguishing agents, and foams, is a potent and stable greenhouse gas that has found little practical use despite the growing importance of trifluoromethyl (CF3) functionality in more structurally elaborate pharmaceuticals, agrochemicals, and materials. Direct nucleophilic trifluoromethylation using CF_3H has been a challenge. Here, we report on a direct trifluoromethylation protocol using close to stoichiometric amounts of CF_3H in common organic solvents such as tetrahydrofuran (THF), diethyl ether, and toluene. The methodology is widely applicable to a variety of silicon, boron, and sulfur-based electrophiles, as well as carbon-based electrophiles.

The trifluoromethyl group is an increasingly important functionality in materials and medicinal chemistry research (*1*). There has been a rapid increase in the development of trifluoromethylation methods as evidenced by ~300 publications since 2008 (*2*). In 1989, the discovery by Prakash and co-workers (*3*) of (trifluoromethyl)trimethylsilane ($TMSCF_3$, **1**), a compound originally prepared by Ruppert (*4*), as a nucleophilic CF_3 transfer reagent made an enormous impact in the field (*5*–*14*). Other higher-boiling silicon-based reagents, such as triethyl ($TESCF_3$) and triisopropyl ($TIPSCF_3$) analogs, were also developed for a variety of applications (*10*, *15*–*17*). Currently, these reagents are synthesized from ozone-depleting CF_3Br gas. At present, use of CF_3Br is being regulated due to Montreal protocol restrictions and, as a result, synthesis of these reagents is becoming increasingly limited and expensive (*18*–*21*). Efficient and new methodologies are needed that use readily available and abundant trifluoromethyl group sources such as CF_3H (*22*, *23*).

Fluoroform (also called trifluoromethane, CF_3H, and HFC-23) is a large-volume by-product in the manufacture of chlorodifluoromethane ($ClCF_2H$ or HCFC-22) used in the production of end products such as Teflon (DuPont), polyvinylidene fluoride (PVDF), refrigerants, fire-extinguishing agents, and foams. It is also a potent and stable greenhouse gas (atmospheric lifetime ~250 years) that has an estimated global warming potential 11,700 times greater than CO_2 (*24*). Large quantities of CF_3H are currently available in storage, and the amount residing in the atmosphere is projected to be about 24.3 kilotons by 2015 (*24*). Current CF_3H mitigation methods involve thermal oxidation, catalytic hydrolysis, and plasma destruction. All of these have economical and operational limitations, and hence conversion of CF_3H to useful and commercially viable products is a much-sought-after goal. However, synthetic use of CF_3H has been challenging because of its low boiling point (–83°C), high pK_a (25 to 28 in water), and low reactivity (as a weak carbon acid). The free trifluoromethyl anion (CF_3^-) generated after deprotonation can be unstable and decompose to fluoride ion (F^-) and singlet difluoromethylene ($:CF_2$) under many reaction conditions due to the concentrated negative charge on the carbon atom.

The use of CF_3H for trifluoromethylation of carbonyl compounds has been explored under specific reaction conditions by Shono, Troupel, Normant, Langlois, and others (*25*–*31*). This was achieved using an electrogenerated base (*25*, *26*) or a strong base to deprotonate CF_3H with subsequent trapping of CF_3^- (trifluoromethyl anion) by dimethylformamide (DMF) to produce a reservoir of trifluoromethylating hemiaminolate species (*27*–*30*). This hemiaminolate species is not capable of reacting with a broad variety of electrophilic silicon, boron, and elemental sulfur centers. Grushin and co-workers have achieved direct copper-mediated trifluoromethylations of haloarenes, haloheteroarenes (*32*) and, more recently, aryl boronic acids (*33*) and α-haloketones (*34*) using CF_3H in DMF. These methods, however, require excess of CF_3H [2 to 3 equivalent (equiv)] and have limited scope. A direct trifluoromethylation method using CF_3H in common solvents [tetrahydrofuran (THF), ether, hexanes, and toluene]

Loker Hydrocarbon Research Institute, Department of Chemistry, University of Southern California, CA 90089, USA.

*To whom correspondence should be addressed. E-mail: gprakash@usc.edu

would be very attractive from a practical point of view (*32*, *33*, *35*). Here, we disclose (*36*) straightforward and practical protocols for the direct nucleophilic trifluoromethylations using stoichiometric amounts of CF_3H.

Initial experiments were performed by dissolving CF_3H in THF and using potassium hexamethyldisilazide, KHMDS (1 M in THF, 1 equiv.) as a base in the presence of trimethylsilyl chloride (TMSCl) at –40°C (see table S1 for a summary of the optimization process). ^{19}F nuclear magnetic resonance (NMR) analysis of the crude reaction mixture showed a new fluorine peak at –67.3 parts per million (ppm), corresponding to $TMSCF_3$ along with other peaks, including that of trimethylsilyl fluoride (TMSF). Change in the reaction temperature, order of addition of reagents, and use of additives or other etheral solvents did not improve the results (see the supplementary materials for a brief discussion). However, use of toluene (a hydrocarbon) as a solvent resolved the impasse, minimizing formation of TMSF under the optimized conditions and leading to >90% conversion to $TMSCF_3$. The pure product was isolated by distillation in 80% overall yield (Fig. 1A). The presence of K^+ as the counter cation of the base appears to be rather important. Using the above conditions, $TMSCF_3$ is obtained as a major product only with KHMDS. Sodium hexamethyldisilazide (NaHMDS) gave $TMSCF_3$ as only a minor product, whereas lithium hexamethyldisilazide (LiHMDS) failed to give the desired product. This observation regarding the importance of the counter cation K^+ has also been noted by others in the past (*37*). On the other hand, other metal-based CF_3-M-CF_3 species, where M is Cu, Ag, or Au, are known and have been observed recently in the gas phase by mass spectrometry (*38*).

We propose that the reaction mechanism to produce $TMSCF_3$ proceeds by deprotonation of CF_3H with KHMDS to generate CF_3^-, which immediately reacts with TMSCl to form a pentacoordinated silicon species (**A**), which eventually loses chloride ion and generates $TMSCF_3$ (Fig. 1B). However, our attempts to observe species **A** by NMR spectroscopy (Fig. 1B) were not successful because the rate of the subsequent reaction is extremely rapid (see fig. S1 and accompanying text). Another mechanistic possibility could be two partial reactions, one between KHMDS and TMSCl to form tris(trimethylsilyl)amine [$N(SiMe_3)_3$], a known silylating agent, and a second between KHMDS and CF_3H to produce CF_3^- followed by a subsequent reaction between tris(trimethylsilyl)amine and CF_3^- to give $TMSCF_3$. However, in the case of all other alkyl-substituted silyl chlorides, none of the trimethylsilylated product was observed (by ^{19}F NMR), suggesting that such a cross-metathesis mechanistic pathway is unlikely.

The developed protocol was extended to prepare other synthetically important alkyl-substituted trifluoromethylated silanes in good yields (Fig. 1), using ether as a solvent because the boiling points of most of the higher trifluoromethylated silanes were very close to the boiling point of toluene. Preparation of higher alkyl-substituted analogs of trifluoromethylated silanes are reported in the literature using trifluoromethyl halides (*4*, *18*–*20*); however, the highest reported yield of (trifluoromethyl)triisopropylsilane was only 9%, whereas with the present procedure, the same compound can be obtained in 78% isolated yield (Fig. 1A). In addition to monotrifluoromethylation reactions, bistrifluoromethylation of dichlorodimethylsilane and dichlorodiethylsilane was achieved in good conversion, although isolation of bis(trifluoromethyl)dimethylsilane was difficult owing to its volatility (boiling point 30°C). The same protocol can also be applied to synthesize tris(trifluoromethyl) phenylsilane [$PhSi(CF_3)_3$] (from trichlorophenylsilane); however, multiple products (based on ^{19}F NMR) were observed in the reaction. Similarly, tetrakis (trifluoromethyl)silane [$Si(CF_3)_4$] (from silicon tetrachloride) was observed along with other

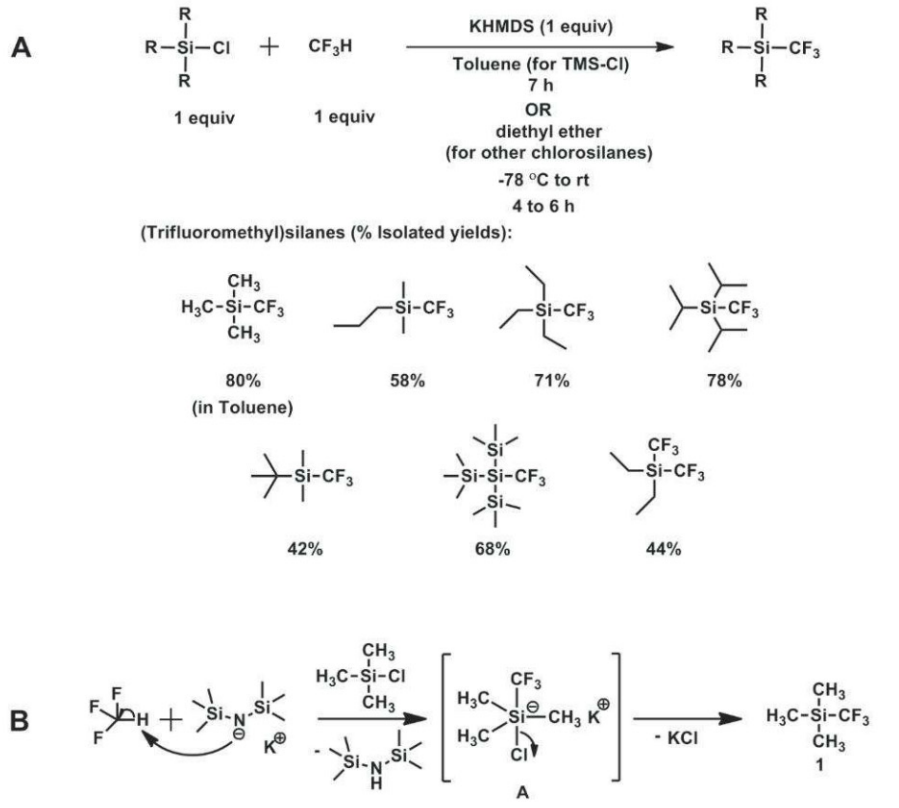

Fig. 1. Direct trifluoromethylation of silyl chlorides using CF_3H. (**A**) Synthesis of various (trifluoromethyl)silanes. (**B**) Plausible mechanism of trifluoromethylation of trimethylsilyl chloride using fluoroform and KHMDS.

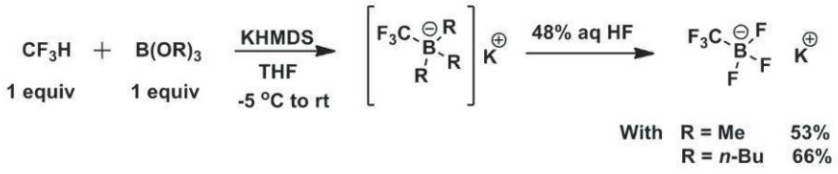

Fig. 2. Direct trifluoromethylation of trialkyl borates using CF_3H.

Fig. 3. Direct trifluoromethylation of elemental sulfur using CF_3H.

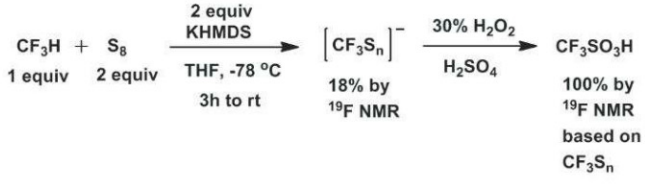

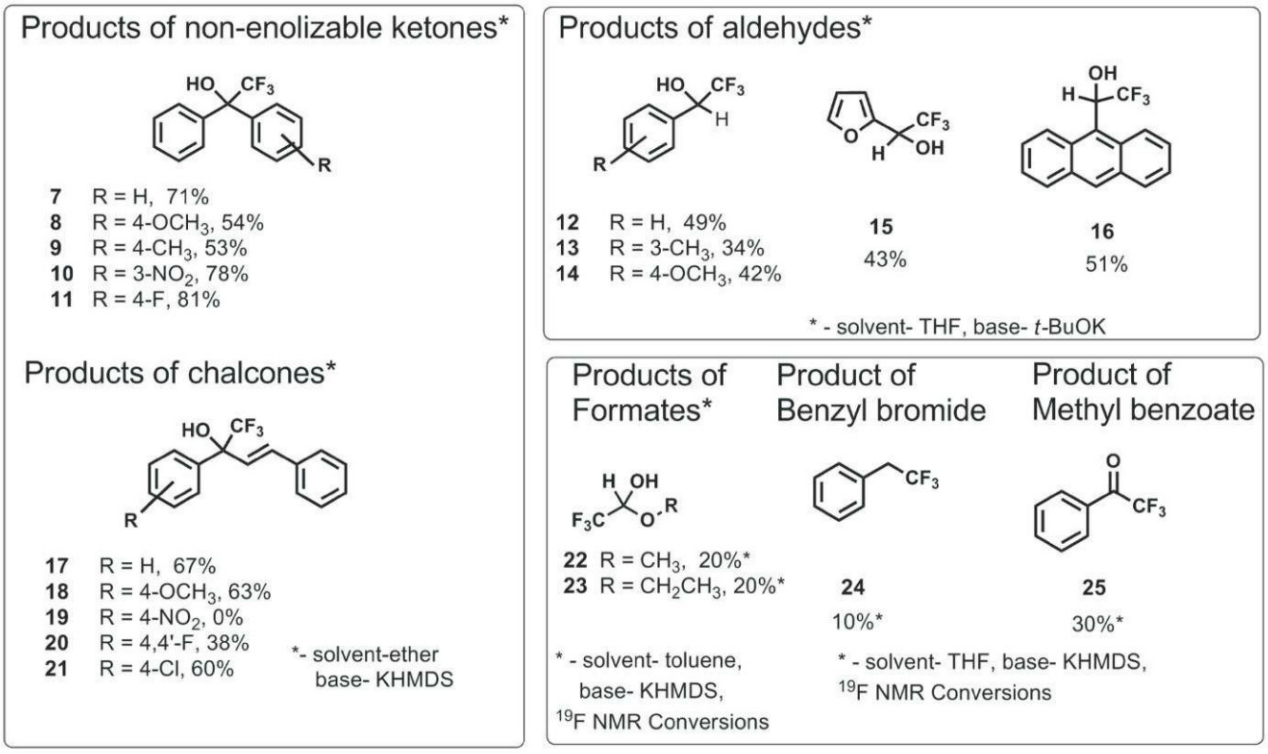

Fig. 4. Trifluoromethylated products of carbon-based electrophiles using CF_3H.

fluorinated products (possibly mono, bis, and tris trifluoromethylated silanes). Due to complexity of the ^{19}F NMR spectra representing multiple products, isolation and purification of these tris and tetrakis (trifluoromethylated) products was not further pursued.

Nucleophilic trifluoromethylation using organoboron reagents, specifically potassium (trifluoromethyl)trifluoroborate (CF_3BF_3K), is also becoming increasingly important. The common electrophiles used include nonenolizable aldehydes, *N*-tosylimines, aryl iodides, and more recently, aryl boronates (*39*–*41*). Synthesis of CF_3BF_3K is reported in the literature (*42*, *43*). However, all of the existing methods use $TMSCF_3$ as the trifluoromethylating reagent to prepare (trifluoromethyl)trialkylborates followed by fluorination using 48% aqueous (aq) HF to make CF_3BF_3K. Hence, a direct trifluoromethylation of trialkyl borates using CF_3H, instead of having to make $TMSCF_3$ from CF_3H, could confer an efficiency advantage. We achieved trifluoromethylation of trialkyl borates [trimethyl borate and tri(*n*-butyl) borate] using CF_3H (1 equiv.) and KHMDS as a base in THF at –5°C followed by gradual warming of the reaction mixture to room temperature. Although potassium trimethoxy(trifluoromethyl) borate [$CF_3B(OMe)_3K$] was formed with good conversion, isolation of the salt in its pure form from the reaction mixture proved to be difficult. This could possibly be due to decomposition of the desired product by further reactions with residual KHMDS. Hence, we decided to fluorinate the $CF_3B(OMe)_3K$ using 48% HF (aq). This transformation occurred smoothly, resulting in the isolation of CF_3BF_3K salt from both $CF_3B(OMe)_3K$ and $CF_3B(O\text{-}nBu)_3K$, respectively, in preparatively useful yields in two steps (Fig. 2).

Another large-volume trifluoromethylated product is trifluoromethanesulfonic acid (CF_3SO_3H), a widely used Brønsted superacid (*44*). Current industrial synthesis of CF_3SO_3H is carried out by electrochemical fluorination of methanesulfonic acid (Simon's Process) (*45*). Although the conversions are high, use of HF is required for the electrolysis. A more recent industrial process is the conversion of trifluoroacetic acid to CF_3SO_3H developed by Rhodia, Inc. (*46*). Direct trifluoromethylation of elemental sulfur using CF_3H and subsequent oxidation of the products obtained would facilitate a straightforward synthesis of CF_3SO_3H. This approach has been attempted by others using the DMF trapping protocol (*44*, *47*), albeit with limited success (1.5% yield based on CF_3H). Using KHMDS in THF, we achieved direct trifluoromethylation of elemental sulfur with stoichiometric amounts of CF_3H with no need for DMF. The intermediate products (trifluoromethylated sulfur species, $[CF_3S_n]^-$) obtained were subjected to complete oxidation using concentrated H_2SO_4/30% H_2O_2 to afford CF_3SO_3H in modest 18% conversion (Fig. 3). The reaction is being further optimized to achieve higher conversions with the aim to make it commercially viable.

Based on our trifluoromethylation results with silanes, borates, and elemental sulfur, we revisited trifluoromethylation of aromatic nonenolizable ketones, aldehydes, chalcones, formate esters, benzyl bromide, and methyl benzoate. In all cases, we were able to trifluoromethylate each of the substrates in moderate to good yields using KHMDS or, in some cases, even potassium *tert*-butoxide (*t*-BuOK) as a base. Importantly, all the reactions were performed without using DMF (Fig. 4 and supplementary materials).

In summary, in contrast to previous methods (*29*, *37*), which have employed excess CF_3H and DMF (and related amides) as trapping agents to stabilize CF_3^- with limited synthetic potential, we have tamed CF_3H under simple conditions to obtain excellent results. Direct nucleophilic trifluoromethylation of silicon, boron, sulfur, and carbon electrophiles has been achieved using stoichiometric amounts of CF_3H in ordinary nonpolar solvents such as THF/ether or toluene and a base, providing a vast potential for the efficient use of CF_3H, with broad applications to medicinal and materials chemistry fields.

References and Notes

1. K. Müller, C. Faeh, F. Diederich, *Science* **317**, 1881 (2007).
2. As of 20 July 2012, based on the search performed in SciFinder Scholar with trifluoromethylation as research topic and number of articles published between 2008 and 2011.
3. G. K. S. Prakash, R. Krishnamurti, G. A. Olah, *J. Am. Chem. Soc.* **111**, 393 (1989).
4. I. Ruppert, K. Schlich, W. Volbach, *Tetrahedron Lett.* **25**, 2195 (1984).
5. G. K. S. Prakash, M. Mandal, *J. Fluor. Chem.* **112**, 123 (2001).
6. G. K. S. Prakash, A. K. Yudin, *Chem. Rev.* **97**, 757 (1997).
7. Y. Ye, M. S. Sanford, *J. Am. Chem. Soc.* **134**, 9034 (2012).
8. Y. Ye, S. H. Lee, M. S. Sanford, *Org. Lett.* **13**, 5464 (2011).
9. N. D. Ball, J. W. Kampf, M. S. Sanford, *J. Am. Chem. Soc.* **132**, 2878 (2010).
10. E. J. Cho *et al.*, *Science* **328**, 1679 (2010).
11. G. G. Dubinina, H. Furutachi, D. A. Vicic, *J. Am. Chem. Soc.* **130**, 8600 (2008).

12. J. F. Hartwig, H. Morimoto, P. Fier (Univ. of Illinois, USA, 2012), pp. 60 U.S. Patent Appl. 20120226041.
13. H. Morimoto, T. Tsubogo, N. D. Litvinas, J. F. Hartwig, *Angew. Chem. Int. Ed.* **50**, 3793 (2011).
14. F. Wang *et al.*, *Angew. Chem. Int. Ed.* **50**, 7153 (2011).
15. G. P. Stahly (Ethyl Corp., USA, 1989), pp. 9 U.S. Patent 4804774A.
16. G. P. Stahly, D. R. Bell, *J. Org. Chem.* **54**, 2873 (1989).
17. T. Hagiwara, T. Kobayashi, T. Fuchikami, *Nippon Kagaku Kaishi* **1997**, 869 (1997).
18. G. Pawelke, *J. Fluor. Chem.* **42**, 429 (1989).
19. J. Grobe, J. Hegge, *Synlett* **1995**, 641 (1995).
20. P. Ramaiah, R. Krishnamurti, G. K. S. Prakash, *Org. Synth.* **72**, 232 (1995).
21. G. K. S. Prakash, A. K. Yudin, D. Deffieux, G. A. Olah, *Synlett* **1996**, 151 (1996).
22. G. K. S. Prakash, J. Hu, G. A. Olah, *J. Org. Chem.* **68**, 4457 (2003).
23. G. K. S. Prakash, J. Hu, G. A. Olah (Univ. of Southern California, USA, 2004), pp. 15 U.S. Patent 6,803,477.
24. W. Han, Y. Li, H. Tang, H. Liu, *J. Fluor. Chem.* **140**, 7 (2012).
25. T. Shono, M. Ishifune, T. Okada, S. Kashimura, *J. Org. Chem.* **56**, 2 (1991).
26. R. Barhdadi, M. Troupel, J. Perichon, *Chem. Commun.* (12): 1251 (1998).
27. B. Folleas, I. Marek, J.-F. Normant, J. L. Saint, *Tetrahedron Lett.* **39**, 2973 (1998).
28. B. Folleas, I. Marek, J.-F. Normant, L. Saint-Jalmes, *Tetrahedron* **56**, 275 (2000).
29. B. R. Langlois, T. Billard, *Synthesis* **2**, 185 (2003).
30. B. R. Langlois, T. Billard, *ACS Symp. Ser.* **911**, 57 (2005).
31. S. Large, N. Roques, B. R. Langlois, *J. Org. Chem.* **65**, 8848 (2000).
32. A. Zanardi, M. A. Novikov, E. Martin, J. Benet-Buchholz, V. V. Grushin, *J. Am. Chem. Soc.* **133**, 20901 (2011).
33. P. Novak, A. Lishchynskyi, V. V. Grushin, *Angew. Chem. Int. Ed.* **51**, 7767 (2012).
34. P. Novák, A. Lishchynskyi, V. V. Grushin, *J. Am. Chem. Soc.* **134**, 16167 (2012).
35. I. Popov, S. Lindeman, O. Daugulis, *J. Am. Chem. Soc.* **133**, 9286 (2011).
36. G. K. S. Prakash, P. V. Jog, P. T. D. Batamack, G. A. Olah (Univ. of Southern California, USA, 2012), pp. 42 PCT. Int. Appl. WO2012148772A1.
37. T. Billard, B. R. Langlois, G. Blond, *Eur. J. Org. Chem.* **2001**, 1467 (2001).
38. N. J. Rijs, R. A. J. O'Hair, *Dalton Trans.* **41**, 3395 (2012).
39. T. Knauber, F. Arikan, G. V. Röschenthaler, L. J. Goossen, *Chem. Eur. J.* **17**, 2689 (2011).
40. V. V. Levin, A. D. Dilman, P. A. Belyakov, M. I. Struchkova, V. A. Tartakovsky, *Tetrahedron Lett.* **52**, 281 (2011).
41. B. A. Khan, A. E. Buba, L. J. Goossen, *Chem. Eur. J.* **18**, 1577 (2012).
42. A. A. Kolomeitsev *et al.*, *Tetrahedron Lett.* **44**, 8273 (2003).
43. G. A. Molander, B. P. Hoag, *Organometallics* **22**, 3313 (2003).
44. G. A. Olah, G. K. S. Prakash, A. Molnar, J. Sommer, *Superacid Chemistry* (Wiley, Hoboken, NJ, ed. 2, 2009).
45. R. E. Banks, Ed., *Preparation, Properties, and Industrial Applications of Organofluorine Compounds* (Ellis Horwood Ltd., Chichester, UK, 1982).
46. G. Forat, J.-M. Mas, L. Saint-Jalmes (Rhone-Poulenc Chimie SA, Fr. 1996), pp. 16 Eur. Patent 735023A1.
47. S. Mukhopadhyay, A. T. Bell, R. V. Srinivas, G. S. Smith, *Org. Process Res. Dev.* **8**, 660 (2004).

Acknowledgments: Support of our work by the Loker Hydrocarbon Research Institute is gratefully acknowledged.

Supplementary Materials

www.sciencemag.org/cgi/content/full/338/6112/1324/DC1
Materials and Methods
Supplementary Text
Figs. S1 to S3
Tables S1 and S2
References (*48*–*54*)

24 July 2012; accepted 11 October 2012
10.1126/science.1227859

Self-Terminating Growth of Platinum Films by Electrochemical Deposition

Yihua Liu, Dincer Gokcen, Ugo Bertocci, Thomas P. Moffat*

A self-terminating rapid electrodeposition process for controlled growth of platinum (Pt) monolayer films from a K_2PtCl_4-NaCl electrolyte has been developed that is tantamount to wet atomic layer deposition. Despite the deposition overpotential being in excess of 1 volt, Pt deposition was quenched at potentials just negative of proton reduction by an alteration of the double-layer structure induced by a saturated surface coverage of underpotential deposited H (H_{upd}). The surface was reactivated for further Pt deposition by stepping the potential to more positive values, where H_{upd} is oxidized and fresh sites for the adsorption of $PtCl_4^{2-}$ become available. Periodic pulsing of the potential enables sequential deposition of two-dimensional Pt layers to fabricate films of desired thickness, relevant to a range of advanced technologies.

Platinum (Pt) is a key constituent in a wide range of heterogeneous catalysts, but its high cost constrains the development of important alternative energy conversion systems such as low-temperature fuel cells (*1*–*3*). Strategies for enhancing catalyst performance and minimizing Pt loadings include alloying and nanoscale engineering of core/shell and related architectures that typically involve spontaneous processes, such as dealloying and segregation, to form Pt-rich surface layers (*4*, *5*).

The deposition of two-dimensional (2D) Pt layers, which are also of interest in thin-film electronics and magnetic materials, is nontrivial because of the step-edge barrier to interlayer transport that results in roughening or 3D mound formation (*6*). In situ scanning tunneling microscopy (STM) of Pt electrodeposition at moderate overpotentials reveals that metal nucleation and growth on Au single-crystal surfaces proceeds by the formation of 3D clusters at defect sites (*7*). At small overpotentials, x-ray scattering indicates that smooth Pt monolayers can be electrodeposited on Au(111), although a long growth time of 2000 s is required (*8*). Voltammetric studies show a potential dependent transition between 2D island versus 3D multilayer growth, although it is only possible to obtain a partial Pt monolayer coverage in the 2D growth regime (*9*).

To circumvent these difficulties, surface-limited place-exchange reactions are being explored. For example, galvanic displacement of an underpotential deposited (upd) metal monolayer, typically Cu, occurs by the desired Pt-group metal, with the exchange resulting in a submonolayer coverage of the noble metal (*10*, *11*). The process can be repeated to form multiple layers by means of a variant known as electrochemical atomic layer epitaxy (*12*). The multistep process typically requires an exchange of electrolytes and some care to control (or avoid) the trapping of the less-noble metal as a minor alloying constituent within the film. The reversible nature of many upd reactions makes it difficult to control deposition processes, especially subnanometer-scale films. Robust additive fabrication schemes are facilitated by irreversible processes analogous to vapor-phase deposition of thin films at low temperatures, although kinetic factors often constrain the quality of the resulting films (*6*).

Prior analytical studies of Pt deposition have largely limited the applied potential to values positive of underpotential deposited H (H_{upd}) and proton reduction. One intriguing exception is Pt deposition from a pH 10, $Pt(NH_3)_2(H_2O)_2^{2+}$-$NaHPO_4$ electrolyte, in which inhibition of the reaction was evident as the potential was scanned into the H_{upd} region, although the magnitude and thus importance of the effect were not examined (*13*). Here, we show that the formation of a saturated H_{upd} layer exerts a quenching or self-terminating effect on Pt deposition, restricting it to a high coverage of 2D Pt islands. When repeated, by using a pulsed potential waveform to periodically oxidize the H_{upd} layer, sequential deposition of discrete Pt layers can be achieved. The process is thus analogous to atomic layer deposition (ALD), but with a rapid potential cycle replacing the time-consuming displacement and replacement of the ambient reactant.

We focus on Pt deposition experiments performed at room temperature in aqueous solutions consisting of 0.5 mol/liter NaCl and 3 mmol/liter K_2PtCl_4, with pH values ranging between 2.5 and 4 (*14*). Apart from this particular electrolyte, self-terminating Pt deposition was observed over a wide range of pH and Cl^- concentrations and was not dependent on the oxidation state (2^+, 4^+) of the Pt halide precursors. To isolate the partial current associated only with the growth process, an electrochemical quartz crystal microbalance

Material Measurement Laboratory, National Institute of Standards and Technology (NIST), Gaithersburg, MD 20899, USA.
*To whom correspondence should be addressed. E-mail: thomas.moffat@nist.gov

(EQCM) was used to track Pt deposition on a Au electrode as the potential was swept in the negative direction. Voltammetry in Fig. 1A shows the onset of Pt deposition at 0.25 V versus a sodium-saturated calomel reference electrode (V_{SSCE}), followed by a substantial current rise to a maximum at −0.32 V_{SSCE} that is close to diffusion-limited $PtCl_4^{2-}$ reduction. Beyond the peak, the deposition rate decreased smoothly as the mass transfer boundary layer thickness expanded. A sharp drop in the current occurred when the potential moved negative of −0.5 V_{SSCE}, eventually reaching a minimum near −0.7 V_{SSCE}, followed by an increase caused by H evolution from water. The gravimetrically determined (with the EQCM) metal deposition rate revealed that the sharp drop below -0.5 V_{SSCE} corresponded to the complete quenching of metal deposition. This remarkable self-termination or passivation process occurred despite the large applied overpotential (>1 V) available for driving the deposition reaction.

The gravimetric data were used to reconstruct the partial voltammogram for Pt deposition: a two-electron process. Good agreement with the measured voltammogram indicates that the current efficiency of Pt deposition is nearly 100% as the potential is swept toward the diffusion-limited value. When the current peak was approached, an apparent loss in efficiency was observed, apparently because nonuniform deposition developed as the $PtCl_4^{2-}$ depletion gradient set up a convective flow field that spanned the electrode. In contrast to the EQCM results, voltammetry with a rotating disk electrode (RDE) provided uniform mass transport that yielded a more symmetric peak (Fig. 1B). The contribution of the proton reduction reaction was isolated by performing voltammetry in the absence of the Pt complex. Merging of the respective voltammograms at negative potentials indicates that quenching of the metal deposition reaction was coincident with the onset of the H_2 evolution reaction. The overlap of the diffusion-limited proton reduction current also indicates the absence of substantial homogeneous reaction between the generated H_2 and $PtCl_4^{2-}$, excluding this reaction as an explanation for the quenching of the Pt deposition reaction.

The two-electron reduction of $PtCl_4^{2-}$ to Pt was not expected to depend on pH, and the onset of appreciable Pt deposition from $PtCl_4^{2-}$ at 0.0 V_{SSCE} shown in Fig. 1D supports this contention. In contrast, sharp acceleration of the deposition rate below −0.2 V_{SSCE} was pH-dependent and correlated with the onset of H_{upd} evident in $PtCl_4^{2-}$-free voltammetry (Fig. 1C). Chronocoulometry studies indicate that the transition between a halide and a H-covered Pt surface occurred in the same regime (*15*). The metal deposition rate increased with H_{upd} coverage and reached a peak value that was independent of pH, whereas the peak potential shifted by −0.059 V/pH, reflecting the importance of H surface chemistry in controlling the Pt deposition process. The onset of proton reduction in the absence of $PtCl_4^{2-}$, marked by the dotted line in Fig. 1, B and C, occurred at essentially the same potential. Thus, the peak deposition rate occurred at the H reversible potential.

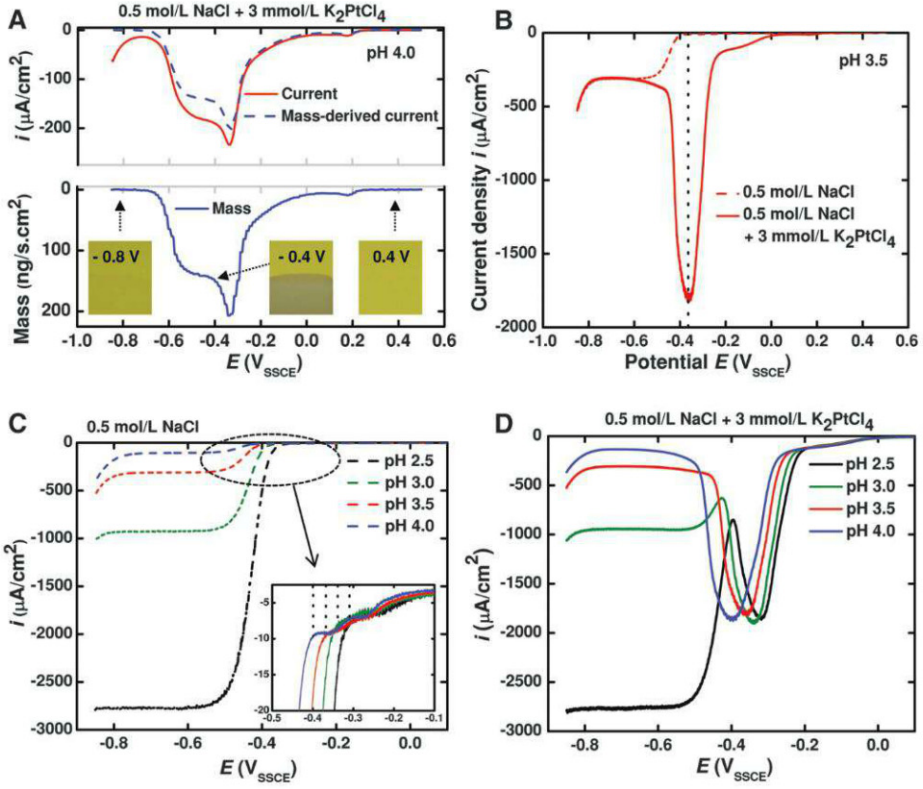

Fig. 1. Gravimetric (**A**) and voltammetric (**B** to **D**) measurements (2 mV/s) of Pt deposition from a NaCl-$PtCl_4^{2-}$ solution using either a static EQCM or an RDE (400 rpm). The insets in (A) are optical images of Pt films grown on 1–cm-wide Au-coated Si(100) wafers for 500 s at the indicated potentials. Voltammetry reveals the effect of pH on the background reactions (on a Pt RDE) and on $PtCl_4^{2-}$ reduction (on a Au RDE).

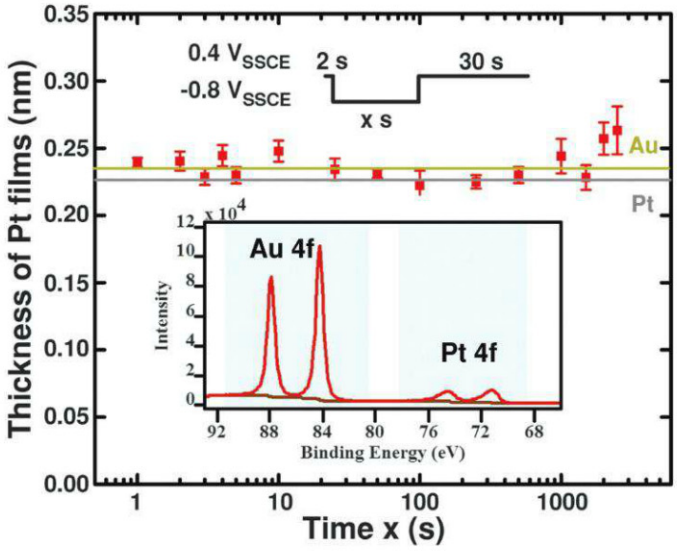

Fig. 2. XPS-derived thickness (red squares) of Pt films as a function of deposition time at −0.8 V_{SSCE} on Au-coated Si wafers from a pH 4 solution. The Au and Pt lines correspond to the (111) d-spacing of the respective bulk metals.

Moving to more-negative potentials, the metal deposition rate declined rapidly, and within 0.1 V of its peak value, the current merged with that attributable solely to diffusion-limited proton reduction, indicating complete quenching of the Pt deposition reaction.Transient studies of H_{ads} on Pt indicate that the coverage did not reach saturation at the reversible H potential but rather occurred 0.1 V below the reversible value (*16*). This potential regime is precisely the one in which the metal deposition reaction is fully quenched. Cyclic voltammetry revealed that the passivation process was reversible, with reactivation being coincident with the onset of H_{upd}

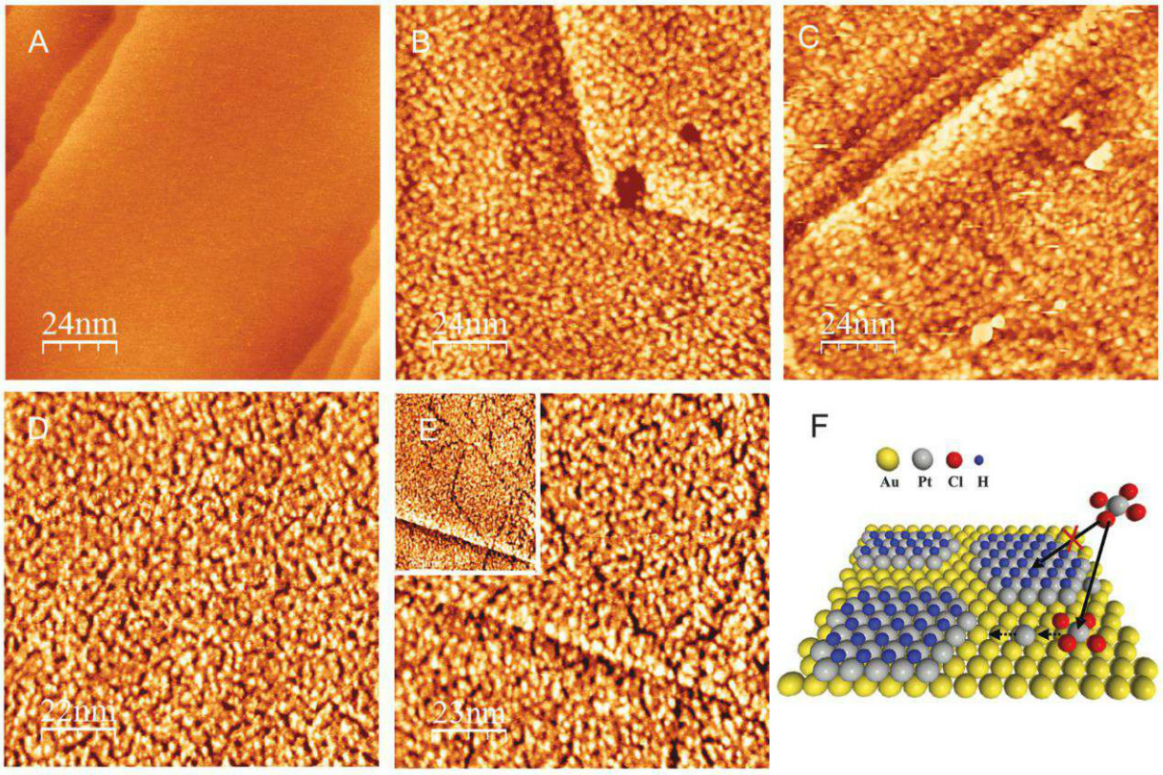

Fig. 3. (**A**) STM images of representative Au(111) surface with monoatomic steps. (**B** and **C**) 2D Pt layers obtained after (B) 5 s and (C) 500 s of deposition at −0.8 V_{SSCE}. (**D**) High-contrast image of 2D Pt layer morphology on Au(111). (**E**) Linear defects in a Pt layer associated with lifting of the reconstructed Au substrate. Inset, lower-magnification image. (**F**) A schematic of H_{upd}-terminated Pt deposition on Au(111).

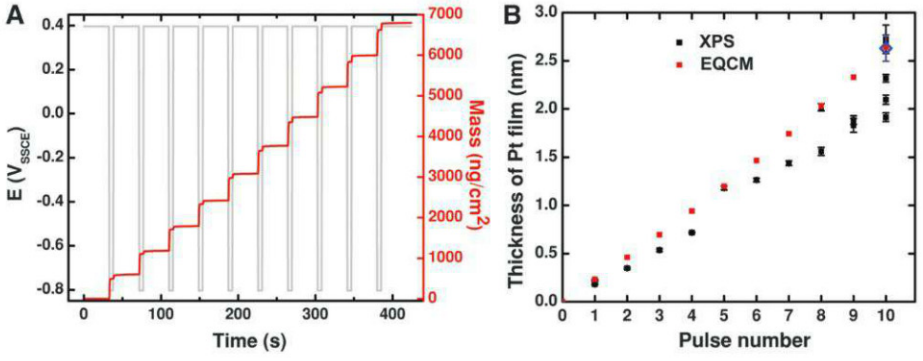

Fig. 4. Sequential deposition of Pt monoatomic layers by pulsed deposition in a pH 4 solution. (**A**) Mass change accompanying each potential pulse. (**B**) EQCM mass increase is converted to thickness and compared with XPS measurements. XPS analysis of the EQCM specimen (blue diamond) and a series of Pt films deposited on Au-coated Si wafers (black squares) are shown.

oxidation (fig. S1 and supplementary text). Self-termination of the metal deposition reaction arose from perturbation of the double-layer structure that accompanies H_{ads} saturation of the Pt surface. Recent theoretical work indicates that the water structure adjacent to a H-covered Pt(111) surface is altered; the centroid of the O atoms within the first water layer is displaced by more than 0.1 nm from the metal surface as the water-water interactions in the first layer become stronger (*17*). In a related development, an EQCM study of Pt in sulfuric acid identified a "potential of minimal mass" near the reversible potential of H reactions (*18*). The gravimetric measurements reflect the impact of H_{upd} on the adjacent water structure, which leads to a minimum in coupling between the electrode and electrolyte, consistent with the recent theoretical result. In addition to H_{upd} perturbation of the water structure, the quenching of the metal deposition reaction occurred at potentials negative of the Pt point of zero charge (pzc), where anions would have been desorbed (*15*). The above combination exerts a remarkable effect whereby $PtCl_4^{2-}$ reduction is completely quenched while diffusion-limited proton reduction continues unabated.

Self-terminating Pt deposition was also examined under potentiostatic conditions. Optical micrographs of a selection of films after 500 s of deposition at various potentials are shown as insets in Fig. 1A. Only the lower half of a Au-coated Si(100) wafer was immersed in solution, where differences in reflectivity and color indicate the anomalous dependence of deposition on potential; specifically, a 33–nm-thick Pt film was deposited at −0.4 V_{SSCE} while a nearly invisible much thinner layer was grown at −0.8 V_{SSCE}.

X-ray photoelectron spectroscopy (XPS) further quantified the composition and thickness of Pt grown as a function of deposition time and potential on (111) textured Au (*14*). For films deposited at −0.8 V_{SSCE}, a representative spectrum with the 4f doublets for the metallic states of Au and Pt is shown in Fig. 2 (inset). The ratio of the Pt and Au peak areas was used to calculate the Pt thickness, assuming it forms a uniform overlayer (*14*, *19*). For deposition times up to 1000 s, the measured thickness varied between 0.21 and 0.25 nm, congruent with the deposition of a Pt monolayer with a thickness comparable to the (111) d-spacing of Pt. Monolayer formation was complete within the first second of stepping the potential to −0.8 V_{SSCE}, and the absence of further growth confirmed the self-terminating nature of the deposition reaction. Beyond 1000 s, an additional increment of Pt deposition was evident. Inspection of the surface with scanning electron microscopy revealed a sparse coverage of spherically shaped Pt particles on the surface attributable to H_2-induced precipitation, a process requiring some heterogeneity and extended incubation to nucleate. Particle formation can be avoided by using shorter deposition times.

STM was used to directly observe the morphology of the Pt overlayer (*14*). Analysis was facilitated by using a flame-annealed Au(111) surface with isolated surface steps, 0.24 ± 0.02 nm in height, that served as fiduciary markers

(Fig. 3A). Pt deposition resulted in three distinct levels of contrast that reflect the surface height, with the lowest level being the original Au terraces (Fig. 3B). The same three-level structure was observed independently of deposition time up to 500 s (Fig. 3C). The middle contrast level corresponds to a high density of Pt islands that covered ~85% of the Au surface, with a step height of ~0.24 nm, consistent with XPS results. Inspection with a higher rendering contrast revealed a ~10% coverage of a second layer of small Pt islands with a step height ranging between 0.23 and 0.26 nm (Fig. 3D). Step positions associated with the flame-annealed substrate were preserved, with negligible expansion or overgrowth of the 2D Pt islands occurring beyond the original step edge. The lateral span of the Pt islands was 2.02 ± 0.38 nm, corresponding to an area of 4.23 ± 1.97 nm^2. Incipient coalescence of the islands was constrained by surrounding (dark) narrow channels, 2.1 ± 0.25 nm wide, that account for the remaining Pt-free portion of the first layer. The reentrant channels correspond to open Au terrace sites that were surrounded by adjacent Pt islands in what amounted to a huge increase in step density relative to the original substrate, the net geometric or electronic effect of which was to block further Pt deposition. The chemical nature of the inter-island region was assayed by exploiting the distinctive voltammetry of Pt and Au with respect to H_{upd} and oxide formation and reduction (fig. S2 and supplementary text).

Similar three-level Pt overlayers have been observed for monolayer films produced by molecular beam epitaxy (MBE) deposition at 0.05 monolayers/min (*20*). Pt-Au intermixing driven by the decrease in surface energy that accompanies Au surface segregation was evident. In the present work, Pt monolayer formation was effectively complete within 1 s, giving a growth rate three orders of magnitude greater than in the MBE-STM study. Exchange of the deposited Pt with the underlying Au substrate was expected to be less developed. However, intermixing and possible chemical contrast (i.e., the ligand effect) were evident on limited sections of the surface that were correlated with the original faulted geometry of the partially reconstructed Au surface. Upon lifting of the reconstruction, the excess Au atoms expelled mark the original fault location as linear 1D surface defects in the Pt overlayer (Fig. 3E). A simplified schematic of the self-terminating Pt deposition process in Fig. 3F describes how the H_{upd} accompanying incremental expansion of the 2D Pt islands can hinder the development of a second Pt layer, presumably by perturbation of the overlying water structure (*17*). This rapid process resulted in a much higher Pt island coverage than has been obtained by other methods, such as galvanic exchange reactions.

Because the saturated H_{upd} coverage is the agent of termination, reactivation for further Pt deposition was possible by removing the upd layer by sweeping or stepping the potential to positive values, e.g., >+0.2 V_{SSCE}, where negligible Pt deposition occurs. Sequential pulsing between +0.4 V_{SSCE} and −0.8 V_{SSCE} enabled Pt monolayer deposition to be controlled in a digital manner. EQCM was used to track the mass gain, showing two net increments per cycle (Fig. 4A). We attributed the mass gain to a combination of Pt deposition [486 ng/cm^2 for a monolayer of Pt(111)], anion adsorption and desorption (41 ng/cm^2 for 7 × 10^{14} Cl^- ion/cm^2, 117 ng/cm^2 for a 0.14 fractional coverage of $PtCl_4^{2-}$) (*7*, *21*), and coupling to other double-layer components such as water. The anionic mass increments were expected to be asymmetric for the first cycle on the Au surface, but once it was covered, subsequent cycles only involved Pt surface chemistry. After correcting for the electroactive surface area of the Au electrode ($A_{real}/A_{geometric}$ = 1.2, derived from reductive desorption of Au oxide in perchloric acid), the net mass gain for each cycle indicates that a near-pseudomorphic layer of Pt was deposited. XPS analysis of Pt films grown in various deposition cycles gave remarkably good agreement with EQCM data (Fig. 4B). The ability to rapidly manipulate potential and double-layer structure, as opposed to the exchange of reactants, offers simplicity, substantially improved process efficiency, and far greater process speed than other surface-limited deposition methods.

References and Notes

1. F. T. Wagner, R. Lakshmanan, M. F. Mathias, *J. Phys. Chem. Lett.* **1**, 2204 (2010).
2. M. K. Debe, *Nature* **486**, 43 (2012).
3. M. T. M. Koper, Ed., *Fuel Cell Catalysis, A Surface Science Approach* (Wiley, Hoboken, NJ, 2009).
4. V. R. Stamenkovic *et al.*, *Nat. Mater.* **6**, 241 (2007).
5. R. R. Adzic *et al.*, *Top. Catal.* **46**, 249 (2007).
6. T. Michely, J. Krug, *Islands, Mounds and Atoms, Patterns and Processes in Crystal Growth Far from Equilibrium* (Springer Series in Surface Science, V42, Springer, New York, 2003).
7. H. F. Waibel, M. Kleinert, L. A. Kibler, D. M. Kolb, *Electrochim. Acta* **47**, 1461 (2002).
8. T. Kondo *et al.*, *Electrochim. Acta* **55**, 8302 (2010).
9. I. Bakos, S. Szabo, T. Pajkossy, *J. Solid State Electrochem.* **15**, 2453 (2011).
10. S. R. Brankovic, J. X. Wang, R. R. Adzic, *Surf. Sci.* **474**, L173 (2001).
11. D. Gokcen, S.-E. Bae, S. R. Brankovic, *Electrochim. Acta* **56**, 5545 (2011).
12. B. W. Gregory, J. L. Stickney, *J. Electroanal. Chem.* **300**, 543 (1991).
13. A. J. Gregory, W. Levason, R. E. Noftle, R. Le Penven, D. Pletcher, *J. Electroanal. Chem.* **399**, 105 (1995).
14. See supplementary materials on *Science* Online.
15. N. Garcia-Araez, V. Climent, E. Herrero, J. Feliu, J. Lipkowski, *J. Electroanal. Chem.* **582**, 76 (2005).
16. D. Strmcnik, D. Tripkovic, D. van der Vliet, V. Stamenkovic, N. M. Markovic, *Electrochem. Commun.* **10**, 1602 (2008).
17. T. Roman, A. Groß, Structure of water layers on hydrogen-covered Pt electrodes. *Cataly. Today*; http://dx.doi.org/10.1016/j.cattod.2012.06.001 (2012).
18. G. Jerkiewicz, G. Vatankhah, S. Tanaka, J. Lessard, *Langmuir* **27**, 4220 (2011).
19. P. J. Cumpson, M. P. Seah, *Surf. Interface Anal.* **25**, 430 (1997).
20. M. O. Pedersen *et al.*, *Surf. Sci.* **426**, 395 (1999).
21. Y. Nagahara *et al.*, *J. Phys. Chem. B* **108**, 3224 (2004).

Acknowledgments: We thank J. J. Mallett for his early observations on the difficulty of electrodepositing Pt films at negative potentials. This work was supported by NIST–Material Measurement Laboratory programs. The x-ray photoelectron spectrometer was provided by NIST–American Recovery and Reinvestment Act funds. Y.L. thanks the NIST–National Research Council Postdoctoral Fellowship Program for support. NIST has filed a provisional patent application (Atomic Layer Deposition of Pt from Aqueous Solutions) based on this work.

Supplementary Materials

www.sciencemag.org/cgi/content/full/338/6112/1327/DC1
Materials and Methods
Supplementary Text
Figs. S1 and S2
References (*22*–*26*)

16 August 2012; accepted 17 October 2012
10.1126/science.1228925

Phase Transformations and Metallization of Magnesium Oxide at High Pressure and Temperature

R. Stewart McWilliams,[1,2]*† Dylan K. Spaulding,[3]‡ Jon H. Eggert,[4] Peter M. Celliers,[4] Damien G. Hicks,[4] Raymond F. Smith,[4] Gilbert W. Collins,[4] Raymond Jeanloz[3,5]

Magnesium oxide (MgO) is representative of the rocky materials comprising the mantles of terrestrial planets, such that its properties at high temperatures and pressures reflect the nature of planetary interiors. Shock-compression experiments on MgO to pressures of 1.4 terapascals (TPa) reveal a sequence of two phase transformations: from B1 (sodium chloride) to B2 (cesium chloride) crystal structures above 0.36 TPa, and from electrically insulating solid to metallic liquid above 0.60 TPa. The transitions exhibit large latent heats that are likely to affect the structure and evolution of super-Earths. Together with data on other oxide liquids, we conclude that magmas deep inside terrestrial planets can be electrically conductive, enabling magnetic field–producing dynamo action within oxide-rich regions and blurring the distinction between planetary mantles and cores.

Magnesium oxide (MgO) is among the simplest oxides constituting the rocky mantles of terrestrial planets such as Earth and the cores of Jupiter and other giant planets. Present in Earth's mantle as an end-member component of the mineral (Mg,Fe)O magnesiowüstite,

it can be abundant in larger planets due to the theoretically expected dissociation of (Mg,Fe)SiO_3 perovskite (*1*). Among common planetary constituents, MgO is thought to be especially resistant to transformation under pressure and temperature, having a high melting temperature (*2*–*7*), a wide electronic band gap under pressure (*1*, *8*, *9*), and a simple phase diagram featuring three phases at the high pressures explored in the present study: the B1 (NaCl)–structured solid found at ambient conditions, the liquid state, and an as-yet-unobserved high-pressure crystalline phase having the B2 (CsCl) structure (*1*–*5*, *9*, *10*).

[1]Geophysical Laboratory, Carnegie Institution of Washington, 5251 Broad Branch Road, NW, Washington, DC 20015, USA. [2]Howard University, 2400 Sixth Street, NW, Washington, DC 20059, USA. [3]Department of Earth and Planetary Science, University of California, Berkeley, CA 94707, USA. [4]Physics Division, Physical and Life Science Directorate, Lawrence Livermore National Laboratory, Livermore, CA 94550, USA. [5]Department of Astronomy and Miller Institute for Basic Research in Science, University of California, Berkeley, CA 94720, USA.

*To whom correspondence should be addressed. E-mail: stewartmcwilliams@gmail.com

†Present address: Grupo de Geociencias, Departamento de Física, Universidad de Los Andes, Bogotá, Colombia

‡Present address: Commissariat à L'Énergie Atomique, Département de Physique Théorique et Appliquée, Bruyères le Châtel, 91297 Arpajon Cedex, France.

To characterize MgO at the elevated pressures and temperatures of planetary interiors, we measured its pressure-volume (P, V) equation of state to 0.6 TPa (6 Mbar) and its temperature (T) and optical reflectivity (R) to beyond 1.4 TPa (14 Mbar) and 50,000 K under shock loading (*11*). We determined shock temperature and corresponding shock velocity (U_S) using the method of decaying shocks (*11*–*14*), in which an optically thick and reflecting shock wave decreases in amplitude as it propagates, revealing—through time-resolved measurement of emission, velocity, and reflectivity—the properties of a continuum of shock states (Fig. 1). Determining the corresponding particle velocity (U_P) in separate experiments (Fig. 2 and fig. S1) allows for the derivation of pressure and volume from our measurements (*11*, *15*).

We observe that the shock temperature does not change monotonically with pressure, as expected for a single phase (*15*, *16*), but instead shows a large anomaly with a temperature minimum at about 0.45 TPa and 8500 K (Figs. 1 and 2). Two additional regions of anomalous behavior (at about 0.65 TPa and beyond 1 TPa) are most evident when examining the specific heat, C_V, of the shock states (Fig. 2B) (*11*–*13*). In broad regions of our data, C_V closely matches the Dulong-Petit limit ($C_V = 6\ R_{gas}$, where R_{gas} is the gas constant per mole of atoms), consistent with the presence of a pure MgO phase above the Debye temperature (~760 K) (*12*, *13*, *15*); in three distinct regions, however, there is substantial deviation from this value. The anomalous values of C_V suggest the influence of latent heats associated with structural, bonding or electronic transitions.

Indeed, beginning with the second transition (0.55 TPa) there is an increase in optical reflectivity (Fig. 2C) from ~0.5%—a value consistent with the optical properties of low-pressure, insulating MgO (*17*) (figs. S2 and S3)—toward ~20%, indicating substantial changes in electronic properties. A simple (Drude-semiconductor) model of the measured reflectivities (*11*–*13*) is consistent with the energy gap between valence and conduction electronic bands nearly vanishing during the second transition (Fig. 2C), resulting in metallic conductivities $>10^4$ S/m above 0.60 to 0.70 TPa (fig. S4) (*11*).

To interpret these experimental results, we constructed a Mie-Grüneisen-Debye, finite-strain equation-of-state (*16*, *18*) for MgO constrained by the shock data (*11*). From this model, we assess phase-transition properties, such as the volume and entropy of transformation (ΔV_{tr} and ΔS_{tr}, respectively). We find that the low-pressure behavior of MgO (to 0.35 TPa and 9500 K) is well described with this model, taking parameters solely from measurements on B1-MgO near

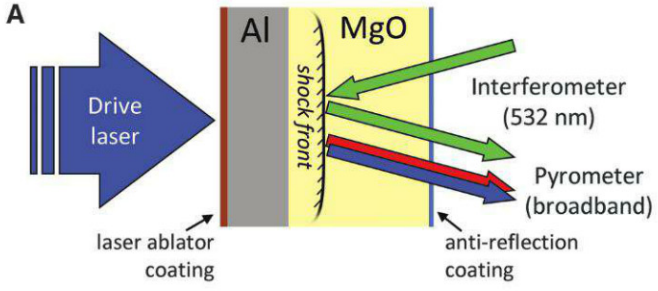

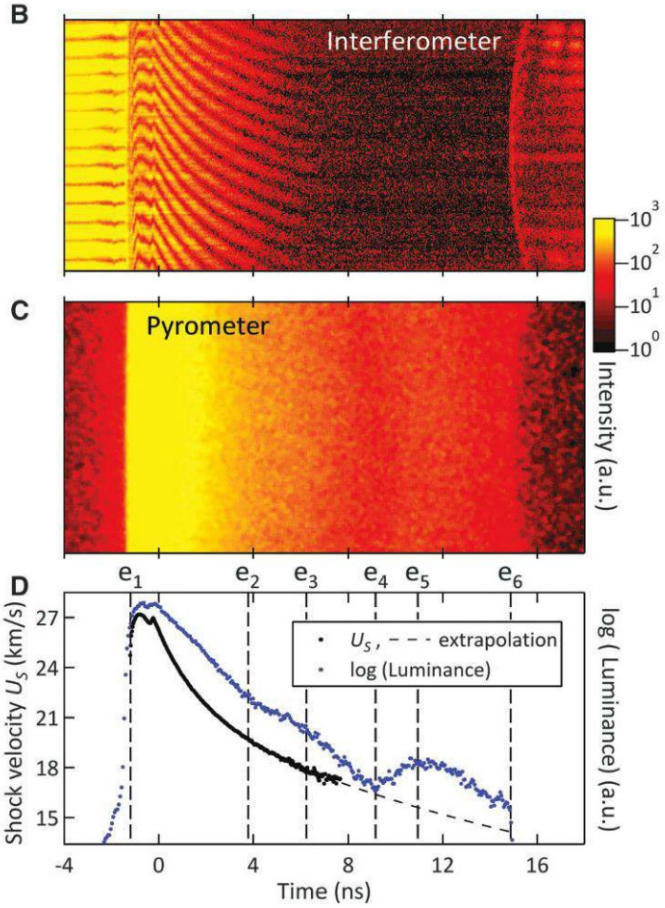

Fig. 1. Schematic of laser-shock experiments (**A**) showing target configuration with drive laser impinging on an Al buffer plate to which the sample (MgO) or a combination of standard (SiO_2) and sample were attached (*11*). Shock velocity, temperature, and reflectivity were determined using velocity interferometry (**B**) and streaked optical pyrometry (**C**) that document intensity (of interference fringes or self-emission, respectively) as a function of distance across the target (vertical axis, ~500 μm full scale) and time (horizontal axis, ~22 ns full scale) (*11*–*14*). Reflectivity and velocity are determined, respectively, from the observed intensity and fringe shift in (B), with shock velocities extrapolated below U_S = 17.3 km/s where reflection from the shock was not detectable (*11*). In the shock-velocity (black dots, dashed line where extrapolated) and emission-intensity (blue dots) records (**D**), events are labeled e_1 to e_6: Entry of the shock into the MgO sample (e_1) and a period of nearly steady shock propagation are followed by steady decay of velocity and emission until e_2, where the rate of emission decay decreases, then increases (e_3), while velocity continues to decay steadily; then emission increases (e_4 to e_5) and decays again before the shock exits the MgO (e_6).

ambient conditions (e.g., pressures below 0.005 TPa) (*19*). Beyond 0.35 TPa, a sequence of phase transformations is required to explain the anomalies in shock temperature, consistent with our specific heat analysis (Table 1).

Several interpretations are possible for the first, most prominent transition, although the observed decrease in shock temperature indicates a positive entropy change (positive latent heat) from low- to high-pressure phases. If the transformation occurs at thermodynamic equilibrium, the data follow a phase boundary having a negative Clapeyron slope and implying a volume change as negative as $\Delta V_{tr}/V \sim -7\%$ (Table 1) (*11*, *15*). This suggests that the first transition corresponds with solid-solid transformation and the second [consistent with positive volume and entropy change (Table 1)] with melting. Indeed, pressure-temperature conditions of the first and second transitions, and Clapeyron slopes obtained assuming equilibrium transformation, are close to theoretically predicted values for the B1-B2 and melting transitions of MgO (Table 1) (*2*). Alternatively, the first transition could be due to melting (*3*), with associated superheating upon shock compression (*12*). In this case, the first transformation can have negligible volume change (Table 1) (*11*), and the second corresponds with a transformation in the fluid.

Our preferred interpretation is that the two transitions are due to B1-B2 (0.45 TPa) and B2-melt (0.65 TPa), respectively. The second transformation is unlikely to be anything other than melting; there is no theoretical evidence for a liquid-liquid transition in MgO (*8*), and known fluid-fluid transitions in other shock-compressed insulators typically occur over a much broader pressure and temperature range (*12*, *13*). Also, the transition from electrically insulating solid to metallic liquid in this interpretation is consistent with theoretical predictions of electronic properties for MgO (*1*, *8*, *9*) (fig. S4) and reflects the melting behavior of other nonmetals such as carbon (*13*), silicon, and sulfur (*20*).

Continuous changes in the reflectivity of the liquid state suggest that liquid electronic properties are strongly sensitive to temperature and pressure (*8*). The large entropy of the first transition relative to typical solid-solid transitions remains poorly understood but is consistent with available theory for MgO (Table 1). The broad region of anomalously high specific heat beyond ~1 TPa and ~33,000 K is similar to that observed at extreme temperatures in carbon and SiO_2 (*12*, *13*) and is similarly attributed here to the onset of complex fluid bonding or to increased electronic specific heat. With this interpretation, we have a self-consistent picture for the phase diagram of MgO (Fig. 3), involving two crystalline phases (B1 and B2) and one liquid phase (*1*–*4*, *9*, *10*).

We conclude that MgO is solid at conditions found in the present Earth (*21*), in large Earth-like planets (*22*) and—based on extrapolations of the melting curve—in Jupiter and its core (*23*) (Fig. 3). The B2 phase of MgO is likely to be stable in the deep mantles of Earth-like planets of more than four Earth masses (*22*) (Fig. 3), so a B1-B2 transition can be relevant to planetary iron-bearing magnesiowüstite (*24*). With the corresponding decrease in volume (up to 7%) and large latent heat of transformation (Table 1), a B1-B2 transition could influence internal structure and dynamics (*22*, *25*), orbital evolution (*25*), and exoplanet mass-radius relationships (*22*). This is particularly true for terrestrial planets exceeding ~8 Earth masses (*22*), where dissociation of perovskite (*1*) could make magnesiowüstite the most abundant mineral of the deep mantle.

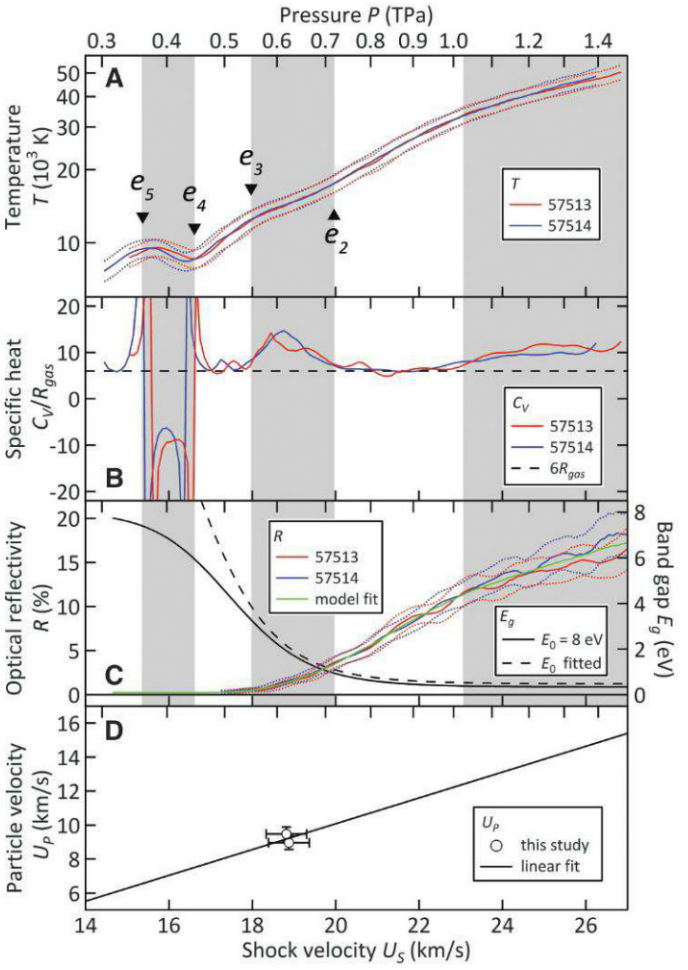

Fig. 2. Shock temperature T (**A**), specific heat C_V (**B**), and shock-front reflectivity R (**C**) measured for MgO in two experiments [blue and red solid curves, systematic uncertainty bounds (*11*) shown by dotted curves (mean ± SD)] are shown as a function of shock-wave velocity (bottom scale) and pressure (top scale), determined from a linear U_S-U_P equation-of-state (**D**) based on a fit (*11*) to data at low pressure (*30*–*33*) (off scale, fig. S1) and high pressure (open symbols, table S1) measured (*34*) relative to SiO_2 (*35*). A Drude-semiconductor model fit to the reflectivity data is shown by the green curve in (C) (*11*); solid and dashed black lines indicate the band gap (E_g) for models constrained to the zero-pressure value for MgO, or not, respectively. Events, labeled as in Fig. 1, correspond to transitions between anomalous (gray shading) and normal (6 R_{gas}) values of C_V.

Table 1. Comparison between experimental and theoretical properties of phase transitions in MgO. Experimental ranges include thermodynamic equilibrium and nonequilibrium [e.g., superheating (*12*)] interpretations of the transitions (*11*). The Clapeyron slope is $(\partial P/\partial T)_B$. Uncertainties are mean ± SD.

		P (TPa)	T (10^3 K)	$(\partial P/\partial T)_B$ (10^{-4} TPa/K)	ΔS_{tr} / R_{gas}	ΔV_{tr} / V (%)
1st transition	Experiment (this study)	0.44 ± 0.08	9.0 ± 0.7	−3.9 ± 3.0	3.9 ± 0.6	−3.8 ± 3.1
	B1-B2 (theory)	0.33 ± 0.04 (*2*)	8.1 ± 0.7 (*2*)	−0.60 ± 0.18 (*2*)	1.9 ± 0.9†	−4.0 ± 0.8† (*9*)
2nd transition	Experiment (this study)	0.65 ± 0.05	14.0 ± 1.1	1.2 ± 0.8	1.6 ± 0.1	4.1 ± 2.9
	Melt (theory)	0.59 ± 0.05 (*2*)	13.6 ± 0.6 (*2*)	0.77 (*2*)	0.5 ± 0.1‡	0.9 ± 0.2‡ (*3*, *8*)

†Upper bound, assuming $\Delta V_{tr}/V$ to be constant along the phase boundary, and calculating ΔS_{tr} from the Clausius-Clapeyron relation $(\partial P/\partial T)_B = \Delta S_{tr}/\Delta V_{tr}$; lower bounds are $\Delta S_{tr} \sim 0$ and $\Delta V_{tr} \sim 0$, obtained if ΔS_{tr} is presumed to be constant along the boundary above zero temperature and infinitesimal (*11*). ‡Estimated assuming that $\Delta V_{tr}/V$ on the melting curve is similar at high pressure for the B1 and B2 phases and using the Clapeyron relation to calculate ΔS_{tr}.

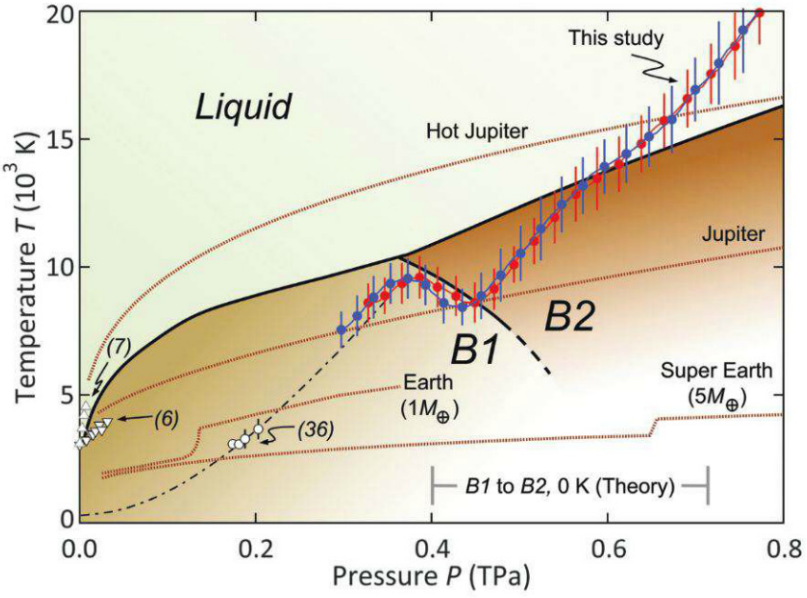

Fig. 3. Phase diagram of MgO constructed from shock temperature data [solid circles, this study, red and blue for two shots; open black circles (*36*)] with B1-phase temperature model (dot-dashed black line) (*36*). Our proposed phase diagram (heavy black lines) is a modification of the recent theoretical phase diagram of (*2*, *4*), in which the melt curve is roughly identical but the B1-B2 transition has moved to higher pressure. Zero-temperature B1-B2 transition pressures from theory (excluding outliers) are given by the gray bracket (*10*). Experimental melting temperatures (*6*, *7*) are open triangles. Also shown are the conditions of planetary interiors for Earth (*21*), a theoretical Earth-like planet of 5 earth masses (Super Earth) (*22*), Jupiter (*23*), and a hot Jupiter-mass planet (average prediction) (*37*); temperature discontinuities at 0.13 and 0.65 TPa in the terrestrial planets correspond to the base of the oxide mantle.

Major end-member oxides of deep planetary interiors (*1*)—SiO_2 (*12*), $MgSiO_3$ (*14*), and MgO—uniformly exhibit high electrical conductivities (σ) in their fluid states at high pressure and temperature, consistent with metallic or semimetallic behavior: $\sigma \sim 10^3$ to 10^5 S/m at $T \sim 5000$ to 15,000 K and $P \sim 0.1$ to 0.7 TPa. Planetary magmas composed of these rocky constituents should likewise be highly conductive at high pressure, as compared with magmas familiar at Earth's surface ($\sigma \sim 10^{-2}$ to 10^2 S/m) (*26*), and would thereby resemble liquid iron alloys making up planetary cores (*27*).

Our experiments therefore reveal a blurring between traditional definitions of planetary mantle and core material: Liquid oxides can be considered either molten mantle constituents or electrically conducting core components. Indeed, for terrestrial planets with extensive melting (i.e., magma oceans) and sufficient interior pressure, oxides could contribute to the dynamo process sustaining a planetary magnetic field. The magnetic Reynolds number $R_m = \mu_0 \sigma v L$ (*28*) for such a magma ocean ($R_m \sim 10^3$ to 10^7) exceeds the critical value required for a self-sustaining field ($R_m > 10^1$ to 10^2), considering flow velocities v appropriate for a terrestrial magma ocean (4 to 40 m/s) (*29*), and distance scales L appropriate for terrestrial mantles (10^6 to 10^7 m); μ_0 is the permeability of free space. Although Earth may be too small ($P < 0.13$ TPa in the mantle) for substantially elevated oxide conductivity, even a modest (order of magnitude) increase in σ over typical magma values can shift R_m in an early-Earth magma ocean from too small ($R_m \sim 10^{-2}$ to 10^2) to large enough to sustain dynamo action. This suggests that an early, short-lived magnetic field could have existed on Earth, perhaps similar to those inferred for Mars and the Moon on the basis of remnant crustal magnetism.

References and Notes

1. K. Umemoto, R. M. Wentzcovitch, P. B. Allen, *Science* **311**, 983 (2006).
2. A. B. Belonoshko, S. Arapan, R. Martonak, A. Rosengren, *Phys. Rev. B* **81**, 054110 (2010).
3. N. de Koker, L. Stixrude, *Geophys. J. Int.* **178**, 162 (2009).
4. D. Alfè, *Phys. Rev. Lett.* **94**, 235701 (2005).
5. A. Aguado, P. A. Madden, *Phys. Rev. Lett.* **94**, 068501 (2005).
6. A. Zerr, R. Boehler, *Nature* **371**, 506 (1994).
7. L. Zhang, Y. W. Fei, *Geophys. Res. Lett.* **35**, L13302 (2008).
8. B. Karki, D. Bhattarai, L. Stixrude, *Phys. Rev. B* **73**, 174208 (2006).
9. A. R. Oganov, M. J. Gillan, G. D. Price, *J. Chem. Phys.* **118**, 10174 (2003).
10. D. Alfe *et al.*, *Phys. Rev. B* **72**, 7 (2005).
11. Materials and methods are available as supplementary materials on *Science* Online.
12. D. G. Hicks *et al.*, *Phys. Rev. Lett.* **97**, 025502 (2006).
13. J. H. Eggert *et al.*, *Nat. Phys.* **6**, 40 (2010).
14. D. K. Spaulding *et al.*, *Phys. Rev. Lett.* **108**, 065701 (2012).
15. Y. B. Zel'dovich, Y. P. Raizer, in *Physics of Shock Waves and High-Temperature Hydrodynamic Phenomena*. W. D. Hayes, R. F. Probstein, Series Eds. (Dover Publications, Inc., Mineola, New York, 2002).
16. R. G. McQueen, S. P. Marsh, J. W. Taylor, J. N. Fritz, W. J. Carter, in *High-Velocity Impact Phenomena*, R. Kinslow, Ed. (Academic Press, New York, 1970), pp. 293–417.
17. G. D. Stevens, L. R. Veeser, P. A. Rigg, R. S. Hixson, *AIP Conf. Proc.* **845**, 1353 (2006).
18. R. Jeanloz, *J. Geophys. Res.* **94**, (B5), 5873 (1989).
19. T. J. Ahrens, Ed., *AGU Handbook of Physical Constants*, vol. II (1995), pp. 45–97.
20. D. A. Young, *Phase Diagrams of the Elements* (Univ. of California Press, Berkeley, 1991).
21. S. Tateno, K. Hirose, Y. Ohishi, Y. Tatsumi, *Science* **330**, 359 (2010).
22. D. Valencia, R. J. O'Connell, D. Sasselov, *Icarus* **181**, 545 (2006).
23. T. Guillot, *Annu. Rev. Earth Planet. Sci.* **33**, 493 (2005).
24. B. J. Wood, *Earth Planet. Sci. Lett.* **174**, 341 (2000).
25. S.-i. Karato, *Icarus* **212**, 14 (2011).
26. F. Gaillard, G. I. Marziano, *J. Geophys. Res. Solid Earth* **110**, 12 (2005).
27. E. Knittle, R. Jeanloz, *Geophys. Res. Lett.* **13**, 1541 (1986).
28. D. J. Stevenson, *Space Sci. Rev.* **152**, 651 (2010).
29. V. Solomatov, in *Origin of the Earth and Moon*, R. M. Canup, K. Righter, Eds. (Univ. of Arizona Press, Tucson, 2000), pp. 323–338.
30. S. P. Marsh, *LASL Shock Hugoniot Data* (Univ. of California Press, Berkeley, 1980).
31. M. S. Vassiliou, T. J. Ahrens, *Geophys. Res. Lett.* **8**, 729 (1981).
32. T. S. Duffy, T. J. Ahrens, *J. Geophys. Res. Solid Earth* **100**, (B1), 529 (1995).
33. L. Zhang, Z. Z. Gong, Y. W. Fei, *J. Phys. Chem. Solids* **69**, 2344 (2008).
34. D. G. Hicks *et al.*, *Phys. Rev. B* **78**, 174102 (2008).
35. M. D. Knudson, M. P. Desjarlais, *Phys. Rev. Lett.* **103**, 225501 (2009).
36. B. Svendsen, T. J. Ahrens, *Geophys. J. R. Astron. Soc.* **91**, 667 (1987).
37. I. Baraffe, G. Chabrier, T. Barman, *Astron. Astrophys.* **482**, 315 (2008).

Acknowledgments: We thank N. Gómez-Pérez, R. J. Hemley, D. C. Swift, R. E. Cohen, D. A. Dalton, and W. Unites for helpful discussions. This work was performed under the auspices of the U.S. Department of Energy by Lawrence Livermore National Laboratory in part under contract W-7405-Eng-48 and in part under contract DE-AC52-07NA27344. We also acknowledge financial support from the U.S. Army Research Office (grant 56122-CH-H), a Krell Institute Department of Energy (DOE) National Nuclear Security Administration (NNSA) graduate fellowship (contract DE-FC52-08NA28752), the DOE/NNSA National Laser User Facility Program, the Miller Institute for Basic Research in Science, and the University of California. Data are available in this manuscript and in the supplementary materials.

Supplementary Materials

www.sciencemag.org/cgi/content/full/science.1229450/DC1
Materials and Methods
Figs. S1 to S6
Tables S1 to S3
References (*38*–*53*)

29 August 2012; accepted 26 October 2012
Published online 22 November 2012;
10.1126/science.1229450

A Bipolar Spindle of Antiparallel ParM Filaments Drives Bacterial Plasmid Segregation

P. Gayathri,[1] T. Fujii,[2]* J. Møller-Jensen,[1]† F. van den Ent,[1] K. Namba,[2,3] J. Löwe[1]‡

To ensure their stable inheritance by daughter cells during cell division, bacterial low-copy-number plasmids make simple DNA segregating machines that use an elongating protein filament between sister plasmids. In the ParMRC system of the *Escherichia coli* R1 plasmid, ParM, an actinlike protein, forms the spindle between ParRC complexes on sister plasmids. By using a combination of structural work and total internal reflection fluorescence microscopy, we show that ParRC bound and could accelerate growth at only one end of polar ParM filaments, mechanistically resembling eukaryotic formins. The architecture of ParM filaments enabled two ParRC-bound filaments to associate in an antiparallel orientation, forming a bipolar spindle. The spindle elongated as a bundle of at least two antiparallel filaments, thereby pushing two plasmid clusters toward the poles.

During bacterial cell division, an equal distribution of replicated plasmids to daughter cells ensures their stable inheritance. Low-copy-number plasmids encode the simplest known DNA segregation machines to perform this task. They comprise a nucleotide-driven (cytomotive) protein filament and a centromere-like DNA region, linked by an adaptor protein. The ParMRC segregation system of *Escherichia coli* R1 plasmid consists of ParM, an actinlike cytomotive protein (*1*) that forms polar, left-handed, double-helical filaments (*2*); ParR, an adaptor protein; and *parC*, a centromeric region (*3*, *4*). Dynamic instability of ParM filaments enables plasmid segregation by a "search and capture" mechanism (*5*, *6*), with ParRC (*7*, *8*) stabilizing the filaments. It has been reported that ParRC binds to both ends of a single ParM filament (*9*, *10*). This leads to a conundrum: How does ParRC bind to two different ends of a polar ParM filament?

Here, we provide a comprehensive description of ParM in the monomeric and filament states. An electron cryomicroscopy (cryo-EM) reconstruction (*11*) (Fig. 1A) provided a subnanometer-resolution map of the polar filament of ParM (resolution of 8.5 Å at FSC 0.5; fig. S1, A to D), polymerized in the presence of adenylyl-imidodiphosphate [AMPPNP, a nonhydrolyzable adenosine triphosphate (ATP) analog]. We determined the crystal structures of a nonpolymerizing mutant, ParM(Leu$^{163\rightarrow}$Arg^{163}, L163R), bound to AMPPNP and ParM(Leu$^{163\rightarrow}$Ala^{163}, L163A) bound to the C-terminal 17-residue peptide corresponding to the ParM-interacting region of ParR (*8*, *10*) (ParR$_{pept}$) and AMPPNP (*11*). Comparison of the crystal structures, including the previously reported apo- and adenosine diphosphate (ADP)–bound forms (*1*), revealed no large differences between the ATP and ADP states of

[1]Medical Research Council (MRC) Laboratory of Molecular Biology (LMB), Hills Road, Cambridge CB2 0QH, UK. [2]Graduate School of Frontier Biosciences, Osaka University, 1-3 Yamadaoka, Suita, Osaka 565-0871, Japan. [3]Riken Quantitative Biology Center, 1-3 Yamadaoka, Suita, Osaka 565-0871, Japan.

*Present address: Riken Quantitative Biology Center, 1-3 Yamadaoka, Suita, Osaka 565-0871, Japan.
†Present address: University of Southern Denmark, Campusvej 55, DK-5230 Odense, Denmark.
‡To whom correspondence should be addressed. E-mail: jyl@mrc-lmb.cam.ac.uk

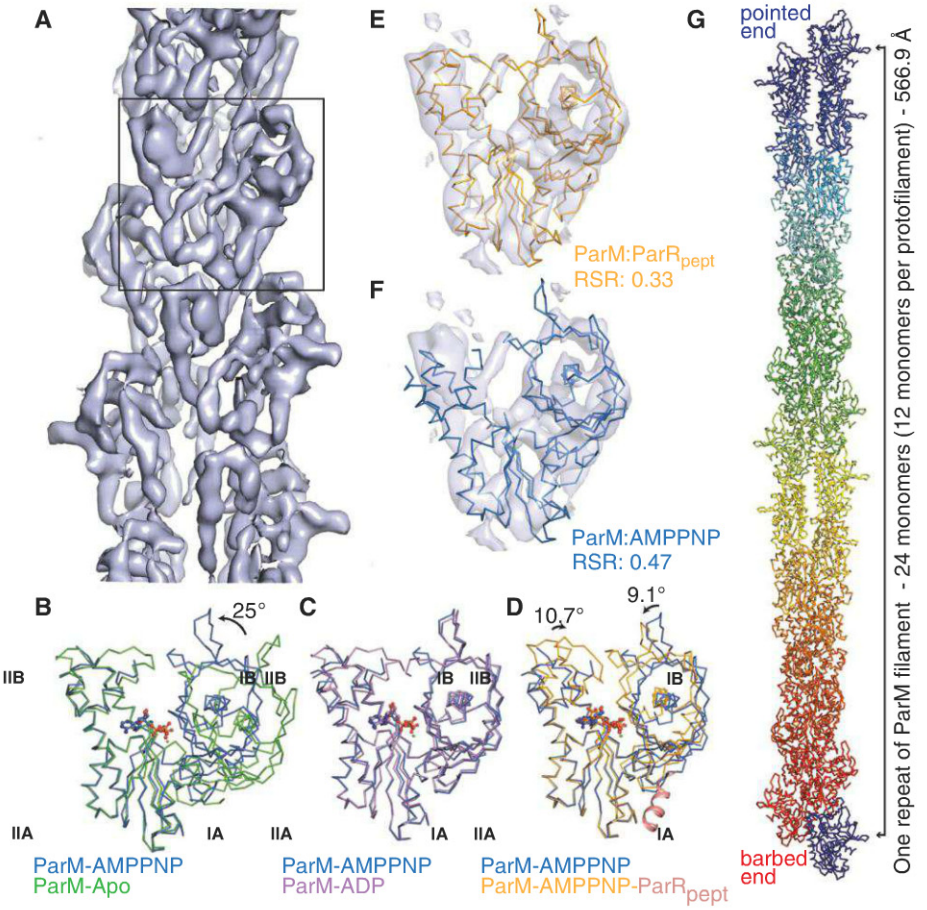

Fig. 1. Conformational cycle of ParM. (**A**) Cryo-EM reconstruction of the ParM filament. Box indicates a monomeric segment. (**B** to **D**) Superposition (using Cα atoms of domain IIA) of the conformations of ParM with the ParM-AMPPNP state (blue; PDB ID: 4A61): (B) unliganded ParM [green (*1*); PDB ID: 1MWK], (C) ParM-ADP state [magenta; (*1*); PDB ID: 1MWM], and (D) ParM with ParR$_{pept}$ and AMPPNP (orange; ParR$_{pept}$ in pink cartoon representation; PDB ID: 4A62). Domain rotations are indicated. (**E** and **F**) Rigid-body fit of ParM monomeric states into the cryoEM reconstruction. Domain I residues were fitted by using Chimera (*24*). Real-space R-factors (RSR) against the map for ParM:AMPPNP (E) and ParM:ParR$_{pept}$ (F) quantify the best fit (movie S1 and fig. S1E). (**G**) A repeat unit of the ParM filament (EMDB: EMD-1980, PDB ID: 4A6).

ParM monomers (Fig. 1, B and C). In contrast, domains IB and IIB showed a rotation of 9.1° and 10.7° toward the nucleotide-binding pocket (Fig. 1D) in the ParM:$ParR_{pept}$ structure, compared with the free monomer. The domain rotations were reminiscent of the transition from G-actin to F-actin (*12*, *13*). Fitting the monomeric structures of ParM into the cryo-EM reconstruction showed that the ParM:$ParR_{pept}$ structure fits best (Fig. 1, E and F, fig. S1E, and movie S1). Thus, the filament conformation of ParM is very similar to ParM:$ParR_{pept}$. The best fit provided a quasi-atomic model of the ParM filament (Fig. 1G) and implies that binding of ParR or ParR*C* locks ParM monomers in the filament-like conformation.

$ParR_{pept}$ was bound in a hydrophobic pocket between domains IA and IIA of ParM (Fig. 2A and fig. S2). The ParM-$ParR_{pept}$ interaction resembled proteins that bind at the barbed end of actin (Fig. 2, A and B). Many actin-binding proteins, including formins (*14*) and Wiskott-Aldrich homology domain 2–containing proteins such as Spire (*15*), insert a helix between the corresponding subdomains 1 and 3 of actin (*16*). The ParM:$ParR_{pept}$ structure modeled onto the ParM filament highlighted a substantial clash between $ParR_{pept}$ and residues 37 to 46 of the next ParM monomer in the protofilament (Fig. 2C). Thus, the ParR-binding site lies within the polymerization interface of ParM, and bound ParR needs to be replaced during elongation. Overlap in the binding site of $ParR_{pept}$ and the polymerization interface occludes all the ParR*C*-binding sites on the ParM filament except those at the barbed end, implying that ParR*C* binds exclusively to this end.

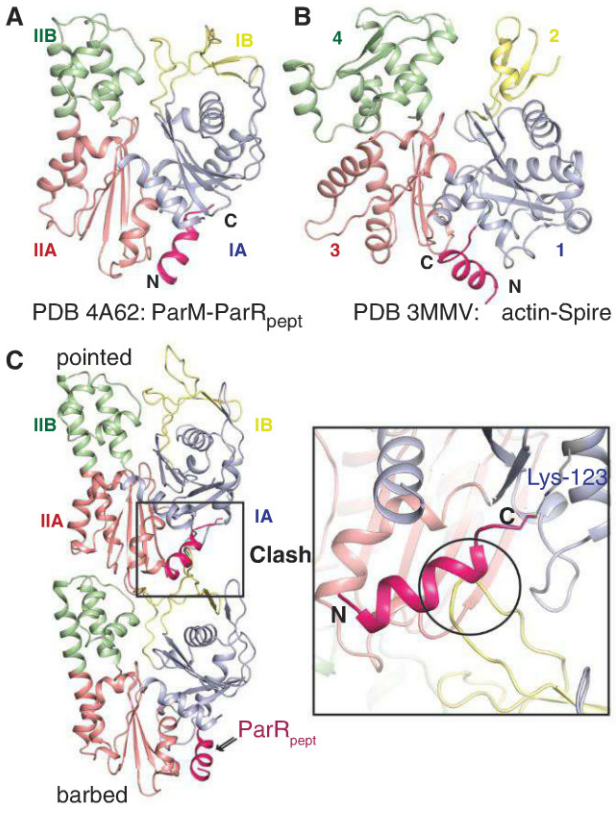

Fig. 2. ParR*C* binds at the barbed end of ParM filaments. (**A** and **B**) The $ParR_{pept}$ binding site corresponds to that of Spire on actin. The helices of the interacting proteins are shown in pink, with the rest in gray. (A) ParM:$ParR_{pept}$ (PDB ID: 4A62), (B) actin:Spire (PDB ID: 3MMV). (**C**) $ParR_{pept}$ binds at the interprotofilament interface of ParM. Two subunits of the ParM filament with hypothetical $ParR_{pept}$ at the binding sites are shown. In that position, $ParR_{pept}$ clashes with loop 37-46 from domain IB of the adjacent subunit.

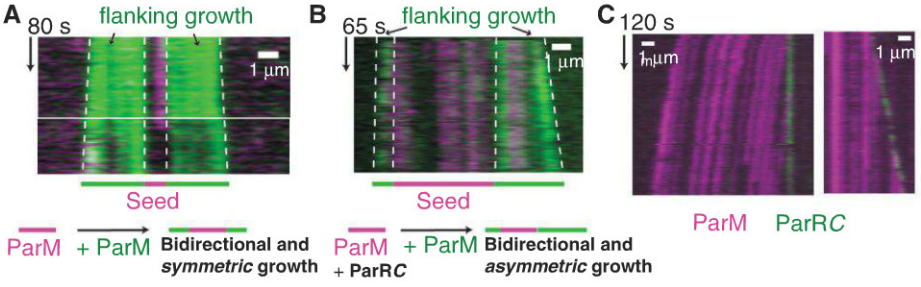

Fig. 3. ParR*C* accelerates growth at one end of ParM filaments. (**A** and **B**) TIRF microscopy kymographs of filaments in dual-label experiments (*11*) (A) without ParR*C* and (B) with ParR*C*. Growth of ParM filaments without ParR*C* is bidirectional and symmetric, with equal slopes on both ends of the kymograph, whereas addition of ParR*C* results in asymmetric growth, with unequal slopes. The relevant boundaries are highlighted. (**C**) Monomers are recruited to the ParR*C*-bound end of ParM filament. Kymograph from a filament labeled with Alexa-568 (magenta) and YOYO-1–labeled ParR*C* (green) are shown.

Our ParM-$ParR_{pept}$ structure supports a forminlike mechanism for the processive movement of ParR*C* (fig. S3). Ten ParR dimers bind *parC* repeats (*7*, *8*), forming a scaffold that allows a forminlike stair-stepping mechanism (fig. S3, B and C) (*17*). The C-terminal helices from the 20 ParRs are localized in a confined area. This probably facilitates ParM filament nucleation by ParR*C* (*18*). It also ensures ParR*C*-bound ParM monomer recruitment upon ParR displacement from the filament (fig. S3D), explaining end tracking of ParM filaments by ParR*C* through insertional polymerization (*6*, *19*). The ParR*C* cap locks the terminal monomers in the filament conformation, thus protecting the filament from dynamic instability.

To confirm the proposed single-end binding of ParR*C*, we examined the effect of ParR*C* on ParM filament elongation by using total internal reflection fluorescence (TIRF) microscopy (*11*). The experiments were performed with nonhydrolyzable AMPPNP to prevent dynamic instability. ParM-AMPPNP elongated symmetrically at both ends from an initial seed of the ParM filament (Fig. 3A and movie S2) (*5*). In the presence of unlabeled ParR*C*, one end of the filaments grew faster, resulting in asymmetric growth (Fig. 3B, fig. S4A, and movie S3). The rates of growth were 9.4 ± 4.1 and 2.5 ± 1.9 monomers per s (numbers after the ± symbol indicate standard deviation from the mean), for fast- and slow-growing ends (n = 32; table S3). Experiments with labeled ParR*C* showed that ParR*C* accelerated growth and recruited ParM monomers at the ParR*C*-bound filament end only (Fig. 3C, fig. S4B, and movie S4), reconfirming insertional polymerization (*6*). The unidirectional elongation by ParR*C* leads us to the key question: What enables bipolar plasmid segregation?

Frequent condensation events were observed between ParM filaments, both with ATP and AMPPNP (Fig. 4A and movies S5 to S8). Furthermore, continuous motion because of interfilament sliding occurred within filament bundles (Fig. 4B, fig. S4C, and movies S9 to S11). A molecular model for the filament sliding and condensation was generated on the basis of two monomers in the crystal packing of ParM:$ParR_{pept}$ (fig. S5A). ParM filament subunits, when superposed sequentially onto the ParM monomers, produced sliding and an antiparallel packing of filaments (Fig. 4C and fig. S5A). Mutation of residues within loop 18-21 [Ser^{19}→Arg^{19} and Gly^{21}→Arg^{21} (S19R and G21R)] at the proposed antiparallel filament interface (Fig. 4, C and D, and fig. S5B) prevented interfilament sliding (movie S12, Fig. 4E, and fig. S4D), because of stronger interactions between filaments caused by alternating charges.

The helical geometry of ParM filament, with 12 subunits per turn, is compatible with a hexagonal

or square packing of ParM filaments in a bundle (fig. S5C) (*4*), in contrast to nonbundling actin filaments with a 13-monomer repeat. Bundles of ParM filaments have been observed in *E. coli* cells expressing ParM at wild-type levels (*20*) and during plasmid partitioning in vivo (*21*). Also, bundles of antiparallel ParM filaments have been described in vitro (*22*).

Antiparallel pairing explains observations of ParR*C* at both ends of ParM filaments (*9*, *10*). Of the 826 filaments we counted, 104, 540, and 182 filaments were observed with ParR*C* at zero, one, and two ends, respectively, consistent with single-end binding and pairing. Bipolar spindles of ParM were observed by TIRF microscopy using ATP. Stable filaments were seen only as elongating spindles with ParR*C* at both ends, pushing plasmids apart at a rate of 22.6 ± 4.8 monomers per s (n = 40; movies S13 and S14 and table S3). Upon loss of ParR*C* at limiting concentrations of ParM (350 to 500 nM), dynamic instability caused spindle disassembly at a rate of 100.3 ± 18.7 monomers per s (n = 61; Fig. 4F, fig. S4E, movies S15 and S16, and table S3).

To demonstrate that the spindles comprised at least two antiparallel filaments, we introduced negatively charged residues within loop 18-21 (S19E, G21E, where E indicates Glu) (Fig. 4D) to weaken the interfilament interaction through repulsive electrostatic forces. We observed spindles (n = 65) that split into the constituent filaments (movie S17 and Fig. 4G). This confirms that spindles are not formed by a single ParM

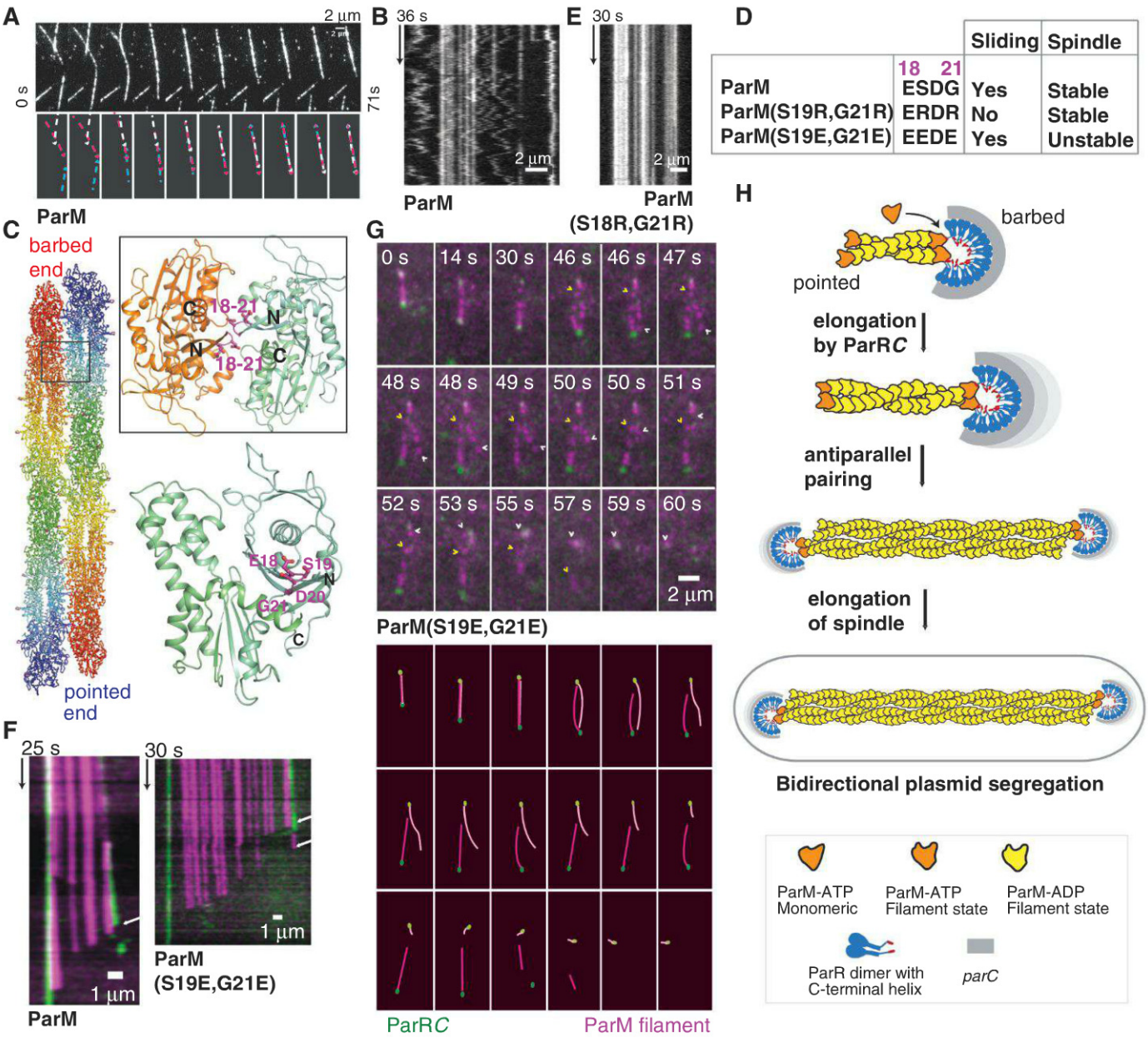

Fig. 4. A bipolar spindle comprises at least two antiparallel ParM filaments. (**A**) ParM-AMPPNP filaments condensing into a bundle (movie S7). (**B**) Kymograph of a bundle of ParM. Static filaments yield straight lines, whereas concerted zigzag motion shows sliding filament movement. (**C**) Atomic model of an antiparallel filament pair. (Inset) Interface involving loop 18-21 in the antiparallel arrangement. D, Asp. (**D**) Interface mutations and their effect on sliding and spindle stability. (**E**) Kymograph of a bundle of ParM(S19R,G21R) filaments that are static because of stronger interfilament interactions. (**F**) Kymographs of disassembling spindles of ParM and ParM(S19E,G21E). Arrows highlight the slopes of disassembly. (**G**) Montage of spindle disassembly events in ParM(S19E,G21E) mutant (movie S17). The spindle splits apart because of repulsive surface charges, demonstrating that the bipolar spindle of ParM (magenta) is formed of more than one filament. The constituent filaments with ParRC (green) bound at one end begin disassembly from the pointed ends. The pointed ends are highlighted with arrowheads. (**H**) Schematic representation of the bipolar spindle model (see also fig. S6).

filament, with ParR*C* attached at both ends (*9*, *10*) (Fig. 4H). ParM filaments in a spindle were protected from dynamic instability by binding of ParR*C* at the barbed end and pairing with another ParR*C*-bound filament at the pointed end (movies S15 to S19; Fig. 4, F to H; and fig. S4, E and F). The trigger for disassembly was either the loss of ParR*C* (movies S15 and S16) or exposure of pointed ends because of unwinding of the antiparallel bundle (movies S17 and S19).

These observations and previously published work (*3*, *4*) provide a comprehensive model of ParMR*C*-mediated plasmid segregation (fig. S6): a critical concentration of ATP-bound monomers in the cell nucleates ParM filaments (or nucleation is ParR*C*-mediated) (*18*). ParR*C* binding rescues the dynamic filaments from disassembly at the barbed end only. ParR*C* speeds up the growth at the barbed end by a forminlike mechanism. The free pointed end remains prone to disassembly unless it pairs up antiparallel with another ParM filament bound to ParR*C*, probably shortly after plasmid replication. Thus, a bipolar spindle of two antiparallel filaments is the minimum unit in plasmid segregation. R1 plasmid has a copy number of about six, which is about the number of filaments within bundles in plasmid-segregating cells (*20*). ParM bundles are stronger than single filaments, which is advantageous when pushing plasmids through the cytoplasm. A single bundle will also ensure concerted segregation of all sister plasmids, as observed in vivo (*21*).

The lateral interaction among dynamic filaments, as in ParMR*C*, may also facilitate contraction in other cytomotive filament systems such as FtsZ in bacterial cell division (*23*). Our model of antiparallel actinlike ParM filaments, without the necessity of bundling factors or motor proteins, provides an attractive conceptual precursor for actin contractile systems, such as muscle.

References and Notes

1. F. van den Ent, J. Møller-Jensen, L. A. Amos, K. Gerdes, J. Löwe, *EMBO J.* **21**, 6935 (2002).
2. D. Popp *et al.*, *EMBO J.* **27**, 570 (2008).
3. K. Gerdes, M. Howard, F. Szardenings, *Cell* **141**, 927 (2010).
4. J. Salje, P. Gayathri, J. Löwe, *Nat. Rev. Microbiol.* **8**, 683 (2010).
5. E. C. Garner, C. S. Campbell, R. D. Mullins, *Science* **306**, 1021 (2004).
6. E. C. Garner, C. S. Campbell, D. B. Weibel, R. D. Mullins, *Science* **315**, 1270 (2007).
7. J. Møller-Jensen, S. Ringgaard, C. P. Mercogliano, K. Gerdes, J. Löwe, *EMBO J.* **26**, 4413 (2007).
8. M. A. Schumacher *et al.*, *Nature* **450**, 1268 (2007).
9. C. L. Choi, S. A. Claridge, E. C. Garner, A. P. Alivisatos, R. D. Mullins, *J. Biol. Chem.* **283**, 28081 (2008).
10. J. Salje, J. Löwe, *EMBO J.* **27**, 2230 (2008).
11. See supplementary materials available on *Science* Online.
12. T. Fujii, A. H. Iwane, T. Yanagida, K. Namba, *Nature* **467**, 724 (2010).
13. T. Oda, M. Iwasa, T. Aihara, Y. Maéda, A. Narita, *Nature* **457**, 441 (2009).
14. T. Otomo *et al.*, *Nature* **433**, 488 (2005).
15. M. Hertzog *et al.*, *Cell* **117**, 611 (2004).
16. R. Dominguez, *Trends Biochem. Sci.* **29**, 572 (2004).
17. B. L. Goode, M. J. Eck, *Annu. Rev. Biochem.* **76**, 593 (2007).
18. J. Møller-Jensen, R. B. Jensen, J. Löwe, K. Gerdes, *EMBO J.* **21**, 3119 (2002).
19. J. Møller-Jensen *et al.*, *Mol. Cell* **12**, 1477 (2003).
20. J. Salje, B. Zuber, J. Löwe, *Science* **323**, 509 (2009); 10.1126/science.1164346.
21. C. S. Campbell, R. D. Mullins, *J. Cell Biol.* **179**, 1059 (2007).
22. D. Popp *et al.*, *Biochem. Biophys. Res. Commun.* **353**, 109 (2007).
23. S. X. Sun, S. Walcott, C. W. Wolgemuth, *Curr. Biol.* **20**, R649 (2010).

Acknowledgments: We acknowledge N. Barry and C. Johnson (MRC-LMB, help with TIRF microscopy and isothermal titration calorimetry); T. Kato (Osaka University, technical support with cryo-EM); beamline support at ID29, ID14-2 (European Synchrotron Radiation Facility, France), and I02 (Diamond Light Source, UK); L. Amos, S. Bullock, A. Carter, and R. Gasper-Schönenbrücher (MRC-LMB, critical reading of the manuscript); and K. Gerdes (Newcastle University) and A. Toste Rêgo (MRC-LMB) (provision of reagents). Support by the MRC (U105184326 to J.L.), Grants-in-Aid for Scientific Research, Ministry of Education, Culture, Sports, Science and Technology (MEXT), Japan (21227006 to K.N.), and FP7-IIF-2008 fellowship (P.G.) is acknowledged. Protein Data Bank (PDB) accession codes: ParM-AMPPNP, 4A61; ParM-AMPPNP-ParR$_{pept}$, 4A62. The EM reconstruction has been deposited in the Electron Microscopy Data Bank (EMD-1980), fitted coordinates in the PDB (4A6J).

Supplementary Materials

www.sciencemag.org/cgi/content/full/science.1229091/DC1
Materials and Methods
Figs. S1 to S6
Tables S1 to S3
References (*24*–*41*)
Movies S1 to S19

20 August 2012; accepted 12 October 2012
Published online 25 October 2012;
10.1126/science.1229091

Kinetic Responses of β-Catenin Specify the Sites of Wnt Control

Ana R. Hernández,* Allon M. Klein,* Marc W. Kirschner†

Despite more than 30 years of work on the Wnt signaling pathway, the basic mechanism of how the extracellular Wnt signal increases the intracellular concentration of β-catenin is still contentious. Circumventing much of the detailed biochemistry, we used basic principles of chemical kinetics coupled with quantitative measurements to define the reactions on β-catenin directly affected by the Wnt signal. We conclude that the core signal transduction mechanism is relatively simple, with only two regulated phosphorylation steps. Their partial inhibition gives rise to the full dynamics of the response and subsequently maintains a steady state in which the concentration of β-catenin is increased.

Kinetic analysis of chemical pathways at steady state can order the steps of a reaction sequence and identify points of control (*1*, *2*). Whether such analysis can be as successful for signaling pathways as it is for mass conversion is unclear. We applied this approach to the canonical Wnt pathway, a fundamental circuit in development and adult homeostasis. Wnt leads to stabilization and accumulation of β-catenin, which then activates transcriptional targets. β-catenin is constantly synthesized but is normally maintained at a low cytoplasmic concentration by degradation. Degradation is mediated by casein kinase 1α (CK1α) and glycogen synthase kinase 3 (GSK3), which sequentially phosphorylate β-catenin, creating a phosphodegron (*3*, *4*). The interaction between the kinases and β-catenin is mediated by two scaffold proteins, Axin1 and adenomatous polyposis coli (APC), forming the so-called destruction complex.

The mechanism by which Wnt inhibits the degradation of β-catenin is still open to debate. Because phosphorylated β-catenin decreases after Wnt stimulation, it is thought that Wnt inhibits phosphorylation of β-catenin, thereby blocking its degradation (*3*–*5*). Inhibition has been proposed to occur by interfering with GSK3 (*6*, *7*), CK1α (*4*), or Axin (*8*, *9*). Wnt is also proposed to inhibit ubiquitylation, rather than phosphorylation (*10*). Moreover, the proposed mechanisms do not explain how β-catenin is maintained at an elevated steady-state level and what prevents it from accumulating indefinitely.

To understand how Wnt controls β-catenin, we examined cultured cells, in which the β-catenin dynamics could be accurately measured. Our analysis focused on sequential β-catenin modifications across two phases: (i) a transient phase of β-catenin accumulation and (ii) a final phase at which β-catenin concentration reaches a new, higher steady state. From a basic conservation law of enzyme kinetics, we deduced the point of Wnt action and revealed a simple core mechanism that couples the Wnt signal to the steady-state amount of β-catenin.

Continuous stimulation of cells by Wnt-3A led to distinct dynamic changes in phosphorylated and total β-catenin (Fig. 1A and fig. S1). The total amount of β-catenin increased 15 to 30 min after exposure to Wnt and reached a steady state in 2 hours that was maintained for several hours. In human colon carcinoma RKO cells, β-catenin concentration increased by a factor of 6 (from 8 ± 1 nM to 52 ± 7 nM) (Fig. 1B). By contrast,

Department of Systems Biology, Harvard Medical School, Boston, MA 02115, USA.

*These authors contributed equally to this work.
†To whom correspondence should be addressed. E-mail: marc@hms.harvard.edu

the amount of GSK3-phosphorylated β-catenin (phospho T41/S37/S33) decreased 80 ± 20% 15 to 30 min after Wnt stimulation and then returned to its initial concentration in 2 hours (Fig. 1, A and D). The amount of CK1α-phosphorylated β-catenin (phospho S45) showed little or no decrease over the first 30 min and then increased above its initial concentration (Fig. 1A). Similar results were observed in all cell lines tested (fig. S1).

The amount of GSK3-phosphorylated β-catenin showed a strong negative correlation with the rate of β-catenin accumulation (Pearson correlation $R = -0.93$) (Fig. 1, C to E). When phosphorylation decreased to a minimum, the rate of β-catenin accumulation was at a maximum (arrows, Fig. 1, C to E). This correlation supports the view that Wnt inhibits phosphorylation to increase β-catenin concentration. When phosphorylation increased and returned to the initial amount, the β-catenin accumulation rate decreased to zero; thereafter, β-catenin was maintained at a high concentration. In this new steady state, degradation must occur because synthesis of the protein remains unchanged during Wnt stimulation (*11*) (fig. S2). These observations suggest that recovery of phosphorylation restores degradation.

We therefore tested whether β-catenin is still degraded during Wnt stimulation. Treatment of Wnt-stimulated cells with a proteasome inhibitor increased β-catenin abundance within 1 hour (Fig. 1F), confirming that β-catenin was being degraded. From Fig. 1B, we calculated that Wnt increases β-catenin lifetime from 16 to 104 min (see supplementary materials), still lower by a factor of 10 than the average protein lifetime (*12*). To determine whether the destruction complex is responsible for mediating degradation after Wnt stimulation, we first blocked GSK3 activity with lithium chloride (LiCl) or silenced APC, Axin1, or CK1α with short hairpin RNA (shRNA) and then added Wnt. Under these conditions, β-catenin phosphorylation dropped but did not fully recover (Fig. 1, G and H, and fig S3). Thus, the destruction complex functions both in the absence and presence of Wnt. However, in the presence of Wnt, the destruction complex must be only partially active because the ratio of GSK3-phosphorylated β-catenin to total β-catenin drops and remains low (Fig. 1I). Inhibition of the destruction complex is not inconsistent with the full recovery of GSK3-phosphorylated β-catenin to its original concentration because the concentration of β-catenin has increased. Therefore, Wnt partially inhibits the destruction complex; recovery of phosphorylation halts the rise in β-catenin, restoring degradation and establishing a new steady state.

These conclusions shape basic features of the Wnt response, but they leave open a number of questions regarding the full dynamics. To determine whether partial inhibition of phosphorylation explains the entire response, or whether Wnt might act elsewhere to inhibit degradation, we used the laws of chemical kinetics to identify constraints on the system behavior. In the simplest model, a protein X (β-catenin) is synthesized with a rate S and degraded by an enzyme E. The protein concentration ($[X]$) is constant only if it is degraded with a flux $k_{deg}[X]$ that equals the synthesis rate, which remains unchanged during Wnt stimulation. In the Michaelis-Menten approximation for an unsaturated enzyme, $k_{deg} = k_{cat}[E]/K_M$. Degradation can be inhibited by lowering the enzyme concentration $[E]$ or its intrinsic catalytic rate k_{cat}, or by lowering the affinity ($1/K_M$). If the enzyme is inhibited by any of these means, k_{deg} is reduced and, as a result, the degradation flux, $k_{deg}[X]$ initially decreases. The protein concentration then increases until the flux equals S once again. The same principle of flux conservation holds when more than one enzymatic step is required for degradation, as for β-catenin (Fig. 2A) (*2*, *13*), and when the reactions do not conform to the Michaelis-Menten approximation (supplementary materials, section S-I). At steady state, the

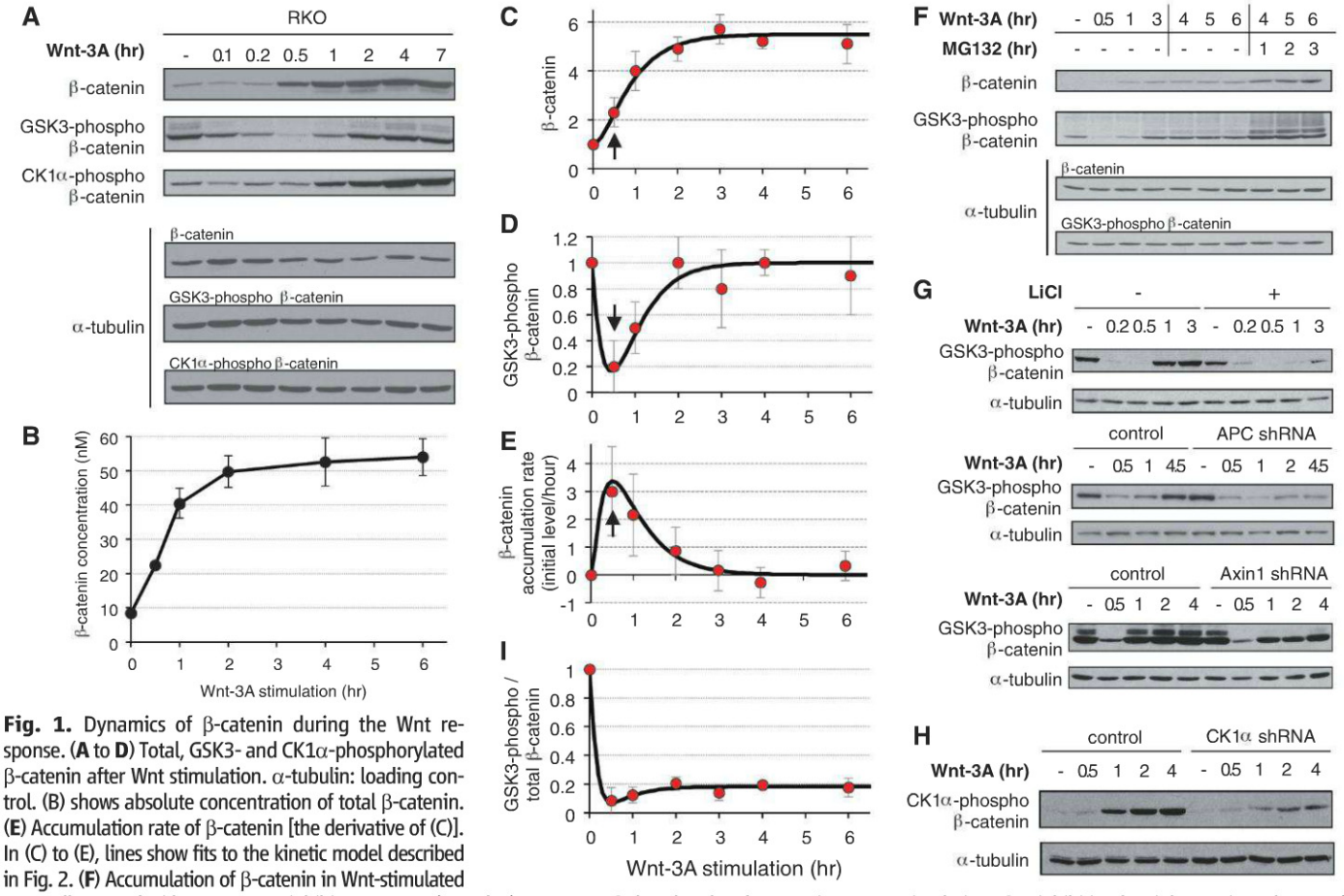

Fig. 1. Dynamics of β-catenin during the Wnt response. (**A** to **D**) Total, GSK3- and CK1α-phosphorylated β-catenin after Wnt stimulation. α-tubulin: loading control. (**B**) shows absolute concentration of total β-catenin. (**E**) Accumulation rate of β-catenin [the derivative of (C)]. In (C) to (E), lines show fits to the kinetic model described in Fig. 2. (**F**) Accumulation of β-catenin in Wnt-stimulated RKO cells treated with proteasome inhibitor MG132. (**G** and **H**) Response of phosphorylated β-catenin to Wnt stimulation after inhibition by LiCl or various shRNAs. (**I**) Ratio of GSK3-phosphorylated β-catenin to total β-catenin relative to initial levels [calculated from (C) and (D)]. Error bars, mean ± SD ($N = 3$ replicates).

net flux through each step equals S irrespective of the point of inhibition.

We use this conservation principle to identify the point of Wnt action. All possible mechanisms lead to just three dynamical outcomes for GSK3-phosphorylated β-catenin (supplementary materials, sections S-I to S-III): First, if inhibition occurs downstream of phosphorylation (Fig. 2A), then GSK3-phosphorylated β-catenin should accumulate to restore the degradation flux (Fig. 2B, black curve). With k_{deg} describing the degradation rate of the phosphorylated protein, its concentration adapts from $S/k_{deg}^{(0)}$ to $S/k_{deg}^{(Wnt)}$ with $k_{deg}^{(Wnt)} < k_{deg}^{(0)}$. Second, if inhibition occurs at the phosphorylation steps, or upstream of them (Fig. 2A), the concentration of GSK3-phosphorylated β-catenin should drop transiently because the influx to that state would be inhibited. Ultimately, the amount of GSK3-phosphorylated β-catenin would return precisely to the initial level because the influx recovers to S, whereas the stability of the phosphorylated protein is unchanged, $k_{deg}^{(Wnt)} = k_{deg}^{(0)}$ (Fig. 2B, red curve). Third, if inhibition occurs both upstream and downstream of phosphorylation, then GSK3-phosphorylated β-catenin levels should first drop (or appear unchanged) until the influx matches S. The protein would then accumulate above its original concentration, reflecting its increased stability with $k_{deg}^{(Wnt)} < k_{deg}^{(0)}$ again (Fig. 2B, blue curve). This three-fold classification resembles the crossover theorem first used to identify control points in the electron transport chain (*2*, *14*).

These dynamic responses derive from basic laws of enzyme kinetics with no particular assumptions about molecular mechanism. The same dynamics also occur if there were feedback on the destruction complex activity (supplementary materials, section S-I). Similarly, the same dynamic responses could occur through activation of the reverse reactions (dephosphorylation or deubiquitylation) (supplementary materials, section S-II). There are two exceptions to the three cases: If β-catenin were degraded independently of phosphorylation, phosphorylated β-catenin should drop without recovering to its initial concentration (supplementary materials, section S-VI). Second, if Wnt causes complete inhibition or saturation of the destruction complex, the degradation flux would not recover, giving an uncontrolled accumulation of β-catenin (supplementary materials, section S-V).

From this analysis, the observed dynamics of GSK3-phosphorylated β-catenin (Figs. 1D and 2C)

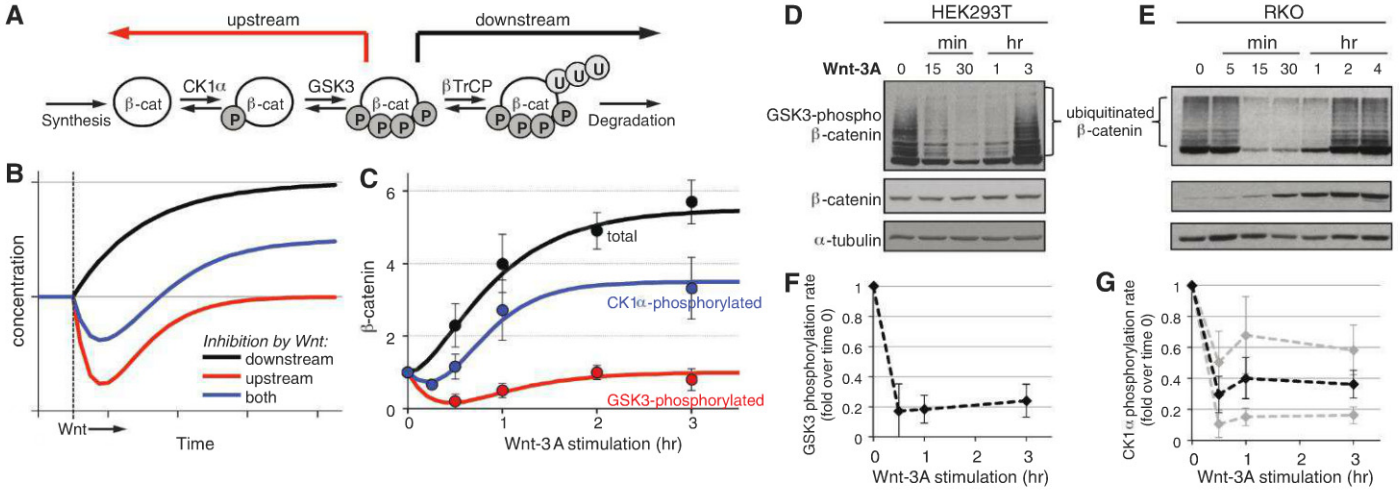

Fig. 2. Flux analysis of the points of Wnt action on β-catenin degradation. (**A**) The β-catenin life cycle. (**B**) The three possible qualitative behaviors of phosphorylated β-catenin in response to Wnt, as predicted by flux analysis. (**C**) Quantification of total, GSK3-, and CK1α-phosphorylated β-catenin in Wnt-stimulated RKO cells. (**D** and **E**) The abundance of ubiquitylated phospho-β-catenin during Wnt stimulation in human embryonic kidney HEK293T (D) and RKO (E) cells. (**F** and **G**) The rates of GSK3- and CK1α-mediated phosphorylation, calculated from the measurements in (C) (supplementary materials, section S-IV). Gray curves show bounds on the CK1α phosphorylation rate: If β-catenin dephosphorylation is rare, the rate is described by the lower bound; if dephosphorylation occurs at a higher rate than phosphorylation and ubiquitylation, the upper bound holds. The black curve shows the dynamics if dephosphorylation and phosphorylation occur at comparable rates. Error bars, mean ± SD (N = 3 replicates).

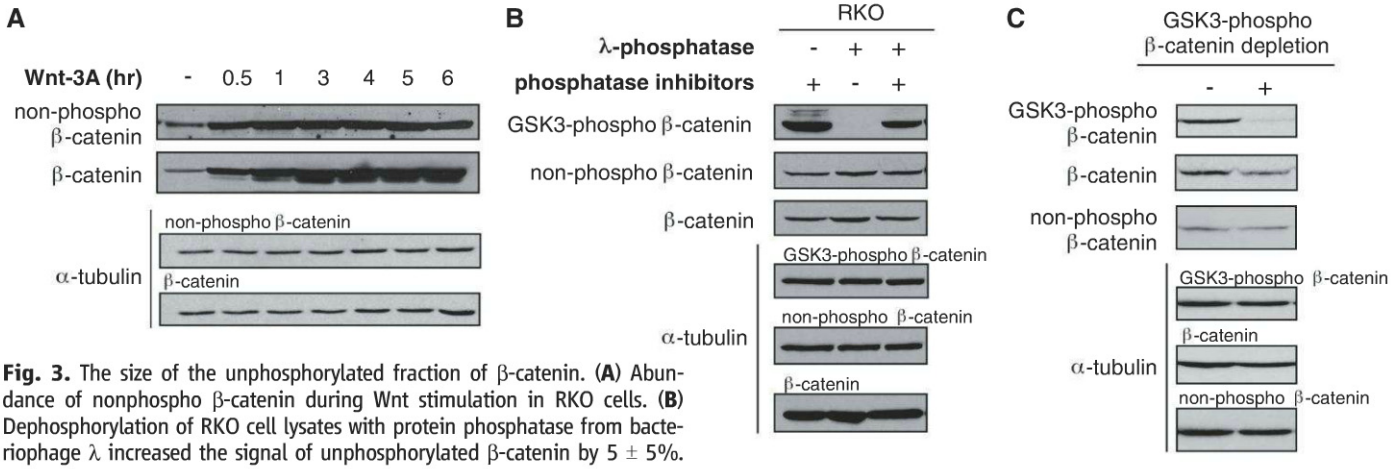

Fig. 3. The size of the unphosphorylated fraction of β-catenin. (**A**) Abundance of nonphospho β-catenin during Wnt stimulation in RKO cells. (**B**) Dephosphorylation of RKO cell lysates with protein phosphatase from bacteriophage λ increased the signal of unphosphorylated β-catenin by 5 ± 5%. (**C**) Immunodepletion of GSK3-phosphorylated β-catenin decreased the signal of total β-catenin by 20 ± 5%. (A) and (B) show qualitative immunoblots; fractions (mean ± SD; N = 3 replicates) were determined by quantitative immunoblots (see supplementary materials).

are consistent with Wnt inhibiting β-catenin degradation at, or upstream, of phosphorylation (Fig. 2B, red curve). We can exclude all other points of inhibition. This mode of inhibition predicts that every intermediate downstream of phosphorylation shows the same dip and full recovery. We confirmed this prediction for ubiquitylated β-catenin in cells stimulated with Wnt (Fig. 2, D and E). Thus, partial inhibition of phosphorylation entirely explains the observed dynamics. Full recovery can occur through mass action alone and does not require feedback. Saturation of the destruction complex has been proposed as a mechanism of Wnt action (*10*), but the dynamics refute this explanation.

To determine how Wnt might affect the individual phosphorylation steps, we applied the same analysis (Fig. 2B). We asked whether Wnt inhibits at or upstream of the priming phosphorylation at S45 by CK1α, or downstream of it, or both. For this analysis, we showed that the majority (80 ± 5%) of CK1α-phosphorylated β-catenin is not phosphorylated by GSK3 (fig. S4). If Wnt only inhibits the GSK3-dependent step, then CK1α-phosphorylated β-catenin should behave similarly to total β-catenin. If Wnt only inhibits the CK1α-dependent step, then CK1α-phosphorylated β-catenin should behave like GSK3-phosphorylated β-catenin. Neither of these occurs. Instead, the accumulation of CK1α-phosphorylated β-catenin is entirely explained by Wnt inhibiting both phosphorylation steps, leading to an initial drop and later accumulation over the initial amount (Fig. 2, B and C). We calculated that the GSK3 and CK1α phosphorylation rates drop in response to Wnt to 24 ± 11% (mean ± SD, $N = 3$) and 16 to 58% (lower/upper bounds) of their initial value, respectively (Fig. 2, F and G) (supplementary materials, section S-IV). Although Wnt might affect the two kinases independently, it seems more likely that Wnt affects a common property of the destruction complex, such as its state of assembly.

It has been suggested that signaling activity may reflect the phosphorylation state, rather than the abundance of β-catenin (*15*). According to this view, β-catenin not phosphorylated by GSK3, called "active" β-catenin, is the transcriptionally active form (*15*); without Wnt, it constitutes 1% of cytoplasmic and nuclear β-catenin (*16*). On addition of Wnt, "active" β-catenin would accumulate massively. For example, a six-fold increase in total β-catenin (Fig. 1B) would translate into a 600-fold increase in "active" β-catenin. Instead, we found that the increase in dephosphorylated β-catenin was comparable to that of total β-catenin (Fig. 3A). Furthermore, in the absence of Wnt, "active" β-catenin was the predominant form (80 ± 5%), as determined by dephosphorylating β-catenin or immunodepleting the GSK3-phosphorylated form (Fig. 3, B and C, and fig. S5). The notion of "active" β-catenin is inconsistent with the observation that almost all β-catenin is unphosphorylated even in the absence of Wnt.

Depictions of signaling pathways have grown exponentially complex with the inclusion of multiple ligands, receptors, extracellular modulators, and downstream targets. Despite this complexity, the core behavior of pathways could be relatively simple. Kinetic analysis of systems, particularly at steady state, provides a powerful strategy to interrogate complex mechanisms; it can provide strong predictions while being insensitive to mechanistic details. In Wnt signaling, β-catenin is subject to a conservation law on the protein flux that permits a few kinetic analyses to resolve long-standing debates about the point of Wnt action. The basic regulatory feature of the pathway is a partial inhibition of two sequential phosphorylation steps without perturbing downstream reactions. Partial inhibition alone establishes the entire dynamics of the β-catenin response. Because a steady state is achieved without saturating the destruction machinery, there in principle can be rapid and facile control of the abundance of β-catenin by tuning its degradation rate through a number of modulators, internal or external to the cell. With a clarification of these central features of the Wnt pathway, we can turn more confidently to its perturbation by drugs and by mutation and to its pathology and pharmacology in different settings.

References and Notes

1. C. H. Schilling, S. Schuster, B. O. Palsson, R. Heinrich, *Biotechnol. Prog.* **15**, 296 (1999).
2. R. Heinrich, T. A. Rapoport, *Eur. J. Biochem.* **42**, 97 (1974).
3. C. Liu *et al.*, *Cell* **108**, 837 (2002).
4. S. Amit *et al.*, *Genes Dev.* **16**, 1066 (2002).
5. M. van Noort, J. Meeldijk, R. van der Zee, O. Destree, H. Clevers, *J. Biol. Chem.* **277**, 17901 (2002).
6. V. F. Taelman *et al.*, *Cell* **143**, 1136 (2010).
7. L. Li *et al.*, *EMBO J.* **18**, 4233 (1999).
8. N. S. Tolwinski *et al.*, *Dev. Cell* **4**, 407 (2003).
9. E. Lee, A. Salic, R. Krüger, R. Heinrich, M. W. Kirschner, *PLoS Biol.* **1**, e10 (2003).
10. V. S. Li *et al.*, *Cell* **149**, 1245 (2012).
11. B. Riggleman, P. Schedl, E. Wieschaus, *Cell* **63**, 549 (1990).
12. F. M. Boisvert *et al.*, *Mol. Cell. Proteomics* **11**, M111.011429 (2012).
13. A. R. Peacocke, *J. Theor. Biol.* **182**, 219 (1996).
14. B. Chance, W. Holmes, J. Higgins, C. M. Connelly, *Nature* **182**, 1190 (1958).
15. F. J. Staal, M. van Noort, G. J. Strous, H. C. Clevers, *EMBO Rep.* **3**, 63 (2002).
16. M. T. Maher, R. Mo, A. S. Flozak, O. N. Peled, C. J. Gottardi, *PLoS ONE* **5**, e10184 (2010).

Acknowledgments: We thank J. Gerhart, M. Springer, X. He, W. Fontana, J. Gunawardena, J. Gray, F. Cong, and R. Deibler for discussions and comments on the manuscript; Y. Ben-Neriah for plasmids; and the Novartis Institutes for Biomedical Research for support of this work. A.M.K. holds a Career Award at the Scientific Interface from the Burroughs Welcome Fund. M.W.K. serves as a paid consultant on the scientific review board of Novartis.

Supplementary Materials

www.sciencemag.org/cgi/content/full/science.1228734/DC1
Materials and Methods
Supplementary Text
Figs. S1 to S6
References (*17*–*25*)

13 August 2012; accepted 22 October 2012
Published online 8 November 2012;
10.1126/science.1228734

Tuning the Electronic Absorption of Protein-Embedded All-*trans*-Retinal

Wenjing Wang, Zahra Nossoni, Tetyana Berbasova, Camille T. Watson, Ipek Yapici, Kin Sing Stephen Lee, Chrysoula Vasileiou, James H. Geiger,* Babak Borhan*

Protein-chromophore interactions are a central component of a wide variety of critical biological processes such as color vision and photosynthesis. To understand the fundamental elements that contribute to spectral tuning of a chromophore inside the protein cavity, we redesigned human cellular retinol binding protein II (hCRBPII) to fully encapsulate all-*trans*-retinal and form a covalent bond as a protonated Schiff base. This system, using rational mutagenesis designed to alter the electrostatic environment within the binding pocket of the host protein, enabled regulation of the absorption maximum of the pigment in the range of 425 to 644 nanometers. With only nine point mutations, the hCRBPII mutants induced a systematic shift in the absorption profile of all-*trans*-retinal of more than 200 nanometers across the visible spectrum.

Light-absorbing protein-chromophore complexes play critical roles in a variety of biological processes such as vision, phototaxis, and photosynthesis. The function of these systems depends on the modulation of the spectroscopic properties through protein-chromophore interactions. The rhodopsin family represents a particularly interesting case, where the λ_{max} (absorption maximum) of the same chromophore is modulated from 420 nm (human short wave–sensitive pigment, hSWS) to 587 nm (sensory rhodopsin I) (*1*, *2*). In all cases, a sole chromophore—retinal in its various isomeric forms—is bound via an iminium (also known as a protonated Schiff base, PSB) through the side chain of a lysine residue (*3*) to various opsins.

Although the mechanism by which rhodopsins alter the absorbance of a single chromophore (the "opsin shift") is still debated, it is generally accepted that wavelength regulation is a result of conformational manipulation of the chromophore and/or directed electrostatics, where the protein

Department of Chemistry, Michigan State University, East Lansing, MI 48824, USA.

*To whom correspondence should be addressed. E-mail: geiger@chemistry.msu.edu (J.H.G.); babak@chemistry.msu.edu (B.B.)

localizes electrostatic potential to various regions of the chromophore [reviewed in (*4*)]. The latter perturbations lead to stabilization or destabilization of the chromophore's ground and excited states that greatly influence the absorption profile (*5*–*8*). Nonetheless, the iminium in all structurally characterized rhodopsins is stabilized, either directly or through a water-mediated network, by a counteranion, which affects the electrostatic environment of the chromophore (*9*, *10*). In contrast, earlier calculations (*11*) and gas-phase experiments with the retinylidene PSB (*12*) have indicated that substantial bathochromically shifted spectra would be obtained in a uniformly neutral electrostatic environment in the absence of a PSB counteranion. With the latter principle in mind, we have reengineered proteins capable of binding retinal as a PSB to investigate the details of subtle interactions that can alter the absorption of a bound cationic chromophore. We propose that mutants designed to achieve a more evenly dispersed electrostatic field across the polyene, should lead to "super-red"–absorbing pigments in the absence of a counteranion proximal to the iminium nitrogen.

To systematically study the correlation between structure and absorption wavelength, we selected the intracellular lipid binding protein family (iLBP), and in particular human cellular retinol binding protein II (hCRBPII), as the target for protein engineering (*13*). Tolerance to mutations and the large binding cavity of iLBPs allow flexibility in the redesign of the protein and enable the binding of a wide range of different ligands (*14*). The relative rigidity of the iLBP fold makes it an ideal scaffold for protein engineering because it is more likely that mutations will not result in structural rearrangement (*14*), allowing their specific effects to be compared directly. In addition, we have shown that the chromophore must be fully embedded within the binding pocket, because exposure to the aqueous media would buffer electrostatic changes that result from mutations along the polyene (*15*). As a result of the latter considerations, hCRBPII was specifically chosen from the iLBP family because it fully encapsulates retinal within its binding cavity.

In prior work, we showed that the correct trajectory of an active-site Lys residue with respect to the electrophilic aldehyde (the Bürgi-Dunitz trajectory) was necessary (*16*, *17*). In that respect, in silico analysis led to the selection of Gln^{108} as the suitable position for the active-site Lys (Fig. 1A). A second mutation, K40L (Fig. 1A), was required because the positively charged Lys residue inhibited the protonation of the Schiff base formed with retinal. Double mutant Q108K:K40L (KL) binds retinal with high affinity (dissociation constant K_d = 29 ± 5 nM) and yields a PSB with λ_{max} = 508 nm, a 68-nm red shift relative to the PSB of retinal with *n*-butylamine in ethanol (λ_{max} = 440 nm). In contrast to the rhodopsins and our earlier engineered protein systems, and as confirmed by KL's crystal structure, a counteranion for the iminium was purposely and successfully omitted. Alternatively, a putative π-cation interaction with Trp^{106} and the possible interaction with the nearby water network could be stabilizing the protonation of the iminium nitrogen (Fig. 1B).

With KL as the starting point, the electrostatic environment around the chromophore was altered by targeting different zones of the polyene through mutations of nearby amino acids (Fig. 1C). Table 1 illustrates modifications to zones II and III of the bound chromophore. Thr^{51}, Thr^{53}, and Tyr^{19} were targeted, as they were situated relatively close to the polyene (fig. S1). As anticipated, the isosteric replacement of Thr^{51} in zone III (near the iminium) with a hydrophobic amino acid (Val) led to a substantial red shift in absorption, presumably by decreasing the negative polarity near the iminium (Table 1, entry 2; fig. S2). Changes to amino acids in zone II (middle of the chromophore) did not produce red-shifted pigments, highlighted by mutations of Thr^{53} and Tyr^{19} with a variety of amino acids, which exhibited maximally a 5-nm red shift when replaced with Cys and Trp, respectively (Table 1, entries 3 and 5; table S2). A large bathochromic shift was again observed as a result of the T51V mutation when combined with T53C and/or Y19W (Table 1, entries 4, 6, and 7; figs. S3 and S4). Changes to zone I (ionone ring end) did not correlate well with electrostatic stabilization of a resonating charge (table S3). In fact, unlike the generally accepted postulate that introduction of negative potential around the ionone ring should lead to more red-shifted pigments [reviewed in (*8*)], introduction of acidic residues in zones I and II resulted in a blue shift (tables S2 and S3). In contrast to the rhodopsins and other engineered systems where a counteranion stabilizes the iminium charge, the present system does not require anionic localization at any point along the polyene because there is no strong ionic interaction at the PSB to counterbalance. The absence of a PSB counteranion yields a conjugated system that is more responsive to subtle changes in its environment, enabling greater bathochromic shift by an overall "softening" (more even distribution) of the electrostatic potential along the polyene.

Further gain in uniformly balancing the electrostatic potential along the polyene came from control of the chromophore's global environment. The estimated dielectric constant inside the binding cavity of proteins (2 to 4) is much lower than that of the aqueous environment (78) (*18*). Because exposure to the aqueous environment increases the polarization of the electrostatic potential across the chromophore and also dampens the effect of weakly polarized groups to stabilize a resonating cationic charge, we sought to further sequester the binding pocket. Examination of the hCRBPII structure identified Arg^{58}, located in the entrance of the binding pocket, as a potential "leak" that could be capped with a larger, hydrophobic residue. A number of amino acids were substituted for Arg^{58} (table S4); the R58W substitution was the most effective in sequestering the binding pocket from the bulk medium.

Table 1 lists the contribution of the R58W mutation when combined with the KL series of proteins discussed above. A substantial red shift is observed for these mutants, clearly surpassing the absorption of human long wave–sensitive (hLWS) pigment with six overall mutations (590 nm; Table 1, entry 7). Consistent with the idea that solvent exposure can buffer the effect of weakly polarizing amino acids, the R58W-containing series of proteins, which have a more sequestered binding pocket, enhance the red shift of mutations that are introduced far from R58W. For example, T53C and Y19W are ~9 Å from Arg^{58}, yet the R58W mutation yields a much greater red shift when either T53C or Y19W are present (539 nm → 585 nm for T53C; 537 nm → 577 nm for Y19W). As noted, the same two mutations alone led to smaller bathochromic shifts, which suggests that isolating the interior of the protein from the bulk medium greatly enhances the red shift induced by substitutions at positions 53 and

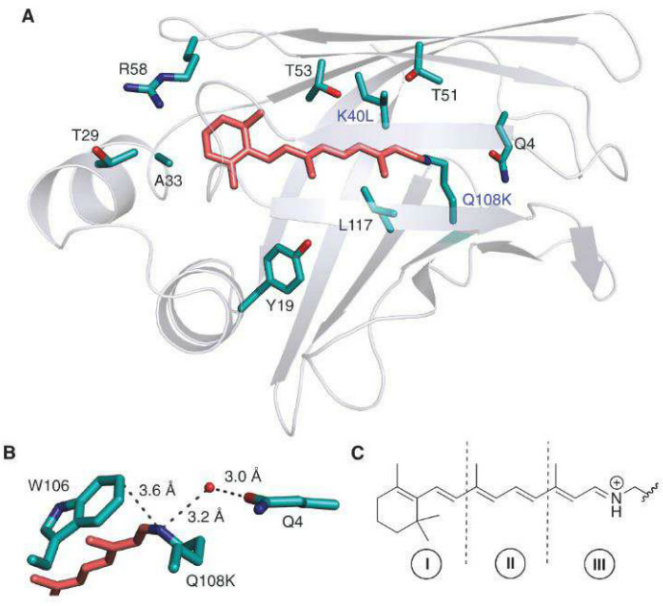

Fig. 1. **(A)** Crystal structure of Q108K:K40L-hCRBPII, with residues most pertinent to this study highlighted. **(B)** Trp^{106} and a close-lying water molecule hydrogen-bonded to Gln^{4} putatively stabilize the protonation of the iminium without the presence of a counteranion. **(C)** Protonated Schiff base of all-*trans*-retinal. The chromophore is divided into three segments to clarify the discussion of mutations that are close to different locations of the polyene.

Table 1. Q108K:K40L hCRBPII (KL)–based mutants.

Entry	Zone	hCRBPII mutant	λ_{max} (nm) R58	Protein shift*		λ_{max} (nm) R58W	Protein shift†		Enhancement (nm)‡
				(nm)	(cm^{-1})		(nm)	(cm^{-1})	
1	—	KL	508	0	0	527	0	0	—
2	III	KL:T51V	533	25	923	570	43	1431	18 (1.7×)
3	II	KL:T53C	513	5	192	540	13	457	8 (2.6×)
4	II+III	KL:T51V:T53C	539	31	1132	585	58	1881	27 (1.9×)
5	II	KL:Y19W	513	5	192	538	11	388	6 (2.2×)
6	II+III	KL:T51V:Y19W	537	29	1063	577	50	1644	21 (1.7×)
7	II+III	KL:T51V:T53C:Y19W	538	30	1098	590	63	2026	33 (2.1×)

*Protein shift with reference to Q108K:K40L; wavenumbers provide a direct correlation to the change in energy. †Protein shift with reference to Q108K:K40L:R58W. ‡Enhancement is calculated as the difference in protein shift between KL-R58W mutants and the KL mutants, and reflects the overall increased red shift in excess of that anticipated from a purely additive effect of R58W. For example, the T51V mutation leads to a 25-nm bathochromic shift (KL versus KL:T51V). A 25-nm red shift would be expected for KL:T51V:R58W versus KL:R58; however, a 43-nm shift is observed. The 18-nm difference in the level of enhancement (factor of 1.7 increase) is a result of the R58W mutation. Numbers in parentheses are relative increases of the protein shift of the KL-R58W mutant series with respect to the KL mutant series.

19. In fact, in all cases, the R58W mutation leads to a factor of ~2 enhancement in red-shifting of the absorption. Although both Cys and Trp can participate in polar interactions, they are also polarizable and could effectively promote conjugation of the positive charge along the polyene in an environment of low dielectric constant.

Inspection of the crystal structures of all available mutants in the PSB region was invaluable to further optimize the binding pocket (representative structure in Fig. 2A). A water network that originates from Thr^{1} to Gln^{4} and extends to the iminium nitrogen apparently contributes to the stability of the charge on the PSB. Putative disruption of this water network by mutation of Gln^{4} in KL-T51V:T53C:Y19W:R58W:T29L to Phe, Trp, Leu, Ala, Asn, and Thr all led to a bathochromic shift from 591 nm up to 610 to 613 nm (table S5). This was akin to removing a polar amino acid residue, such as Thr^{51}, from zone III. A bathochromic shift was gained with the Q4R mutation (622 nm), presumably as a result of increased positive electrostatic potential in zone III, which further destabilizes the localization of the positive charge on the iminium nitrogen. Evident from the crystal structure of KL-T51V:T53C:Y19W:R58W:T29L:Q4R is the absence of the hydrogen-bonded water network (Fig. 2B). Although the iminium nitrogen is ~6 Å away from the Arg^{4} guanidinium, the decreased dielectric constant of the binding pocket translates to higher sensitivity in zone III. Disruption of the putative cation-stabilizing water network was only possible at this late stage of design, having provided the necessary and sufficient means to stabilize the resonating charge along the polyene by earlier mutations. As a point of comparison, the KL:Q4W protein binds retinal to produce a pigment that absorbs maximally at 533 nm, but with a depressed iminium pK_a (8.3 for KL versus 6.2 for KL:Q4W). This is presumably the result of insufficient stabilizing elements, both in the PSB region and along the length of the chromophore.

A final push to gain the most bathochromically shifted pigment focused on further encapsulation of the binding pocket from the aqueous environment. The Ala^{33} position, residing on the α helix that functions as a lid for ligand entry, provided a likely candidate (Fig. 2C). A series

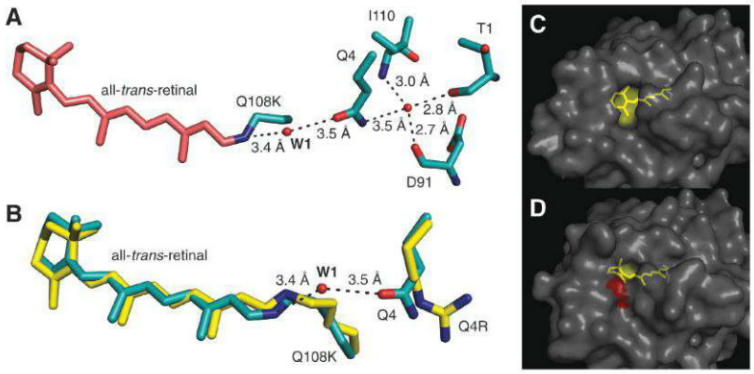

Fig. 2. (**A**) Crystal structure of Q108K:K40L:T51V:T53C:Y19W:R58W:T29L hCRBPII with Thr^{1}, Gln^{4}, Asp^{91}, and Ile^{110} highlighted to show hydrogen bonding to W1, extending to the iminium nitrogen. (**B**) Overlay of the crystal structures of Q108K:K40L:T51V:T53C:Y19W:R58W:T29L hCRBPII (591 nm, cyan structure) and Q108K:K40L:T51V:T53C:Y19W:R58W:T29L:Q4R hCRBPII (622 nm, yellow structure) illustrates that the mutation of Gln^{4} results in the loss of the ordered water molecule (**W1**), leading to further bathochromic shift of the retinylidene protein complex. As exemplified in the latter two structures, all mutants that have an ordered water molecule adopt the *cis*-imine geometry. Conversely, *trans*-imine geometry is observed in all Gln^{4} mutants without the ordered water molecule. (**C**) Crystal structure of Q108K:K40L:T51V:T53C:Y19W:R58W:T29L hCRBPII (591 nm) illustrates the opening near Ala^{33}. (**D**) Crystal structure of Q108K:K40L:T51V:T53C:Y19W:R58W:T29L:A33W hCRBPII (606 nm) shows substantial closing of the orifice (A33W surface shown in red).

of Ala^{33} mutants of the KL-T51V:T53C:Y19W:R58W:T29L:Q4F protein were produced (table S6). Incorporation of A33W led to further red-shifting of the absorption (636 nm), likely as a result of sequestering and increasing the polarizability of the binding pocket (Fig. 2D) (*19*). The nonamutant KL-T51V:T53C:Y19W:R58W:T29L:Q4R:A33W produced the most bathochromically shifted retinylidene-bound protein complex reported thus far, with a λ_{max} of 644 nm (**M11**, Fig. 3). To put this in context, the most red-shifted retinylidene PSB previously observed (measured in vacuum) peaks at 610 nm, whereas 620 nm was considered to be the theoretical maximum (*12*).

Wavelength regulation toward the most red-shifted hCRBPII mutant (**M11**, 644 nm) showed that removal of the negative polarity in zone III is necessary. Conversely, introduction of negatively polarized residues in this region should result in a blue shift by localizing the cation on the iminium nitrogen. Replacement of Lys^{40} with Ser (**M3**, 482 nm) reversed the polarity in zone III and produced a blue-shifted pigment relative to KL. The same was true for the absorption of Q108K:T51D double mutant, which blue-shifted to 474 nm (**M2**). Further, introduction of L117E (also in zone III) generated the most hypsochromically shifted mutant (**M1**, 425 nm), which is comparable to hSWS pigment.

The ultraviolet-visible (UV-vis) spectra and solutions of a number of hCRBPII mutants bound with retinal are shown in Fig. 3. The figure depicts the regulation of wavelength of a single chromophore, over a 219-nm range, through the redesign of the electrostatic potential of the protein's interior. The hCRBPII mutants not only recapitulate the wavelength regulation observed with the pigmented rhodopsins, but also display red shifts beyond the postulated limit for any retinylidene PSB. These mutants show that extensive wavelength regulation is possible with little contribution from conformational effects. The latter conclusion was based on analysis of crystal structures for this series of mutants that showed little change in the planarity of the chromophore (figs. S6 and S7). As expected, maximal hypsochromicity is achieved by localizing the positive charge on the iminium nitrogen.

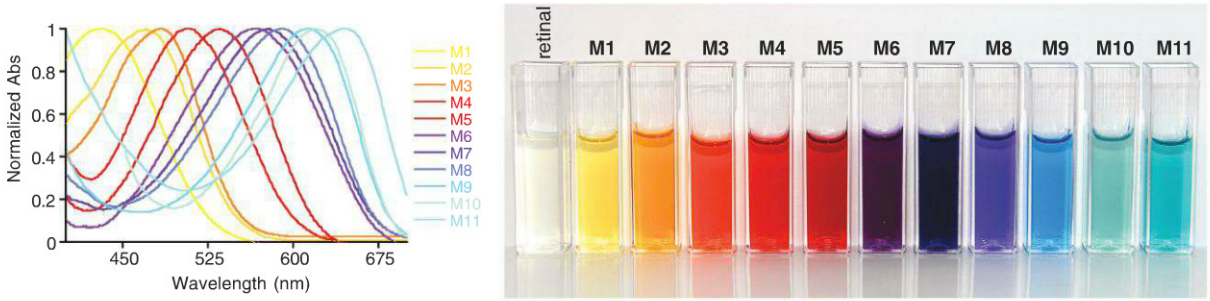

Entry	Pigments	λ_{max} nm	Protein shift nm (cm^{-1})	K_d, nM
1	*n*Bu-retinylidene PSB	440	---	---
2	hSWS	420	-20 (-1,082)	---
M1	Q108K:T51D:L117E	425	-15 (-802)	53±15
M2	Q108K:T51D	474	34 (1,630)	23±6
M3	Q108K:K40S	482	42 (1,980)	28±12
3	sensory rhodopsin II	487	47 (2,193)	---
4	rod-rhodopsin	500	60 (2,727)	---
M4	Q108K:K40L	508	68 (3,042)	29±5
5	hMWS	530	90 (3,859)	---
M5	Q108K:K40L:T51V	533	93 (3,966)	19±7
6	hLWS	560	120 (4,870)	---
7	bacteriorhodopsin	570	130 (5,183)	---
M6	Q108K:K40L:T51V:R58W	570	130 (5,183)	63±4
M7	Q108K:K40L:T51V:Y19W:R58W	577	137 (5,396)	86±6
8	sensory rhodopsin I	587	147 (5,691)	---
M8	Q108K:K40L:T51V:T53C:Y19W:R58W:T29L	591	151 (5,807)	55±5
M9	Q108K:K40L:T51V:T53C:Y19W:R58W:T29L:Q4W	613	173 (6,414)	65±8
M10	Q108K:K40L:T51V:T53C:Y19W:R58W:T29L:Q4R	622	182 (6,650)	70±6
M11	Q108K:K40L:T51V:T53C:Y19W:R58W:T29L:Q4R:A33W	644	204 (7,199)	42±6

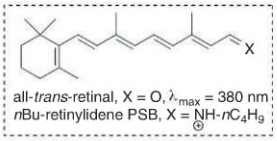

Fig. 3. Normalized UV-vis spectra of a selected group of hCRBPII mutants (**M1** to **M11**). As indicated in the table, the absorption of the mutants spans from 425 nm (**M1**) to 644 nm (**M11**). For comparison, the wavelengths of various rhodopsins are included. The pigments in the cuvettes were generated by incubation of all-*trans*-retinal (72 μM in 100 mM phosphate buffer, pH 7.3, shown in the left cuvette) with hCRBPII mutants **M1** to **M11** (80 μM protein; the same concentration of retinal was used in all cuvettes). Protein shift is defined as the difference between the absorbance of *n*-butylamine retinylidene PSB and the absorbance of retinal-bound hCRBPII mutants; wavenumbers given in parentheses provide a direct correlation to the change in energy. The binding constants for the hCRBPII mutants (shown as dissociation constants K_d) indicate strong binding of retinal with the proteins.

Extreme bathochromic shifting, on the other hand, depends not on a reversal of polarity but on an even distribution of electrostatic potential across the entire polyene, keeping in mind that a strong interaction of a counteranion to the PSB is not present in these mutants (*20*). To this end, it is of utmost importance not only to embed the chromophore within the binding pocket, but also to enclose the binding cavity from the bulk medium and distribute the cationic charge evenly along the polyene. Embedding the chromophore enables it to respond to electrostatic perturbations, and this is enhanced by enclosure of the binding pocket. A balanced distribution of the cationic charge across the polyene is generated by evenly distributed neutral electrostatic potential in the binding pocket, leading to "super-red" pigments.

References and Notes

1. K. Palczewski, *J. Biol. Chem.* **287**, 1612 (2012).
2. J. L. Spudich, C. S. Yang, K. H. Jung, E. N. Spudich, *Annu. Rev. Cell Dev. Biol.* **16**, 365 (2000).
3. K. Palczewski, *Annu. Rev. Biochem.* **75**, 743 (2006).
4. M. B. Nielsen, *Chem. Soc. Rev.* **38**, 913 (2009).
5. P. B. Coto, A. Strambi, N. Ferré, M. Olivucci, *Proc. Natl. Acad. Sci. U.S.A.* **103**, 17154 (2006).
6. G. G. Kochendoerfer, S. W. Lin, T. P. Sakmar, R. A. Mathies, *Trends Biochem. Sci.* **24**, 300 (1999).
7. S. W. Lin *et al.*, *J. Biol. Chem.* **273**, 24583 (1998).
8. R. Rajamani, Y. L. Lin, J. Gao, *J. Comput. Chem.* **32**, 854 (2011).
9. T. P. Sakmar, R. R. Franke, H. G. Khorana, *Proc. Natl. Acad. Sci. U.S.A.* **86**, 8309 (1989).
10. T. P. Sakmar, R. R. Franke, H. G. Khorana, *Proc. Natl. Acad. Sci. U.S.A.* **88**, 3079 (1991).
11. B. Honig, A. D. Greenberg, U. Dinur, T. G. Ebrey, *Biochemistry* **15**, 4593 (1976).
12. J. Rajput *et al.*, *Angew. Chem. Int. Ed.* **49**, 1790 (2010).
13. E. Li, A. W. Norris, *Annu. Rev. Nutr.* **16**, 205 (1996).
14. K. Gunasekaran, A. T. Hagler, L. M. Gierasch, *Proteins* **54**, 179 (2004).
15. K. S. S. Lee *et al.*, *ChemPlusChem* **77**, 273 (2012).
16. H. B. Bürgi, J. D. Dunitz, *Acc. Chem. Res.* **16**, 153 (1983).
17. C. Vasileiou *et al.*, *J. Am. Chem. Soc.* **129**, 6140 (2007).
18. J. J. Dwyer *et al.*, *Biophys. J.* **79**, 1610 (2000).
19. Addition of hydroxylamine to two hCRBPII mutants examined the ability to enclose the binding cavity with mutations of Arg^{58} and Ala^{33}. Reaction of the retinylidene with hydroxylamine would require ready access of the reagent to the PSB. A rapid disappearence of the PSB was observed upon addition of hydroxylamine to the hCRBPII mutant that retained Arg^{58} and Ala^{33}. Conversely, the protein containing the R58W and A33W mutations resisted change in the presence of hydroxylamine (see supplementary materials for further details).
20. The calculated electrostatic potential of **M10** (622 nm) projected onto the bound retinylidine chromophore is compared to that of **M4** (508 nm) in fig. S5. The comparison shows that to achieve the red shift observed in **M10**, the chromophore experiences an even distribution of a neutral electrostatic potential across its length.

Acknowledgments: Supported by NIH grant R01-GM54082. We thank the U.S. Department of Energy (DOE), Office of Science, Basic Energy Sciences, Chemical Sciences, Geosciences and Biosciences Division (grant DE-FG02-06ER15822 to J.H.G.) and the beamline staff at LS-CAT 21-ID (supported by the DOE Office of Energy Research under contract W-31-109-ENG-38). The Advanced Photon Source is supported by the DOE, Office of Science, Basic Energy Sciences, under contract W-31-109-ENG-38. PDB accession codes for the crystal structures used in this study: 4EXZ (Q108K:K40L); 4EEJ (Q108K:K40L:T51V:T53C:Y19W:R58W:T29L:Q4R); 4GKC (Q108K:K40L:T51V:T53C:Y19W:R58W:T29L:Q4A); 4EFG (Q108K:K40L:T51V:T53C:Y19W:R58W:T29L); 4EDE (Q108K:K40L:T51V:T53C:Y19W:R58W:T29L:A33W). Michigan State University has applied for a patent titled "Colorimetric and Fluorescent Proteins" (U.S. patent pending, serial no. 13/636,499) related to the design methods and materials presented in this work.

Supplementary Materials

www.sciencemag.org/cgi/content/full/338/6112/1340/DC1
Materials and Methods
Figs. S1 to S7
Tables S1 to S7
References (*21*–*29*)

15 June 2012; accepted 19 October 2012
10.1126/science.1226135

Identity and Function of a Large Gene Network Underlying Mutagenic Repair of DNA Breaks

Abu Amar M. Al Mamun,[1] Mary-Jane Lombardo,[1]*† Chandan Shee,[1]* Andreas M. Lisewski,[1] Caleb Gonzalez,[1]‡ Dongxu Lin,[1]§ Ralf B. Nehring,[1] Claude Saint-Ruf,[2]|| Janet L. Gibson,[1] Ryan L. Frisch,[1] Olivier Lichtarge,[1,3] P. J. Hastings,[1] Susan M. Rosenberg[1,3,4,5]¶

Mechanisms of DNA repair and mutagenesis are defined on the basis of relatively few proteins acting on DNA, yet the identities and functions of all proteins required are unknown. Here, we identify the network that underlies mutagenic repair of DNA breaks in stressed *Escherichia coli* and define functions for much of it. Using a comprehensive screen, we identified a network of ≥93 genes that function in mutation. Most operate upstream of activation of three required stress responses (RpoS, RpoE, and SOS, key network hubs), apparently sensing stress. The results reveal how a network integrates mutagenic repair into the biology of the cell, show specific pathways of environmental sensing, demonstrate the centrality of stress responses, and imply that these responses are attractive as potential drug targets for blocking the evolution of pathogens.

Repair of DNA double-strand breaks (DSBs) by homologous recombination in *Escherichia coli* is nonmutagenic in unstressed cells but, under stress, switches to a mutagenic mode that is activated by stress responses (*1*, *2*) (Fig. 1A). It is, therefore, a mechanism of stress-induced mutagenesis (SIM): mechanisms in bacterial, yeast, and human cells that promote mutation and potentially accelerate evolution when cells are maladapted to their environment [reviewed (*3*–*6*)].

Mutagenic repair of DNA breaks in *E. coli* requires proteins that mend DSBs by homologous recombination; error-prone DNA polymerases; and activation of the SOS DNA-damage response, the RpoS (σ^S)–controlled general or starvation stress response, and the RpoE (σ^E) membrane protein stress response (*7*). The σ^E response promotes spontaneous DNA breakage in some DNA regions (*8*) (Fig. 1A). The SOS response is activated by DSBs and promotes mutation via transcriptional up-regulation of DNA polymerases (Pols) IV and V. However, break repair remains nonmutagenic unless the σ^S general or starvation response is also activated (*1*, *2*). The σ^S response licenses the use of Pols IV, II, and V in DSB repair (*7*) and thus throws the switch to mutagenesis under stress (Fig. 1A) in plasmids (*1*) and chromosomes of plasmid-free cells (*2*).

We performed genetic screens for comprehensive discovery of genes required for stress-induced mutagenesis (Methods in supplementary materials and fig. S1). We used a colony–color papillation screen and minitransposon Tn*10*dCam-insertion mutagenesis, which allows isolation of non-null alleles of essential genes in addition to knock outs (*9*). Mutants lacking known genes required in DSB-dependent SIM show fewer papillae (Fig. 1B and table S1). A total of 83 genes that facilitate SIM were identified: 76 new and 7

[1]Department of Molecular and Human Genetics, Baylor College of Medicine, Houston, TX 77030–3411, USA. [2]U1001 INSERM, Université Paris, Descartes, Sorbonne Paris cité, site Necker, 156 rue de Vaugirard, 75730 Paris Cedex 15, France. [3]Department of Biochemistry and Molecular Biology, Baylor College of Medicine, Houston, TX 77030, USA. [4]Department of Molecular Virology and Microbiology, Baylor College of Medicine, Houston, TX 77030, USA. [5]The Dan L. Duncan Cancer Center, Baylor College of Medicine, Houston, TX 77030, USA.

*These authors contributed equally to this work.
†Present address: Seres Health, Inc., 1 Memorial Drive, Cambridge, MA 02142, USA.
‡Present address: Department of Systems Biology (Unit 950), University of Texas M.D. Anderson Cancer Center, 7435 Fannin Street, Houston, TX 77054, USA.
§Present address: Department of Cell Biology, Yale University, 333 Cedar Street, New Haven, CT 06520, USA.
||Present address: U1001 INSERM, Université Paris Descartes, Sorbonne Paris Cité, Site Cochin, 24 rue du Faubourg St. Jacques, 75014 Paris, France.
¶To whom correspondence should be addressed. E-mail: smr@bcm.edu

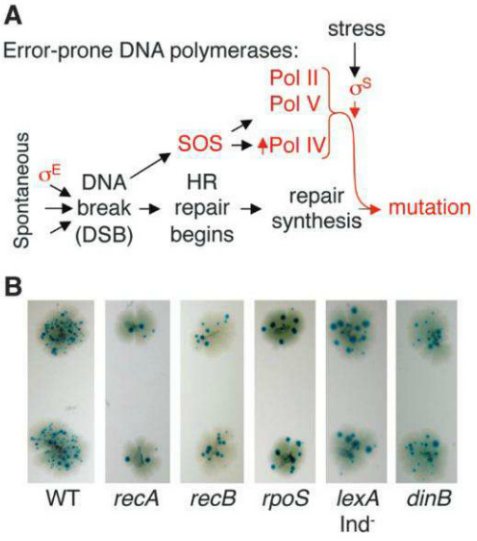

Fig. 1. (**A**) Roles of stress responses in mutagenic repair of DNA DSBs by homologous recombination (HR) [reviewed, (*7*)]. (**B**) Primary screen for DSB-dependent SIM-deficient mutants. Blue papillae in the white colonies are Lac$^+$ mutant clones formed after prolonged starvation stress (*8*). (**C**) Identities of 93 SIM-network genes and results of secondary screens. [1]Previously known, found in this screen. [2]Previously known, not found in this screen. [3]Identified on the basis of genes discovered in this screen. (p), transposon inserted in the promoter (table S12). Superscripts S, E, and SOS indicate decreased σ^S activity, σ^E activity, and spontaneous SOS induction, respectively (table S7).

C

Class	Mutant genes for stress-induced mutation
Regulators	*arcA*(p)^E, *argR*, *barA*, *crp*^{3}, *cyaA*, *fruR*^{E}, *glnK*^{S}, *hdfR*^{S}, *ihfA*, *lexA*^{2,SOS}, *lrp*^{E}, *mall*, *metJ*^{S}, *nagC*, *nusA*^{2}, *phoU*^{E}, *ppk*^{1}, *rpoE*(p)^E, *rpoS*^{1,S}, *treR*, *uvrY*^{SOS}
Proteases, chaperones	*cspC*^{S}, *groES*(p)^1, *hfq*^{S}, *ldcA*, *lon*^{E}, *pepP*, *prc*
DNA replication, repair	*dinB*^{2}, *ligA*(p), *polB*^{2}, *recA*^{1,SOS}, *recB*^{1,SOS}, *recC*^{1,SOS}, *recF*^{2}, *ruvA*^{2}, *ruvB*^{2}, *ruvC*^{2}, *sulA*^{1}, *umuC*^{2}
Electron transfer	*cyoA*^{S,E}, *cyoD*^{S,E}, *fre*^{S,E}, *hemL*^{S,E}, *hscB*^{S}, *mdh*^{S,E}, *nuoC*^{S,E}, *nuoG*^{S,E}, *nuoH*^{S,E}, *nuoJ*^{S,E}, *nuoK*^{S,E}, *nuoL*^{S,E}, *pgi*^{S,SOS}, *sdhB*^{S,E}, *sdhD*^{S,E}, *ubiA*^{S,E}, *ubiD*^{S,E}, *ubiE*^{S,E}, *ubiH*^{S,E}, *ubiX*^{S,E}
Metabolism	*apaH*^{S,E}, *argD*, *cysD*(p), *lipB*^{E}, *pgl*, *rbsK*^{S}, *speD*^{S}, *speE*^{S}
Cellular processes	*acrA*, *acrB*, *dsbA*, *dsbC*, *proL*, *pstB*^{E}, *pstC*^{E}, *rppH*^{E}, *srlA*, *tatC*, *trxB*^{E}, *znuA*, *znuC*^{E}
Unknown functions	*apaG*, *ybjT*, *yfjL*(p), *ygfA*^{E}, *yhhK*, *yicC*, *yjcC*, *yifE*^{S}, *yigP*^{E}, *yqgE*, *yqiC*, *ytjB*(p)

previously known (Fig. 1C). Nine additional previously known genes were not identified, most for reasons that we understand (outlined in table S2), and one was identified by candidate-gene approach (supplementary text S1). We define a network of ≥93 genes (83+9+1) (Fig. 1C and annotations in table S2). All were reconstructed in nonmutagenized cells by using deletion alleles (tables S3 and S4) for nonessential genes and were verified in quantitative SIM assays: 30 showed weak (W, 1.5 to 3); 34 showed moderate (M, 3.1 to 9); and 29 showed strong (S, >9) fold decreases in mutation rate (table S3). In supplementary texts S2 and S3, we estimate total and essential genes likely to have been missed.

We confirmed the mutation-deficient phenotypes of a large representative sample of SIM-deficient mutants using two additional, different assays for DSB-dependent SIM (Fig. 2 and table S5): one (Tet) for frameshift (*2*) and one (Nal) for base-substitution mutations, both in I-Sce I endonuclease–cleaved chromosomes of starved plasmid-free cells. Both require the σ^S and SOS stress responses, DSB repair proteins, DNA Pols IV and V, and either starvation or artificial up-regulation of the σ^S starvation-stress response, all of which characterize DSB-dependent SIM (*2*) (table S5). Thus, SIM is neither plasmid-specific nor specific to genes selected during the stress [previous concerns (*10*)]. We confirmed phenotypes of 43 of 52 mutants tested (Fig. 2 and table S5). Those confirmed showed significant correlation of strength of defect between different mutation assays (Lac papillation, Lac quantitative, Tet, and Nal) (tables S1 and S6). Of the remaining nine, all but two displayed sensitivity to SDS-EDTA (tables S1 and S7), a characteristic of cells with membrane stress (σ^E)–response defects (*11*). σ^E functions in SIM by promoting spontaneous DNA breaks and so is not required when DSBs are provided by I-Sce I (*8*), as is the case in these assays. Thus, the overwhelming majority of genes tested are confirmed as deficient in DSB-dependent base-substitution and frameshift SIM at the three unlinked sites sampled (*lac*, *tet*, and *gyrA*). A summary of SIM-deficient phenotypes of the network mutants in the four mutation assays used is given in table S1.

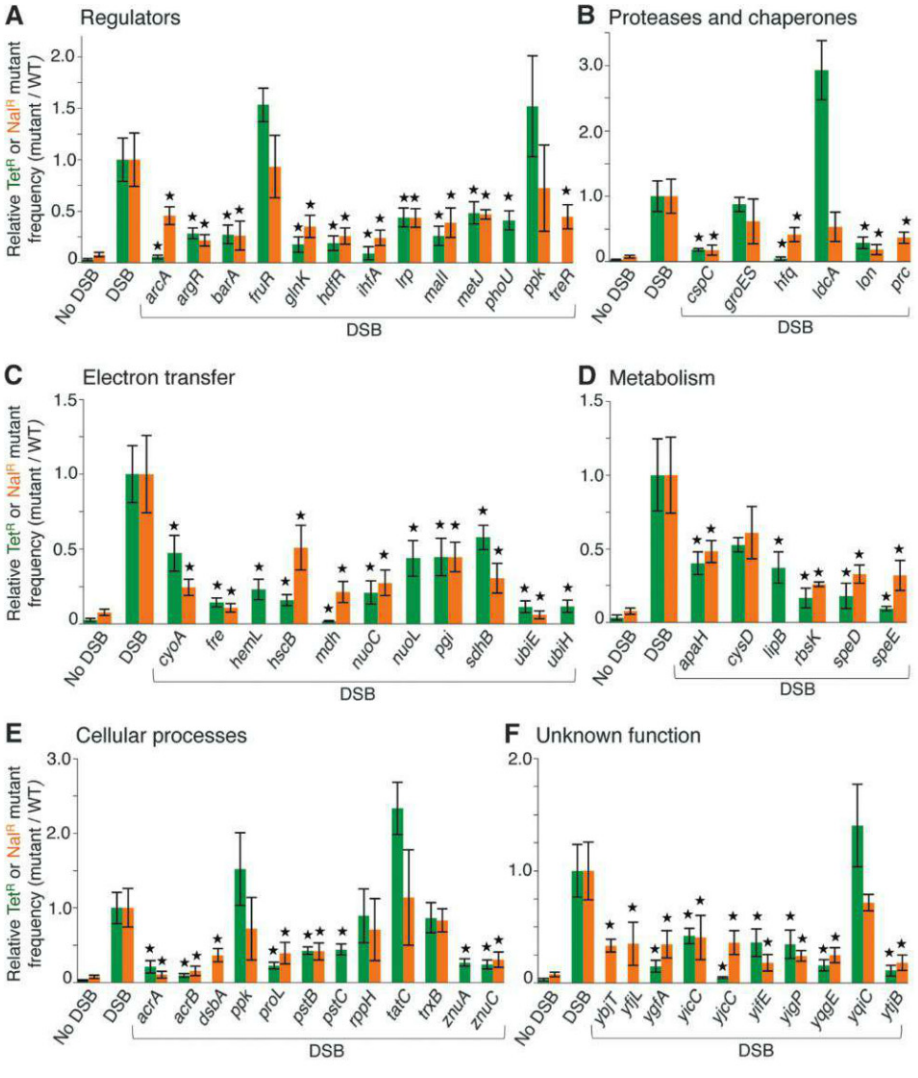

Fig. 2. (**A** to **F**) Validation of mutants in chromosomal Tet frameshift and Nal base substitution SIM assays. *Significantly SIM-deficient (*P* values in table S5, two-tailed Student's *t* test). Relative mutant frequencies, mutant frequency divided by that of the WT-DSB (I-Sce I–positive) controls assayed in parallel. Means ± SEM ($n \geq 3$ experiments each), for this and all figures.

The 93 SIM genes constitute a functional network. First, protein-protein interaction data (*12*) show highly significant clustering for the SIM genes (Fig. 3, A and B, and fig. S2). Second, comparison with the Many Microbial Microarrays Database (*13*) shows that genes in the SIM network are highly significantly coexpressed under various conditions (Fig. 3B), which supports their common function. Highly significant correlations in protein-protein interaction and gene coexpression with the strong class are strengthened by the addition of moderate and weak classes (Fig. 3B) and are also seen in each class individually, with significance increasing from weak to strong (fig. S3).

The largest class of genes identified encodes electron transfer chain (ETC) proteins, which function in oxidative phosphorylation (*14*) (Fig. 1C). These proteins promote mutation by acting upstream of activation of the σ^S general or starvation stress response during starvation, presumably because they sense stress, as follows.

We tested all network proteins for possible activation of the σ^S response (Fig. 1C and tables S1 and S7). We identified 31 bona fide σ^S response–deficient mutants by flow cytometric analysis of the yellow fluorescent protein (YFP) gene expression from the σ^S-regulated promoter P_{yiaG} (*15*) (select ETC mutants, Fig. 4A; the rest of the mutants, fig. S4, A and B, and table S8). These mutants showed normal expression of the cyan fluorescent protein (CFP) gene from a P_{lac} promoter-*cfp* fusion gene (*16*) (Fig. 4B and fig. S4C), and so do not have reduced transcription overall, but instead are deficient in expression of σ^S-controlled genes. The decreases in σ^S-dependent gene expression were not due to delays reaching stationary phase, when σ^S is induced (Fig. 4C and fig. S5). These proteins might promote SIM by activation of the σ^S response, acting upstream of σ^S, sensing and communicating stress.

We examined one representative mutant of each protein machine or pathway of the following groups of the ETC: (i) NuoC, NuoG, NuoH, NuoJ, NuoK, and NuoL subunits of NADH: ubiquinone oxidoreductase I (*17*); (ii) CyoA and CyoD subunits of cytochrome bo′ oxidase (*14*); and (iii) UbiA, UbiD, UbiE, UbiH, and UbiX, which catalyze biosynthesis of ubiquinone (UQ) (*18*). First, we find that the SIM deficiency of representative ETC mutants is suppressed, and SIM is partially or mostly restored, by provision of increased σ^S via *arcB*, *arcA*, or *rssB* mutations (fig. S6), which up-regulate σ^S levels (*19*). Mutation is partially restored (Fig. 4, D to F, and table S9), which supports the hypothesis that the ETC proteins act upstream of ArcB, ArcA, and RssB in increasing σ^S levels (model in Fig. 4L). The incomplete restoration of mutation (Fig. 4,

D to F; fig. S7; and table S9) indicates that, in addition to their role upstream of ArcBA and RssB promoting σ^S accumulation, these proteins also promote SIM via some other route(s).

Second, double-mutant (epistasis) analyses for ETC mutations combined with Δ*rpoS* show that these genes act in a single SIM-activating pathway with σ^S. We analyzed double mutants of Δ*rpoS* with 9 of the 20 ETC mutations (Fig. 4, G to I; fig. S8; and table S10) in standard Lac-mutation assays, as well as in strains with the mutation rate elevated by an I-Sce I endonuclease–generated DSB near *lac* (*1*), for greater sensitivity for additive decreases in mutation rate. The decrease in mutation rate for, e.g., the *nuoC rpoS* double mutant, with or without I-Sce I–induced DSBs, is near that of the *rpoS* single mutant (Fig. 4, G and H; fig. S8; and table S10), which indicates action in a single pathway. Similar results for *cyoD*, *ubiE, fre*, *hemL*, *hscB*, *mdh*, *pgi*, and *sdhD* mutants carrying the *rpoS* mutation (Fig. 4, G to I; fig. S8; and table S10) indicate that *rpoS* is fully epistatic with these ETC mutants, which shows action in the same pathway. All genetic analyses of σ^S-upstream genes are summarized in table S1.

A model for the action of the ETC in starvation-sensing and mutation is shown in Fig. 4L (described in supplementary text S4). In it, during starvation, consumption of specific energy sources malate and succinate, during either an internal autophagy-like recycling process or external cannibalism, acts both upstream of σ^S activation and downstream to promote mutation. Activation of the σ^S response is a critical hub in the network, supported by a large allocation of network genes (Fig. 3A, green), which demonstrates its importance to mutagenesis. Generalization of the roles of the σ^S response (*7*) and supporting network proteins in the chromosomal Tet and Nal assays (Fig. 2 and table S5) indicates that this large network segment (and hub) is generally important to *E. coli* mutagenesis.

Mutants defective for *rpoE*, encoding the σ^E-response transcriptional activator, are sensitive to membrane disruption by SDS with EDTA (*11*). Forty-four mutants are sensitive to SDS-EDTA (fig. S9 and tables S1 and S7). Thirty-three of these also show decreased transcription from the σ^E-dependent *rpoH*P3 promoter (*20*), which confirms their σ^E-response deficiency (Fig. 4J, fig. S9, and table S11). Thus, these genes function upstream of activation of the σ^E response, sensing and transducing the stress signal, which supports the hypothesis that some or all of these may function in SIM via activation of σ^E. The remaining 11 genes might also encode σ^E-response activators during SIM, but merely were not confirmed with this particular σ^E-dependent promoter in these assay conditions (table S11 legend and summarized in tables S1 and S7).

We screened for network mutants defective in the SOS response by sensitivity to ultraviolet (UV) light. Twenty-six show UV sensitivity (table S7 and summary in table S1), which suggests defects in tolerance or repair of DNA damage. Of these, *lexA*, *recA*, and *recB* activate SOS in response to spontaneous DNA breaks (*21*). We identified three mutants not identified previously as SOS upstream (*pgi*, *recC*, and *uvrY*) by their defects in spontaneous SOS induction using a flow cytometric assay of cells that express the green fluorescent protein (GFP) gene from an SOS-dependent promoter (*21*) (Fig. 4K). It is possible that more of the UV-sensitive mutants are SOS-induction defective under starvation-stress SIM conditions, which differ from conditions of the GFP

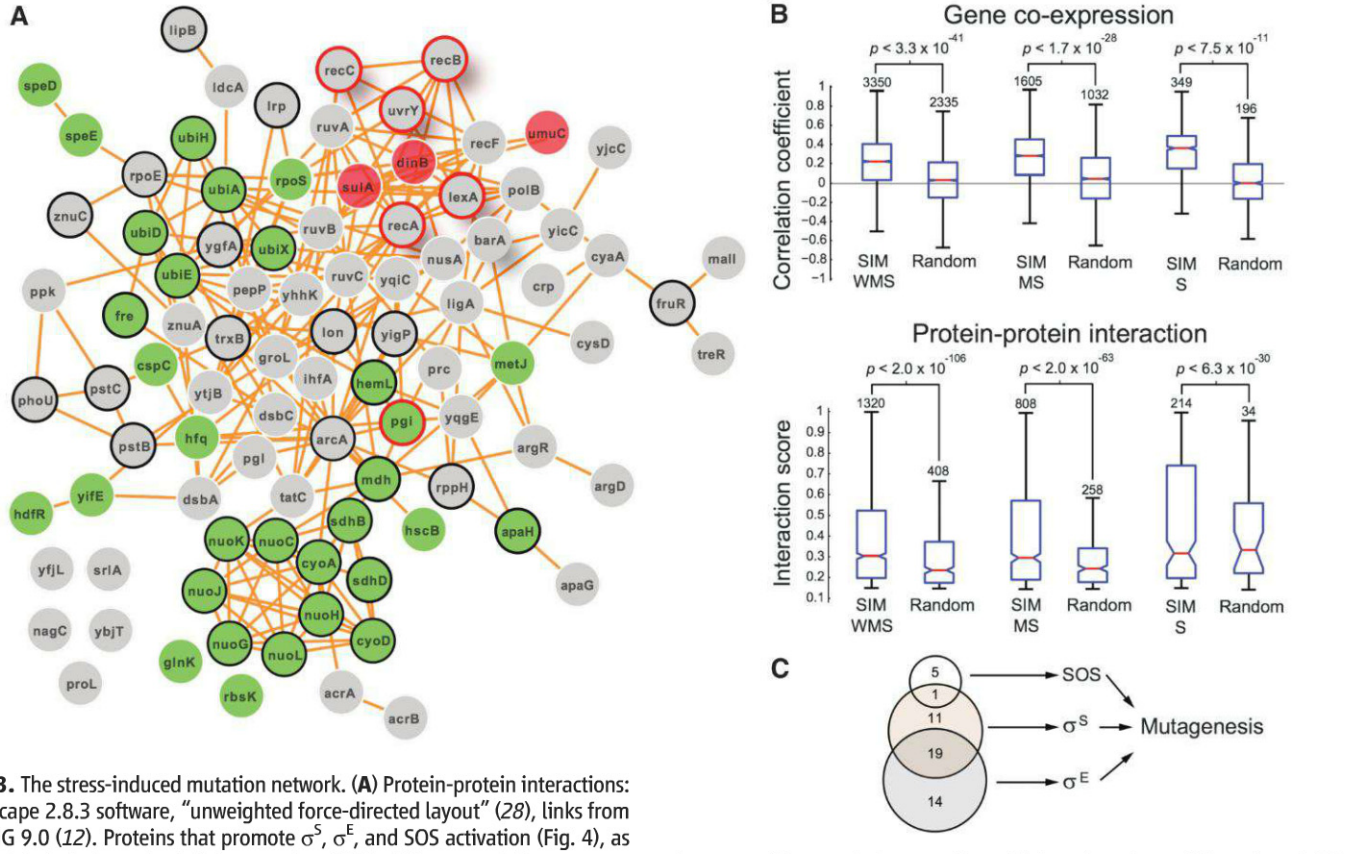

Fig. 3. The stress-induced mutation network. (**A**) Protein-protein interactions: CytoScape 2.8.3 software, "unweighted force-directed layout" (*28*), links from STRING 9.0 (*12*). Proteins that promote σ^S, σ^E, and SOS activation (Fig. 4), as green, black circle, and red circle, constitute 54% of the network. Downstream of SOS (*7*), solid red. (**B**) Coexpression and protein-protein interaction are significantly more clustered than random controls. Gene expression data (*13*). The 93 SIM genes, (92 × 93)/2 = 4278 pairs, show correlation coefficient distributions (top): bars, entire range; boxes 25th and 75th percentile; red bars, mean. Of 4278 pairs, 3350 show positive correlation coefficient; 928 lie below the zero threshold level. High statistical significance for the strong phenotype (S) genes is increased by addition of moderate (M) and weak (W) (table S3). (Bottom) Significantly more protein-protein interactions for SIM than random genes. Of 4278 pairs, 1320 show positive interaction scores; 2958 pairs do not. *P* values: sign test of the probability of failure to reject the null hypothesis "number of positively correlated pairs is the same as in the random control." (**C**) Allocation of network genes upstream of stress responses (data summarized in tables S1 and S7).

assay. All genetic analyses described in the preceding paragraphs are summarized in table S1.

Taken together, our data suggest that as much as 54% of the SIM network proteins (50 out of 93) promote SIM by activating the σ^S, σ^E, and/or SOS stress responses (Fig. 3C and tables S1 and S7). Most of the network is devoted to sensing stress and communicating the signal (Fig. 3A).

The fraction of the network not implicated in action upstream of the three stress responses clusters into two groups of coincident gene expression (fig. S10). One group mirrors expression patterns of the σ^S and SOS groups, whereas the other does not and may represent a separate pathway. Of those genes upstream of stress responses, all are correlated roughly equally for protein-protein interactions and gene coexpression and similarly to all SIM genes (fig. S11).

Our data show that mutagenic DNA break repair (*1*, *2*), previously known to require 16 proteins, is supported by a network of ≥93 proteins, all demonstrated to promote the mutagenesis mechanism. We demonstrated (in the case of the σ^S controllers) and implicated (for SOS and

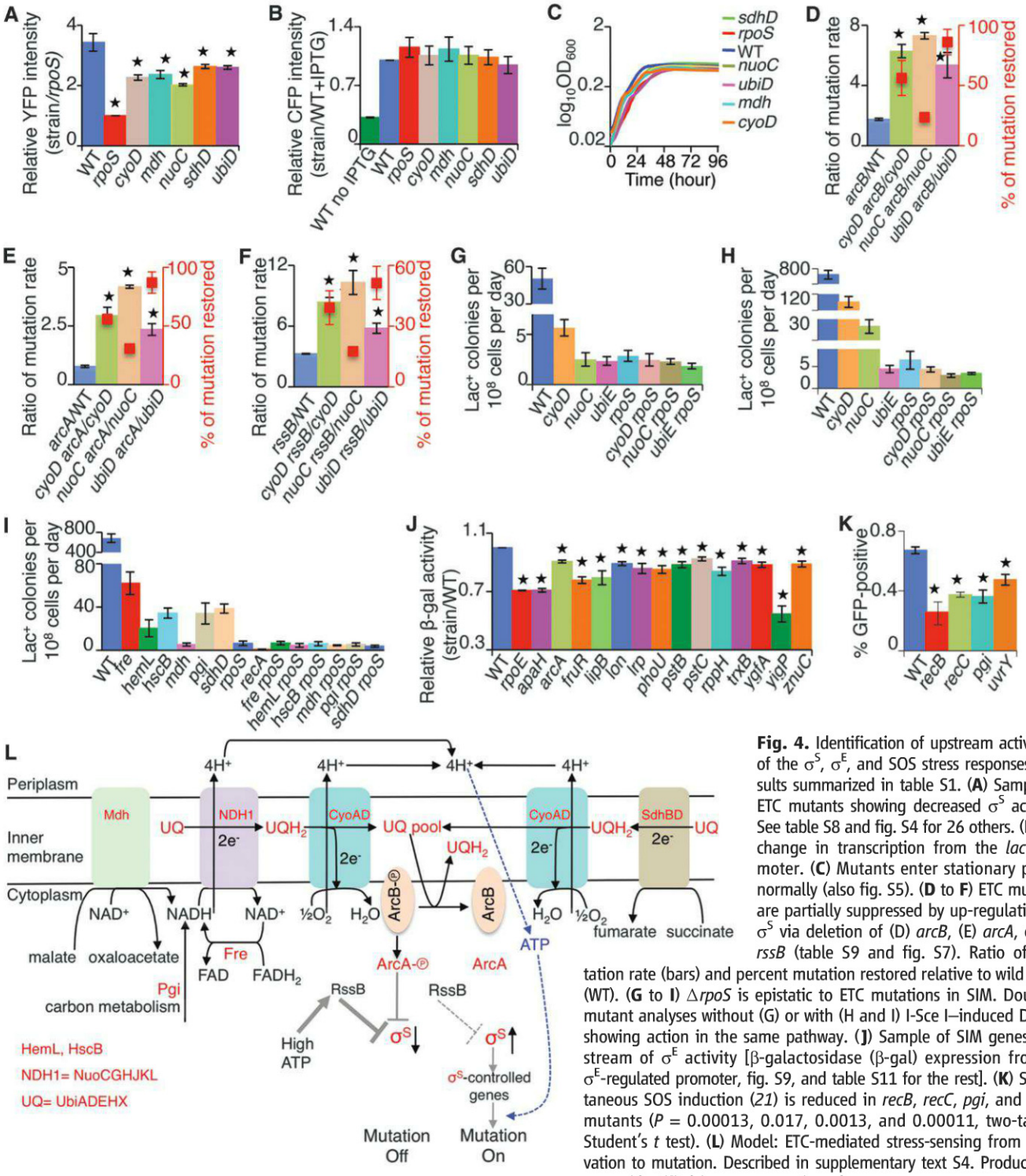

Fig. 4. Identification of upstream activators of the σ^S, σ^E, and SOS stress responses. Results summarized in table S1. (**A**) Sample of ETC mutants showing decreased σ^S activity. See table S8 and fig. S4 for 26 others. (**B**) No change in transcription from the *lac* promoter. (**C**) Mutants enter stationary phase normally (also fig. S5). (**D** to **F**) ETC mutants are partially suppressed by up-regulation of σ^S via deletion of (D) *arcB*, (E) *arcA*, or (F) *rssB* (table S9 and fig. S7). Ratio of mutation rate (bars) and percent mutation restored relative to wild type (WT). (**G** to **I**) Δ*rpoS* is epistatic to ETC mutations in SIM. Double-mutant analyses without (G) or with (H and I) I-Sce I–induced DSBs, showing action in the same pathway. (**J**) Sample of SIM genes upstream of σ^E activity [β-galactosidase (β-gal) expression from a σ^E-regulated promoter, fig. S9, and table S11 for the rest]. (**K**) Spontaneous SOS induction (*21*) is reduced in *recB*, *recC*, *pgi*, and *uvrY* mutants (P = 0.00013, 0.017, 0.0013, and 0.00011, two-tailed Student's t test). (**L**) Model: ETC-mediated stress-sensing from starvation to mutation. Described in supplementary text S4. Products of genes identified in screens are in red.

in parasites grown in Fy-deficient cells were significantly reduced by a factor of almost three (Fig. 4C and D). These data suggest that infected cells internalize PF4 and that the Fy molecule largely mediates the phenomenon.

Our data show that the intraerythrocytic killing of falciparum parasites by platelets requires platelet-iRBC contact, release of PF4, and binding of PF4 to the Fy receptor. Although platelets release PF4 into the medium of cultured *P. falciparum*, the levels measured in our experiments were insufficient to kill the parasites. Instead, our data suggest that after binding to iRBCs, platelets release PF4, resulting in locally high concentrations. The released PF4 then binds to the surface of the infected cell. PF4 binding is greatest in red cells with mature parasites, and these parasites are more likely to be TUNEL positive, i.e., dead. Not all PF4-bound cells were colabeled by TUNEL, suggesting that there may be a delay between the binding of PF4, the death of parasites, and the subsequent fragmentation. Others have reported that the bactericidal activity of PF4 and related platelet antimicrobial proteins is exerted via disruption of cell metabolism and membrane potential, although the exact mechanisms remain unclear (*25*, *26*). A similar cytocidal or cytostatic mechanism may also operate on the metabolically active maturing parasite. Interestingly, depletion of PF4 rescues otherwise susceptible mice in the *P. berghei*–induced experimental cerebral malaria model (ECM) (*14*). However, ECM is mediated through an unrelated pathology and is not associated with parasite death. Erythrocyte Fy is essential for the killing of *P. falciparum* by platelets and PF4. Our data show that Fy binds PF4. There is more binding in Fy-positive than Fy-negative cells. There is also more PF4 present internally in Fy-positive erythrocytes compared with Fy-deficient cells. We therefore deduce that PF4 binding to Fy mediates both the increased concentration of PF4 on the surface of the cell and the observed intraerythrocytic accumulation of the protein through transport from the surface of the cell, although we have yet to demonstrate this formally. A genetic lack of Fy renders an infected cell impervious to killing by both PF4 and platelets and is associated with less surface binding and internalized PF4. In normally resistant mice, platelet deficiency leads to a more severe outcome (*1*, *2*), but Fy deficiency has no effect (*27*), possibly indicating a different effector pathway in the mouse.

The vast majority of individuals living in Western and Central equatorial Africa are Duffy-antigen negative (*22*). An obvious implication of our findings is the potential lack of platelet-mediated protection against malaria in these individuals and the possibility that this has an impact on disease severity and outcome. Although the available epidemiological and clinical data are insufficient to directly compare disease severity and outcome in humans with different Duffy alleles (*28*–*30*), *P. falciparum* infections are most common in equatorial Africa and result in the highest global rates of death (*31*, *32*).

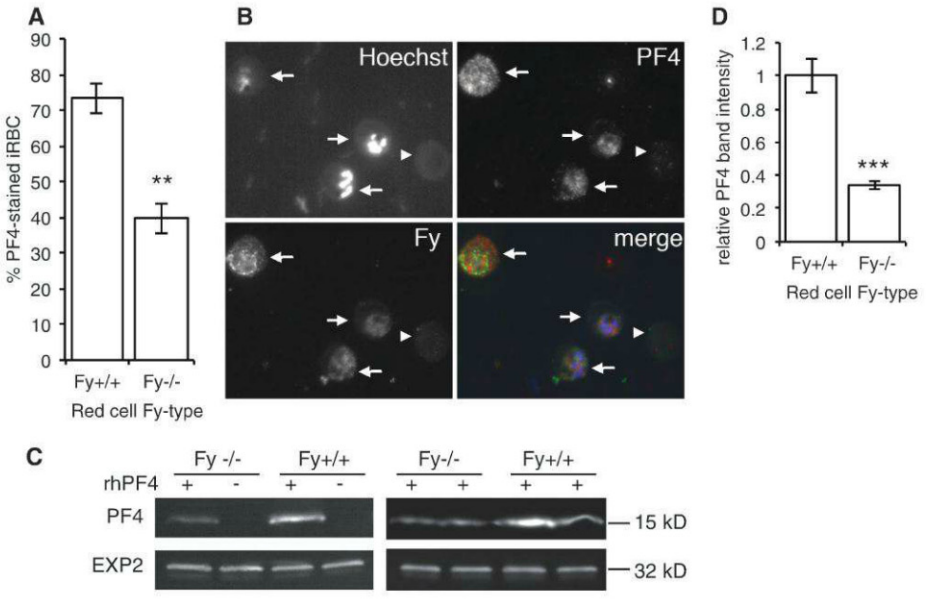

Fig. 4. Requirement of Duffy antigen for PF4 binding and internalization by iRBC. (**A**) Percentage of anti-PF4 stained *P. falciparum* 3D7 iRBC grown in Fy-expressing ($Fy^{+/+}$) or Fy-deficient ($Fy^{-/-}$) cells after treatment with human platelets for 24 hours. Error bars represent mean proportions (±SEM) determined in three independent experiments. The blood from three different Fy-negative donors was tested. $^{**}P = 0.002$ compared with $Fy^{+/+}$ cells. (**B**) Immunofluorescent assay images of PF4-treated iRBC stained with Hoechst (blue), antibody to PF4 (red), and antibody to Fy (green). rhPF4 was added to synchronized ring-stage parasites for 24 hours. Arrowheads indicate uninfected cells, and arrows indicate iRBC (PF4 and Fy costained). (**C**) Immunoblot analysis of PF4 in rhPF4-treated *P. falciparum* 3D7 parasites. Immunoblots (using antibodies to PF4 or EXP2) of saponin-purified trophozoites, treated before purification with or without rhPF4 (0.5 μM) for 2 hours. Parasites were grown in Fy-deficient ($Fy^{-/-}$) or sufficient ($Fy^{+/+}$) red cells. (**D**) Quantification of the PF4 immunoblot analysis. Error bars represent the mean pixel intensity (±SEM) of the PF4 immunoreactive bands relative to EXP2 [shown in (C)]. $^{***}P < 0.001$ compared with $Fy^{+/+}$ cells.

References and Notes

1. B. J. McMorran *et al.*, *Science* **323**, 797 (2009).
2. B. Polack, F. Delolme, F. Peyron, *Haemostasis* **27**, 278 (1997).
3. F. Peyron, B. Polack, D. Lamotte, L. Kolodie, P. Ambroise-Thomas, *Parasitology* **99**, 317 (1989).
4. A. D. Adedapo, C. O. Falade, R. T. Kotila, G. O. Ademowo, *J. Vector Borne Dis.* **44**, 266 (2007).
5. L. M. Erhart *et al.*, *Am. J. Trop. Med. Hyg.* **70**, 8 (2004).
6. P. Gérardin *et al.*, *Am. J. Trop. Med. Hyg.* **66**, 686 (2002).
7. R. D. Horstmann, M. Dietrich, U. Bienzle, H. Rasche, *Blut* **42**, 157 (1981).
8. S. Ladhani, B. Lowe, A. O. Cole, K. Kowuondo, C. R. Newton, *Br. J. Haematol.* **119**, 839 (2002).
9. K. Chotivanich *et al.*, *J. Infect. Dis.* **189**, 1052 (2004).
10. A. Pain *et al.*, *Proc. Natl. Acad. Sci. U.S.A.* **98**, 1805 (2001).
11. L. H. Miller, S. J. Mason, D. F. Clyde, M. H. McGinniss, *N. Engl. J. Med.* **295**, 302 (1976).
12. J. E. Peterson *et al.*, *Am. J. Hematol.* **85**, 487 (2010).
13. M. B. Zucker, I. R. Katz, *Proc. Soc. Exp. Biol. Med.* **198**, 693 (1991).
14. K. Srivastava *et al.*, *Cell Host Microbe* **4**, 179 (2008).
15. C. F. Ockenhouse, N. N. Tandon, C. Magowan, G. A. Jamieson, J. D. Chulay, *Science* **243**, 1469 (1989).
16. Y. Q. Tang, M. R. Yeaman, M. E. Selsted, *Infect. Immun.* **70**, 6524 (2002).
17. M. R. Yeaman *et al.*, *Biochim. Biophys. Acta* **1768**, 609 (2007).
18. A. Chaudhuri *et al.*, *J. Biol. Chem.* **269**, 7835 (1994).
19. M. C. Szabo, K. S. Soo, A. Zlotnik, T. J. Schall, *J. Biol. Chem.* **270**, 25348 (1995).
20. Z. H. Lu *et al.*, *J. Biol. Chem.* **270**, 26239 (1995).
21. M. Kashiwazaki *et al.*, *Int. Immunol.* **15**, 1219 (2003).
22. R. E. Howes *et al.*, *Nat Commun* **2**, 266 (2011).
23. S. Lauer *et al.*, *EMBO J.* **19**, 3556 (2000).
24. B. U. Samuel *et al.*, *J. Biol. Chem.* **276**, 29319 (2001).
25. Y. Q. Xiong, A. S. Bayer, M. R. Yeaman, *J. Infect. Dis.* **185**, 348 (2002).
26. M. R. Yeaman, A. S. Bayer, S. P. Koo, W. Foss, P. M. Sullam, *J. Clin. Invest.* **101**, 178 (1998).
27. N. Akimitsu *et al.*, *Parasitol. Res.* **93**, 499 (2004).
28. S. J. Allen, A. O'Donnell, N. D. Alexander, J. B. Clegg, *QJM* **89**, 779 (1996).
29. K. Marsh *et al.*, *N. Engl. J. Med.* **332**, 1399 (1995).
30. R. Tripathy *et al.*, *Pediatrics* **120**, e454 (2007).
31. S. I. Hay *et al.*, *PLoS Med.* **6**, e1000048 (2009).
32. World Health Organization, *World Malaria Report 2011* (WHO, Geneva, 2011).

Acknowledgments: We thank the Australian Red Cross Blood Services in Hobart and Brisbane for providing red blood cells and antibodies, the platelet donors, and C. Flowers and R. McWhirter for phlebotomy. We also acknowledge funding support from the National Health and Medical Research Council of Australia (grants 605524 and 490037), the Australian Cancer Research Foundation, the National Collaborative Research Infrastructure Strategy of Australia, The Bill and Melinda Gates Foundation Grand Challenges Explorations, The Howard Hughes Medical Institute, Australian Research Council (grant DP120100061 and Future Fellowship to J.G.B.), and the Victorian State Government Operational Infrastructure Support Scheme. Ethics approval for the platelet donations was received from the Human Research Ethics Committee (Tasmania) Network (H0009004). Data are deposited in the Dryad Repository: http://dx.doi.org/10.5061/dryad.8sb5h

Supplementary Materials

www.sciencemag.org/cgi/content/full/338/6112/1348/DC1
Materials and Methods
Figs. S1 to S9
References (*33*–*36*)

15 August 2012; accepted 25 October 2012
10.1126/science.1228892

Developmental Progression to Infectivity in *Trypanosoma brucei* Triggered by an RNA-Binding Protein

Nikolay G. Kolev,[1] Kiantra Ramey-Butler,[2] George A. M. Cross,[3] Elisabetta Ullu,[2,4]* Christian Tschudi[1]*

Unraveling the intricate interactions between *Trypanosoma brucei*, the protozoan parasite causing African trypanosomiasis, and the tsetse (*Glossina*) vector remains a challenge. Metacyclic trypanosomes, which inhabit the tsetse salivary glands, transmit the disease and are produced through a complex differentiation and unknown program. By overexpressing a single RNA-binding protein, *Tb*RBP6, in cultured noninfectious trypanosomes, we recapitulated the developmental stages that have been observed in tsetse, including the generation of infective metacyclic forms expressing the variant surface glycoprotein. Thus, events leading to acquisition of infectivity in the insect vector are now accessible to laboratory investigation, providing an opening for new intervention strategies.

Reproducing the life cycle of infectious organisms in vitro offers unique opportunities for studying pathogenesis and for developing intervention strategies. The protozoan parasite *Trypanosoma brucei* is the causative agent of sleeping sickness in humans, and the related disease "nagana" in livestock, which remain a public health challenge in sub-Saharan Africa. Human African trypanosomiasis is fatal if left untreated, and the livestock disease profoundly impacts on the economic development of affected countries. The blood-feeding tsetse fly (*Glossina* subspecies) vector transmits the disease, and its range determines the distribution of the disease. Bloodstream forms (BSFs) are taken up with the bloodmeal, and in the fly midgut stumpy forms (SFs) differentiate into procyclic forms that are no longer infectious to mammals (*1*). Several morphological and metabolic changes take place during this developmental stage, including repositioning of the kinetoplast (the mitochondrial genome) midway between the posterior pole and the nucleus, elaboration of mitochondrial cisternae, silencing of variable surface glycoprotein (VSG) expression, VSG coat loss, and expression of procyclin on the cell surface (*1*). Procyclics then move from the midgut to the proventriculus, the terminal portion of the foregut, where they elongate and become epimastigotes, with the kinetoplast positioned next to the nucleus in the anterior position. Epimastigotes undergo asymmetric division to produce a long epimastigote, which probably degenerates, and a short epimastigote, which instead goes on to colonize the salivary glands where it attaches to the epithelium. Attached epimastigotes divide and ultimately differentiate into mature nondividing metacyclics that detach from the epithelium and are found in the lumen of the salivary glands. During metacylogenesis, the mitochondrion regresses to the single tubule characteristic of BSFs, indicating that mitochondrial function is inhibited; the VSG coat, synthesized from VSG genes in metacyclic-type transcription units (metacyclic expression sites), reappears; endocytosis increases; and the cells reacquire infectivity to mammals (*1*). Although the intricate nature of trypanosome development in the fly has been recognized for more than a century (*2*), the molecular mechanisms are still mysterious, due in part to experimental challenges of studying parasites in the fly.

RNA-binding proteins (RBPs) are important regulators of trypanosome gene expression as mediators of posttranscriptional control (*3*). A survey of the *T. brucei* transcriptome in infected tsetse tissues by high-throughput RNA sequencing (RNA-Seq) revealed that the mRNA abundance for *RBP6* (Tb927.3.2930, containing a single RNA-recognition motif) is increased by a factor of 13 (relative to midgut-derived procyclics) in trypanosomes from the proventriculus (fig. S1). Experimentally induced RBP6 overexpression in cultured noninfectious procyclics resulted in the appearance of developmental stages that have been previously described in tsetse; namely, long and short epimastigotes and metacyclic trypomastigotes (Fig. 1A and figs. S2 to S4). The prevalence of metacyclics depended on RBP6 expression levels (fig. S5), and we also observed asymmetrically dividing long epimastigotes (fig. S6).

Metacyclics generated in vitro featured a kinetoplast at the cell's posterior pole (Fig. 1B and fig. S4), an undulating membrane (Fig. 1C), and BSF-like motility and, like BSFs, they did not adhere to glass. Metacyclic-like cells also displayed a range of mitochondrial architectures from multibranched to tubular (Fig. 1C and fig. S7), an indication of mitochondrial regression (*4*), which is distinctive of BSFs. Relative to procyclics and epimastigotes, metacyclics generated in vitro had higher levels of calflagin (Fig. 1B and fig. S8), mirroring results from salivary-gland metacyclics (*5*). Compared to procyclics and epimastigotes, metacyclics also showed higher internalization of the fluid-phase marker dextran 10,000 (fig. S9)—an indication of active endocytosis, which is a characteristic feature of BSFs (*4*). Up to 20% of the metacyclic-like cells could be purified by DEAE-cellulose chromatography, which combined with the gradation in mitochondrial regression (fig. S7) and calflagin expression (fig. S8), suggested that the cultures contained metacyclics at different stages of differentiation.

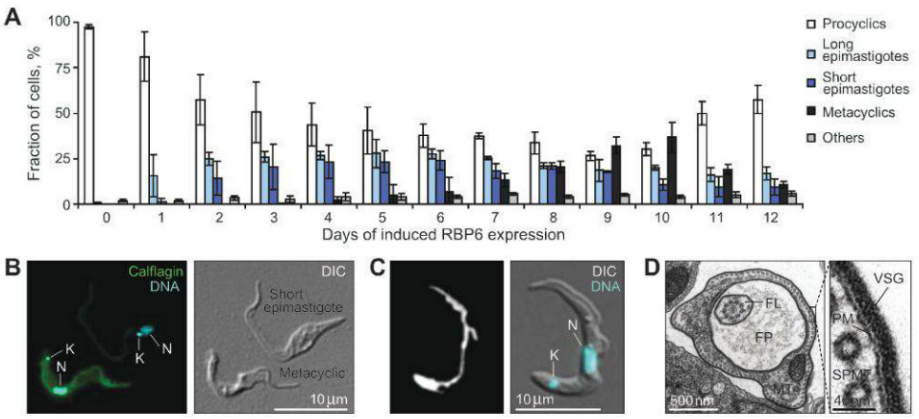

Fig. 1. *T. brucei* RBP6 induces metacyclogenesis. (**A**) Timeline for the appearance of different cell types upon induction of RBP6 expression (three independent experiments; error bars, SD). (**B**) Immunofluorescent detection of calflagin (K, kinetoplast; N, nucleus) in a culture induced to express RBP6 for 10 days DIC, differential interference contrast. (**C**) Live-cell imaging of the mitochondrion in a metacyclic cell with Mitotracker Deep Red FM. (**D**) Transmission electron microscopy confirms the presence of a variant surface glycoprotein (VSG) coat. Shown is a transverse section across the flagellar pocket (FP), which, like bloodstream form trypomastigotes, contains fibrous material (MT, mitochondrion; FL, flagellum; PM, plasma membrane; SPMT, subpellicular microtubules).

[1]Department of Epidemiology of Microbial Diseases, Yale School of Public Health, New Haven, CT 06536, USA. [2]Department of Internal Medicine, Yale School of Medicine, New Haven, CT 06536, USA. [3]Laboratory of Molecular Parasitology, The Rockefeller University, New York, NY 10065, USA. [4]Department of Cell Biology, Yale School of Medicine, New Haven, CT 06536, USA.

*To whom correspondence should be sent. E-mail: elisabetta.ullu@yale.edu (E.U.); christian.tschudi@yale.edu (C.T.)

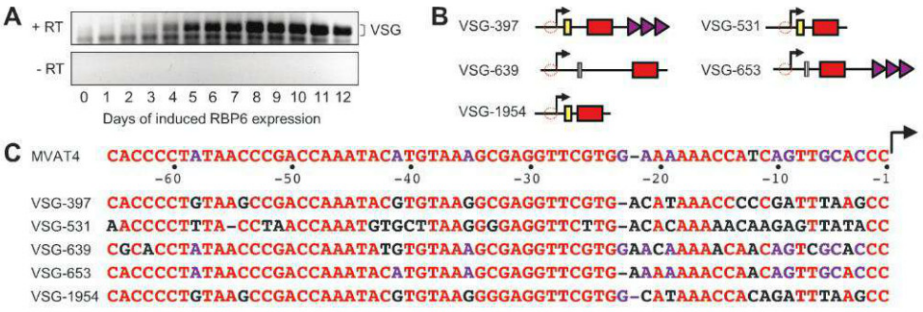

Fig. 2. *T. brucei* RBP6 induces the expression of monocistronic VSG genes. (**A**) RT-PCR detection of expressed VSG genes in cultures containing metacyclic cells. Ethidium bromide–stained agarose gel for samples processed with (+RT) or without (–RT) reverse transcriptase are shown. The identity of amplified products was confirmed by cloning and sequencing. (**B**) Diagrams of the genomic context of the VSG genes with metacyclic-type Pol I promoters. Red rectangles, VSG genes; purple triangles, subtelomeric or telomeric repeats; yellow rectangles, ribosomal mobile element (RIME) sequences; gray rectangles, 70–base pair repeats; bent arrows, transcription start sites; red circles, Pol I promoters. (**C**) Alignment of the metacyclic Pol I promoters of expressed VSG genes to a previously characterized metacyclic promoter sequence of the MVAT4 gene (*6*). Bent arrow indicates the position of the putative transcription start site. Red and purple indicate ≥60% and <60% sequence conservation, respectively.

The hallmark of metacyclogenesis is the reacquisition of a VSG coat (*1*, *4*). We detected the VSG coat by transmission electron microscopy (Fig. 1D) and the mRNA for several VSGs by reverse transcriptase–polymerase chain reaction (RT-PCR) and RNA-Seq (Fig. 2A and table S1). The VSG transcripts with highest expression were derived from monocistronic expression sites (Fig. 2B and fig. S10) with metacyclic-type RNA polymerase I (Pol I) VSG promoters (Fig. 2C) (*6*), underscoring the identity of the metacyclics generated in vitro. Cultures containing these cells produced *T. brucei* infections in BALB/c (table S2) and c57BL/6 mice (table S3), and trypanosomes were detected in the bloodstream as early as day 3 after inoculation. Bloodstream stumpy forms, which initiate colonization of the fly midgut (*4*), were also present (fig. S11). In contrast, no trypanosomes were detected in mice inoculated with uninduced RBP6 cells grown in parallel or in tet-induced parental Lister 427 (29-13) cells.

Our results underscore the critical role for RBPs in the regulation of gene expression in trypanosomes and provide a robust in vitro system for recapitulating trypanosome developmental stages in the insect vector, including the production of infectious metacyclics.

References and Notes

1. R. Sharma *et al.*, *Trends Parasitol.* **25**, 517 (2009).
2. D. Bruce, A. E. Hamerton, H. R. Bateman, F. P. Mackie, *Proc. R. Soc. Lond. B* **81**, 405 (1909).
3. M. Wurst *et al.*, *Mol. Microbiol.* **83**, 1048 (2012).
4. K. Vickerman, *Br. Med. Bull.* **41**, 105 (1985).
5. B. Rotureau, I. Subota, J. Buisson, P. Bastin, *Development* **139**, 1842 (2012).
6. M. L. Ginger *et al.*, *Eukaryot. Cell* **1**, 1000 (2002).

Acknowledgments: We thank A. Savage and S. Aksoy for assistance with the infectivity assays, J. Bangs for providing the immunofluorescence protocol and advice, D. Engman for the antibody against calflagin, and M. Chaudhuri for the antibody against alternative oxidase. Supported by grants AI028798 (E.U.), AI043594 (C.T.), AI021729 (G.A.M.C.), and AI076879 (S. Aksoy) from the National Institute of Allergy and Infectious Diseases (NIAID) of the U.S. National Institutes of Health (NIH). The content is solely the responsibility of the authors and does not necessarily represent the official views of the NIAID or the NIH. The sequence data from this study have been submitted to the National Center for Biotechnology Information Sequence Read Archive under accession nos. SRP002243 and SRA059559.

Supplementary Materials

www.sciencemag.org/cgi/content/full/338/6112/1352/DC1
Materials and Methods
Figs. S1 to S11
Tables S1 to S3
References (*7*–*10*)

3 September 2012; accepted 24 October 2012
10.1126/science.1229641

Acute Inflammation Initiates the Regenerative Response in the Adult Zebrafish Brain

Nikos Kyritsis,[1] Caghan Kizil,[1] Sara Zocher,[1] Volker Kroehne,[1] Jan Kaslin,[1,2] Dorian Freudenreich,[1] Anne Iltzsche,[1] Michael Brand[1]*

The zebrafish regenerates its brain after injury and hence is a useful model organism to study the mechanisms enabling regenerative neurogenesis, which is poorly manifested in mammals. Yet the signaling mechanisms initiating such a regenerative response in fish are unknown. Using cerebroventricular microinjection of immunogenic particles and immunosuppression assays, we showed that inflammation is required and sufficient for enhancing the proliferation of neural progenitors and subsequent neurogenesis by activating injury-induced molecular programs that can be observed after traumatic brain injury. We also identified cysteinyl leukotriene signaling as an essential component of inflammation in the regenerative process of the adult zebrafish brain. Thus, our results demonstrate that in zebrafish, in contrast to mammals, inflammation is a positive regulator of neuronal regeneration in the central nervous system.

After a traumatic brain injury in the telencephalon, zebrafish can efficiently restore the tissue architecture and replace the lost neurons upon neurogenic activity of the ventricularly located radial glial cells (*1*–*4*). However, the signaling mechanisms involved in the activation of those stem cell niches after injury (reactive proliferation) and the production of new neurons (regenerative neurogenesis) from neurogenic progenitors are largely unknown.

Immune cell activation is among the first responses detected in the tissue after a severe central nervous system injury in both mammals and zebrafish (*5*–*9*). Various types of immune cells from the bloodstream (leukocytes) or resident in the brain tissue (microglia) accumulate in the injured tissue, secrete cytokines and chemokines to modulate the environment, and are responsible for the removal of cell debris and accumulated metabolites, as has been shown in mammals (*10*). Acute neuroinflammation in mammals has generally been considered to have a negative effect on neurogenesis and regeneration by promoting the formation of a glial scar and hampering the proliferation of the precursor cells and the migration, survival, maturation, and integration of the newborn neurons into the existing circuitry (*11*–*15*). In contrast, the inflammatory

[1]Deutsche Forshungsgemeinschaft–Center for Regenerative Therapies Dresden (CRTD)–Cluster of Excellence, Technische Universität Dresden, Fetscherstraße 105, 01307 Dresden, Germany. [2]Australian Regenerative Medicine Institute (ARMI), Monash University, Wellington Road, Clayton, Victoria 3800, Australia.

*To whom correspondence should be addressed. E-mail: michael.brand@biotec.tu-dresden.de

response observed at the lesion site after injury in the zebrafish brain does not hamper the regeneration of the neurons (*3*). Thus, we hypothesized that an acute inflammatory reaction in fish might provide a context in which the molecular programs for regenerative neurogenesis could be initiated.

First, we characterized the inflammatory response upon traumatic brain injury, which leads to the activation of microglia and leukocytes that can be detected with L-plastin immunostaining (Fig. 1A) (*16*). After the brain lesion, the number of microglia and leukocytes in the injured telencephalic hemisphere increased significantly, and those elevated levels persisted for several days (Fig. 1, A to C). Based on the morphological transformation of the L-plastin–positive cells, as well as the elevated expression levels of the proinflammatory cytokines interleukin-8 (IL-8), IL-1β, and tumor necrosis factor–α, we concluded that an active inflammatory response takes place rapidly after traumatic brain injury (fig. S1). These results suggest that lesion in the adult zebrafish brain induces a bona fide inflammatory response characterized by proliferation (*3*) and a change of microglia morphology, which resolves within a few days without indications of chronic inflammation.

Because traumatic brain injury induces active inflammation yet leads to efficient neural regeneration in zebrafish, we hypothesized that the inflammatory response might directly activate radial glial cells. In order to test this hypothesis, we sought to experimentally dissect the traumatic brain injury from the inflammatory response by injecting immunogenic zymosan A BioParticles (*15*) conjugated with fluorophores, using cerebroventricular microinjection (fig. S2, A to D) (*17*). In this way, the processes of the

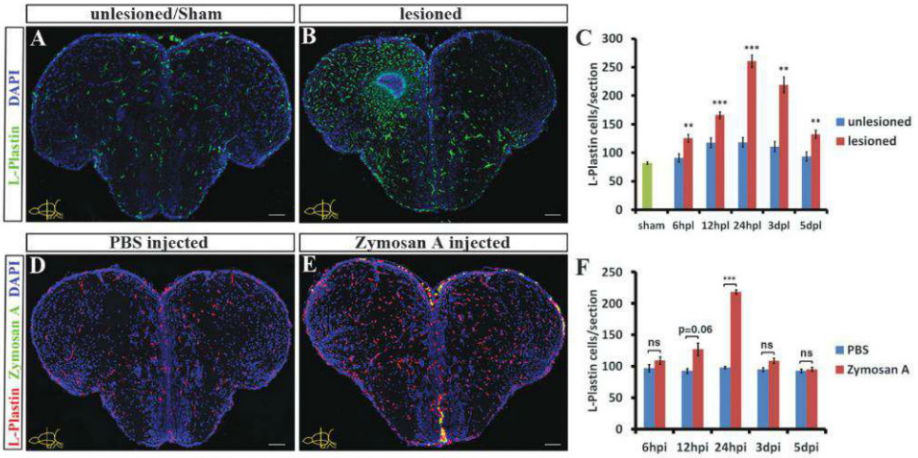

Fig. 1. Leukocytes infiltrate the brain rapidly after traumatic injury and sterile infection. (**A** and **B**) Immunohistochemistry (IHC) for L-plastin in unlesioned and lesioned telencephalons. (**C**) Quantification of the L-plastin cells in sham-operated, lesioned, and unlesioned telencephalic hemispheres in time course. (**D** and **E**) IHC for L-plastin in phosphate-buffered saline (PBS)– and zymosan A–injected brains. (**F**) Quantification of the L-plastin cells in PBS- and zymosan A–injected brains in time course. ns, not significant; $^{**}P < 0.01$, $^{***}P < 0.001$; scale bars, 100 μm; $n = 3$ brains for every experiment.

Fig. 2. Inflammation is sufficient and necessary for the initiation of reactive proliferation and reactive neurogenesis. (**A** and **B**) IHC for S100β and PCNA in PBS- or zymosan A–injected zebrafish brains. (**C**) Quantification of S100β/PCNA-positive cells in PBS and zymosan A–injected brains. (**D** and **E**) IHC for HuC/D and BrdU. (**F**) Quantification of the HuC/D/BrdU double-positive cells between PBS and zymosan A injections. (**G** and **H**) IHC for S100β and PCNA. (**I**) Quantification of proliferating radial glia in both lesioned and unlesioned hemispheres between Dex- and vehicle-treated animals. (**J** and **K**) IHC for HuC/D and BrdU. (**L**) Quantification of the newborn neurons (HuC/D/BrdU double-positive cells). $^{*}P < 0.05$, $^{**}P < 0.01$, $^{***}P < 0.001$; scale bars, 100 μm; $n = 4$ brains for every experiment.

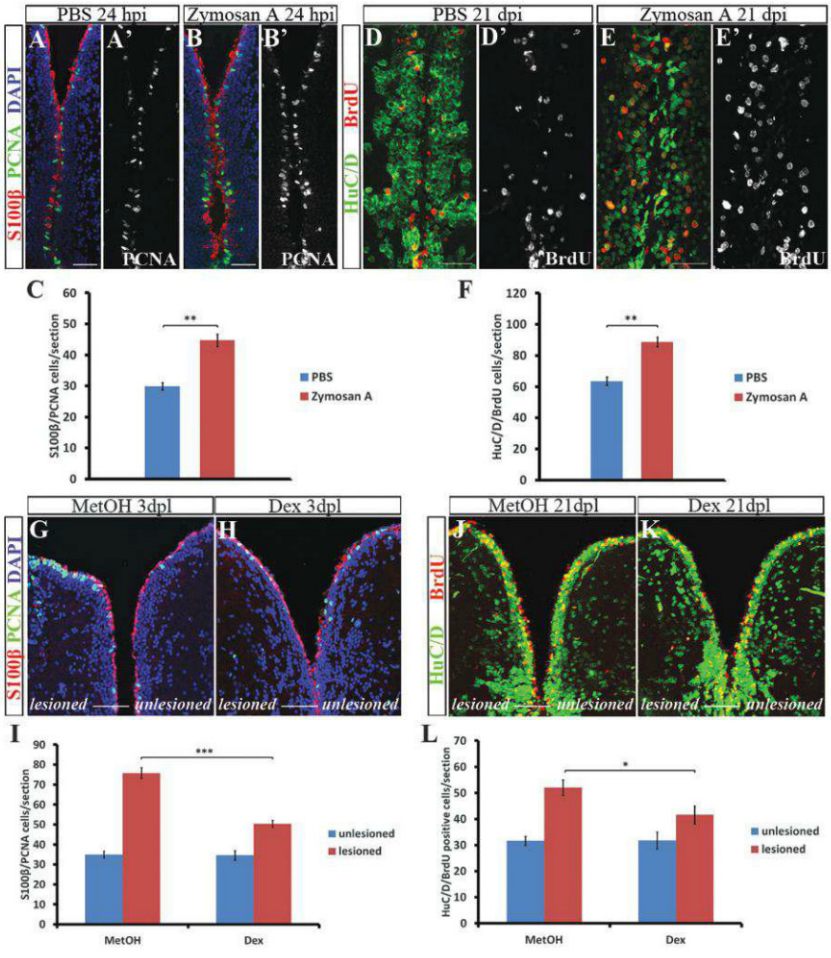

radial glial cells were not injured, and only sterile inflammation was induced. Similar to the response after traumatic brain injury, zymosan A injections led to a significant increase in the number of L-plastin–positive cells at 24 hours after injection, and the response was resolved 2 days later (Fig. 1, D to F). We also found that leukocytes engulf the yeast particles and undergo extensive shape changes from ramified to amoeboid morphology, and the levels of proinflammatory cytokines increase similarly as in the lesioned brains (fig. S2, E to L). These results indicate that zymosan A–induced sterile inflammation can mimic aspects of the inflammatory conditions after traumatic brain injury, whereas at the same time there is no effect on cell viability, as shown by TUNEL (terminal deoxynucleotidyl transferase–mediated deoxyuridine triphosphate nick-end labeling) and hematoxylin and eosin staining (figs. S3 and S4).

After traumatic brain injury, radial glial cells are activated, increase their proliferation levels significantly, and produce neurons to compensate for the neuronal loss (*3*, *4*). To test whether induced inflammation would lead to similar outcomes without a lesion, we performed proliferating cell nuclear antigen (PCNA) immunostaining (marking proliferative cells) and S100β immunostaining (marking radial glial cells) on zymosan A–injected brains 1 day after the injection (Fig. 2, A and B). When we quantified the double-positive cells, we observed a significant increase of 49.7 ± 12.0% in the zymosan A–injected fish when compared to vehicle-injected fish (Fig. 2C), indicating that acute inflammation can enhance progenitor cell proliferation in the adult zebrafish brain. To test whether the increase in the proliferation of the progenitors leads to elevated levels of neurogenesis, after injecting zymosan A into the brain ventricle, coupled with bromodeoxyuridine (BrdU) pulses, we found that the number of newborn neurons was increased significantly by 39.7 ± 1.3% as compared to vehicle-injected fish (Fig. 2, D to F).We performed similar experiments in the cerebellum, where the same effect of increased progenitor proliferation and neurogenesis was observed (fig. S5).

Our data suggest that the inflammatory response might be one of the molecular cues that imminently precede the activation of radial glial cells. Thus, to analyze whether the inflammatory response was necessary for the initiation of the reactive proliferation, we immunosuppressed the

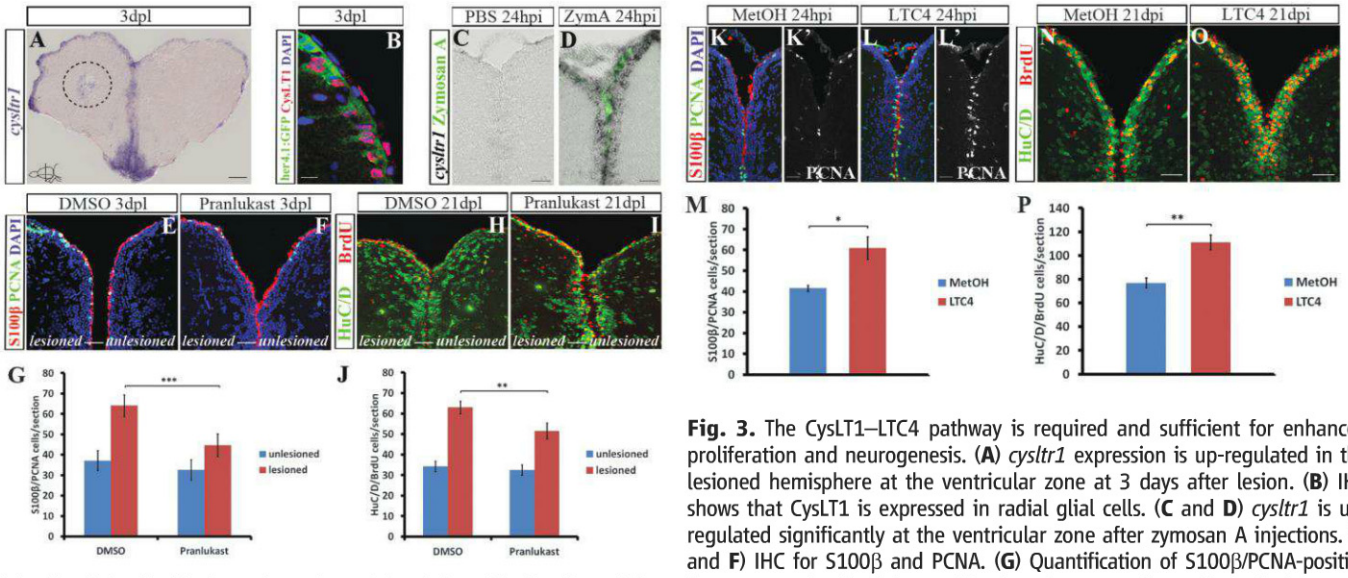

Fig. 3. The CysLT1–LTC4 pathway is required and sufficient for enhanced proliferation and neurogenesis. (**A**) *cysltr1* expression is up-regulated in the lesioned hemisphere at the ventricular zone at 3 days after lesion. (**B**) IHC shows that CysLT1 is expressed in radial glial cells. (**C** and **D**) *cysltr1* is up-regulated significantly at the ventricular zone after zymosan A injections. (**E** and **F**) IHC for S100β and PCNA. (**G**) Quantification of S100β/PCNA-positive cells in dimethyl sulfoxide (DMSO)– and Pranlukast-injected brains. (**H** and **I**) IHC for HuC/D and BrdU. (**J**) Quantification of HuC/D/BrdU-positive cells in DMSO- and Pranlukast-injected brains. (**K** and **L**) IHC for S100β and PCNA in MetOH- and LTC4-injected brains (**M**) LTC4 injections initiate the reactive proliferation response. (**N** and **O**) IHC for HuC/D and BrdU. (**P**) LTC4 injections induce reactive neurogenesis. *$P < 0.05$, **$P < 0.01$, ***$P < 0.001$; scale bar in (A), 200 μm; scale bar in (B), 10 μm; scale bars in (C), (D), (K), (L), (N), and (O), 100 μm; dashed circle in (A) indicates the lesion site; $n = 3$ brains for every experiment.

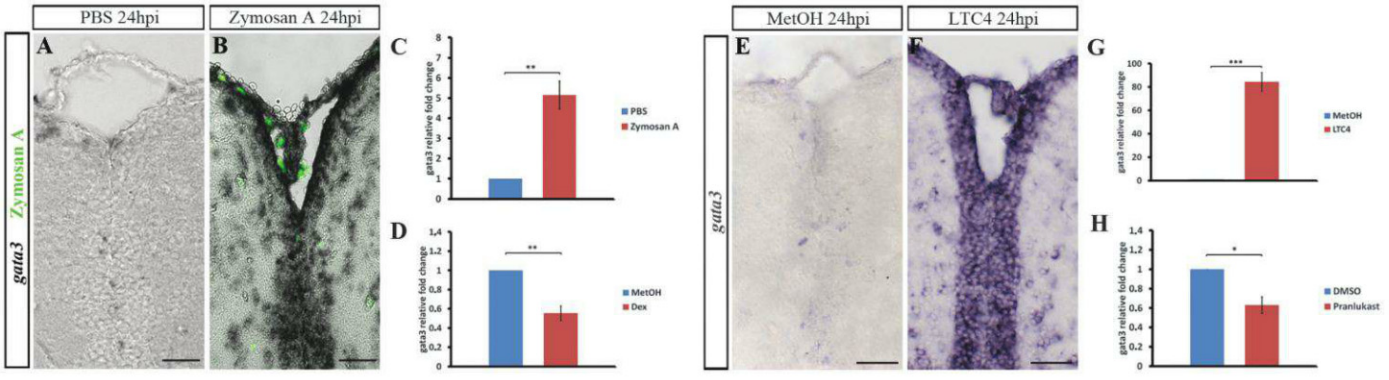

Fig. 4. Inflammation is sufficient and necessary for inducing regeneration-specific molecular programs. (**A** and **B**) *gata3* is induced at the ventricular zone 24 hours after zymosan A injections in comparison to vehicle injections. (**C**) Relative fold change of *gata3* expression between vehicle and zymosan A injections. (**D**) Relative expression levels of *gata3* at 3 days after lesion in immunosuppressed and control animals. (**E** and **F**) *gata3* is induced significantly in the ventricular region 24 hours after LTC4 injection, in comparison to vehicle-injected brains. (**G**) Relative expression levels of *gata3* in vehicle- and LTC4-injected brains. (**H**) Quantification graph indicates that *gata3* expression reduces significantly after Pranlukast injection, in comparison to vehicle-injected telencephalons. *$P < 0.05$, **$P < 0.01$, ***$P < 0.001$; scale bars, 100 μm; $n = 3$ brains for every experiment).

zebrafish by administering the anti-inflammatory drug dexamethasone (Dex). After determining the efficiency of the immunosuppression assay (fig. S6), we concluded that Dex treatment did partially suppress the immune system of the adult zebrafish, and hence we could proceed to test the effect during regeneration. We killed the lesioned (control and immunosuppressed) fish at 3 days after lesion and analyzed the proliferation response of the radial glial cells (Fig. 2, G to I). We observed that compared to the control brains, the reactive proliferation response in the lesioned brains was significantly reduced after immunosuppression (61.2 ± 2.2%). We subsequently tested the effect of immunosuppression on reactive neurogenesis.The number of newborn neurons was significantly lower (55.8 ± 1.8%), as shown by HuC/D and BrdU double labeling (Fig. 2, J to L). To examine whether Dex had any effect on the constitutive proliferation and neurogenesis, we performed the immunosuppression assay also in unlesioned animals, where no difference was detected between control and immunosuppressed animals (fig. S7). This finding shows clearly that Dex impedes only the regenerative response, without any additional effect on brain homeostasis. Moreover, we examined the effect of immunosuppression in the caudal fin, and we observed that immunosuppressed animals could not regenerate their caudal fins (fig. S8).

Because inflammation is involved in the activation of reactive proliferation and neurogenesis, we performed a transcriptome screen to identify possible molecular players involved in the regenerative response. We determined that *cysteinyl leukotriene receptor 1* (*cysltr1*) was induced after traumatic brain injury, especially in the lesioned hemisphere (Fig. 3A). By using the transgenic line *Tg(her4.1:GFP)*, which marks radial glial cells, we found that CysLT1 is predominantly expressed in those cells (Fig. 3B and fig. S9A). After zymosan A injection, *cysltr1* expression was also up-regulated in the ventricular zone (Fig. 3, C and D), suggesting that the inflammatory response after lesion might enhance leukotriene signaling in radial glial cells. Next, we analyzed the need for CysLT1 signaling in the reactive proliferation of the radial glial cells and the subsequent neurogenesis by injecting Pranlukast, an antagonist of CysLT1 (*18*, *19*), into the ventricle after lesion. When we analyzed the proliferation response of the glial cells, we observed that compared to vehicle-injected fish, injury-induced proliferation levels were reduced significantly, by 54.9 ± 5.5% in lesioned and Pranlukast-injected telencephalons (Fig. 3, E to G). We subsequently found that the number of newborn neurons was significantly reduced by 33.5 ± 4.6% in the Pranlukast-injected telencephalons as compared to the vehicle-injected ones (Fig. 3, H to J).

Then, we hypothesized that the leukotriene signaling pathway itself might increase the proliferation of radial glial cells and the overall neurogenesis response. To test this hypothesis, we injected leukotriene C4 (LTC4), one of the ligands for CysLT1, which had been sufficient to enhance its receptor expression through a feedback mechanism (fig. S9, B and C) and had not caused an inflammatory response itself (fig. S10), into the ventricle of the zebrafish brain without lesion. We analyzed the proliferation of the glial cells at 24 hours after injection. Compared to control injections, LTC4-injected brains displayed significantly elevated levels of progenitor proliferation (46.7 ± 0.8%) (Fig. 3, K to M). Additionally, we observed that LTC4 injection also significantly increased the consequent neurogenesis at 21 days after injection (44.4 ± 4.7%) (Fig. 3, N to P).

Our data suggest a role of the inflammatory response and immune cells in reactive proliferation of the radial glial cells and consequently enhanced neurogenesis. However, it is known that zebrafish radial glial cells proliferate constitutively and that newborn neurons are formed continuously (*4*, *20*–*24*). This poses the question of whether the inflammatory outcome enhances cell proliferation and neurogenesis by amplifying the already-existing signals of adult neurogenesis or initiates an injury-induced molecular program specific to the regenerative response. To address this question, we took advantage of the injury-induced expression of the zinc-finger transcription factor Gata3 as a marker (*25*). We have previously shown that *gata3* is induced only after traumatic brain injuries in the adult zebrafish telencephalon, whereas it is undetectable under homeostatic conditions. We found that zymosan A injections were sufficient to induce *gata3* expression at the ventricular zone at 24 hours after injection, similar to the lesion model (Fig. 4, A to C). Additionally, by immunosuppression studies we found that inflammation is required for the induction of *gata3* expression, because after zymosan A injection, *gata3* expression is reduced significantly upon immunosuppression (Fig. 4D). Moreover, in a Gata3 knockdown background, reactive proliferation ceased upon zymosan A injection (fig. S11).

LTC4 injection without the lesion was able to activate *gata3* expression in the adult zebrafish telencephalon (Fig. 4, E to G). When we blocked the CysLT1 activity using Pranlukast, *gata3* expression levels were significantly diminished after lesions (Fig. 4H). Together these data indicate that the inflammatory response, including the LTC4 signaling activity, initiates regeneration programs that are distinct from the constitutive neurogenesis in the adult zebrafish brain.

In mammals, which cannot efficiently regenerate neurons after injuries, several studies have shown that acute inflammation impedes adult neurogenesis and regenerative capacity (*13*, *26*). Our results suggest that acute inflammation can promote central nervous system regeneration, because it provides cues necessary for the initiation of reactive proliferation and regenerative neurogenesis in the adult zebrafish brain (fig. S12). Our findings reveal a signaling pathway in zebrafish that couples the inflammatory response to efficient enhancement of stem cell activity and the initiation of neural regeneration. Thus, the zebrafish offers an opportunity to study the crosstalk between the inflammatory response and successful regeneration programs in the central nervous system of a regeneration-capable vertebrate, with the aim of translating such findings into potential therapeutic applications to treat traumatic brain injuries and neurodegenerative disorders.

References and Notes

1. E. V. Baumgart, J. S. Barbosa, L. Bally-Cuif, M. Götz, J. Ninkovic, *Glia* **60**, 343 (2012).
2. N. Kishimoto, K. Shimizu, K. Sawamoto, *Disease Models Mechanisms* **5**, 200 (2012).
3. V. Kroehne, D. Freudenreich, S. Hans, J. Kaslin, M. Brand, *Development* **138**, 4831 (2011).
4. C. Kizil, J. Kaslin, V. Kroehne, M. Brand, *Dev. Neurobiol.* **72**, 429 (2012).
5. B. Finsen, T. Owens, *FEBS Lett.* **585**, 3806 (2011).
6. G. J. Lieschke, N. S. Trede, *Curr. Biol.* **19**, R678 (2009).
7. D. J. Loane, K. R. Byrnes, *Neurotherapeutics* **7**, 366 (2010).
8. P. Martin, Y. Feng, *Nature* **459**, 921 (2009).
9. R. M. Ransohoff, M. A. Brown, *J. Clin. Invest.* **122**, 1164 (2012).
10. A. Nimmerjahn, F. Kirchhoff, F. Helmchen, *Science* **308**, 1314 (2005).
11. C. T. Ekdahl, J. H. Claasen, S. Bonde, Z. Kokaia, O. Lindvall, *Proc. Natl. Acad. Sci. U.S.A.* **100**, 13632 (2003).
12. M. T. Fitch, J. Silver, *Exp. Neurol.* **209**, 294 (2008).
13. B. D. Hoehn, T. D. Palmer, G. K. Steinberg, *Stroke* **36**, 2718 (2005).
14. M. L. Monje, H. Toda, T. D. Palmer, *Science* **302**, 1760 (2003).
15. P. G. Popovich *et al.*, *J. Neuropathol. Exp. Neurol.* **61**, 623 (2002).
16. M. J. Redd, G. Kelly, G. Dunn, M. Way, P. Martin, *Cell Motil. Cytoskeleton* **63**, 415 (2006).
17. C. Kizil, M. Brand, *PLoS ONE* **6**, e27395 (2011).
18. G. L. Yu *et al.*, *Brain Res.* **1053**, 116 (2005).
19. W. P. Zhang, E. Q. Wei, R. H. Mei, C. Y. Zhu, M. H. Zhao, *Acta Pharmacol. Sin.* **23**, 871 (2002).
20. B. Adolf *et al.*, *Dev. Biol.* **295**, 278 (2006).
21. P. Chapouton, R. Jagasia, L. Bally-Cuif, *BioEssays* **29**, 745 (2007).
22. H. Grandel, J. Kaslin, J. Ganz, I. Wenzel, M. Brand, *Dev. Biol.* **295**, 263 (2006).
23. J. Kaslin, J. Ganz, M. Brand, *Philos. Trans. R. Soc. London Ser. B* **363**, 101 (2008).
24. I. Rothenaigner *et al.*, *Development* **138**, 1459 (2011).
25. C. Kizil *et al.*, *Developmental Cell* 10.1016/j.devcel.2012.10.014 (2012).
26. R. E. Iosif *et al.*, *J. Neurosci.* **26**, 9703 (2006).

Acknowledgments: We thank A. Menge for cryosections and paraffin sections, G. Kempermann and C. L. Antos for useful discussions, T. Chavakis for discussions and critical reading on the manuscript, N. Trede for discussion and assistance with the immunosuppression assay, and M. Redd for kindly providing us the L-plastin antibody. This work was supported by research grants from the Deutsche Forschungsgemeinschaft (SFB-655), European Union (ZF Health, EC Grant Agreement HEALTH-F4-2010-242048), and Technical University of Dresden.

Supplementary Materials

www.sciencemag.org/cgi/content/full/science.1228773/DC1
Materials and Methods
Figs. S1 to S12
Tables S1 and S2
Reference (*27*)

13 August 2012; accepted 24 October 2012
Published online 8 November 2012;
10.1126/science.1228773

Sexually Dimorphic BDNF Signaling Directs Sensory Innervation of the Mammary Gland

Yin Liu,[1] Michael Rutlin,[1]* Siyi Huang,[1] Colleen A. Barrick,[2] Fan Wang,[3] Kevin R. Jones,[4] Lino Tessarollo,[2] David D. Ginty[1]†

How neural circuits associated with sexually dimorphic organs are differentially assembled during development is unclear. Here, we report a sexually dimorphic pattern of mouse mammary gland sensory innervation and the mechanism of its formation. Brain-derived neurotrophic factor (BDNF), emanating from mammary mesenchyme and signaling through its receptor TrkB on sensory axons, is required for establishing mammary gland sensory innervation of both sexes at early developmental stages. Subsequently, in males, androgens promote mammary mesenchymal expression of a truncated form of TrkB, which prevents BDNF-TrkB signaling in sensory axons and leads to a rapid loss of mammary gland innervation independent of neuronal apoptosis. Thus, sex hormone regulation of a neurotrophic factor signal directs sexually dimorphic axonal growth and maintenance, resulting in generation of a sex-specific neural circuit.

Sexually dimorphic body structures require differentially assembled neural circuits to control gender-specific physiological functions and behaviors. One sexually dimorphic organ is the mammary gland, the milk-producing apocrine gland of female mammals. In mice, the initial stages of mammary gland development are virtually identical in males and females, until embryonic day 13 (E13). Then, in response to androgens secreted by the male gonads, the male glands begin to regress, such that sexual dimorphism is first observable at E14 (*1*, *2*). By birth, each of the 10 mammary glands of the female mouse contains a clearly defined nipple and an elaborate ductal tree that is densely innervated by sensory neurons (fig. S1), whereas the male glands are barely detectable. To investigate how development of neuronal innervation coordinates with sexually dimorphic mammary gland organogenesis, we performed immunostaining using an antibody against the neuron-specific class III β-tubulin (Tuj1) to visualize neuronal fibers associated with rudimentary mammary glands from E11 to E14. In both males and females, Tuj1$^+$ fibers innervate the mammary rudiments shortly after their appearance, and the number of Tuj1$^+$ fibers associated with mammary rudiments is comparable for the two sexes until early E13 (Fig. 1, A to D and G, and figs. S2 and S3). These Tuj1$^+$ fibers associated with mammary rudiments at this stage are from sensory neurons, most likely emanating from dorsal root ganglia (DRGs) (fig. S4). The number of Tuj1$^+$ fibers innervating female mammary rudiments dramatically increases from late E12 to late E13, whereas fibers innervating male rudiments increase until early E13, but then they are rapidly lost during the subsequent 8 hours. As a result, a sexually dimorphic pattern of mammary gland sensory innervation is generated by late E13, before male gland regression (Fig. 1, E to G, and fig. S3). As sexually dimorphic development of neuronal populations in both the central nervous system and the peripheral nervous system has been linked to steroid hormone–regulated apoptotic cell death (*3*–*7*), we asked whether male-specific axonal loss from mammary rudiments is the result of apoptosis or, alternatively, axon pruning (*8*). In *Bax*$^{-/-}$ embryos, in which apoptosis in sensory ganglia is eliminated (*9*), mammary gland innervation at late E13 exhibits a sexually dimorphic pattern, which is quantitatively indistinguishable from that seen in wild-type embryos (fig. S3). Thus, formation of sexually dimorphic mammary gland innervation is not due to apoptotic loss of male sensory neurons; rather, it is a result of sensory axon pruning from the male gland beginning at early E13.

We next analyzed mammary gland innervation in embryos exposed to the androgen receptor antagonist flutamide, testosterone propionate, or the nonaromatizable androgen dihydrotestosterone (DHT), as well as in androgen-insensitive (*Tfm*) mice (*10*). It is remarkable that, in flutamide-treated embryos, sensory fibers projecting to the male mammary rudiments fail to be pruned, and quantification of fiber density shows no difference between the two sexes at late E13 (Fig. 1, H to K, and N). Similarly, the amount of mammary gland innervation in *Tfm* male embryos is comparable to both flutamide-treated male embryos and wild-type female embryos at late E13 (fig. S5). Conversely, in both testosterone- and DHT-treated embryos, sensory fibers projecting to female mammary rudiments are lost within 8 hours (Fig. 1, L, M, and O, and fig S5). Thus, androgen receptor activation is both necessary and sufficient for pruning of sensory axons and, thus, generation of the sexually dimorphic pattern of mammary gland sensory innervation before male gland regression.

The sexually dimorphic pattern of mammary gland innervation results from extension of new sensory fibers into female glands and a coincident pruning of fibers associated with male glands. This suggests that signaling pathways essential for promoting and maintaining axonal projections to female glands are either absent or disrupted in E13 males, presumably because of androgen receptor activation. To identify signals that mediate development of mammary gland sensory innervation in the female, we assessed the expression patterns of the four neurotrophins at E13 because neurotrophins play key roles in primary sensory neuron development (*11*, *12*). Brain-derived neurotrophic factor (BDNF) emerged as a candidate because it is robustly expressed in the developing mammary gland at this stage, whereas the other neurotrophins are not (Fig. 2A and figs. S6 and S7). Staining on tissue sections showed that BDNF is expressed in mammary mesenchymal cells, not in mammary epithelial cells (Fig. 2A, inset). To determine whether the BDNF receptor TrkB is expressed in sensory neurons that innervate the female mammary rudiments, we analyzed *TrkB*^{GFP} knock-in mice (*13*) and found that virtually all Tuj1$^+$ fibers projecting to the female mammary rudiments express TrkB at E13 (Fig. 2B). Experiments using a TrkB antibody that recognizes the extracellular domain of TrkB (TrkB^{ECD} antibody) confirmed that TrkB is present on most or all axon terminals surrounding female glands at E13 (Fig. 3C). Furthermore, we generated a *TrkB*^{CreERT2} knock-in mouse line and used it to permanently label sensory neurons that express TrkB at E13. Postnatally, the labeled fibers innervate the ductal tree structure, but not the nipple, of female mammary glands (fig. S8).

To ask whether BDNF-TrkB signaling is necessary for establishing sensory innervation of the female mammary gland, we assessed mammary gland innervation in mouse lines harboring targeted mutations of either *Bdnf* or *TrkB*. Female embryos with a homozygous null mutation in *Bdnf* exhibited very few sensory fibers associated with the mammary rudiments at E13 (Fig. 2, C to E). Moreover, both *TrkB* null and *TrkB* conditional mutant embryos in which *TrkB* is ablated exclusively in primary sensory neurons showed a dramatic reduction in female mammary gland innervation at E13 (Fig. 2F and fig. S9). To determine whether BDNF-TrkB signaling is required at E13 for maintaining female mammary gland sensory innervation, we used a chemical-genetic strategy that enables precise temporal inhibition of TrkB signaling in vivo. *TrkB*^{F616A} knock-in mice harbor a single–amino acid substitution in the TrkB adenosine triphosphate binding pocket that allows specific and potent inhibition of endogenous TrkB kinase signaling by the small-molecule inhibitor 1NMPP1 (*14*). Five hours of 1NMPP1 exposure at E13 resulted in a dramatic reduction in mammary gland innervation of *TrkB*$^{F616A/F616A}$

[1]The Solomon H. Snyder Department of Neuroscience, Howard Hughes Medical Institute, The Johns Hopkins University School of Medicine, Baltimore, MD 21205, USA. [2]Mouse Cancer Genetics Program, Center for Cancer Research, National Cancer Institute–Frederick, National Institutes of Health, Frederick, MD 21702, USA. [3]Department of Cell Biology, Duke University Medical Center, Durham, NC 27710, USA. [4]Department of Molecular, Cellular, and Developmental Biology, University of Colorado, Boulder, CO 80309, USA.

*Present address: Department of Biology, National Center for Behavioral Genomics, Brandeis University, Waltham, MA 02454, USA. †To whom correspondence should be addressed. E-mail: dginty@jhmi.edu

female embryos compared with that of vehicle-treated $TrkB^{F616A/F616A}$ females, whereas 1NMPP1 had no effect on wild-type females (Fig. 2, G to K). Thus, BDNF-TrkB signaling is required in sensory neurons for establishment and maintenance of mammary gland innervation, and disrupting BDNF-TrkB signaling in the female at E13 leads to rapid axonal pruning and a male-type pattern of mammary gland sensory innervation.

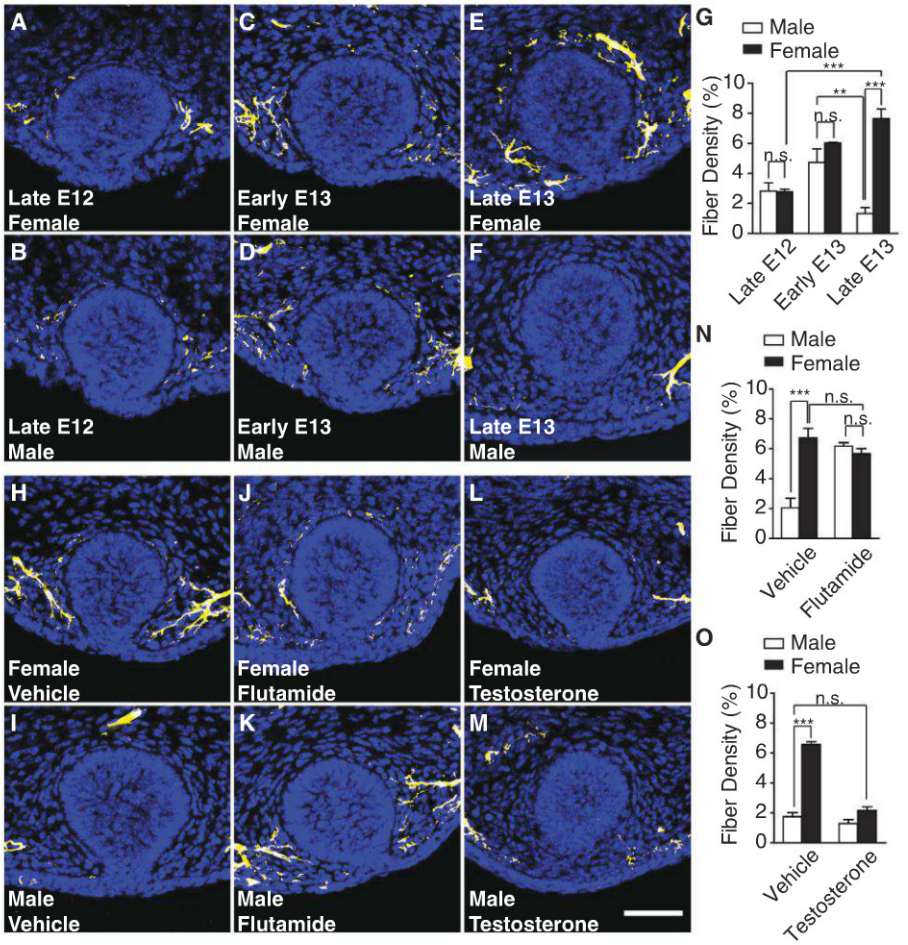

Fig. 1. Androgen-dependent, male-specific axon pruning leads to sexually dimorphic mammary gland innervation before male gland regression. (**A** to **F**) Tuj1 (yellow) and TO-PRO-3 (blue, nucleic acid stain) staining of mammary gland sections of embryos at different stages. This staining was used in all subsequent mammary gland innervation analyses unless otherwise specified. (**G**) Quantification of mammary gland innervation. (**H** to **O**) Mammary gland innervation of embryos treated with vehicle, flutamide, or testosterone propionate (8 hours). The vehicle group shown in (H) and (I) is the control for flutamide treatments; controls for the testosterone treatments were similar (not shown). Each experiment was done at least three times. (N) and (O) are quantifications of the data shown in (H) to (M). All statistical analyses shown in this figure and all subsequent figures (except Fig. 2, E and F) were done using two-way ANOVA with a Bonferroni post hoc test. Shown are the means ± SEM, $n \geq 5$ embryos for each bar, $^{*}P < 0.05$; $^{**}P < 0.01$; $^{***}P < 0.001$; n.s., not significant. Scale bar: 50 μm.

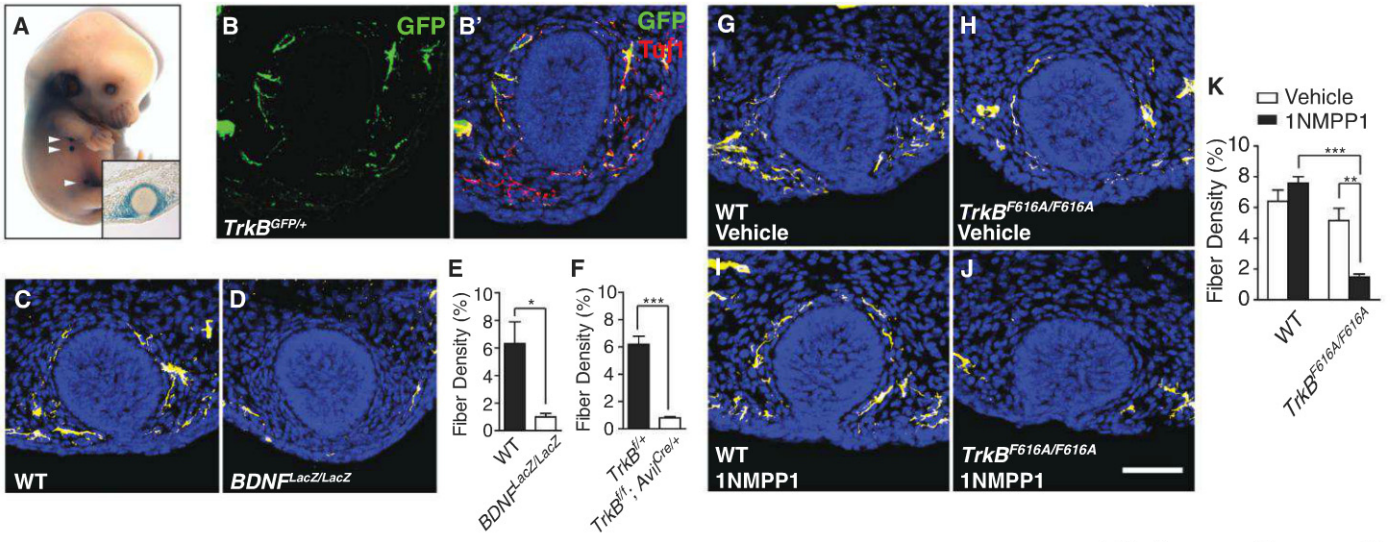

Fig. 2. BDNF-TrkB signaling is required for sensory innervation of the female mammary gland at E13. (**A**) Whole-mount X-gal staining of a late E13 female $BDNF^{LacZ/+}$ embryo (*21*). (Inset) Cross section of one mammary gland. Arrows: rudimentary mammary glands (five on each side of the body, glands nos. 1 and 5 are located behind the limbs). (**B** and **B'**) Costaining of GFP, Tuj1, and TO-PRO-3 of a late E13 female $TrkB^{GFP/+}$ mammary gland. (**C** to **F**) Mammary gland innervation of late E13 female wild-type (WT), $BDNF^{lacZ/LacZ}$ (null), $TrkB^{f/+}$, and $TrkB^{f/f}$; $Avil^{Cre/+}$ embryos. [The $Avil^{Cre/+}$ mouse is a sensory neuron–specific Cre driver mouse line (*22*). Statistical analyses in (E) and (F) were done using Student's *t* test.] (**G** to **K**) Mammary gland innervation of late E13 wild-type and $TrkB^{F616A/F616A}$ female embryos that had been exposed to either vehicle or 1NMPP1 for 5 hours. For each bar, $n \geq 3$ embryos in (E), (F), and (K). Scale bar: 50 μm.

We next asked whether BDNF-TrkB signaling is absent or disrupted in E13 male glands and thus would account for the androgen-dependent axon pruning and the sexually dimorphic pattern of mammary gland sensory innervation. The androgen receptor is expressed in both the male and female mammary mesenchyme but not in DRG sensory neurons at E13 (figs. S10 and S14), which suggests that the site of androgen action is the rudimentary mammary gland itself. We next tested whether BDNF expression in mammary mesenchymal cells differs in males and females. This appears not to be the case, as X-gal staining of *BDNF*$^{LacZ/+}$ embryos shows that BDNF expression in the male mammary mesenchyme is comparable to that of the female at late E13 (Fig. 3, A and B, and fig. S11). We next examined TrkB expression and, to our surprise, found that male mammary mesenchymal cells robustly express TrkB (Fig. 3D). This pattern of TrkB expression in the male mammary mesenchyme is not observed in female glands at the same stage and neither is it seen in the glands of either sex 1 day earlier, at E12 (Fig. 3C and fig. S12). These findings raise the possibility that BDNF is sequestered by TrkB on male mammary mesenchymal cells at E13, which prevents BDNF-TrkB signaling in sensory fibers associated with the male mammary rudiments and leads to pruning of fibers in the male and the sexually dimorphic mammary gland innervation pattern.

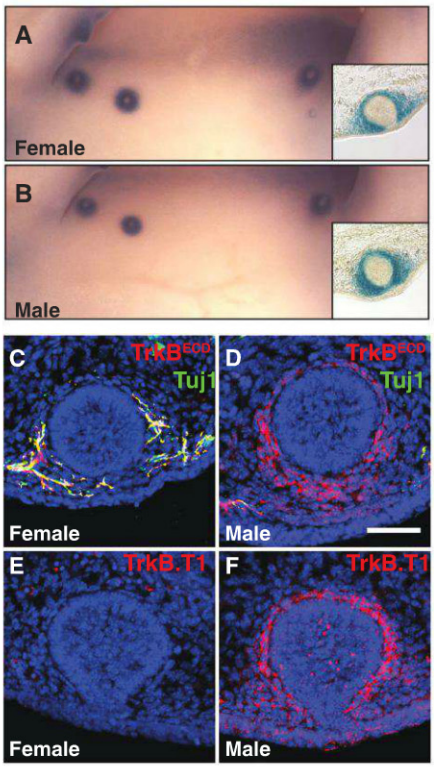

Fig. 3. The truncated form of TrkB is expressed in E13 male mammary mesenchymal cells. (**A** and **B**) X-gal staining of late E13 female and male *BDNF*$^{LacZ/+}$ embryos, respectively. (**C** to **F**) Mammary gland sections of late E13 male and female embryos were stained with TO-PRO-3 (blue) and, in addition, (C and D) with TrkB^{ECD} and Tuj1 antibodies or (E and F) with a truncated form–specific TrkB antibody (TrkB.T1). Staining observed in the female section in (E) is due to nonspecific antibody binding to blood cells. All experiments were done at least three times. Scale bar: 50 μm.

We tested this model by exploring the nature of TrkB expression in the male mammary mesenchyme, its androgen dependence, and the requirement of mesenchymal TrkB for generating the male pattern of mammary gland sensory innervation. Thus far, two isoforms of TrkB generated by alternative splicing have been described in mice: a full-length form, with the intracellular tyrosine kinase domain required for canonical receptor tyrosine kinase signaling and BDNF-dependent axonal growth (*15*, *16*), and a truncated form, called TrkB.T1, which lacks the tyrosine kinase domain and, instead, has a unique, short, C-terminal intracellular domain (*17*). Both TrkB forms bind to BDNF and become internalized together with ligand (*18*, *19*), which demonstrates their ability to sequester BDNF. Immunostaining using a TrkB.T1-specific antibody that recognizes the C-terminal intracellular domain

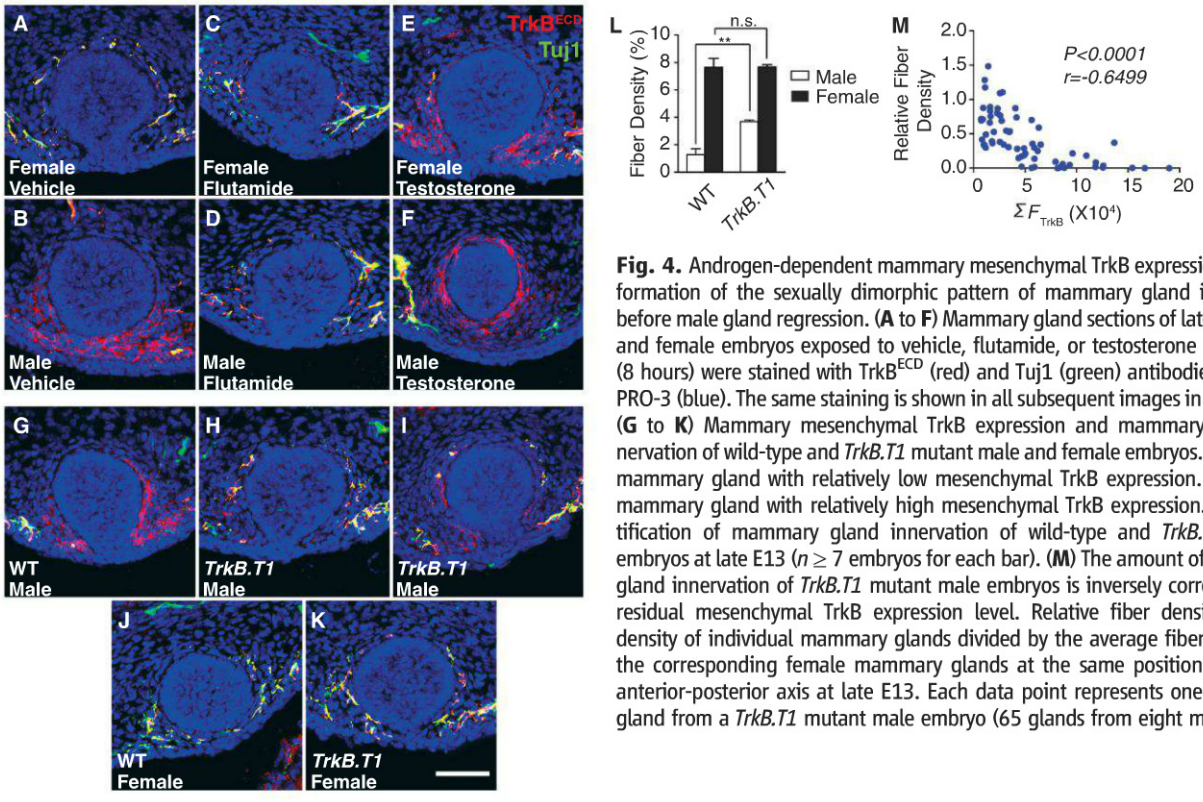

Fig. 4. Androgen-dependent mammary mesenchymal TrkB expression controls formation of the sexually dimorphic pattern of mammary gland innervation before male gland regression. (**A** to **F**) Mammary gland sections of late E13 male and female embryos exposed to vehicle, flutamide, or testosterone propionate (8 hours) were stained with TrkB^{ECD} (red) and Tuj1 (green) antibodies, and TO-PRO-3 (blue). The same staining is shown in all subsequent images in this figure. (**G** to **K**) Mammary mesenchymal TrkB expression and mammary gland innervation of wild-type and *TrkB.T1* mutant male and female embryos. (H) A male mammary gland with relatively low mesenchymal TrkB expression. (I) A male mammary gland with relatively high mesenchymal TrkB expression. (**L**) Quantification of mammary gland innervation of wild-type and *TrkB.T1* mutant embryos at late E13 ($n \geq 7$ embryos for each bar). (**M**) The amount of mammary gland innervation of *TrkB.T1* mutant male embryos is inversely correlated with residual mesenchymal TrkB expression level. Relative fiber density is fiber density of individual mammary glands divided by the average fiber density of the corresponding female mammary glands at the same position along the anterior-posterior axis at late E13. Each data point represents one mammary gland from a *TrkB.T1* mutant male embryo (65 glands from eight mice).

of TrkB.T1 revealed that TrkB.T1 is robustly expressed in the male mammary mesenchyme at E13, whereas it is undetectable in the female gland (Fig. 3, E and F). In complementary experiments, in situ hybridizations using two different probes to distinguish between full-length TrkB and TrkB.T1 transcripts show that there is an undetectable amount of full-length TrkB mRNA in mammary mesenchymal cells of either sex (fig. S13). These findings indicate that sexually dimorphic expression of TrkB in mammary mesenchymal cells at E13 is the result of differential transcription of the *TrkB* gene and expression of the truncated form of TrkB exclusively in the male gland.

We next asked whether TrkB expression in male mammary mesenchymal cells is androgen-dependent. Double immunostaining for green fluorescent protein (GFP) and the androgen receptor on mammary gland sections of $TrkB^{GFP/+}$ knock-in embryos showed that TrkB-expressing cells surrounding the male mammary rudiment are indeed a major subset of androgen-expressing mammary mesenchymal cells (fig. S14). TrkB expression in mammary mesenchymal cells, assessed by $TrkB^{ECD}$ antibody labeling, is abolished in male embryos treated with flutamide and, conversely, it is dramatically induced in female embryos treated with testosterone (Fig. 4, A to F). Experiments that assessed GFP levels in mammary mesenchymal cells of $TrkB^{GFP/+}$ embryos treated with flutamide are consistent with these $TrkB^{ECD}$ antibody labeling experiments and indicate that androgens control TrkB expression through regulation of *TrkB* gene transcription in mammary mesenchymal cells (fig. S15). Moreover, the increase of TrkB expression in the female mammary mesenchyme after testosterone treatment is temporally coincident with the loss of sensory innervation of female glands (fig. S16). Thus, TrkB transcription in the mammary mesenchyme is androgen-dependent and inversely related to the amount of sensory fibers associated with the rudimentary gland.

To determine whether the truncated form of TrkB expressed in the male mammary mesenchyme at E13 plays an essential role in the sexually dimorphic patterning of mammary gland innervation, we analyzed mammary gland innervation in *TrkB.T1* mutant mice in which the exon encoding the C-terminal residues unique to TrkB.T1 is missing (*20*). These mice do not express TrkB.T1, but they do express normal levels of full-length TrkB. Because TrkB.T1 is not expressed in DRG neurons at E13 (fig. S17), performing experiments using *TrkB.T1* mutant mice allowed us to address the role of TrkB.T1 without directly affecting BDNF-TrkB signaling in DRG neurons themselves. We examined mammary mesenchymal TrkB expression in *TrkB.T1* mutant male embryos by immunostaining using the $TrkB^{ECD}$ antibody and quantifying immunofluorescence signals in the mammary mesenchyme (fig. S18). The specificity of the $TrkB^{ECD}$ antibody was confirmed using late E13 male $TrkB^{GFP/GFP}$ (null) embryos (fig. S19). Our analysis revealed a significant reduction in, but not a complete loss of, TrkB expression in mammary mesenchyme of male *TrkB.T1* mutant embryos at late E13, as compared with wild-type males (Fig. 4, G to I, and fig. S18). Although the residual TrkB protein found in *TrkB.T1* mutant embryos lacks the TrkB.T1-specific C terminus, it is likely capable of associating with BDNF because it does contain the extracellular domain of TrkB (fig. S20). Quantification of mammary gland innervation revealed a significant increase in fiber density in *TrkB.T1* mutant males compared with wild-type males at late E13, and no significant difference between *TrkB.T1* mutant females and wild-type females (Fig. 4, G to L). Moreover, because we observed that the amount of residual TrkB varies between glands and embryos (Fig. 4, H and I), we assessed the relation between the amount of residual TrkB expression and relative fiber density for individual glands from several *TrkB.T1* mutant males. This analysis revealed a strong inverse correlation between the amount of residual mesenchymal TrkB observed in individual mammary glands of *TrkB.T1* mutant males and the number of sensory fibers associated with these glands (correlation coefficient: $r = 0.6499$, $P < 0.0001$) (Fig. 4M). We conclude that androgen-dependent expression of the truncated form of TrkB in male mammary mesenchyme is required for inhibition of BDNF-TrkB signaling in sensory fibers, axonal pruning, and generation of the male-type pattern of mammary gland sensory innervation at late E13 (fig. S21). Thus, sex hormone–dependent modulation of neurotrophic factor signaling is a mechanism that controls sexually dimorphic development of the mammalian nervous system.

References and Notes

1. G. W. Robinson, *Nat. Rev. Genet.* **8**, 963 (2007).
2. M. E. Dunbar *et al.*, *Development* **126**, 3485 (1999).
3. E. J. Nordeen, K. W. Nordeen, D. R. Sengelaub, A. P. Arnold, *Science* **229**, 671 (1985).
4. L. L. Wright, A. J. Smolen, *Int. J. Dev. Neurosci.* **5**, 305 (1987).
5. R. B. Simerly, *Annu. Rev. Neurosci.* **25**, 507 (2002).
6. J. A. Morris, C. L. Jordan, S. M. Breedlove, *Nat. Neurosci.* **7**, 1034 (2004).
7. N. G. Forger, *Neuroscience* **138**, 929 (2006).
8. L. K. Low, H. J. Cheng, *Philos. Trans. R. Soc. Lond. B Biol. Sci.* **361**, 1531 (2006).
9. T. D. Patel, A. Jackman, F. L. Rice, J. Kucera, W. D. Snider, *Neuron* **25**, 345 (2000).
10. M. F. Lyon, S. G. Hawkes, *Nature* **227**, 1217 (1970).
11. M. Bibel, Y. A. Barde, *Genes Dev.* **14**, 2919 (2000).
12. E. J. Huang, L. F. Reichardt, *Annu. Rev. Neurosci.* **24**, 677 (2001).
13. L. Li *et al.*, *Cell* **147**, 1615 (2011).
14. X. Chen *et al.*, *Neuron* **46**, 13 (2005).
15. R. Klein, L. F. Parada, F. Coulier, M. Barbacid, *EMBO J.* **8**, 3701 (1989).
16. J. K. Atwal, B. Massie, F. D. Miller, D. R. Kaplan, *Neuron* **27**, 265 (2000).
17. R. Klein, D. Conway, L. F. Parada, M. Barbacid, *Cell* **61**, 647 (1990).
18. S. Biffo, N. Offenhäuser, B. D. Carter, Y. A. Barde, *Development* **121**, 2461 (1995).
19. R. H. Fryer, D. R. Kaplan, L. F. Kromer, *Exp. Neurol.* **148**, 616 (1997).
20. S. G. Dorsey *et al.*, *Neuron* **51**, 21 (2006).
21. J. A. Gorski, S. R. Zeiler, S. Tamowski, K. R. Jones, *J. Neurosci.* **23**, 6856 (2003).
22. S. da Silva *et al.*, *Proc. Natl. Acad. Sci. U.S.A.* **108**, 3395 (2011).

Acknowledgments: We thank members of the Ginty laboratory for assistance and discussions throughout the course of this project, and A. Kolodkin and R. Kuruvilla for comments on the manuscript. This work was supported by NIH grants NS34814 (D.D.G.), EY014998 (K.R.J.), and DE019440 (F.W.). D.D.G. is an investigator of the Howard Hughes Medical Institute. BDNFlox mice are covered under U.S. patent no. 4,959,317, which is licensed to Bristol-Myer Squibb Company, with the right to grant sublicenses. The mice are available for noncommercial biomedical research under a Material Transfer Agreement with the University of Colorado.

Supplementary Materials

www.sciencemag.org/cgi/content/full/338/6112/1357/DC1
Materials and Methods
Figs. S1 to S21
References (*23*–*30*)

1 August 2012; accepted 16 October 2012
10.1126/science.1228258

Mice Lacking a *Myc* Enhancer That Includes Human SNP rs6983267 Are Resistant to Intestinal Tumors

Inderpreet Kaur Sur,[1,2] Outi Hallikas,[3] Anna Vähärautio,[1,3] Jian Yan,[1] Mikko Turunen,[3] Martin Enge,[1] Minna Taipale,[1,3] Auli Karhu,[4] Lauri A. Aaltonen,[4] Jussi Taipale[1,3]*

Multiple cancer-associated single-nucleotide polymorphisms (SNPs) have been mapped to conserved sequences within a 500-kilobase region upstream of the *MYC* oncogene on human chromosome 8q24. These SNPs may affect cancer development through altered regulation of *MYC* expression, but this hypothesis has been difficult to confirm. We generated mice deficient in Myc-335, a putative *MYC* regulatory element that contains rs6983267, a SNP accounting for more human cancer-related morbidity than any other genetic variant or mutation. In Myc-335 null mice, *Myc* transcripts were expressed in the intestinal crypts in a pattern similar to that in wild-type mice but at modestly reduced levels. The mutant mice displayed no overt phenotype but were markedly resistant to intestinal tumorigenesis induced by the *APCmin* mutation. These results establish that a cancer-associated SNP identified in human genome-wide association studies has a functional effect in vivo.

Genome-wide association (GWA) studies have identified polymorphisms upstream of the *MYC* gene that are associated with increased risk for multiple different cancer types [e.g., breast (*1*), bladder (*2*), prostate (*3*), and colon (*4*)]. Several lines of evidence suggest that the

identified polymorphisms affect function or expression of the *MYC* oncogene. Isolated elements containing the polymorphic sequences have enhancer activity in transgenic mice (*5*, *6*), and chromatin conformation-capture assays suggest that in cultured cells the elements are located close to the *MYC* promoter sequences (*7*–*9*) despite being more than 300 kb away in linear sequence. Moreover, it has been shown that the cell line DLD-1 that is heterozygous for the polymorphism rs6983267 differentially expresses the *MYC* alleles (*9*), suggesting that this polymorphism affects the level of expression of *MYC*. The single-nucleotide polymorphism (SNP) rs6983267 affects binding of the transcription factor TCF7L2 that is centrally important in colorectal tumorigenesis (*5*, *10*), providing a plausible mechanism of action for this polymorphism. Despite all these lines of evidence, direct analyses comparing *MYC* expression between individuals with different genotypes have been inconclusive or negative (*5*, *10*).

[1]Science for Life Center, Department of Biosciences and Nutrition, Karolinska Institutet, Stockholm, Sweden. [2]Clinical Research Center, Karolinska University Hospital, Stockholm, Sweden. [3]Genome-Scale Biology Program, Institute of Biomedicine, University of Helsinki, Biomedicum, Post Office Box 63 (Haartmaninkatu 8), University of Helsinki, FI-00014 Helsinki, Finland. [4]Genome-Scale Biology Program, Department of Medical Genetics, University of Helsinki, Biomedicum, Post Office Box 63 (Haartmaninkatu 8), University of Helsinki, FI-00014 Helsinki, Finland.

*To whom correspondence should be addressed. E-mail: jussi.taipale@ki.se

It is possible that the effect of the polymorphisms on *MYC* expression has not been robustly detected because single-nucleotide substitutions are expected to alter binding of only one transcription factor out of many that bind to a given regulatory element. Thus, the polymorphisms are expected to have only a minor impact on normal *MYC* expression. However, even when a polymorphism has minor impact, the activity of the element containing it could be required for tumorigenesis.

Because the region containing rs6983267 is conserved in mice, we used a mouse genetic model to evaluate the functional role of the SNP in Myc expression and tumorigenesis. However, converting the risk allele that mice normally carry to the protective allele would be expected to mimic the effect of the SNP in humans, potentially requiring sample sizes that are similar to those used in human GWA studies (hundreds to thousands of mice). To yield an allele with a stronger effect, we instead generated a gene-targeted mouse in which the entire regulatory element containing rs6983267 (Myc-335 hereafter) can be conditionally deleted. This allele allowed us also to test the possibility that the Myc-335 element would be required for tumorigenesis.

Mice carrying the Myc-335 conditional allele (Myc-335 cKO) were generated by flanking with loxP sites a 1740-bp region that lies 335 kb upstream of the *Myc* transcription start site. The Myc-335 cKO mice were crossed to a deletor mouse strain to generate the Myc-335 null (Myc-335^{-}) allele (Fig. 1A). Deletion of the Myc-335 element was confirmed by polymerase chain reaction (PCR) analysis of the genomic DNA (Fig. 1A), and the mice were further intercrossed to generate Myc-335$^{-/-}$ mice.

Loss of Myc is embryonic lethal and, even in heterozygous form, affects body size of newborn mice by compromising placental function (*11*, *12*). However, the Myc-335$^{-/-}$ mice are viable and fertile and display no overt phenotype, indicating that loss of Myc-335 does not equal loss of Myc. Because rs6983267 increases risk for colorectal and prostate cancers and mice do not develop prostate tumors, we analyzed the intestinal morphology and function of the Myc-335$^{-/-}$ mice in more detail. Histological analysis of the intestines of Myc-335$^{-/-}$ mice, at postnatal day 1 (p1), showed normal morphology. The proliferation of the Myc-335$^{-/-}$ intestinal epithelium, as judged by the immunohistochemistry (IHC) analysis of the Ki-67 marker, was also comparable to that of the wild-type littermates. Furthermore, we detected an apparently normal pattern of Myc expression in the developing intestinal crypts of both the wild-type and the Myc-335$^{-/-}$ animals by IHC analysis (Fig. 1B and fig. S1). The intestinal epithelia of adult mice also showed normal histology and Myc expression in the crypts, including cells located adjacent to Paneth cells (*13*, *14*). Analysis of Paneth cells by morphology (Fig. 1C), Goblet cells by periodic-acid Schiff base (PAS) staining (fig. S2), and Lgr5 expression by quantitative PCR (qPCR) (fig. S3) suggested

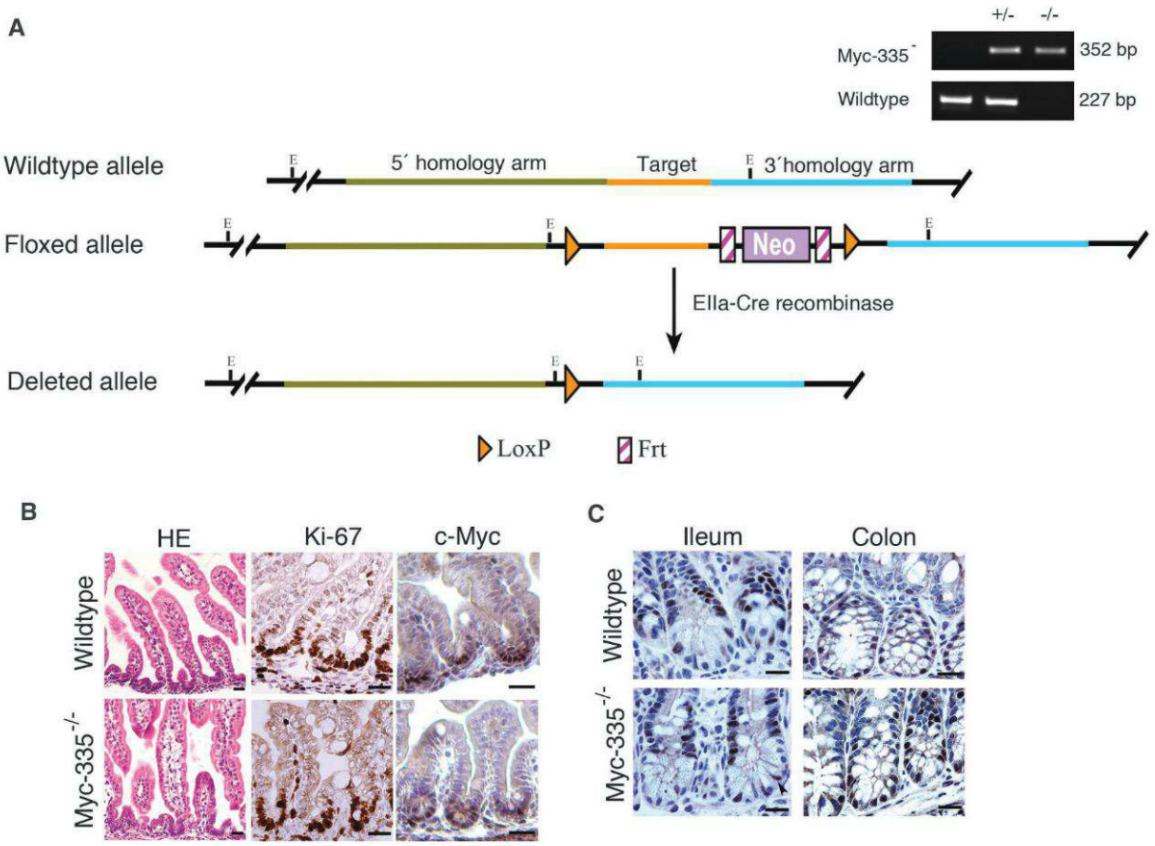

Fig. 1. Generation of the Myc-335 null allele. (**A**) Schematic representation of the targeting strategy. E depicts the EcoRI restriction sites. (Inset) Genotyping PCR analysis of the wild-type and Myc-335 null alleles. (**B**) Normal intestinal morphology and proliferation in Myc-335$^{-/-}$ mice at p1. Hematoxylin and eosin (HE) stains of sections show normal morphology in Myc-335$^{-/-}$ mice. IHC analysis showed normal proliferation (Ki-67) and restriction of the c-Myc expression to the developing crypts. Scale bars indicate 10 μm. (**C**) c-Myc expression detected in the crypts of adult Myc-335$^{-/-}$ mice. The arrowhead points to an Myc-positive cell located between two Paneth cells. Scale bars, 20 μm.

Fig. 2. Myc-335 deletion affects *Myc* transcription. (**A**) qPCR analysis showing decreased expression of *Myc* in Myc-335$^{-/-}$ mice (n = 3) compared with wild-type control (n = 3), $P < 0.04$ (Student's t test). Error bars denote one standard deviation. (**B**) Exon array analysis, showing decreased expression of *Myc* in Myc-335$^{-/-}$ mice. Hexagonal binning density plot of normalized RNA expression signal ($\log_2$) for each exon of a wild-type (x axis) and a Myc-335$^{-/-}$ (y axis) male mouse from the same litter are shown. The density scale is at right. Myc exons (red) are expressed at a slightly lower level in the Myc-335$^{-/-}$ mouse as compared with the wild-type colon. (**C**) Loss of major peak of transcription factor Tcf7l2 binding upstream of *Myc* in the Myc-335$^{-/-}$ animals (y axes, extended read coverage). (Inset) Tcf7l2 binding site within this peak. Red denotes the SNP rs6983267 associated with the risk allele in humans, which is normally present in mice.

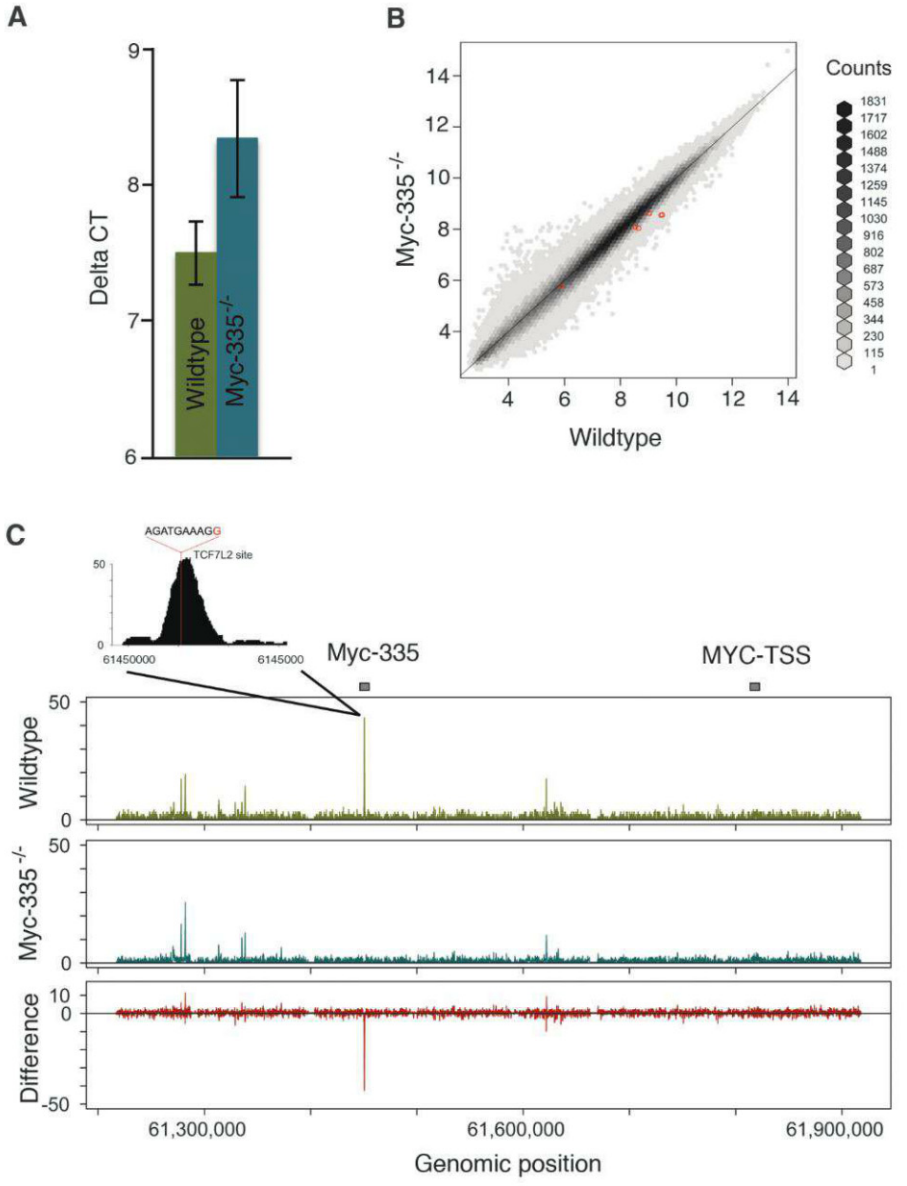

Fig. 3. Reduced incidence of polyp formation in *Apc*$^{min/+}$; Myc-335$^{-/-}$ mice at 4 months of age. (**A**) Microscopic image of intestine showing abundant polyps in *Apc*$^{min/+}$ mice compared with the *Apc*$^{min/+}$; Myc-335$^{-/-}$ mice. Scale bars, 2 mm. (**B**) Box plot summarizing the total numbers of polyps from both small intestine and colon observed per animal (n = 9 for each group). The ends of the whiskers denote the minimum and maximum of each group. The line within the box denotes the median. Student's t test, $P < 0.00038$.

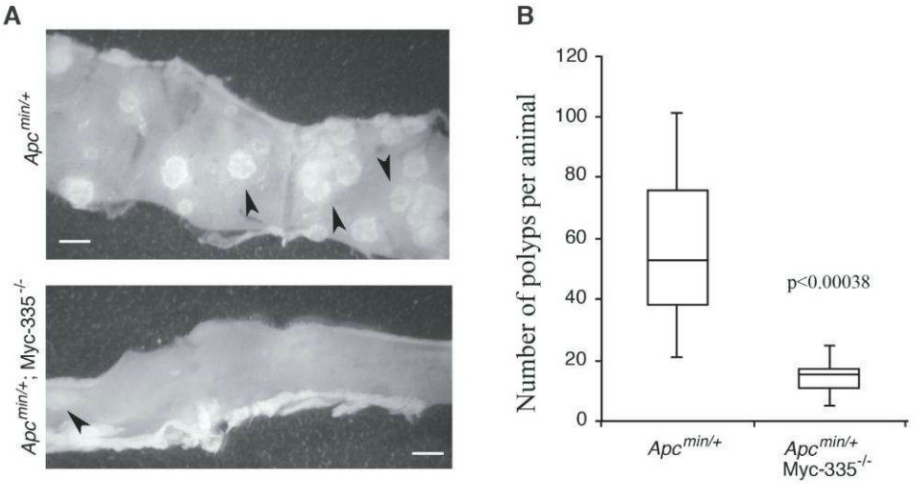

that the loss of Myc-335 did not have a major impact on intestinal cell differentiation. This result is consistent with the lack of effect of Myc loss on homeostasis of intestinal epithelium (*15*–*17*).

A significant difference in *Myc* RNA expression was not observed by qPCR from the duodenum of the Myc-335$^{-/-}$ mice at p1. However, we detected a decreased expression of *Myc* transcripts in the colon of the Myc-335$^{-/-}$ mice both by qPCR and exon array analysis at p1 (Fig. 2, A and B). Chromatin immunoprecipitation and sequencing (ChIP-seq) analysis for Tcf7l2 in adult mouse colon confirmed that, also in mice, the highest peak of Tcf7l2 binding within 1 Mb of *Myc* is located at Myc-335. Binding within this region was completely abolished in the colon of Myc-335$^{-/-}$ mice, and no obvious compensatory changes in binding pattern of Tcf7l2 were observed at other regions within 1 Mb of *Myc* (Fig. 2C). These results indicate that Myc-335 contains a major Tcf7l2 binding site and that its loss results in a modest decrease of *Myc* expression in the mouse colon. However, the Myc-335$^{-/-}$ mice are viable and fertile, indicating that the Myc-335 element is dispensable for function of the mouse intestine under standard mouse housing conditions.

The Myc-335 element was first identified as a conserved element containing a cancer-associated SNP that affects binding of TCF7L2 (*5*, *8*), the transcription factor that is activated in most cases of colorectal cancer (*18*, *19*). Thus, even though Myc-335 is not critical for normal intestinal function, it could still be required for tumorigenesis. To test this, we crossed the Myc-335$^{-/-}$ mice to the *Apc^{min}* mouse strain that spontaneously develops tumors in the small intestine and colon. These tumors are dependent on the activity of Myc (*20*–*22*) and the T cell factor/lymphoid enhancer factor (TCF/LEF) family of transcription factors (*23*–*25*). We generated *Apc$^{min/+}$*; Myc-335$^{-/-}$ mice and scored the number of polyps in the small intestine and colon of these mice at 4 months of age. We found a lower total number of polyps in the intestines of *Apc$^{min/+}$*; Myc-335$^{-/-}$ (n = 9) mice compared with that in the control *Apc$^{min/+}$* mice (n = 9; P < 0.00038; Fig. 3). The effect was observed primarily at the level of frequency of occurrence of tumors. From these results, we conclude that, in laboratory mice, Myc-335 functions as a tumor-specific enhancer element that is dispensable for normal intestinal function but required for tumorigenesis.

Most associations identified by using GWA studies map to noncoding regions whose function is largely unknown. This has been used as an argument against the validity of the GWA approach [for example, (*26*)]. GWA studies have implicated the region containing the SNP rs6983267 as being responsible for more human cancer-associated morbidity than any other known inherited variant or mutation. Our results presented here validate this region by showing that the Myc-335 enhancer has a critical role in intestinal tumorigenesis in mice. Because MYC-335 does not contain other SNPs with similar P values to rs6983267 (*5*), our use of the Myc-335 deletion allele does not affect the conclusion that rs6983267 is the causative SNP in humans.

Our results also highlight the fact that, although a disease-associated polymorphism typically has a relatively modest effect size, the element that it affects can be critically important for the underlying pathological process. In particular, MYC is a promising target for cancer therapy (*27*) that has been difficult to target by direct inhibitors (*28*). Our results suggest that MYC expression could be decreased by inhibitors targeting MYC-335. In a broader context, our finding that the phenotypic effect of Myc-335 loss is tumor-specific suggests that normal growth control and pathological growth induced by cancer can use different mechanisms.

References and Notes

1. F. R. Schumacher *et al.*, *Cancer Res.* **67**, 2951 (2007).
2. L. A. Kiemeney *et al.*, *Nat. Genet.* **40**, 1307 (2008).
3. L. T. Amundadottir *et al.*, *Nat. Genet.* **38**, 652 (2006).
4. B. W. Zanke *et al.*, *Nat. Genet.* **39**, 989 (2007).
5. S. Tuupanen *et al.*, *Nat. Genet.* **41**, 885 (2009).
6. N. F. Wasserman, I. Aneas, M. A. Nobrega, *Genome Res.* **20**, 1191 (2010).
7. N. Ahmadiyeh *et al.*, *Proc. Natl. Acad. Sci. U.S.A.* **107**, 9742 (2010).
8. M. M. Pomerantz *et al.*, *Nat. Genet.* **41**, 882 (2009).
9. J. B. Wright, S. J. Brown, M. D. Cole, *Mol. Cell. Biol.* **30**, 1411 (2010).
10. M. M. Pomerantz *et al.*, *Cancer Res.* **69**, 5568 (2009).
11. N. C. Dubois *et al.*, *Development* **135**, 2455 (2008).
12. A. Trumpp *et al.*, *Nature* **414**, 768 (2001).
13. T. Sato *et al.*, *Nature* **469**, 415 (2011).
14. T. Sato *et al.*, *Nature* **459**, 262 (2009).
15. M. D. Bettess *et al.*, *Mol. Cell. Biol.* **25**, 7868 (2005).
16. J. C. Cohen *et al.*, *BMC Dev. Biol.* **4**, 4 (2004).
17. V. Muncan *et al.*, *Mol. Cell. Biol.* **26**, 8418 (2006).
18. H. Clevers, *Cell* **127**, 469 (2006).
19. J. Taipale, P. A. Beachy, *Nature* **411**, 349 (2001).
20. D. Athineos, O. J. Sansom, *Oncogene* **29**, 2585 (2010).
21. N. A. Ignatenko *et al.*, *Cancer Biol. Ther.* **5**, 1658 (2006).
22. K. Yekkala, T. A. Baudino, *Mol. Cancer Res.* **5**, 1296 (2007).
23. T.-C. He *et al.*, *Science* **281**, 1509 (1998).
24. V. Korinek *et al.*, *Science* **275**, 1784 (1997).
25. P. J. Morin *et al.*, *Science* **275**, 1787 (1997).
26. J. McClellan, M. C. King, *Cell* **141**, 210 (2010).
27. L. Soucek *et al.*, *Nature* **455**, 679 (2008).
28. G. Evan, *Science* **335**, 293 (2012).

Acknowledgments: We thank S. Miettinen and A. Zetterlund for technical assistance. This work was supported by the Academy of Finland grant 140753, postdoctoral researcher's project 134073, Finnish Center of Excellence in Cancer Genetics Research 250345, European Union Framework Program 7 project SYSCOL, European Research Council project GROWTHCONTROL, the Sigrid Juselius Foundation, the Finnish Cancer Society, the Swedish Cancer Society, the Center for Biosciences at Karolinska Institutet, and Vetenskapsrådet.

Supplementary Materials

www.sciencemag.org/cgi/content/full/science.1228606/DC1
Materials and Methods
Figs. S1 to S3
Tables S1 and S2
References (*29*–*32*)

9 August 2012; accepted 15 October 2012
Published online 1 November 2012;
10.1126/science.1228606

Evolution of an MCM Complex in Flies That Promotes Meiotic Crossovers by Blocking BLM Helicase

Kathryn P. Kohl,[1] Corbin D. Jones,[2,3] Jeff Sekelsky[1,2,4]*

Generation of meiotic crossovers in many eukaryotes requires the elimination of anti-crossover activities by using the Msh4-Msh5 heterodimer to block helicases. Msh4 and Msh5 have been lost from the flies *Drosophila* and *Glossina*, but we identified a complex of minichromosome maintenance (MCM) proteins that functionally replace Msh4-Msh5. We found that REC, an ortholog of MCM8 that evolved under strong positive selection in flies, interacts with MEI-217 and MEI-218, which arose from a previously undescribed metazoan-specific MCM protein. Meiotic crossovers were reduced in *Drosophila rec*, *mei-217*, and *mei-218* mutants; however, removal of the Bloom syndrome helicase (BLM) ortholog restored crossovers. Thus, MCMs were co-opted into a novel complex that replaced the meiotic pro-crossover function of Msh4-Msh5 in flies.

Crossovers (COs) between homologous chromosomes can be beneficial or detrimental, depending on their context (*1*). Meiotic COs increase genetic diversity and promote accurate chromosome segregation, whereas mitotic COs can lead to loss of heterozygosity, potentially triggering tumorigenesis. Mitotic COs are prevented by "anti-CO" proteins. A key anti-CO protein is the Bloom syndrome helicase BLM, which generates non-CO products by unwinding recombination intermediates that might otherwise be processed into COs (*2*). In meiosis, CO formation is encouraged through inhibition of anti-CO proteins. The budding yeast Msh4-Msh5 heterodimer antagonizes the BLM ortholog Sgs1 (*3*). Msh4 and Msh5 are found in all metazoans for which sequence is available, except *Drosophila* species and their fellow schizophoran *Glossina morsitans*, the tsetse fly (figs. S1 and S2). The lack of recognizable orthologs of these

proteins suggests that these species evolved another protein or complex to block the anti-CO activity of BLM.

Like *Saccharomyces cerevisiae Msh4* and *Msh5* mutants, the only defects in *Drosophila rec*, *mei-217*, and *mei-218* mutants are in meiotic recombination (*4*–*9*). REC is orthologous to MCM8 (*6*); MCMs have properties reminiscent of Msh4-Msh5. MCM2 through MCM7, which are essential for replication in eukaryotes, form a heterohexamer that encircles DNA (*10*). Similarly, Msh4-Msh5 is thought to encircle recombination intermediates (*11*). In both cases, this activity is regulated by adenosine triphosphate (ATP) binding and hydrolysis (*10*, *11*).

MEI-217 initially appeared to be novel, because BLAST searches failed to identify homologs outside dipterans, and searches of the Conserved Domain Database (CDD) (*12*) did not detect any domains. BLAST searches with MEI-218 identified a single putative ortholog in metazoans (figs. S1 and S2). A CDD search returned a hit to the MCM domain in the C terminus of MEI-218, but the score was low and the match covered only one-third of the domain (fig. S3A). To verify the presence of this domain, we conducted structure-based searches with PHYRE (Fig. 1A) (*13*). This analysis revealed that the C terminus of MEI-218 has a structure similar to that of the AAA adenosine triphosphatase (ATPase) domain of MCMs (fig. S3B). Canonical MCMs have both an N-terminal MCM domain and a C-terminal ATPase domain. The N-terminal domain is present in vertebrate MEI-218 but not in *Drosophila* MEI-218. However, PHYRE with MEI-217 shows that its predicted structure is similar to the MCM N-terminal domain. Because MEI-217 and MEI-218 are encoded by overlapping open reading frames on the same transcript (*7*), we infer that they evolved from an MCM-like protein represented by a single polypeptide in other metazoans.

The shared phenotypes and MCM domains suggest that REC, MEI-217, and MEI-218 function together in meiotic recombination. To distinguish them from the replicative MCMs, we refer to REC, MEI-217, and MEI-218 as "mei-MCMs." Because MCM2 through MCM7 function together as a heterohexamer, we investigated whether the mei-MCMs form a complex. MEI-217 interacted strongly with both the C-terminal third of MEI-218 and REC (Fig. 1, B and C), which suggests that the mei-MCMs form a complex. This complex likely also contains one or more replicative MCMs. A meiosis-specific mutation in *Mcm5* causes the same phenotypes as *mei-MCM* mutants (*14*), making MCM5 a strong candidate to be a component of the complex.

Noting the genetic and biochemical similarities between mei-MCMs and Msh4-Msh5, we hypothesized that the mei-MCMs antagonize *Drosophila melanogaster* BLM (DmBLM) in lieu of Msh4-Msh5. This hypothesis predicts that removing DmBLM should compensate for *mei-MCM* mutations; in budding yeast, the CO defect in *msh4* mutants is suppressed by removing Sgs1 (*3*). Few COs were made in *rec* and *mei-218* single mutants, resulting in high nondisjunction (NDJ) of meiotic chromosomes (Fig. 2A). In contrast, mutations in *mus309*, which encodes DmBLM, caused only a mild reduction in COs and correspondingly low levels of NDJ. Strikingly, *mus309* mutations suppressed the high-NDJ phenotype of *rec* and *mei-218* mutants (Fig. 2A). Furthermore, the low CO rate in *rec* mutants returned to an approximately wild-type rate in *mus309 rec* double mutants (Fig. 2B, fig. S4, and tables S1 to S4); this finding indicates that mei-MCMs are not essential for generating meiotic COs if DmBLM is absent, thereby supporting our hypothesis that mei-MCMs oppose the known anti-CO activities of DmBLM (*15*, *16*).

mei-MCMs appear to functionally replace Msh4-Msh5 in Schizophora, and presumably

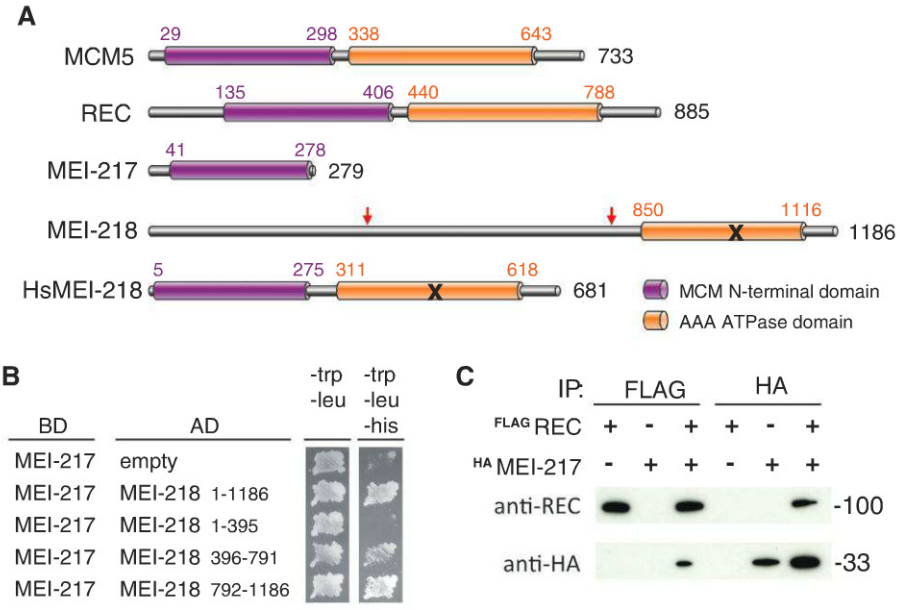

Fig. 1. (**A**) Structural domains identified through PHYRE. "MCM N-terminal domain" corresponds to Protein Data Bank fold ID 3f9v and "AAA ATPase domain" to fold ID 3f8t. The "x" on *Drosophila* and human (Hs) MEI-218 symbolizes changes in the ATP binding and hydrolysis motifs predicted to abolish ATPase activity (fig. S3B). Red arrows on MEI-218 indicate segments used in yeast two-hybrid analysis. (**B**) Yeast two-hybrid interactions between MEI-217 and MEI-218. Cells expressing the indicated fusions to the GAL4 DNA binding domain (BD) or activating domain (AD) were streaked onto selective media. Growth on –trp –leu –his indicates an interaction. (**C**) Coimmunoprecipitation of REC and MEI-217. Epitope-tagged mei-MCMs were coexpressed in insect cells, immunoprecipitated with antibodies to the indicated epitope tags, blotted, and probed with antibodies to REC and to the hemagglutinin (HA) tag (*19*).

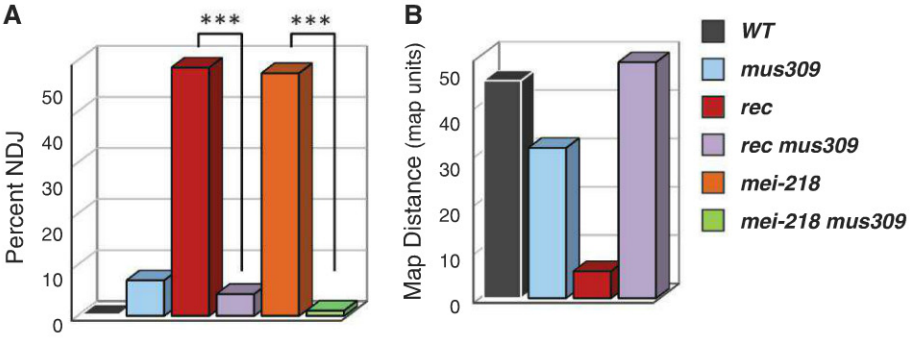

Fig. 2. (**A**) X chromosome nondisjunction (NDJ) across more than 1500 individuals for each genotype except *mei-218; mus309* ($n = 383$). ***$P < 0.0001$. (**B**) Summed map distance in map units (equivalent to centimorgans) across five intervals spanning ~20% of the genome for more than 1000 individuals for each genotype (*19*). $P < 0.0001$ for all comparisons except wild-type versus *mus309 rec*, $P = 0.0674$.

[1]Curriculum in Genetics and Molecular Biology, University of North Carolina, Chapel Hill, NC 27599, USA. [2]Department of Biology, University of North Carolina, Chapel Hill, NC 27599, USA. [3]Carolina Center for Genome Sciences, University of North Carolina, Chapel Hill, NC 27599, USA. [4]Program in Molecular Biology and Biotechnology, University of North Carolina, Chapel Hill, NC 27599, USA.

*To whom correspondence should be addressed. E-mail: sekelsky@unc.edu

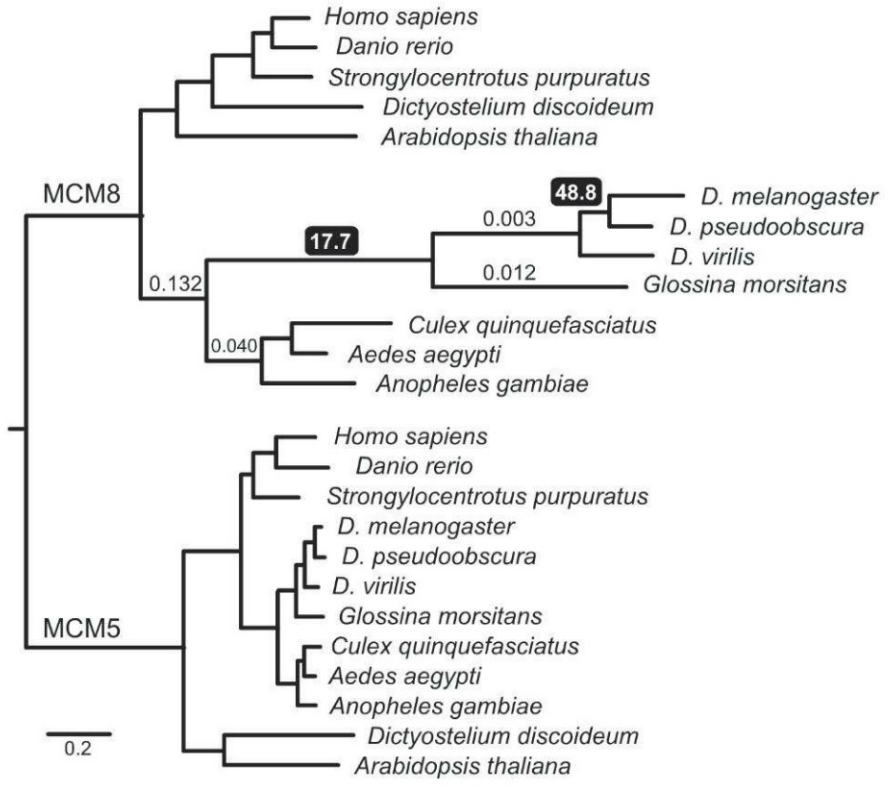

Fig. 3. Maximum likelihood tree from an alignment of the conserved MCM domains of MCM8/REC and MCM5 from diverse taxa. Branch lengths indicate the number of substitutions per site (see scale). Numbers above branches show dN/dS estimates for selected branches; those with black background highlight branches with dN/dS estimates greater than 1, suggesting positive selection. See fig. S6 for more description and additional dN/dS estimates.

evolved to do so in response to natural selection. Several evolutionary scenarios could lead to this result (fig. S5), but most predict that there would be evidence of adaptive divergence of *mei-MCM* genes in Schizophora. REC was previously noted to be highly diverged in *Drosophila* (*6*, *17*); we found that *Glossina* MCM8/REC is similarly divergent (Fig. 3). The presence or absence of MCM8 correlates with that of its functional partner MCM9 throughout eukaryotes, except in *Drosophila* and *Glossina*, which retained MCM8/REC while losing MCM9 (figs. S1 and S2). The loss of MCM9 suggests that MCM8 evolved a novel function in an ancestor to Schizophora.

Divergence in *rec* and loss of MCM9 occurred after the split between mosquitos and higher flies 200 to 250 million years ago, but prior to the emergence of the Schizophora 65 million years ago. To test whether patterns of sequence evolution were consistent with positive selection leading to the divergence of *rec*, we estimated the ratio between the rate of base pair substitutions at nonsynonymous sites (dN) and the rate at synonymous sites (dS) among dipterans in *MCM8/rec*. We compared 15 evolutionary models, ranging from conservation of dN/dS ratios across all taxa surveyed to allowing free evolution of dN/dS ratios along all branches, and including models testing specific hypotheses about the evolution of *rec* along different branches of the insect phylogeny. The best-fitting model ($P = 0.0002$ versus the next best model) supports the hypothesis that rapid protein-coding divergence was driven by positive selection prior to the split of tsetse flies from fruit flies (Fig. 3, fig. S6, and table S5). Thus, we infer that natural selection likely drove the repurposing of REC into its new role as an antagonist of DmBLM. Recent evolution of *rec* shows much lower levels of nonsynonymous changes, suggesting subsequent functional constraint (fig. S6). MEI-217 and MEI-218 have also diverged substantially from the ancestral MCM structure: They split into two polypeptides, and MEI-218 acquired an N-terminal extension (figs. S7 and S8).

Our data show that flies evolved a novel MCM complex to antagonize the anti-CO functions of BLM during meiosis—a role held by Msh4-Msh5 in other organisms. Although we do not know what evolutionary forces ultimately drove the loss of Msh4-Msh5 and the repurposing of mei-MCMs, it is tempting to speculate that these forces also led to another fundamental meiotic difference in *Drosophila* and *Glossina* relative to mosquitoes: the absence of recombination in males, which was first noted in *Drosophila* by Morgan 100 years ago (fig. S5) (*18*). Resolving the conundrum of why the mei-MCMs supplanted Msh4-Msh5 will require a deeper understanding of both the evolutionary origins of the mei-MCMs and the functional differences between mei-MCMs and Msh4-Msh5.

References and Notes

1. S. L. Andersen, J. Sekelsky, *Bioessays* **32**, 1058 (2010).
2. W. K. Chu, I. D. Hickson, *Nat. Rev. Cancer* **9**, 644 (2009).
3. L. Jessop, B. Rockmill, G. S. Roeder, M. Lichten, *PLoS Genet.* **2**, e155 (2006).
4. P. Ross-Macdonald, G. S. Roeder, *Cell* **79**, 1069 (1994).
5. N. M. Hollingsworth, L. Ponte, C. Halsey, *Genes Dev.* **9**, 1728 (1995).
6. H. L. Blanton *et al.*, *PLoS Genet.* **1**, e40 (2005).
7. H. Liu, J. K. Jang, J. Graham, K. Nycz, K. S. McKim, *Genetics* **154**, 1735 (2000).
8. B. S. Baker, A. T. C. Carpenter, *Genetics* **71**, 255 (1972).
9. E. A. Manheim, J. K. Jang, D. Dominic, K. S. McKim, *Mol. Biol. Cell* **13**, 84 (2002).
10. D. Remus *et al.*, *Cell* **139**, 719 (2009).
11. T. Snowden, S. Acharya, C. Butz, M. Berardini, R. Fishel, *Mol. Cell* **15**, 437 (2004).
12. A. Marchler-Bauer *et al.*, *Nucleic Acids Res.* **39**, D225 (2011).
13. L. A. Kelley, M. J. Sternberg, *Nat. Protoc.* **4**, 363 (2009).
14. C. M. Lake, K. Teeter, S. L. Page, R. Nielsen, R. S. Hawley, *Genetics* **176**, 2151 (2007).
15. M. D. Adams, M. McVey, J. J. Sekelsky, *Science* **299**, 265 (2003).
16. M. McVey, S. L. Andersen, Y. Broze, J. Sekelsky, *Genetics* **176**, 1979 (2007).
17. Y. Liu, T. A. Richards, S. J. Aves, *BMC Evol. Biol.* **9**, 60 (2009).
18. T. H. Morgan, *Science* **36**, 719 (1912).
19. See supplementary materials on *Science* Online.

Acknowledgments: We thank K. McKim for helpful discussions and for sharing unpublished results, and N. Crown and other members of the Sekelsky laboratory for helpful comments on the manuscript. Supported by NIH grant GM061252 (J.S.), NSF grant MCB-0618691 (J.S., C.D.J., and G. C. Copenhaver), and NIH grant 5T32GM007092 (K.P.K.). Alignments and trees were submitted to TreeBASE (http://purl.org/phylo/treebase/phylows/study/TB2:S13435).

Supplementary Materials

www.sciencemag.org/cgi/content/full/338/6112/1363/DC1
Materials and Methods
Figs. S1 to S8
Tables S1 to S7
References (*20*–*43*)

31 July 2012; accepted 5 October 2012
10.1126/science.1228190

Tissue Engineering

Cell Culture Enters the Third Dimension

Scientists have been culturing mammalian cells in flat petri dishes for decades, but a new generation of tools and techniques is now letting them grow three-dimensional cultures that more closely mimic the biology of real tissues. **By Alan Dove**

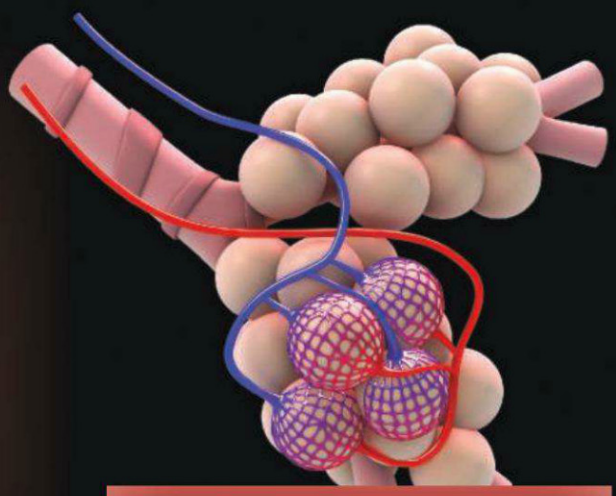

Ingber's team built a "lung-on-a-chip," with epithelial cells growing on flexible membranes to form 3-D structures that resemble alveoli and microfluidic devices feeding and maintaining the cells.

In 1907, Anatomist Ross Harrison removed developing neural tubes from frog embryos, placed them in a solution of frog lymph on a coverslip, and inverted the mixture over a glass slide with a depression in it so the explanted tissue could grow in a hanging drop. Neurons in these first tissue cultures continued their normal three-dimensional growth patterns, allowing Harrison to see how nerve fibers extended themselves during development.

Later generations of cell biologists moved tissue culture into two-dimensional petri dishes, where lines of transformed cells could establish uniform monolayers that were much easier to maintain and subculture than Harrison's hanging drops. These 2-D cultures revolutionized virology and molecular biology. However, flat cells on a plastic plate are at best mediocre models for complex tissues in the body, and researchers kept trying to develop systems that would combine 3-D physiological relevance with 2-D convenience.

Now, advances in materials engineering, manufacturing, and cell biology are finally starting to turn 3-D cell culture from a finicky, specialized technique into a mainstream tool for biologists. The result is a slew of new platforms and methods, ranging from simple, easy-to-use products for growing tiny cellular spheres to esoteric technologies that recapitulate entire organs in vitro.

A LITTLE MOLD CAN BE A GOOD THING

"[Some] of the problems through the years have been that the formats for 3-D cell culture have been expensive, cumbersome, [and] difficult to work with," says Jeff Morgan, president and chief executive officer of **Microtissues** in Providence, Rhode Island. However, many scientists have been willing to tolerate these problems in order to use 3-D cultures. Indeed, even Harrison's original hanging-drop method remains a staple technique in some areas of cell biology, despite its limitations.

Hoping to make 3-D systems more convenient and flexible, Morgan and his colleagues found a surprisingly simple solution: agarose. Cells grown on the ubiquitous gelling reagent can't stick to its surface. That would be a disaster for conventional 2-D cultures, which depend on surface adhesion to form monolayers, but Microtissues turns nonadhesion into an asset. In the company's system, cells fall into tiny wells molded into the surface of the agarose, where they form spherical structures.

"Microtissues' 3-D petri dish is a micromolded nonadhesive hydrogel that the cells don't attach to, which allows them to attach to each other," says Morgan, adding that in this case "the cells are actually self-assembling." The resulting spheroids form tight connections between cells, creating gap junctions and other features of intact tissues. So far, investigators have grown more than 40 different cell lines this way, including both primary and transformed cells.

Rather than sell preformed agarose plates, the company sells molds that researchers can autoclave and reuse as many times as necessary, casting new plates whenever they need them. The molds fit into standard 12- or 24-well plastic cell culture dishes. Within each well, a mold can create 96 microwells, so pipetting a

UPCOMING FEATURES

The Connectome—January 18, 2013

Genomics—February 15, 2013

Proteomics—March 1, 2013

CREDIT: (© ISTOCKPHOTO.COM/ERAXION

single aliquot of suspended cells into the dish will create 96 individual spheroids. That's a lot easier than creating an equivalent number of hanging drop cultures. "A hanging drop might dry out, and a 96-well plate for the hanging drop is 96 pipetting steps. In our case we've got one pipetting step in a gel that makes 96 spheroids, and they're in a hydrogel that's stable for two weeks and beyond for long-term culture," says Morgan. The number of cells in the aliquot determines the size of the spheroids, making the system easy to modify.

Researchers are already using the molds for a variety of studies. For example, "there's exciting work with stromal-cancer cell interactions," says Morgan, adding that by creating spheroids with mixed cell types tumor biologists can manipulate and study the interactions directly. To do this, researchers simply combine the two cell types into the desired ratio, pipet them onto a gel, and after they settle, the cells form a mixed spheroid with the different cell types interacting. In another project, investigators are seeding tumor stem cells into the agarose plates, allowing individual wells to host microtumors derived from single cells.

CLIMBING THE SCAFFOLD

No matter how flexible a platform appears to be, though, no 3-D culture system will cover all applications. "We appreciate that there's no single technology for all needs, there's horses for courses in many respects, and the investigator will select the tools and technologies most appropriate to enable them to answer their biological question," says Stefan Przyborski, chief scientific officer of **Reinnervate** in Sedgefield, United Kingdom.

Reinnervate is one of several companies offering scaffold-based 3-D culture systems. Instead of growing into spheroids of a fixed size, cells in a scaffold can form sheets that mimic many types of animal tissues. In the early 2000s, Przyborski and his colleagues at Durham University were studying xenograft tumors that formed when they transplanted stem cells into animals. "The stem cells were producing all these complex tumors and tissues, and one of the major challenges of stem cell science is to be able to reproduce that level of complexity in vitro," says Przyborski.

To do that, he created thin, highly porous membranes from polystyrene—the same material used for standard tissue culture plates. Cells can grow inside the porous membrane and form 3-D structures with multiple layers. Researchers can manipulate the system to recreate different types of environments, for example by placing the membrane at the bottom of a culture dish so that it only receives nutrients from one side, or suspending it to expose it to the medium on both sides. Because the scaffold is polystyrene, investigators can also coat it with collagen or other matrix molecules used with traditional 2-D cultures. Reinnervate now sells the membranes under the Alvetex brand name, in versions precut for standard cell culture dishes.

Though product manufacturers are taking pains to make 3-D culture user-friendly, newcomers to the technique should still expect some learning experiences. Technical support from the vendor is crucial. "We have technical services to help [customers] overcome any issues, help them optimize the system, and get the most out of the technology," says Przyborski.

Algimatrix, which is derived from the tissues of marine sponges, has no growth factors in it. However, it allows researchers to fine-tune their cells' environment.

Besides adapting established cell lines from 2-D to 3-D culture, scientists may find themselves puzzling over other parts of their research routines. "One of the questions we get regularly is 'how do you visualize cells in 3-D,' because when you think about it all the imaging technologies are all built around 2-D cell culture," says Przyborski. Reinnervate offers coaching on 3-D culture visualization as well as other common obstacles new users encounter.

Some problems of scaffold-based cell culture aren't easy to solve though, at least not yet. One major challenge is that current scaffolding systems aren't amenable to standard passaging techniques, so researchers have to restart new 3-D cultures from established 2-D lines periodically. Przyborski and his colleagues are working on methods that will address that, and are also developing perfusion techniques to feed scaffold-grown cells continuously. "If we maintain the cell line in 3-D, it adapts and becomes different and actually is more in vivo-like, so then you get more accurate data," says Przyborski.

AN EXPANDING MATRIX OF CHOICES

Researchers who want to start using 3-D cultures will find themselves in good company; growing more tissue-like structures has become a major focus of both basic and applied research labs. "There have been technologies developed in the past few years that have enabled better 3-D cell culture, and also there's a movement towards getting more in vivo-like data from cell systems," says David Welch, associate director of global market development for primary and stem cell systems at **Life Technologies** in Carlsbad, California.

Don Finley, product manager at **Sigma-Aldrich** in St. Louis, Missouri, concurs: "3-D cell culture is perceived as a way to better mimic the in vivo situation and what's in the human without actually having to use humans." That motivation is especially powerful in the pharmaceutical industry, where recent clinical trial failures have highlighted the need for more continued>

CREDIT: © ISTOCKPHOTO.COM/CUNFEK

Tissue Engineering

predictive preclinical assays for drug efficacy and toxicity.

To help scientists move their cells into the third dimension, Life Technologies now offers three scaffolding products with different features: Geltrex, Cellstart, and Algimatrix. "Geltrex is derived from mouse tumors, and it contains within it a lot of growth factors and other things that can stimulate cell growth," explains Welch. Cellstart, meanwhile, consists of exclusively human and recombinant materials, for researchers doing clinical research where animal components could cause rejection and other side effects. Algimatrix, which is derived from the tissues of marine sponges, has no growth factors in it. However, it allows researchers to fine-tune their cells' environment. "You can change the hardness or the rigidity of the structure by adding a supplement, so you can make it softer or harder, and that makes it more or less amenable to different environments and different cell types," says Welch.

Algimatrix isn't the only tunable scaffold on the market. Hydromatrix, made by **Alphagenix** in West Lafayette, Indiana, is composed of synthetic peptide nanofibers. Altering the concentration of the Hydromatrix solution adjusts the 3-D architecture of the self-assembling peptides. The company also makes a scaffold called Maxgel, which includes human extracellular matrix components. Sigma-Aldrich carries both products, and also sells specially designed cell culture bioreactors manufactured by **3-D Biotek** in North Brunswick, New Jersey. "I see this as a toolkit, and we're at a stage where researchers are going to have to do what they do and help us understand what works best with different cell lines," says Finley.

The diversity of choices underscores the need for tinkering and experimentation in getting a new 3-D cell culture system working. "It probably depends on the cell type and the application," says Welch, adding that "not all matrices or technologies that have been developed work for all cell types." Lisa Masterson, a product manager at Sigma-Aldrich, agrees: "I don't really see any one particular matrix, whether it be synthetic or native, as being a huge winner at this point."

PATIENT ON A CHIP

As lab suppliers and their early adopter customers work to set up relatively simple 3-D cell cultures, some scientists are pushing the far edge of the field into the realm of science fiction. One of them is Don Ingber, director of the **Wyss Institute at Harvard University** in Boston, Massachusetts. Flush with $37 million in funding from the Defense Advanced Research Projects Agency, Ingber and his colleagues are now building what amounts to a miniature person: a series of 3-D cell cultures and microfluidic devices that will form 10 interconnected artificial organs, providing a sophisticated in vitro model of human physiology.

Several of the organs are already working, and they're enabling previously impossible experiments. "If you work on the lung and you want to get access to the lumen, [when] you have epithelial cells from a lung in a matrix gel in 3-D, they form spheroids, and you really can't get to the center," says Ingber. Animal models have normal lung lumens, but can't be studied for long periods or manipulated as extensively as cultured cells. To get around that, Ingber's team built a "lung-on-a-chip," with epithelial cells growing on flexible membranes to form 3-D structures that resemble alveoli and microfluidic devices feeding and maintaining the cells. That system revealed that breathing motions may play a crucial role in the pathogenesis of bacterial pneumonia.

In another project, the team built a gut-on-a-chip, which allows human intestinal cells to grow in the presence of peristaltic straining forces. The cells organize themselves into villi, with gene expression patterns that mimic real human intestine. Moreover, the researchers were able to co-culture bacteria on top of the artificial gut without killing the cells. "We can start putting bacteria on the lumenal face of the intestinal epithelium, and the human epithelial cells are perfectly happy. Normally in a 2-D culture we'd call that contamination and you'd have to kill the dish," says Ingber.

Ingber concedes that the organ-chip prototypes have been difficult to build, particularly when it comes to introducing small numbers of cells into the minuscule growth chambers, but once established, the systems can survive for as long as a month. Microperfusion systems keep the cells alive, obviating the need for constant feeding and subculturing.

The investigators are now trying to iron out the bugs in the chips' production, with an eye toward making them more widely available for research. "I think it's one of these things where it's not like any one technical thing is such a hurdle, it's just putting it all together so people who know nothing about cells can use it," says Ingber.

Ultimately, the researchers hope to recapitulate enough human biology in chip-based systems to provide reliable preclinical models of pathogenesis and drug activity. Replacing racks of mouse cages with incubators full of automated homunculi may sound far-fetched, but it's exactly what Ingber intends to do: "I think one by one we'll replace animal models."

FEATURED PARTICIPANTS

3-D Biotek
www.3dbiotek.com

Alphagenix
purdueresearchpark.com/businessprofiles/alphagenix-inc

Life Technologies
www.lifetechnologies.com

Microtissues
www.microtissues.com

Reinnervate
www.reinnervate.com

Sigma-Aldrich
www.sigmaaldrich.com

Wyss Institute at Harvard University
wyss.harvard.edu

Alan Dove is a science writer and editor based in Massachusetts.

DOI: 10.1126/science.opms.p1200070

New Products: Tissue Enigineering

3-D HANGING DROP PLATES

The new Perfecta3D Hanging Drop Plates allow researchers to form and test reproducible 3-D cell cultures in a 96-well format. The unique design of the Perfecta3D Hanging Drop Plates simplifies and streamlines spheroid formation, culture, and subsequent testing of the 3-D cellular constructs without the aid of coatings or matrices. Spheroid cultures grown in Perfecta3D Hanging Drop Plates allow researchers to easily mimic tissue metabolic and proliferative gradients, capture complex cell-matrix and cell-cell interactions, conduct co-cultures, and monitor cell growth easily and regularly. Media and compounds can be added or removed from the top of the plate without requiring new equipment, and spheroids can be harvested for analysis. Users simply pipet a cell suspension into each channel; the channel shape causes the drop to securely hang from the bottom of the well. One spheroid forms per well, and the spheroid diameter is controlled by the cell type and number of cells added to each well.

3D Biomatrix

For info: 734-272-4688 | www.3dbiomatrix.com

3-D CULTURE CELL HARVESTING KIT

3-D cultures exhibit cellular behaviors and morphologies similar to those seen in vivo; however, the adaptation of 3-D culture models for studying biochemical processes has been impeded by the challenge of separating intact or 3-D grown cells from extracellular proteins comprising the 3-D matrix. The Cultrex 3D Culture Cell Harvesting Kit is based on a nonenzymatic approach that prevents biochemical degradation during processing and overcomes the problems associated with extracting cells from 3-D culture in BME or Laminin I. The quality of the harvested cells is ideal for Western blotting and RNA and DNA analysis. This new kit provides an optimized and standardized solution for the isolation and normalization of cell lysates from 3D Culture Matrix, BME, or Laminin I for subsequent biochemical analysis.

AMS Biotechnology

For info: +44-(0)-1235-828200 | www.amsbio.com

CELL CULTURE PLATFORM

The Cytoo 2D+ Cell Culture Platform is based on the of use micropatterns on plates to drive/control the behavior and localization of cells in cultures. Modifying cell shape can be a very efficient way to modify cell functions, including cell fate and differentiation. Cells are exquisite mechano-sensing systems and adapt permanently to their boundary conditions. Thus, contrary to the frequent opinion that classical 2-D culture on infinite adhesive substrates are more representative of cell behavior (as cells are 'free' to spread and move), these conditions introduce a considerable, and unnoticed, variability in cell functions. 2D+ Technology controls the 3-D shape of cultured cells by controlling the 2-D topology of cell adhesion and setting the cell shape in the *z* axis. Since each micropattern is identical (several hundred per well), cells perform in a reproducible and consistent manner. Thus, fewer precious primary cells and less replicates per data point are needed.

Cytoo

For info: +33-(0)-438-884705 | www.cytoo.com

3-D CELLULAR IMAGING SOFTWARE

Volocity 6.0 is a 3-D cellular imaging software featuring a suite of high-performance tools for exploring, interacting, and publishing 3-D imaging data from cells, tissues, and organisms and how they behave over time. The software is designed as a universal solution that provides users with significant functionality to visualize, analyze, and validate 3-D fluorescence images from a wide range of confocal microscopy, wide-field, and high-content screening systems, and is fully integrated for a seamless user experience. Beyond simple cells, the Volocity software can also organize and relate measurements according to biological classification such as nuclei, membranes, organelles, and proteins, making it easier and faster to perform an analysis and understand the results. The updated interface also enables users of all skill levels to perform complex and challenging biological measurements, thereby extending the power of 3-D analysis to a wider population of potential users.

PerkinElmer

For info: 877-754-6973 | www.perkinelmer.com

STEM CELL CULTURE MEDIUM

Stemline Pluripotent Culture Medium is a novel human pluripotent stem cell culture medium that provides a consistent environment for the long-term maintenance and growth of healthy pluripotent stem cells. Stemline Pluripotent Culture Medium performs equivalently to the leading medium for maintaining pluripotency and optimal growth rates and is produced more efficiently than traditional media, resulting in lower costs. Culturing pluripotent stem cells can be challenging as many media's undefined, heterogenous mixtures can cause inconsistent growth rates and undesired spontaneous differentiation. The Stemline Pluripotent Stem Cell Culture Medium is serum-free, composed of fully defined components and has 80% less basic fibroblast growth factor than the leading pluripotent stem cell culture medium. This provides a consistent environment for long-term maintenance of optimal growth rates, viability, and pluripotency.

Sigma Life Science

For info: 800-325-3010 | www.sigma.com/stemlinepsc

Electronically submit your new product description or product literature information! Go to **www.sciencemag.org/products/newproducts.dtl** for more information.

Newly offered instrumentation, apparatus, and laboratory materials of interest to researchers in all disciplines in academic, industrial, and governmental organizations are featured in this space. Emphasis is given to purpose, chief characteristics, and availability of products and materials. Endorsement by *Science* or AAAS of any products or materials mentioned is not implied. Additional information may be obtained from the manufacturer or supplier.

Science Careers Advertising

For full advertising details, go to ScienceCareers.org and click For Employers, or call one of our representatives.

Tracy Holmes
Worldwide Associate Director
Science Careers
Phone: +44 (0) 1223 326525

THE AMERICAS

E-mail: advertise@sciencecareers.org
Fax: 202-289-6742

Tina Burks
East Coast/West Coast/South America
Phone: 202-326-6577

Allyson Rosen
Midwest/Canada/Corporate
Phone: 202-326-6578

Marci Gallun
Sales Administrator
Phone: 202-326-6582

Online Job Posting Questions
Phone: 202-312-6375

EUROPE & REST OF WORLD

E-mail: ads@science-int.co.uk
Fax: +44 (0) 1223 326532

Ben Asfaha
Phone: +44 (0)1223 326529

Lucy Nelson
Phone: +44 (0)1223 326527

Kelly Grace
Phone: +44 (0) 1223 326528

JAPAN

Yuri Kobayashi
Phone: +81-50-3696-5100
E-mail: ykobayas@aaas.org

CHINA & TAIWAN

Ruolei Wu
Phone: +86-1367-1015-294
E-mail: rwu@aaas.org

All ads submitted for publication must comply with applicable U.S. and non-U.S. laws. *Science* reserves the right to refuse any advertisement at its sole discretion for any reason, including without limitation for offensive language or inappropriate content, and all advertising is subject to publisher approval. *Science* encourages our readers to alert us to any ads that they feel may be discriminatory or offensive.

Science Careers
From the journal *Science* AAAS

STANFORD
SCHOOL OF MEDICINE

Director of Translational Research

The Department of Medicine at Stanford University is recruiting a Director of Translational Research to lead the translational research program of the Department. The faculty position is at the Associate Professor or Professor level in the Medical Center Line or the University Tenure Line. The predominant criterion for appointment in the University Tenure Line is a major commitment to research and teaching. The major criteria for appointment for faculty in the Medical Center Line shall be excellence in the overall mix of clinical care, clinical teaching, scholarly activity that advances clinical medicine, and institutional service appropriate to the programmatic need the individual is expected to fulfill. Faculty rank will be determined by the qualifications and experience of the successful candidate and the appointment will be in the appropriate Division depending on the successful applicant's area of expertise. The successful candidate should be an accomplished investigator with a national reputation in translational research. Candidates must have an MD, PhD, or MD/PhD degree.

He/she will work with the Department leadership to guide the Department in all aspects of translational research, including the recruitment of translational investigators to form a core research group. The Director of Translational Research will lead the Departmental effort to serve as the bridge between basic and clinical investigation and reach out to investigators in other Departments at Stanford and engage them in multidisciplinary translational research. The Director will work with the training programs in the Department to involve trainees in translational research and guide them in collaborative investigative teams. The successful candidate must have leadership skills, administrative experience, a record of outstanding research accomplishments, and strong mentoring skills. A track record of translating discoveries from the laboratory into patient care is critical. A history of involvement and leadership with investigation in both academics and industry is highly desirable. The Department of Medicine benefits from an outstanding scientific and clinical environment at Stanford, including active collaborations with the clinical and basic science departments and the Stanford Institutes.

Candidates should submit a detailed letter of interest and curriculum vitae to: **Gretchen Picache, Department of Medicine, Stanford University School of Medicine, 1070 Arastradero Rd, Rm 255, Palo Alto CA 94304, Mail Code:5850; gpicache@stanford.edu.**

Stanford University is an equal opportunity employer and is committed to increasing the diversity of its faculty. It welcomes nominations of and applications from women and members of minority groups, as well as others who would bring additional dimensions to the University's research, teaching and clinical missions.

In **2013, CNRS** is **recruiting 307** permanent **researchers**

in all scientific fields
life sciences, chemistry, environmental sciences and sustainable development, humanities and social sciences, computer sciences, engineering, mathematics, physics, nuclear and particle physics, earth sciences and astronomy.

Online registration at www.**cnrs**.fr
from **December 3, 2012**
Registration deadline **January 7, 2013**

cnrs
www.cnrs.fr

Georgia Tech College of Sciences

The **Georgia Institute of Technology** is one of the top ranked educational/research institutions in the country and ranks as one of the best places to work. As part of significant growth in the biological sciences, the **School of Applied Physiology and School of Biology** are seeking applications for two tenure-track positions in the area of **Developmental Molecular Biology**, with an interest in regenerative biology, neural, cranio-facial and/or musculo-skeletal systems using genetics, cellular and systems physiology and/or chemical/synthetic biology. Candidates will be favored whose research integrates well with the Institute's existing strengths in molecular and cell biology, biomedical engineering and computational sciences. Georgia Tech has a strong interdisciplinary environment where collaborations between faculty in science, engineering and computing are encouraged.

It is anticipated that these positions will be filled at the assistant/associate professor level, but outstanding senior candidates with exceptional records are encouraged to apply. Candidates should upload a letter of application, full curriculum vitae, statement of research interests and plans, and arrange for three letters of reference to **http://searches.biology.gatech.edu**. Review of applications begins **January 15, 2013** and will continue until positions are filled.

Georgia Tech is a unit of the University System of Georgia and an Affirmative Action/Equal Opportunity Employer and requires compliance with Immigration Control Reform Act of 1986.

GEORGIA INSTITUTE OF TECHNOLOGY

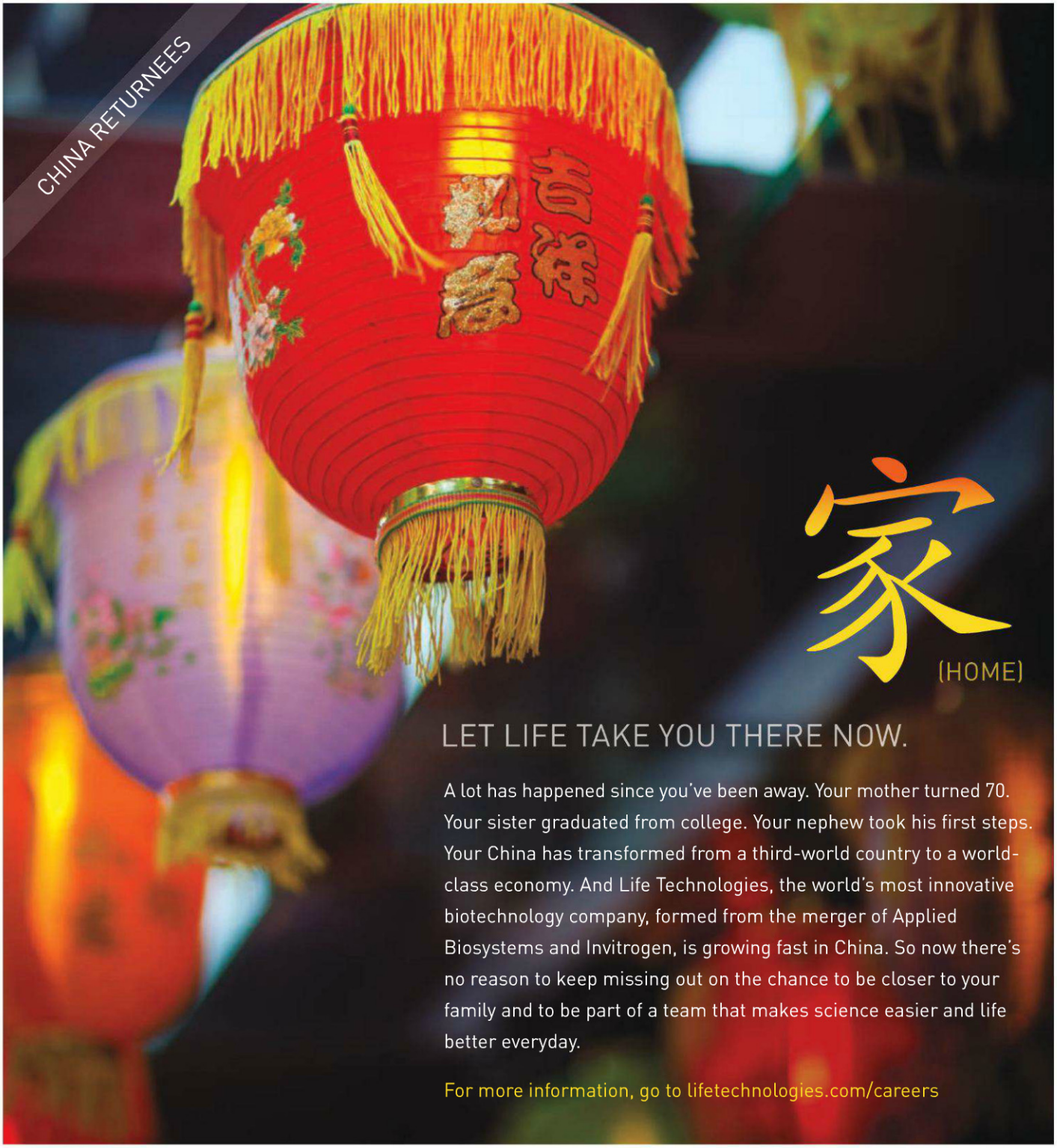

We want to hear from you. Email us at cn.recruit@lifetech.com

life technologies™

Life Technologies is an Equal Employment Opportunity/Affirmative Action employer. ©2012 Life Technologies Corporation. All rights reserved.
The trademarks mentioned herein are the property of Life Technologies Corporation or their respective owners. CO03056 0712

Invitrogen™ Applied Biosystems® Gibco® Molecular Probes® Novex® TaqMan® Ambion® Ion Torrent™

Science Careers online @sciencecareers.org

THE MBI FELLOWS

Mechanobiology Institute, Singapore
National University of Singapore

The MBI Fellowships provides talented young scientists a rare opportunity to set up research programs of their own as an alternative to traditional post-doctoral positions. Recent Ph.D. graduates with proven excellence in research are given the resources to work as junior principal investigators, free from financial constraints and distraction by formal teaching responsibilities and grant applications. MBI Fellows will exercise independence in their research projects with no supervision but under the care of the MBI Faculty Mentorship Programme. The Faculty Mentors are formed by a group of senior and well-reputed international scientists who are appointed as Principal Investigators at MBI.

The Goal is for MBI Fellows to receive the training to become independent principal investigators in Academic or Research Institutions.

The MBI Fellows program is an integral part of the Mechanobiology Institute's mission to nurture scientists during their most creative years and will yield a new generation of leaders more rapidly than traditional programs. In MBI's vibrant and multi-disciplinary environment and with state-of-the-art research facilities, MBI Fellows will gain the training for interdisciplinary and innovative research that will position them as highly marketable scientists.

Candidates for the MBI Fellowship Programme must accompany their applications with nomination letters from their research advisor or other distinguished scientist from the applicant's field or institution. Two additional letters of support by persons familiar with the candidate's research and academic accomplishments also should be forwarded to:

Prof. Michael Sheetz
Director
MBI Fellowship Programme
The Mechanobiology Institute, Singapore
National University of Singapore
T-Lab , 5 A Engineering Drive 1
Singapore 117411
E-mail : mbihr@nus.edu.sg
Website : http://mbi.nus.edu.sg/

NUS National University of Singapore | MBI MECHANOBIOLOGY INSTITUTE Singapore

NUS National University of Singapore | MBI MECHANOBIOLOGY INSTITUTE Singapore

FACULTY RECRUITMENT

Mechanobiology Institute, Singapore
National University of Singapore

The Mechanobiology Institute, Singapore is a multi-disciplinary institute committed to developing new paradigms for biomedical research by focusing on the quantitative analysis of function. We are seeking outstanding candidates for tenure-track positions with a background in molecular and cell biology, biophysics, biology-related engineering, or computer sciences and a commitment to collaborative interdisciplinary research. With an open lab environment and extensive central facilities support, successful candidates can address critical mechanical problems for understanding human health and disease processes. Successful candidates will hold joint appointments through relevant departments at the National University of Singapore or other Singapore Universities.

Please submit your application along with curriculum vitae, full publication list, research plans and names of three external referees to :

Prof. Michael Sheetz
Director
The Mechanobiology Institute, Singapore
National University of Singapore
T-Lab , 5 A Engineering Drive 1
Singapore 117411
E-mail : mbihr@nus.edu.sg
Website : http://mbi.nus.edu.sg/

WASHINGTON STATE UNIVERSITY

CHAIRPERSON
DEPARTMENT OF VETERINARY MICROBIOLOGY AND PATHOLOGY
WASHINGTON STATE UNIVERSITY
PULLMAN, WA

The College of Veterinary Medicine at Washington State University seeks a distinguished researcher and academic leader to be Chairperson of the Department of Veterinary Microbiology and Pathology (VMP) (**http://www.vetmed.wsu.edu/depts-vmp/index.aspx**). As one of the foremost pathobiology departments in the nation, VMP's mission is to enhance animal and public health through training veterinary medical students, graduate students and residents, conducting global outreach, and performing biomedical research in immunology, infectious diseases, food safety, genomics, and pathology. VMP's strong, extramurally funded research programs benefit from close collaborative ties with the USDA/ARS Animal Disease Research Unit, and other College of Veterinary Medicine entities including the Washington Animal Disease Diagnostic Laboratory, the newly founded Paul G. Allen School for Global Animal Health, and the School for Molecular Biosciences. VMP excellence in teaching is supported by the first-in-the-nation College Teaching Academy, whose mission is to enhance educational enterprises at all levels. The Chairperson's portfolio includes fiscal management of VMP, participation in and promotion of mentoring and professional development for faculty members, and fostering curricular development and scholarship in teaching. The successful candidate will have a record of academic leadership, productive, sustained, extramurally funded, internationally recognized research, and excellence in graduate education. Applicants must hold an earned doctorate in microbiology, immunology, pathology, veterinary medicine, medicine or a related discipline and be eligible for academic appointment at the level of Professor.

Review of applications will begin **January 7, 2013**. To apply or obtain more detailed information go to **www.wsujobs.com**. For questions or confidential expressions of interest about this position candidates may email or telephone **Ms. Sue Zumwalt** at **szumwalt@vetmed.wsu.edu** or **509.335.6027**.

WSU is an EO/AA Educator Employer.

Director Position

Institute of Plant & Microbial Biology
Academia Sinica,Taiwan

Academia Sinica, Taiwan, invites applications and nominations for the position of Director of the Institute of Plant and Microbial Biology (IPMB). The initial appointment is for three years (renewable for a second term), and will also carry the title of Research Fellow. It requires no Taiwan citizenship and much of the scientific affairs can be conducted in English.

As the pre-eminent academic research institution in Taiwan, Academia Sinica is devoted to basic and applied research in mathematics and physical sciences, life sciences, and humanities and social sciences. PMB consists of 29 laboratories, engaged in research leading to the better understanding of biological processes in both plants and microbes. Current foci include cell biology, cereal genetics and genomics, epigenetics, programmed growth and development, molecular phylogeny/evolution, plant-microbe and plant-environment interactions. IPMB is well funded and equipped with modern research facilities managed by experienced research specialists. IPMB maintains a high research standard with a high-quality publication record. For details about Academia Sinica and IPMB, please see **http://www.sinica.edu.tw**

Interested candidates should have a PhD or equivalent degree, with outstanding research accomplishments and demonstrated leadership ability. Besides pursuing a rigorous research program at IPMB, the successful candidate is expected to build on the existing strengths of IPMB, develop new research thrusts, and provide intellectual leadership in relevant basic and applied plant/microbial sciences in Taiwan.

Applications and nominations, including complete curriculum vitae, a publication list, and three letters of recommendation, should be submitted to **Dr.Wen-Hsiung Li**, **Academia Sinica, 128 Academia Road, Section 2, Nankang, Taipei 115, Taiwan** or by Email to: **zomslin@gate.sinica.edu.tw**. Screening of applications/nominations will begin immediately, and will continue until the position is filled.

St. Jude Children's Research Hospital
ALSAC • Danny Thomas, Founder
Finding cures. Saving children.

CHAIR, DEPARTMENT OF HEMATOLOGY

St. Jude Children's Research Hospital is seeking a Chair for the Department of Hematology at the rank of full member. A commensurate appointment at the full professor rank at the University of Tennessee is included. The position requires visionary thinking to build on St. Jude's foundation of excellence within an interdisciplinary environment. The successful candidate should have an M.D. or M.D./Ph.D. with a strong research interest, proven extramural funding and solid clinical background. The candidate must possess strong administrative and communication skills, a commitment to education and training, and strong leadership capabilities.

St. Jude's hematologists are an integral part of a multidisciplinary team that includes oncologists, bone marrow transplant therapists, radiation therapists, pathologists, radiologists, infectious disease specialists, basic scientists and biostatisticians. The Hematology department has a substantial clinical program including one of the largest pediatric sickle cell disease populations in the U.S. and an established NIH-funded research program with ample opportunities in basic and clinical research. There are twelve faculty members equally distributed between clinical and basic science. The department supports a strong translational research program in gene therapy as well as diverse research and clinical programs in molecular control of blood cell development and regulation, sickle cell disease, hemophilia, thrombophilia, marrow failures and platelet disorders. Further opportunities are available for collaboration and integration with a broad array of programs at the LeBonheur Children's Hospital and the University of Tennessee-Memphis.

St. Jude is a leading institution in pediatric hematology-oncology, and the future chair is expected to be a leader in his/her field as well as an active member of the St. Jude leadership. St. Jude ranks number 1 in pediatric cancer hospitals and is on the *Fortune* magazine's list of 100 best places to work. All patients accepted for treatment at St. Jude are treated without regard to the family's ability to pay.

The campus is located on 70 acres in downtown Memphis on the bluffs of the Mississippi River. Memphis offers a low-cost of living as well as numerous cultural attractions, including historic sites like Beale Street, two symphony orchestras, opera and ballet companies, great music (home of Elvis' Graceland and Sun Studios), many museums, and a dynamic live theatre community. Memphis is home to the Memphis Grizzlies Basketball Team, hosts the St. Jude PGA Golf Tournament, and is a stop on the Kroger St. Jude Tennis Tour.

Interested individuals are asked to submit a cover letter and C.V. to:

Arthur Nienhuis, MD
St. Jude Children's Research Hospital
262 Danny Thomas Place
Memphis, TN 38105
Email: arthur.nienhuis@stjude.org

St. Jude is an equal opportunity employer and a drug-free workplace.
Candidates receiving offers of employment are subject to pre-employment drug testing and background checks.

www.stjude.org

Jefferson Science Fellowship

The National Academies is pleased to announce a call for nominations and applications for the 2013 Jefferson Science Fellows program. Initiated by the Secretary of State in 2003, this fellowship program engages the American academic science, technology, engineering and medical communities in the design and implementation of U.S. foreign policy.

Jefferson Science Fellows (JSF) spend one year at the U.S. Department of State or the U.S. Agency for International Development (USAID) for an on-site assignment in Washington, D.C. that may also involve extended stays at U.S. foreign embassies and/or missions.

The fellowship is open to tenured, or similarly ranked, academic scientists, engineers and physicians from U.S. institutions of higher learning. Nominees/applicants must hold U.S. citizenship and will be required to obtain a security clearance.

The deadline for 2013-2014 program year applications/nominations is **January 14, 2013**. To learn more about the Jefferson Science Fellowship and to apply, visit the JSF web at:

www.nas.edu/jsf

THE NATIONAL ACADEMIES
Advisers to the Nation on Science, Engineering, and Medicine

WASHINGTON STATE UNIVERSITY
HEALTH SCIENCES

FACULTY POSITIONS
MEDICAL SCIENCES

Washington State University Division of Health Sciences, located on the Riverpoint campus in Spokane, invites applications for two tenure-track faculty positions at the rank of Assistant or Associate Professor and one at the rank of Professor in its new Medical Sciences section. Applicants must have an earned doctorate degree in the basic, clinical, or translatonal medical sciences. Successful candidates will be expected to maintain an active, extramurally funded research program, to mentor graduate students and fellows, and to teach in the professional and/or graduate curricula. The successful candidate for the Professor position will additionally be expected to take a leadership role in rapidly expanding medical research in Spokane, including recruitment of faculty and programmatic development.

Areas of research interest are open, but preference will be given to candidates completing research in the areas of planned growth in our program including molecular, cellular, physiological and systems biology approaches to: neurosciences/behavioral neurosciences (sleep, addictions, pain, anesthesia), senescence and immortality (stem cells, cancer, aging, regenerative medicine), microbiology (antimicrobial resistance, virology), and metabolic diseases (obesity, diabetes, renal and cardiovascular disease). Washington State University is substantially building its research and graduate education capacity in the medical sciences. The Medical Sciences section also participates in preclinical medical education in the WWAMI program, which is a collaborative medical education program with the University of Washington School of Medicine.

Screening of applications will begin immediately and will continue until a suitable candidate is identified. To apply visit: **www.wsujobs.com**. Applications must include a current curriculum vitae and letter of application describing professional goals, research, and teaching experience. Before interviews commence four letters of reference will be required. **Contact Kim Noe, Administrative Manager**, at **knoe@wsu.edu** or **509-358-7515** for questions, assistance with the application process or confidential expressions of interest.

Women and minorities are particularly encouraged to apply. Washington State University Is An Equal Opportunity/affirmative Action Educator And Employer.

Penn Dental Medicine

The Department of Anatomy and Cell Biology (ACB) at the University of Pennsylvania School of Dental Medicine (SDM) invites applications for full-time tenure track or tenured faculty positions at the **Assistant Professor, Associate Professor or Professor** level.

We are seeking candidates with outstanding academic accomplishments in cellular and/or molecular biology to complement our departmental research strengths. A strong track record of extramural grant funding, as well as an interest in teaching basic sciences to dental students are required. Preference will be given to candidates who can foster new and enhance existing inter-disciplinary, translational, and collaborative research, both within the ACB Department and across the SDM. Departmental interests include muscle physiology, mechanobiology, extracellular matrix synthesis in fibrosis, mechanisms of lysosomal signaling, and craniofacial development; the SDM excels in immunology, microbial pathogenesis, and oral cancers.

Applicants with a PhD or dual degree (DMD-PhD, MD-PhD, DVM-PhD) are invited to submit a statement of research and teaching interests, curriculum vitae, and names with contact information for three references. Review of applications will begin **January 1, 2013**, and continue until the position is filled. Anticipated start date is September 2013. Applicants can apply directly at the University of Pennsylvania website: **http://facultysearches.provost.upenn.edu/applicants/Central?quickFind=51131** or by submitting materials to the Chair of the Search Committee:

Elisabeth R. Barton, PhD
Dept. of Anatomy and Cell Biology
School of Dental Medicine
University of Pennsylvania
240 S. 40th Street
Philadelphia, PA 19104
ACB2013@dental.upenn.edu

The University of Pennsylvania is an Equal Opportunity Affirmative Action Employer; women and minority candidates are strongly encouraged to apply.

The CAS-MPG Partner Institute for Computational Biology is searching for "Group Leader" in Shanghai, China

The CAS-MPG Partner Institute for Computational Biology is an internationally focused research institute based in Shanghai, China and jointly operated by the Chinese Academy of Sciences (CAS) and the German Max Planck Society (MPG). Work at this institute is driven by the accelerating importance of statistical and computational methods in modern biology, and we specialize in innovative research at the boundaries between disciplines.

PICB would be delighted to receive applications for Group Leader positions from scientists working in the following research areas:

- Genomics;
- Epigenomics;
- Functional genomics;
- Computational biology;
- Biostatistics;
- Biomathematics.

PICB will offer a competitive salary package to successful applicants, including a basic salary, position allowance, related welfare and housing benefits.

Interested applicants should send a covering letter, 3 letters of recommendation, a curriculum vitae, a brief summary of past achievements, a research proposal and at least three representative publications to:

Prof. Xinguang Zhu
CAS-MPG Partner Institute for Computational Biology
320 Yueyang Road, Shanghai 200031
Tel: **86-21-54920481**
Fax: **86-21-54920451**
E-mail: **zhuxinguang@picb.ac.cn**

JAAS 江苏省农业科学院 Jiangsu Academy of Agricultural Sciences

Open position as Deputy Director and Full Professor in the Institute of Agricultural Facility and Equipment

Jiangsu Academy of Agricultural Sciences (JAAS) is a professional agricultural research and extension institution that has been established since 1932. JAAS ranks at the top of provincial agricultural academies in China in terms of the comprehensive strength in agriculture. JAAS's headquarter and main research facilities are located in Nanjing, Jiangsu,China.

Currently, JAAS is seeking a deputy director with the rank of full professor in the area of agricultural facility and equipment researches. Applicant should have a commitment to scientific excellence and the enthusiasm, energy, and innovative thinking necessary to lead a dynamic institute with a broad and diverse portfolio. Applicant must possess a faculty position already beyond the assistant professor level in a university or the equivalent position in a research institution. In addition, the candidate should demonstrate excellent records of research accomplishment and has a command of bilingual language for English and Chinese, both in spoken and written.

Successful applicant will be offered a competitive package, including sufficient laboratory space, startup funding, relocation fee and competitive salary commensurate with experience, in addition to a housing allowance, and other employee benefits. Applicant can go to **www.jaas.ac.cn** for application details.

In addition, more information for other regular faculty positions from JAAS relevant to a variety of disciplines in agriculture is also available at **www.jaas.ac.cn**.

Contact information
E-mail: **rsc-gbk@jaas.ac.cn**; Tel: **086-25-84390037**

ASSISTANT/ASSOCIATE PROFESSOR MAMMALOGY AND CONSERVATION ECOLOGY

JOB #: 38124

The Pennsylvania State University seeks applicants for a tenure-track position at the rank of Assistant or Associate Professor in the research area of mammalogy and conservation ecology. This is an academic-year appointment with both research and teaching responsibilities. The successful candidate is expected to interact with scientifically diverse faculty across campus and develop an internationally recognized, extramurally supported research program related to mammal conservation and management that addresses population/community response to management options, habitat change and manipulation, and/or anthropogenic stressors. The successful candidate will join the Department of Ecosystem Science and Management http://ecosystems.psu.edu/, which includes faculty and staff with expertise in wildlife and fisheries, forests, soils, water, and wood products and is a campus center of excellence in the science and management of renewable natural resources, providing faculty with ample opportunities to interact within a world-class university. See full position announcement including all required qualifications and application information at **http://apptrkr.com/299147** Employment will require successful completion of background check(s) in accordance with University policies. Penn State is committed to affirmative action, equal opportunity, and the diversity of its workforce.

PENNSTATE 1855

ROSALIND FRANKLIN UNIVERSITY
OF MEDICINE AND SCIENCE

Advocate Lutheran General Hospital
Inspiring medicine. Changing lives.

Vice Dean for Translational Research (RFUMS)
Medical Director of the Russell Institute for Research and Innovation (RIRI) at Advocate Lutheran General Hospital (ALGH)

The Chicago Medical School at Rosalind Franklin University of Medicine and Science (RFUMS) and Advocate Lutheran General Hospital (ALGH) invite applications for the full-time position of Vice Dean for Translational Research (RFUMS) and Medical Director of the Russell Institute for Research and Innovation (RIRI) at Advocate Lutheran General Hospital (ALGH).

The Vice Dean for Translational Research Director of the Russell Foundation Research Institute will: •Possess an MD or MD/PhD degree •Have extensive clinical and translational research experience and capabilities •Be expected to either currently maintain or have previously maintained a long-standing active research program with extramural funding •Have a broad research perspective with appreciation and knowledge across wide ranges of biomedical research •Posses the ability to bridge the gap between basic science, translational, and clinical research. Interested applicants should submit, electronically, a cover letter, curriculum vitae, including teaching and research interests and three names of reference to Rosalind Franklin University of Medicine and Science Human Resources web site via **http://rosalindfranklin.peopleadmin.com/postings/3395**. Applications will be accepted until **January 31, 2013**.

TOYOTA TECHNOLOGICAL INSTITUTE 豊田工大

Positions Open
Toyota Technological Institute

Toyota Technological Institute has two openings for "Principal Professor" positions in its School of Engineering. For more information, please refer to the following website:
http://www.toyota-ti.ac.jp/bosyu/index_E.html

Research fields:

1. Advanced Energy Technology and Related Sciences
This field covers fundamental studies and applied research on advanced energy technology, including new concepts and systems for the generation, storage, and utilization of energy as well as innovative propulsion mechanisms. It also covers basic and applied studies of materials and their functions for advanced energy technology.

2. Science and technology for advanced instrumentation and/or information processing
This field covers new devices and systems for advanced information processing and/or communication technology, including quantum information technology and leading instrumentation technology for ultra-sensitive measurements and/or bio-medical studies and diagnosis. It also covers large-scale computation in cyber-physical space and related technology for advanced sensor networks.

The "Principal Professor" will serve as the head of a "unit laboratory", that consists of the Principal Professor, one associate professor, and two research assistants, i.e., one assistant professor and one post-doctoral fellow. Alternatively, two post-doctoral fellows can be hired in place of an assistant professor. All the expenses for hiring these unit members will be covered by TTI. A start-up grant of about one hundred million Japanese yen (ca. one million US dollars) is available. In addition, a research budget of about ten million Japanese yen (ca. one hundred thousand US dollars) will be given each year to promote research programs for a period of five years. At the end of this five-year term, the principal professor will be given a formal evaluation, as described on our web page.

Start date: Fiscal year 2013 (on the date of the earliest convenience)

Documents: Please refer to our web site

Deadline: March 31, 2013

Inquiries: Search Committee Chair, Vice President Dr. Shuji Tanaka
(Phone) **+81-52-809-1775** (E-mail) **tanaka_mat@toyota-ti.ac.jp**

The Toyota Technological Institute is an Equal Opportunity Employer and Educator.

Assistant/Associate Professor

Saw Swee Hock School of Public Health
National University of Singapore

NUS National University of Singapore
Saw Swee Hock School of Public Health

The National University of Singapore (NUS) Saw Swee Hock School of Public Health is recruiting full-time Assistant and Associate Professors into its Health Services and Policy domain and Infectious Diseases Program. More details of the appointment are available at:
http://sph.nus.edu.sg/index.php/about/careers

Qualifications:
Applicants should have completed or be about to complete a doctoral degree in public health, sociology, economics, business, management, informatics, industrial engineering or other related fields.

Responsibilities:
Establishing an independent research agenda through extramural funding; developing collaborative, multidisciplinary research; curricula design and teaching; graduate student advising, and providing service to the community and field of public health.

Applicants should send a statement of interest, CV and names of three character referees to:

Ms Kong Yeean Leng Email: **ephkyl@nus.edu.sg**

DIRECTOR
Fermi National Accelerator Laboratory

Fermilab

The Board of Directors of Fermi Research Alliance, LLC (FRA) has initiated a search for a new Director of the Fermi National Accelerator Laboratory in Batavia, Illinois. The position, for a term of five years with the possibility of extension for a mutually agreed time, will be available July 1, 2013. The Search Committee welcomes applications and nominations for this position. It is recommended that applications be accompanied by curriculum vitae and other information bearing on the candidates' qualifications for the Directorship. Relevant qualifications include visionary leadership capability, internationally recognized scientific achievement, management experience and accomplishments at a national laboratory or complex research setting, and broad communications skills.

The membership of the Search Committee, its charge, and provision for submitting confidential input to the Committee are posted at **http://www.fnal.gov/pub/directorsearch**

Communications should be sent as soon as possible, preferably before **January 15, 2013**, and should be addressed to:

Ezra Heitowit
Executive Secretary for the Fermilab Director Search Committee
Fermi Research Alliance, LLC
Suite 400
1111 19th Street, NW
Washington, DC 20036 USA
e-mail: heitowit@fnal.gov

The two members of FRA are the University of Chicago and Universities Research Association, Inc. FRA operates Fermilab under contract with the U.S. Department of Energy. For more information about FRA and Fermilab visit **http://fra-hq.org** and **http://www.fnal.gov**, respectively.

FRA is an Equal Opportunity Employer.

Science Careers online @sciencecareers.org

AAAS is here – helping scientists achieve career success.

Every month, over 400,000 students and scientists visit ScienceCareers.org in search of the information, advice, and opportunities they need to take the next step in their careers.

A complete career resource, free to the public, *Science* Careers offers a suite of tools and services developed specifically for scientists. With hundreds of career development articles, webinars and downloadable booklets filled with practical advice, a community forum providing answers to career questions, and thousands of job listings in academia, government, and industry, *Science* Careers has helped countless individuals prepare themselves for successful careers.

As a AAAS member, your dues help AAAS make this service freely available to the scientific community. If you're not a member, join us. Together we can make a difference.

To learn more, visit **aaas.org/plusyou/sciencecareers**

AAAS + U = Δ

UCDAVIS

TENURE TRACK POSITION – ASSISTANT PROFESSOR
Food Chemistry

The Department of Food Science and Technology is currently seeking to fill a faculty position, which includes the expectation that the appointee will conduct mission-oriented research and outreach of relevance to the California Agricultural Experiment Station We seek applications from individuals who have or can establish a strong extramurally funded research program in an advanced contemporary area of chemistry or biochemistry that can be broadly described as impacting food. The research approach will endeavor to produce significant scholarly achievements that impact one or more areas of contemporary food science including food security, quality, safety, health, toxicology, processing-efficiency and food sustainability. Candidates are expected to have a PhD (or equivalent) and demonstrated ability in chemistry, biochemistry, food science or a related discipline. Postdoctoral experience is highly desirable. Selection will be based in part on a record of research publications in internationally recognized peer-reviewed journals, and the ability to obtain extramural funding. The specific research program will depend upon the expertise and interests of the candidate. The successful applicant will be expected to develop an independent, internationally recognized research program and contribute to the mission of the College of Agricultural and Environmental Sciences and the California Agricultural Experiment Station (**http://caes.ucdavis.edu/facstaff/rmap/aes-overview**), teach at the undergraduate and graduate level, and supervise graduate student research.

Applicants should submit online at **https://recruit.ucdavis.edu** a letter of application, curriculum vitae (including list of publications), a statement of research, a separate statement describing teaching interests and background; PDF files of three publications; undergraduate and graduate academic transcripts and names, addresses including e-mail, and telephone numbers of three references. The position is open until filled; but to assure full consideration, completed online applications should be submitted no later than **February 1, 2013**, for a targeted start date of **July 1, 2013**.

UC Davis is an Affirmative Action/Equal Employment Opportunity Employer and is dedicated to recruiting a diverse faculty community. We welcome all qualified applicants to apply, including women, minorities, individuals with disabilities and veterans.

BCM
Baylor College of Medicine

FACULTY POSITION
Alkek Center for Molecular Discovery

The Alkek Center for Molecular Discovery (ACMD) has recently been established at BCM with a mandate to utilize high-throughput technology to facilitate translational research and drug development. Applications are invited for a tenure-track or non-tenured faculty position at any rank, expressly for those with a strong record of research accomplishment and productivity and who use mass spectrometry to investigate problems in metabolomics. The successful applicant will enjoy a faculty appointment in the Department of Molecular and Cellular Biology and join other faculty members from this and other outstanding discovery-based research departments who are currently appointed to the Center. The ACMD offers competitive start-up packages and salaries together with newly renovated research space and access to numerous shared resources as well as other Centers operated by BCM. BCM occupies a central location within the highly interactive Texas Medical Center research community and has a prominent position with other institutions that make up the Gulf Coast Consortium.

Applicants will be reviewed as they are received, although priority will be given to applications completed by **December 31, 2012**. Applicants should submit a curriculum vitae, statement of research interests and contact information for three individuals who have agreed to provide letters of reference as a single PDF file by applying online at **http://www.medschooljobs.org** to job vacancy **#228355**.

Baylor College of Medicine is an Equal Opportunity/Affirmative Action/Equal Access Employer.

St. Jude Children's Research Hospital
ALSAC • Danny Thomas, Founder
Finding cures. Saving children.

POSTDOCTORAL POSITIONS IN MAMMALIAN ORGANOGENESIS

POSTDOCTORAL POSITIONS are available to study the cellular and molecular processes controlling vertebrate organogenesis using available mouse models. We are particularly interested in understanding the cellular and molecular mechanisms regulating the development of the visual system and the lymphatic vasculature using in vivo and 3D organ culture systems.

Highly motivated individuals who recently obtained a PhD or MD degree and have a strong background in molecular and developmental biology are encouraged to apply. Interested individuals should send their curriculum vitae, a brief description of their research interests, and the names of three references to:

Guillermo Oliver, PhD
Member
Department of Genetics
St. Jude Children's Research Hospital
332 N. Lauderdale, Memphis, TN 38105
E-mail: guillermo.oliver@stjude.org
www.stjude.org/oliver

An Equal Opportunity Employer

www.stjude.org

Oakland University

Tenure-Track Assistant Professor Position in Biochemistry
Department of Biological Sciences

The Department of Biological Sciences at Oakland University invites applications for a candidate with a strong background in biochemistry, investigating key problems in **cellular metabolism**. Special consideration will be given to candidates studying enzyme or protein function using biochemical approaches. A PhD and at least two years of post-doctoral experience are required, in addition to strong research track record evidenced by publications. Laboratory space and a competitive startup package will be provided. The successful candidate is expected to develop a vigorous, extramurally funded research program, to teach effectively at the undergraduate and graduate levels, and to mentor undergraduate and graduate students (MS and PhD).

The Department of Biological Sciences (**http://www2.oakland.edu/biology/**) is a vibrant and growing department that places the highest priority on research excellence. The faculty have wide range of research interests, including inflammatory response, host-parasite interactions, metalloproteins, chromatin modifications, development of tubular organs, stem cells, flagellar motility, hypertension, oxidative damage in muscle, population dynamics and stream ecology. Oakland University is a state-supported institution of 20,000 students. It is located on a beautiful 1,600-acre campus in the heart of Oakland County, 25 miles north of Detroit.

Applications should be submitted by January 5, 2013. Applications should include a cover letter, curriculum vitae, detailed statement of research plans, teaching philosophy, 3 representative publications, and a list of 3 or more references. Application is set online at **http://academicjobs.oakland.edu/postings/447**. Inquiries should be addressed to: **Arik Dvir, Chair, Department of Biological Sciences (dvir@oakland.edu).**

Oakland University is an Affirmative Action/Equal Opportunity Employer and encourages applications from women and minorities.

Women in Science Booklet

Science and the L'Oréal Foundation present

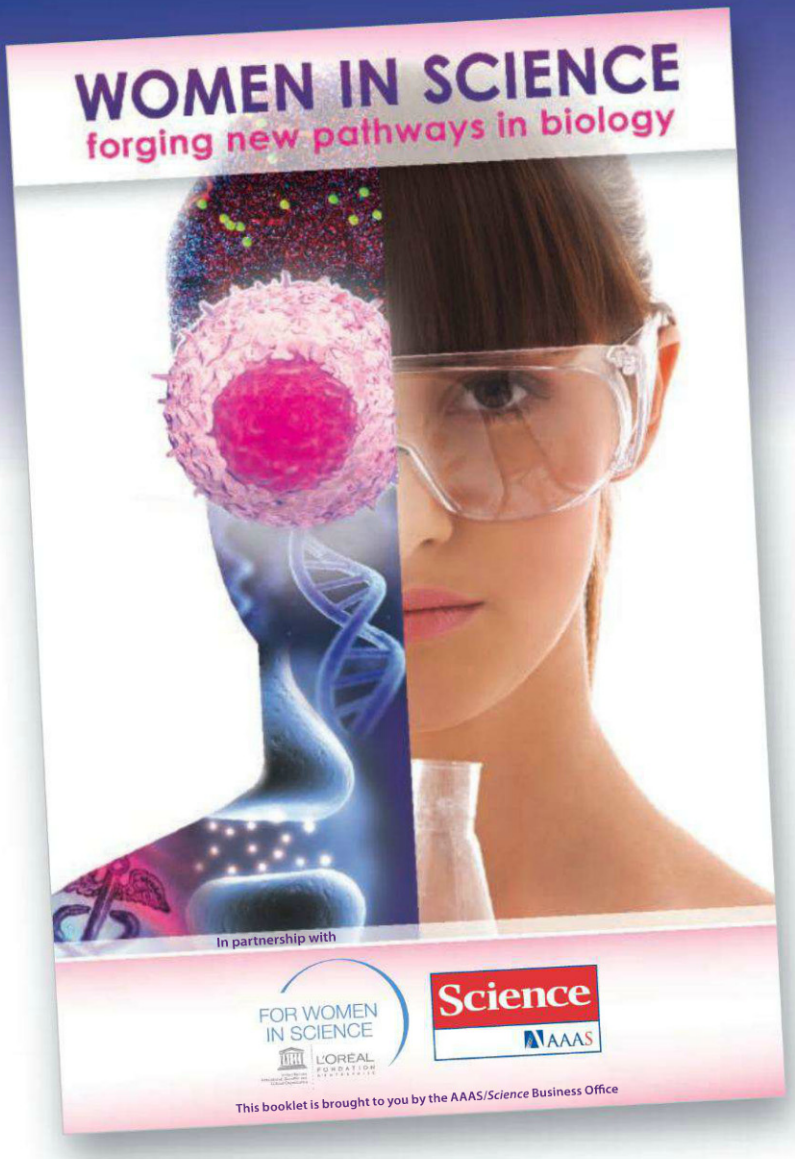

Read inspiring profiles of women making a difference in biology.

Free download at ScienceCareers.org/LOrealWIS

Georgia Health Sciences University
Cancer Center

Faculty Positions in Cancer Inflammation and Tolerance

Georgia Health Sciences University Cancer Center is undergoing an unprecedented expansion in basic science and related translational medicine programs as part of a new initiative to achieve designation as an NCI Cancer Center. As part of this process we invite applications for positions for Assistant, Associate or Full Professor. We are particularly interested in individuals with expertise that complements the research interests in the existing Cancer Center Programs in the area of chronic inflammation that creates tolerance to protect tumors and healthy tissues from immune-mediated injury, and how to manipulate tolerogenic mechanisms for clinical benefit. Individuals working in the field of cancer inflammation and immunology are particularly encouraged to apply. Other areas of interest include, but are not limited to, aspects of inflammation and immunology research that facilitate understanding of cancer immunology and immunotherapy.

Applicants must have a strong track record of independent research and active extramural research funding. Applicants with NCI funding and experience of working in an NCI-designated Cancer Center are particularly encouraged to apply, but other applicants with funding and interests in a relevant research area will also be considered. Successful applicants will join a collaborative group of basic research scientists using animal models and who work closely with oncologists to promote translational research in immunotherapies to treat cancer and autoimmune syndromes. Strategic program interests include developing better cancer vaccines, and elucidating novel targets to manipulate immune responses to treat cancer and other chronic inflammatory syndromes. Applications in these priority research areas are especially welcomed.

A competitive salary and start-up package, commensurate with experience and academic qualifications, is available. A summary of research interests, curriculum vitae and names of three references should be sent to **Dr. Rhea-Beth Markowitz, Faculty Recruitment Coordinator, rbmarkowitz@georgiahealth.edu**.

The Georgia Health Sciences University is an Equal Opportunity Affirmative Action, and Equal Access Employer. The Georgia Health Sciences University has a strong interest in promoting diversity in its faculty and women and minority candidates are encouraged to apply.

Georgia Health Sciences University
Cancer Center

Faculty Positions in Genomic Medicine

Georgia Health Sciences University Cancer Center is undergoing an unprecedented expansion in the basic and population sciences programs as part of an initiative to achieve designation as an NCI Cancer Center. As part of this process we invite applications for positions for **Assistant, Associate or Full Professor** in the area of genomics in personalized medicine. Individuals working with NextGen sequencing, epigenomics, pharmacogenomics, and the functional genomics analysis of tumors to steer clinical management of patients and predict progression and outcome are particularly encouraged to apply.

Applicants must have active extramural research funding, ideally from NCI; a strong track record of independent research; and, ideally, experience of working in an NCI-designated Cancer Center. Successful applicants will join a collaborative program that works closely to promote translational research with the clinical research oncologists. Organizational strategic interests include the relationship between obesity, HPV, and smoking as etiological risk factors for cancer. Applications in these research areas are especially welcomed.

A competitive salary and start-up package, commensurate with experience and academic qualifications is available. A summary of research interests, curriculum vitae, and names of three references should be sent to **Dr. Rhea-Beth Markowitz, Faculty Recruitment Coordinator, rbmarkowitz@georgiahealth.edu**.

The Georgia Health Sciences University is an Equal Opportunity Affirmative Action, and Equal Access Employer. The Georgia Health Sciences University has a strong interest in promoting diversity in its faculty and women and minority candidates are encouraged to apply.

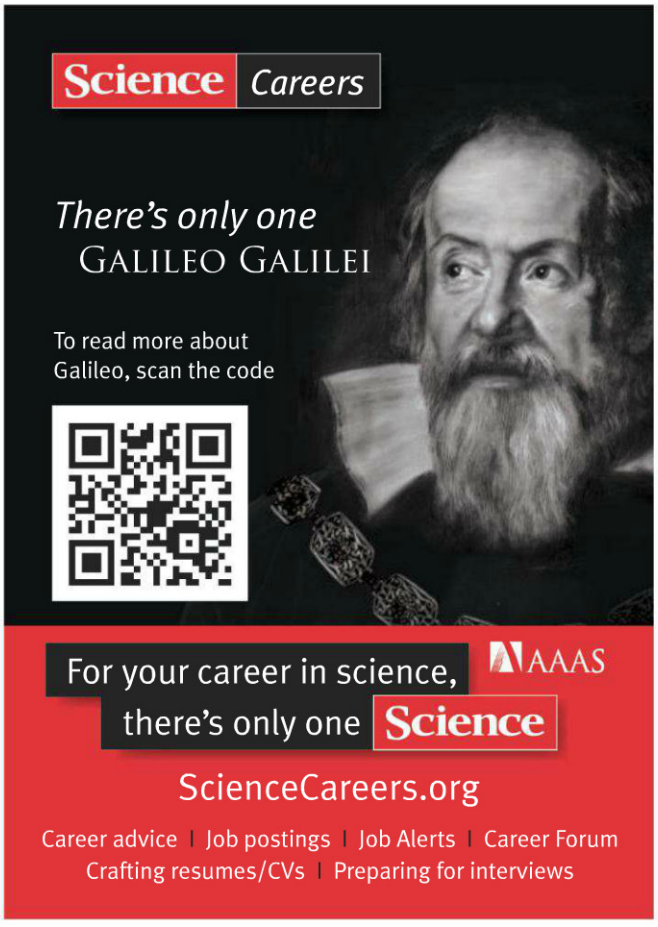

Georgia Health Sciences University
Cancer Center

Faculty Positions in Tumor Angiogenesis

Georgia Health Sciences University Cancer Center is undergoing an unprecedented expansion in the basic and population sciences programs as part of an initiative to achieve designation as an NCI Cancer Center. As part of this process, we invite applications for tenure-track positions at **Assistant, Associate or Full Professor** levels in the general area of tumor angiogenesis. Individuals studying novel therapeutic approaches of targeting the tumor vasculature to steer clinical management of patients are particularly encouraged to apply.

Applicants must have active extramural research funding, ideally from NCI, and a strong track record of independent research. Applicants with experience of working in an NCI-designated Cancer Center are especially encouraged to apply. Successful applicants will join a collaborative team of scientists who work closely to promote translational research with the clinical research oncologists and interact with the GHSU Vascular Biology Center. Organizational strategic interests include the relationship between obesity, HPV and smoking as etiological risk factors for cancer. Applications in these research areas are particularly welcome.

These positions come with a competitive salary and start-up package, commensurate with experience and academic qualifications. A summary of research interests, curriculum vitae and names of three references should be sent to **Dr. Rhea-Beth Markowitz, Faculty Recruitment Coordinator, rbmarkowitz@georgiahealth.edu**.

The Georgia Health Sciences University is an Equal Opportunity Affirmative Action, and Equal Access Employer. The Georgia Health Sciences University has a strong interest in promoting diversity in its faculty and women and minority candidates are encouraged to apply.

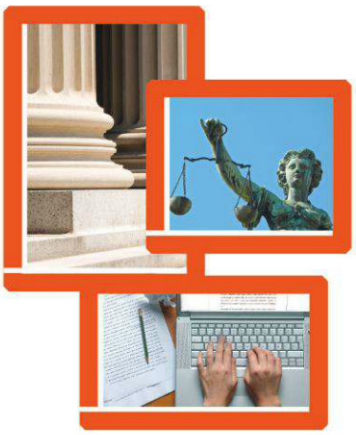

Nontraditional Careers: Opportunities Away From the Bench

Webinar

Want to learn more about exciting and rewarding careers outside of academic/industrial research? View a roundtable discussion that looks at the various career options open to scientists and strategies you can use to pursue a nonresearch career.

Now Available On Demand
www.sciencecareers.org/webinar

Produced by the *Science*/AAAS Business Office.

Science Careers
From the journal *Science* AAAS

POSITIONS OPEN

厦门大学
环境与生态学院

FACULTY POSITIONS
Xiamen University
College of the Environment and Ecology

A top educational institution in China, Xiamen University is known for its academic excellence and magnificent coastal campuses. The newly established College of the Environment and Ecology (CEE) focuses its research programs on costal and wetland ecosystems, environmental science, and technology. CEE is searching for excellent scientists/eminent scholars with research interests complementing existing strength. Qualified candidates of any nationalities will be nominated for national/provincial talent plans with excellent startup packages and compensations. For details, please visit **website: http://cee.xmu.edu.cn. E-mail: ceezp@xmu.edu.cn.**

UNIVERSITY of ROCHESTER MEDICAL CENTER

INNATE IMMUNOLOGIST
Faculty Position

The Immunology and Infectious Disease Program at the University of Rochester School of Medicine and Dentistry (Rochester, New York) is recruiting for a tenure-track faculty (open-rank) position in innate immunology. We seek an energetic and creative scientist whose research synergizes with major institutional strengths in human and mouse adaptive immunology in infectious and inflammatory disease. The successful candidate will join a highly collaborative and multidisciplinary research community and should strengthen research interests in how microbial and environmental factors modify immunity through innate cell recruitment and activation.

Qualified candidates should have a successful research background in basic and/or translational science focused on innate immunity. Candidates with a strong record of accomplishments and innovation should apply online at **website: http://www.rochester.edu/jobopp, job number 177923** and forward a single PDF containing cover letter, curriculum vitae, contact information for three references and statement of current research and future plans to **e-mail: dina_marcoccia@urmc.rochester.edu.**

Review of applications will start January 2, 2013.

The University of Rochester has a strong commitment to principles of diversity and, in that spirit, actively encourages applications from groups underrepresented in higher education.

Find your future here.

↓

Science Careers
From the journal *Science* AAAS

www.ScienceCareers.org

POSITIONS OPEN

UNIVERSITY of ROCHESTER MEDICAL CENTER

SYSTEMS BIOLOGIST in Immunology and infectious Disease
Faculty Position

The Immunology and Infectious Disease Program at the University of Rochester School of Medicine and Dentistry (Rochester, New York) is recruiting for a tenure-track faculty (open-rank) position to use systems biology approaches to understand inflammation and infectious disease. We seek an energetic and creative scientist whose research synergizes with major institutional strengths in human and mouse immunology. The successful candidate will join a highly collaborative and multidisciplinary research community focused on immunological disease. The candidate's expertise will complement a number of major NIH funded center awards and contracts at the University of Rochester that focus on translational studies of immunity including the Respiratory Pathogens Research Center (RPRC), the Autoimmunity Center of Excellence (ACE), the Center for Biodefense Immune Modeling (CBIM), the Center of Excellence in Influenza Research and Surveillance (NYICE), and a Developmental Center for AIDS Research (DCFAR).

Qualified candidates should have a successful research background in basic and/or translational science in immunology from a systems biology perspective. Candidates with a strong record of accomplishments should apply online at **website: http://www.rochester.edu/jobopp, job number 177923** and forward a single PDF containing cover letter, curriculum vitae, contact information for three references and statement of current research and future plans to **e-mail: dina_marcoccia@urmc.rochester.edu.**

Review of applications will start January 2, 2013.

The University of Rochester has a strong commitment to principles of diversity and, in that spirit, actively encourages applications from groups underrepresented in higher education.

Loyola University Chicago (LUC), College of Arts and Sciences, Department of Biology invites applications for **DEPARTMENT CHAIRPERSON**, a tenure-track position at the **FULL PROFESSOR** rank. Candidates from all areas of Biology will be considered. The Department, located in the Quinlan Life Sciences Education and Research Center, serves approximately 1,500 undergraduate majors, 55 students in a Medical Sciences M.A. program, and 25 students in a thesis-based M.S. program, and contributes courses to Biochemistry, Bioinformatics, Forensic Sciences, Exercise Physiology, Nursing, and Neuroscience. The Institute of Urban Environmental Sustainability will provide additional opportunities for interdepartmental collaborations (**website: http://luc.edu/biology**). The successful candidate will be expected to lead a department of 20 tenure-track and 18 full-time, non-tenure-track faculty and to promote excellence in teaching and scholarship. A Ph.D. degree and leadership experiences in Biology or closely related fields are required. Candidates should complete an online application at **website: http://careers.luc.edu**, with a cover letter; curriculum vitae; a personal statement about their philosophy of departmental leadership; and a detailed description of their research and teaching interests. Candidates should submit names and e-mail addresses of three individuals prepared to write about their professional qualifications for the position. Review of applications will begin December 15, 2012, and applications will be accepted until the position is filled. *LUC is an Equal Opportunity/Affirmative Action Employer with a strong commitment to hiring for its mission and diversifying its faculty. LUC seeks candidates who will contribute to its strategic plan to deliver a transformative education in the Jesuit Catholic tradition. Information on LUC's mission and philosophy of transformative education is found at* **websites: http://luc.edu/mission/missionandidentity** *and* **http://luc.edu/transformativeed**, *respectively. Applications from women and minorities are especially encouraged.*

SYMPOSIUMS

CiRA International Symposium 2013

"Raising the next generation of stem cell research"

March 11-12, 2013 | Kyoto, JAPAN

Call for Poster Presentation

Abstracts Due: January 18, 2013

Registration and further information
http://www.cira.kyoto-u.ac.jp/

Confirmed Speakers

Kevin Eggan	Harvard University
John Gurdon	Gurdon Institute
Konrad Hochedlinger	Harvard Stem Cell Institute
Hiromitsu Nakauchi	University of Tokyo
Shin-Ichi Nishikawa	RIKEN
Hideyuki Okano	Keio University
Mahendra Rao	NIH
Hans Schöler	Max Planck Institute
Austin Smith	University of Cambridge
Deepak Srivastava	Gladstone Institute
Amy Wagers	Harvard University
Ian Wilmut	University of Edinburgh
Shinya Yamanaka	CiRA, Kyoto University
Richard Young	Whitehead Institute

Center for iPS Cell Research and Application
Kyoto University

SYMPOSIUMS

INTERNATIONAL SOCIETY FOR NEUROCHEMISTRY
AMERICAN SOCIETY FOR NEUROCHEMISTRY

Satellite Symposium

UNVEILING THE SIGNIFICANCE OF LIPID SIGNALING IN NEURODEGENERATION AND NEUROPROTECTION

April 17 - 19, 2013
Hyatt Regency Cancun, Cancun, Mexico

The purpose of this meeting is to honor and recognize the academic contributions of Dr. Nicolas Bazan to advancing lipid signaling in neuroscience and ophthalmology, as well as his dedicated service to the ASN and ISN.

In addition, this satellite meeting will integrate signaling mediated by different lipids to neurological disorders. This integrative approach will stimulate vigorous discussions on mechanisms and novel strategies for prevention and treatment of neurological diseases

Visit our website:
www.ISN-BrainLipids.org

Honoree
Nicolas G. Bazan, M.D., Ph.D.
(New Orleans, LA)

ORGANIZING COMMITTEE

Chair -
Grace Sun, Ph.D.
(Columbia, MO)

Co-Chair -
W. Gibson Wood, Ph.D.
(Minneapolis, MN)

Abstracts are encouraged for poster presentations

Selected abstracts will be chosen for oral presentation

Proof 994

AWARDS

Federal Ministry of Education and Research

bccn

"Bernstein Award" 2013
Young Scientists Research Award in Computational Neuroscience

The German Federal Ministry of Education and Research (BMBF) has established the "National Network for Computational Neuroscience" with six high-performing "Bernstein Centers for Computational Neuroscience" as the major structural elements.

The "Bernstein Award" is equipped with up to 1.25 Mio Euros in the form of a grant over a period of five years. It will be awarded to a highly qualified young researcher, considering the candidates' verifiable research profile in the field of Computational Neuroscience and the scientific concept for a future young research group. Young researchers can apply for their own position and group. The group funded by the "Bernstein Award" will become an integral part of the National Network for Computational Neuroscience. Future announcements of the "Bernstein Award" are in the scope of the Ministry's planning.

The grant is provided for a scientific project of a young research group headed by a postdoc regardless of nationality. The project will be conducted at a German university or research institution – within or outside the Bernstein Centers. It is a prerequisite for funding that the university or research institution concerned employs the young researcher during the funding period and supports him/her with the basic equipment in terms of laboratory space and other infrastructure. A statement made to that effect by the receiving institution must be included with the project outline to be submitted.

Deadline for applications is April 15th, 2013.

For more detailed information about the "Bernstein Award" including application conditions please visit

http://www.nncn.de
or
http://www.gesundheitsforschung-bmbf.de/en/2476.php

Download your free copy today.

ScienceCareers.org/booklets

From technology specialists to patent attorneys to policy advisers, learn more about the types of careers that scientists can pursue and the skills needed in order to succeed in nonresearch careers.

Science Careers
From the journal *Science* AAAS

POSITIONS OPEN

BIOINFORMATICIST/COMPUTATIONAL BIOLOGIST

As part of an ongoing expansion into core research clusters, the Department of Biological Sciences, Bowling Green State University (BGSU) seeks tenure-track Bioinformaticist/Computational Biologist applicants at the **ASSISTANT PROFESSOR** level. Demonstrated experience in applying next generation sequencing and other high throughput technologies to dissect genomes, genes, and pathways is sought with the strongest candidates combining bioinformatics and experimental approaches, irrespective of research area. Research complementing existing faculty interests in genomic, transcriptomic, and metagenomic analyses is preferred. Ph.D. required; postdoctoral experience preferred. Successful candidates are expected to develop highly productive, externally funded research, and contribute to the graduate (Ph.D./M.S., n=90) and undergraduate programs. Ample laboratory space and resources are available for research program expansion. Electronically submit (one PDF file; Subject: Bioinformatics Search) cover letter, curriculum vitae, statements of research plans and teaching perspective, and representative publications to **e-mail: dmclean@bgsu.edu** along with three reference letters by January 11, 2013. A background check is required for employment. Questions? Contact **George Bullerjahn** at **e-mail: bullerj@bgsu.edu**. Further information about our department can be found at **website: http://www.bgsu.edu/departments/biology**.

BGSU is an Affirmative Action/Equal Opportunity Employer/Educator and encourages applications from women, minorities, veterans, and persons with disabilities.

Stop searching for a job; start your career today.

Science Careers
From the journal *Science* AAAS
www.ScienceCareers.org

☑ More scientists agree —we are the most useful website.
www.ScienceCareers.org

MARKETPLACE

Widely Recognized Original & Guaranteed
KlenTaq1
8¢/u Truncated Taq DNA Polymerase Withstand 99°C
US Pat #5,436,149 **e-mail:** abpeps@msn.com
Call:AB Bioscience, LLC 1•800•383•3362
Fax: 314•968•8988 **www.abpeps.com**

Announcing our new partnership with NASA Federal Credit Union

Dear Member:

AAAS is committed to offering you member benefits that fit your needs and make your membership more valuable.

With that in mind AAAS is embarking on a new partnership with NASA Federal Credit Union that will provide you with access to a wide range of financial tools and products. Like AAAS, NASA Federal Credit Union is dedicated to serving the scientific community. This shared perspective is just one of the many reasons that we are embarking on this partnership.

As you may know, we have recently ended our banking relationship with Bank of America, but we're confident that our new partnership with NASA FCU will provide you with a superior banking experience. NASA FCU offers members better ways to save and smarter ways to borrow with friendly, professional service – along with anytime, anywhere account access.

Moreover, unlike other financial institutions that have public stockholders, NASA FCU is a not-for-profit financial cooperative where being a member means being an owner, too. And as a member/owner, you will enjoy unique benefits like: better loan rates, higher dividends and state-of-the-art products and services.

We'll be sending you more information about this great new benefit over the coming months. In the meantime, be sure to visit **nasafcu.com/AAASpackage** to apply for the new AAAS Platinum Advantage Rewards or Platinum Cash Rewards credit cards. You can also take a sneak peek at the AAAS Check Card and Checks coming soon.

Sincerely,

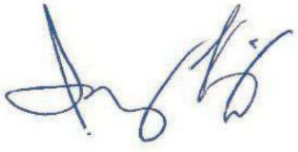

Ian King
Director of Marketing and Membership, AAAS

Easy
access to what you need

lifetechnologies.com

Simple ordering for all the products from our trusted brands

Supply Centers

Instant, on-site access to key research tools

Instruments & Services Portal

Centralized management of instrument use & care

Your valuable feedback has influenced upgrades to our current e-solution options, and inspires new ideas for how we can simplify the way you buy our products and do business with us.

Tell us how we're doing at **lifetechnologies.com/contactus**

life technologies™

For research use only. Not intended for any animal or human therapeutic or diagnostic use. ©2012 Life Technologies Corporation. All rights reserved. The trademarks mentioned herein are the property of Life Technologies Corporation or their respective owners. TaqMan® is a registered trademark of Roche Molecular Systems, Inc., used under permission and license. C027334 1012